SEISMIC HAZARD ASSOCIATED WITH THE SPRINGBANK FAULT, NORTH CANTERBURY PLAINS

A thesis
submitted in partial fulfilment
of the requirements for the Degree
of
Master of Science in Engineering Geology
at the
University of Canterbury
by

Beatriz Elena Estrada

University of Canterbury
2003

Frontispiece: Southwest view across the study area in the North Canterbury Plains illustrating the best topographic expression of the Springbank Fault (arrow). Photograph taken from an experimental model aircraft adapted by James Grindey.

ABSTRACT

This study contains an evaluation of the seismic hazard associated with the Springbank Fault, a blind structure discovered in 1998 close to Christchurch. The assessment of the seismic hazard is approached as a deterministic process in which it is necessary to establish: 1) fault characteristics; 2) the maximum earthquake that the fault is capable of producing, and 3) ground motions estimations.

Due to the blind nature of the fault, conventional techniques used to establish the basic fault characteristics for seismic hazard assessments could not be applied. Alternative methods are used including global positioning system (GPS) surveys, morphometric analyses along rivers, shallow seismic reflection surveys and computer modelling. These were supplemented by using multiple empirical equations relating fault attributes to earthquake magnitude, and attenuation relationships to estimate ground motions in the near-fault zone.

The analyses indicated that the Springbank Fault is a reverse structure located approximately 30 km to the northwest of Christchurch, along a strike length of approximately 16 km between the Eyre and Ashley River. The fault does not reach the surface, but it is associated with a broad anticline whose maximum topographic expression occurs close to the mid-length of the fault.

Two other reverse faults, the Eyrewell and the Sefton Faults, are inferred in the study area. These faults, together with the Springbank and the Hororata Faults, are interpreted as part of a system of thrust/reverse faults propagating from a decollement located at mid-crustal depths of approximately 14 km beneath the Canterbury Plains.

Within this fault system, the Springbank Fault is considered to behave in a seismically independent way, with a fault slip rate of ~0.22 mm/yr, and the capacity of producing a reverse-slip earthquake of moment magnitude ~6.4, with an earthquake recurrence of 3,000 years.

An earthquake of the above characteristics represents a significant seismic hazard for various urban centres in the near-fault zone including Christchurch, Rangiora, Oxford, Amberley, Kaiapoi, Darfield, Rolleston and Cust. Estimated peak ground accelerations for these towns range between 0.14 g to 0.5 g.

ACKNOWLEDGEMENTS

I would like to thank many people not only for their contribution to this thesis but also for making my time in New Zealand a wonderful kiwi experience:

- To my supervisors Jarg Pettinga and Jocelyn Campbell for all their help and support during this study, and for always understanding my English even when I was no sure about what I was trying to say
- To Mr Finnemore who made possible the seismic reflection surveys undertaken for this study, and also for *always* answering my questions
- To Peter Stafford for his constant and generous help with the attenuation relationships and for providing me with the software necessary for their application
- To the river monitoring program team of Environment Canterbury, especially Tony Boyle and Brodie Young for allowing me to access to the topographic river data of the study area
- To Richard Allmendinger for kindly providing me with his software for fold analysis and for his technical support
- To Geonet, especially Hugh Cowan and Brian Ferris for supplying the earthquake data of the study area
- To Indo-Pacific Ltd for allowing me to analyse the seismic line where the Springbank Fault was initially discovered
- To the landowners in the study area for giving me their permission to access to their farms to carry out my field work
- To Tim for all his help and support since the first day we met in the Department
- To my classmates and all the people in the Department of Geological Sciences of the University of Canterbury, especially: PJ, Danette, Emma, Mike, DB, Andrew, Scott, Grim, Sarah, Gus, Myriam, Calum, Sam, Erica, Cathy, Rob, John, Julie Anne…
- To the NZODA scholarship and John Pickering who made possible this experience
- Y finalmente a mi familia en Colombia por su constante apoyo.

TABLE OF CONTENTS

CHAPTER 4. SPRINGBANK FAULT EVOLUTION AND STRUCTURAL MODEL

CHAPTER 5. SEISMIC HAZARD ASSOCIATED WITH THE SPRINGBANK FAULT

LIST OF FIGURES

CHAPTER 1

CHAPTER 2

CHAPTER 3

CHAPTER 4

CHAPTER 5

ATTACHED MAPS

LIST OF TABLES

Chapter 1
INTRODUCTION

1.1 INTRODUCTION

The Springbank Fault is a blind structure discovered in 1998 approximately 30 km to the northwest of Christchurch city. Due to the blind nature of the fault, its topographic expression is not evident and was only recognized when Indo-Pacific Ltd carried out seismic reflection surveys in the north Canterbury Plains (Campbell et al., 2000).

Although faults with similar characteristics have proven to represent a significant seismic hazard for several urban centres (for example Northridge in 1994) no further studies regarding the potential seismic hazard of the Springbank Fault have been undertaken prior to this study. The principal aim of this study is to characterise the Springbank Fault and evaluate its potential seismic hazard on nearby urban centres. To achieve this, and because of the blind character of the fault, conventional techniques used in seismic hazard analysis are supplemented with alternative and indirect methods of investigation.

This research is focused on establishing the location, extent and geometric/structural characteristics of the Springbank Fault, even where no evident topographical expression is available. These characteristics are used in turn, to estimate the maximum earthquake magnitude that the fault is capable of producing, and finally, to estimate ground motions at selected places.

The research is presented in six chapters:

- Chapter 1 outlines the objectives of the research, and the tectonic setting in which the Springbank Fault is evolving, together with a description of the study area and a brief explanation of the methods and techniques used

- Chapter 2 describes the evident topographic expression of the Springbank Fault and analyses its subtle geomorphologic expression in order to establish the fault location and extent
- Chapter 3 provides a description of the near-surface character of the fault and an analysis of the earthquake activity in the study area
- Chapter 4 provides a possible structural evolution model for the study area
- Chapter 5 integrates the information from the previous chapters in order to establish the fault characteristics to be used in the assessment of the seismic hazard of the Springbank Fault; and
- Chapter 6 discuss the possible uncertainties regarding the methodology of investigation, summarises the conclusions, considers their implications and provides recommendations for further studies.

1.2 OBJECTIVES

The main aim of this study is the structural and seismogenic characterisation of the Springbank Fault, and the evaluation of its associated seismic hazard. To accomplish this, the project includes the following objectives:

1. Undertake detailed geomorphological mapping along the fault, the associated wider zone of active earth deformation, and the fault-related micro-topographic features
2. Determine the subsurface fault zone geometry
3. Estimate the fault slip rate
4. Define the approximate timing of the most recent earthquake ruptures
5. Analyse levels of micro-earthquake activity and associated focal mechanisms
6. Estimate ground motions and fault hazard assessment for a scenario earthquake.

The complete characterisation of the Springbank Fault requires an understanding of the regional tectonic setting, as well as the local tectonic and structural setting in which the fault is evolving.

1.3 OUTLINE OF THE TECTONIC SETTING OF NEW ZEALAND

This section explains the general tectonic plate distribution in New Zealand and the main fault systems accommodating the tectonic movement, together with the main characteristics of the Springbank Fault and its position within this tectonic setting. This section is based on several key publications including Norris et al. (1990), Berryman and Beanland (1991), Knuepfer (1992), Cowan et al. (1996) and Pettinga et al. (2001).

New Zealand is located at the boundary between the Australian and Pacific plates. The motion between these plates forms an opposite dipping and obliquely convergent subduction zone. The relative plate displacements along the plate margin range from 50 mm/yr in the north to 40 mm/yr in the centre, and 30 mm/yr in the south (Figure 1.1). Numerous active faults within New Zealand accommodate the plate motion. Two major fault zones, the Alpine Fault and Marlborough Fault Zone (MFZ) in the South Island, can be interpreted as a trench-trench transform fault zone, linking the subduction zones (Figure 1.1). A southeast dipping subduction zone at the southwest end of the country, the Pysegur trench, also called the Fiordland subduction zone, is linked to a major northwest-dipping subduction zone in the northeast, the Hikurangi subduction zone.

Most of the plate motion accommodated through this trench-trench transfer zone occurs in the Alpine Fault, an approximately 480 km linear structure along the west part of South Island. The Alpine Fault dips to the east, strikes oblique to the present plate convergence vector, and accommodates at least 75% of the plate boundary motion.

In the northeast of South Island, the Marlborough Fault System (MFS) transfers the motion between the Alpine Fault and the Hikurangi Subduction Zone. The MFS consists of dextral strike-slip and oblique-slip faults. Several studies have proposed that deformation has progressively migrated southward on to the younger faults of this system.

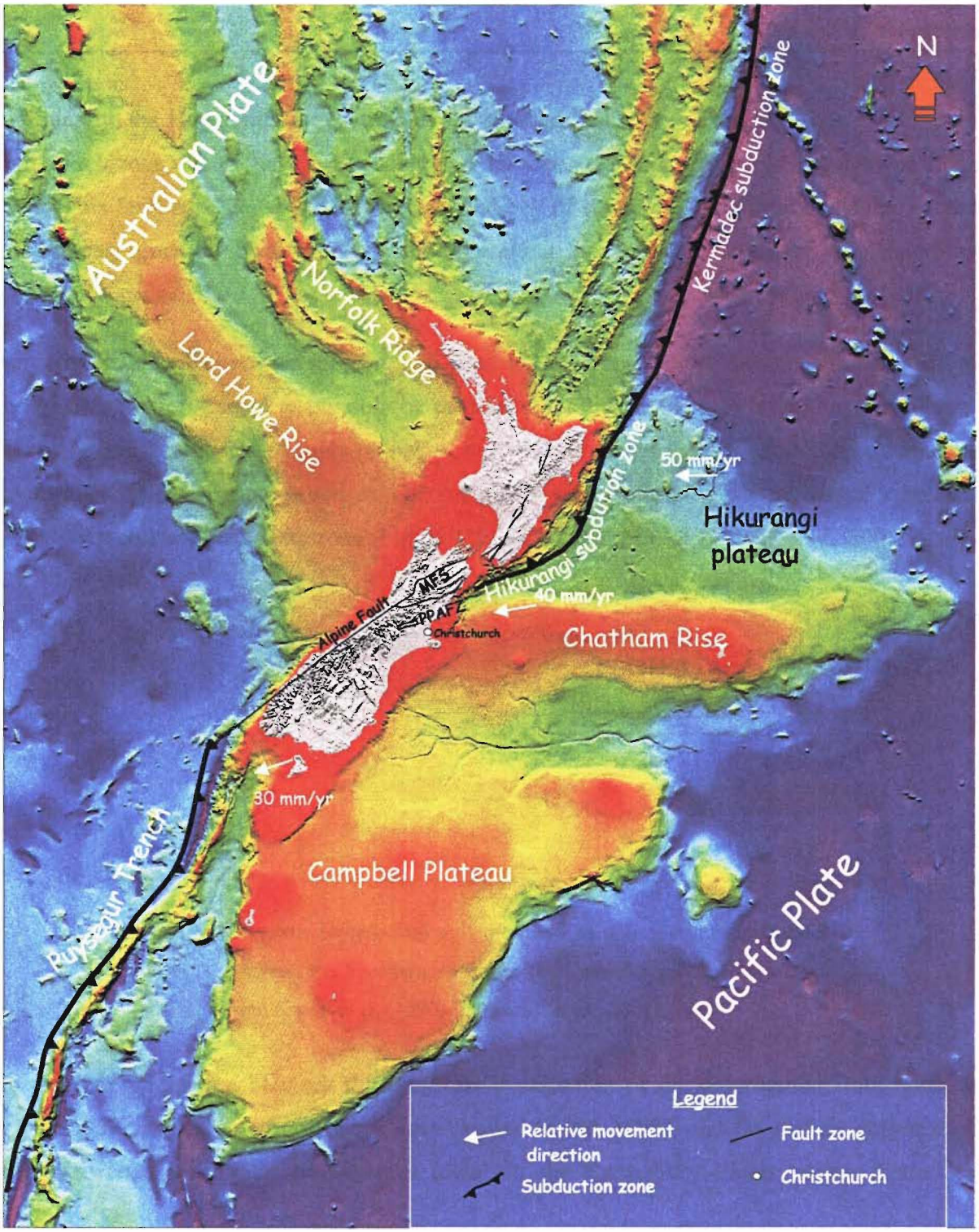

Figure 1.1: Tectonic setting of New Zealand. The location of some key elements of the plate boundary zone are illustrated. The movement along the opposite dipping subduction zones, the Puysegur trench and the Hikurangi subduction zone, at the SW and NE of the country, is accommodated by the Alpine and the Marlborough Fault System (MFS). The Porters Pass-Amberley Fault Zone (PPAFZ) south of the MFS is also represented. Numbered arrows show rates of relative plate convergence (The undersea New Zealand information is reproduced with permission from NIWA).

Traditionally, the Hope Fault is regarded as the southern boundary of the MFS but, to the south another fault zone, the Porter's Pass-Amberley Fault Zone (PPAFZ), is developing (Cowan et al., 1996). This fault zone consists of a disseminated belt of strike-slip and thrust faults that extend east-northeast from the Southern Alps foothills along the northern margin of the Canterbury Plains.

Alternatively, the area between the Southern Alps and the Canterbury Plains constitutes a diffuse zone of deformation related to the oblique continental collision. Beneath the Canterbury Plains, systems of thrust fault-related folds propagate eastwards from the Alpine Fault. This broad zone of deformation has been interpreted as a part of a two–sided deforming wedge, associated with a mid to lower crustal detachment zone (Figure 1.2; Norris et al., 1990; Pettinga et al., 2001).

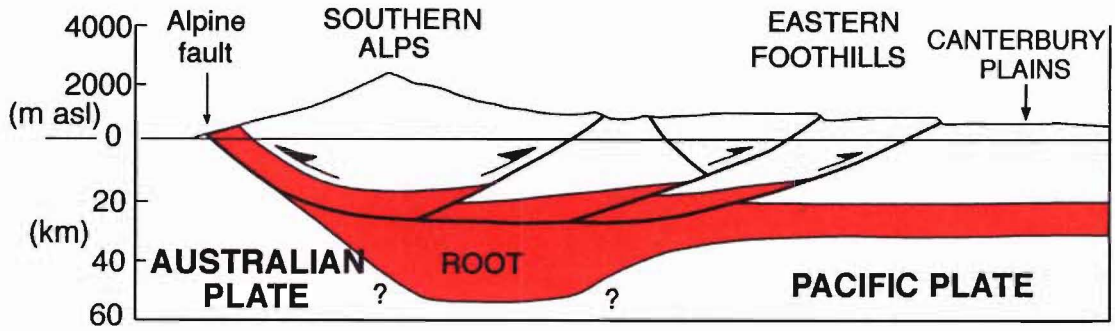

Figure 1.2: Schematic representation of the two-side deforming wedge model between the Southern Alps and the Canterbury Plains (modified from Norris et al. (1990) in Pettinga et al., 2001)

The complex interaction between the progressive migration of the deformation from north to south into the north Canterbury region (represented by the MFS), and the diffuse deformation zone (associated with fault propagation folds) in the Canterbury Plains causes distinctive structural styles.

Different structural domains have been recognized (Pettinga et al., 1998, 2001). Each domain presents different tectonic characteristics related to fault style, geometry, and rates of deformation. For the Canterbury region, eight structural domains have been documented as illustrated in Figure 1.3 and Table 1.1.

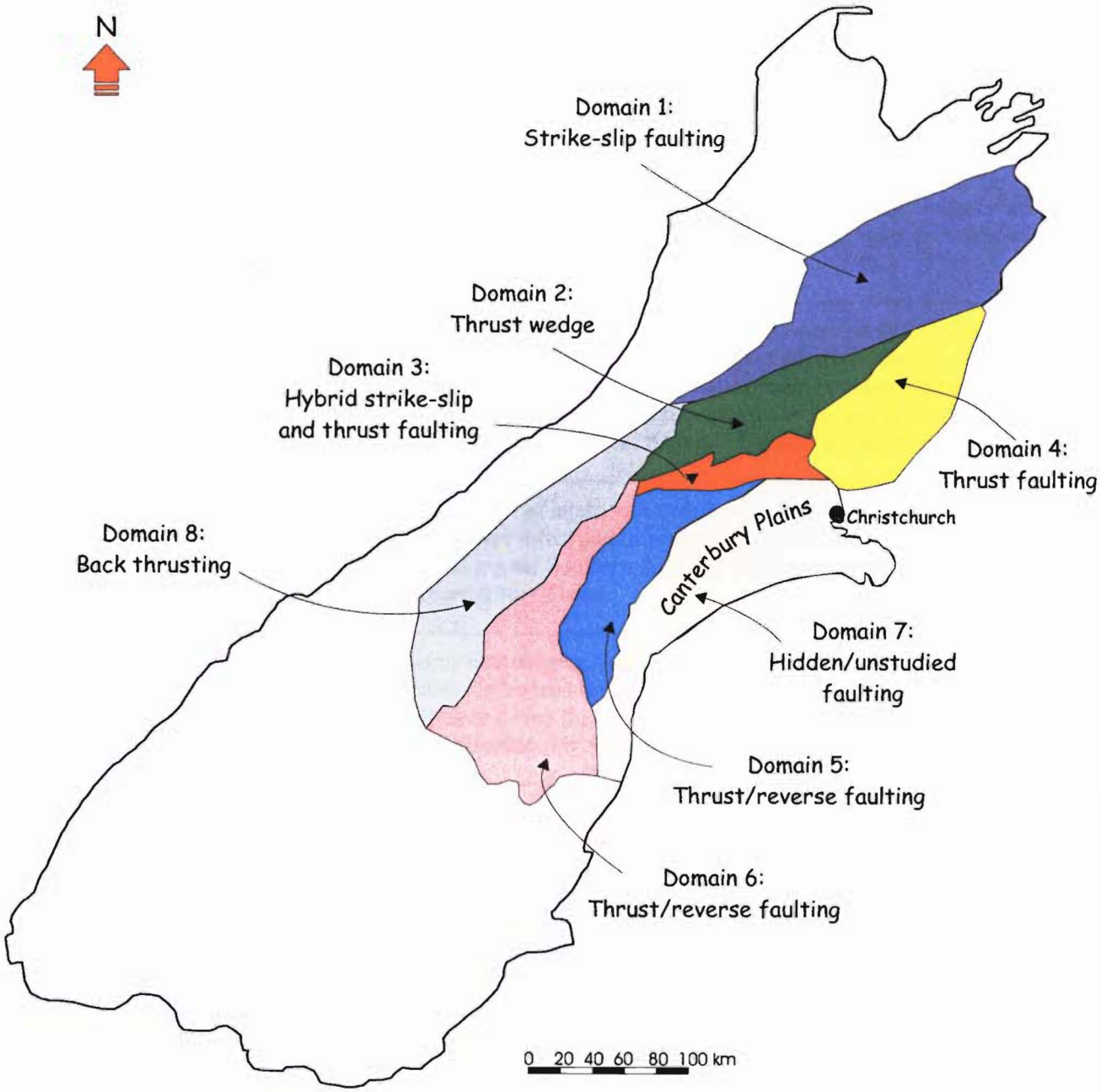

Figure 1.3: Different structural domains within the Canterbury Region (modified from Pettinga et al, 1998, 2001).

Table 1.1: Structural domains in Canterbury (Modified from Pettinga et al., 1998; 2001)

DOMAIN	BRIEF DESCRIPTION
Domain 1: Marlborough Fault System	Major fault system of northeast trending strike-slip faults that transfer crustal shortening associated with subduction of the Pacific plate onto the west-facing Alpine Fault.
Domain 2: West Culverden Fault Zone	West dipping system of thrust/reverse faults and associated fault-propagation folds that represents the eastern margin of the wedge-shaped structural domain of the Southern Alps in north Canterbury. This fault system is interpreted as backthrusts to the east of the Alpine Fault zone and is inferred to extend to mid and lower crustal depths beneath the Southern Alps and Canterbury foothills.
Domain 3: Porter's Pass-Amberley Fault Zone	Juvenile hybrid system of interconnected east-northeast trending strike-slip transfer faults, oblique thrust and/or reverse faults with associated fault propagated folds that occur along the Southern Alps foothills and range-front at the west margin of the Canterbury Plains.
Domain 4: North Canterbury Fold and Fault Belt	Region of mainly east dipping thrust/reverse faults associated with strongly asymmetric folds that extend through the northeast part of the onshore Canterbury region, and offshore across the continental shelf and slope. The faults are well expressed as topographic ridges separated by fault-controlled synclinal valleys.
Domain 5: Central Canterbury Rangefront Fault Zone	Complex array of faults, folds, and associated warping along the west margin of the Canterbury Plains. This constitutes the eastern most expression of the double-sided wedge described by Norris et al. (1900).
Domain 6: South Canterbury Zone	This domain comprises the margin of the Southern Alps double-sided wedge style of thrust deformation.
Domain 7: Canterbury Plains	System of north and northeast trending active faults and folds are emerging from beneath the aggradation gravels of Pleistocene fluvio-glacial outwash in the Canterbury Plains. This system is the result of the tectonic shortening, crustal thickening and uplift taking place in the region.
Domain 8: Southern Alps Zone	The deformation here is dominated by oblique, reverse/thrust faulting, inferred to be driven by backthrusting off the dipping Alpine Fault.

1.3.1 THE SPRINGBANK FAULT

The Springbank Fault is located approximately 30 km northwest of Christchurch, within a complex interaction between domains 3, 4, and 7. The fault was first recognized in 1998, when Indo-Pacific Ltd undertook seismic reflection surveys across the north Canterbury Plains. At that time, the Springbank Fault was identified as a major northeast trending thrust/reverse fault dipping to the northwest, with a broad fault-related fold developing at the tip of the fault and backthrust structures developed to the northwest.

The seismic stratigraphy indicated that, close to the surface, the fault dips ~60° to the northwest, without breaking into the top reflectors of the profile. The strata overlying the tip of the Springbank Fault closest to the surface have been broadly folded in response to the reverse-slip movement along the fault plane. These initial characteristics allow the classification of the Springbank Fault as a blind thrust/reverse structure.

The best surface expression of the fault, its associated fold, occurs between the Cust and Eyre Rivers, close to the Springbank settlement (Figure 1.4). This landform was only recognized as the Springbank Fault-related fold after the Indo-Pacific seismic reflection survey conducted in 1998. Prior to this survey, no surface expression related to the Springbank Fault had been recognised or mapped in the field (Pettinga, *personal communication, 2002*).

The impetus from this study came from the realization that this previously unrecognized fault represents a significant earthquake source within 30 km of Christchurch city.

1.4 DESCRIPTION OF THE STUDY AREA

1.4.1 LOCATION

The study area is centred on a proposed location of the Springbank Fault defined prior to this study. The area comprises 38x40 km and is situated to the northwest of Christchurch city, in the north Canterbury Plains (Figure 1.4).

Other urban centres are also located within or near to the study area, including Rangiora, Kaiapoi, oxford, as well as the rural townships of Cust and Springbank.

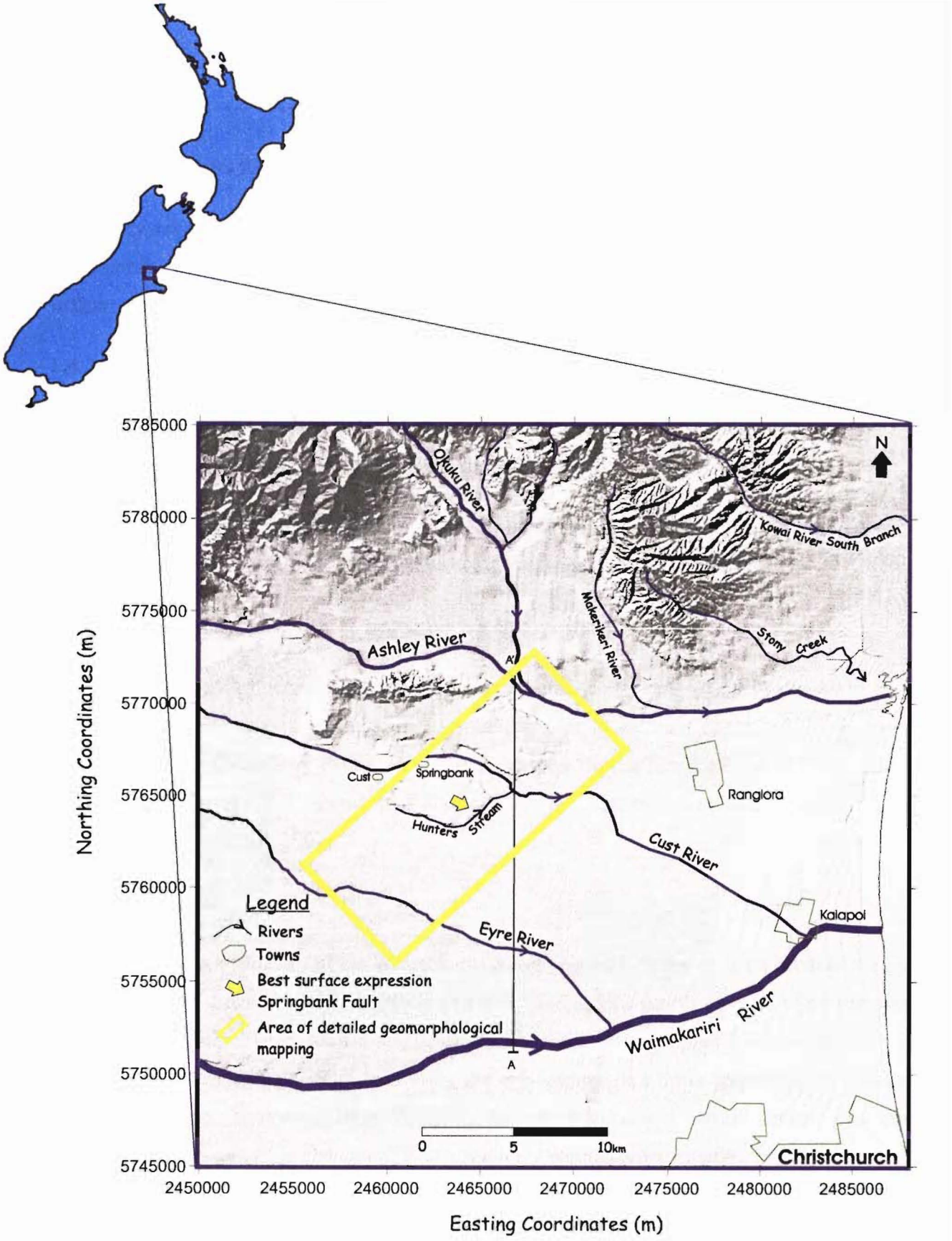

Figure 1.4: Digital elevation model (DEM) of the study area. Yellow rectangle shows area of detailed geomorphological mapping, and yellow arrow illustrates the location of the best topographic expression of the Springbank Fault. The location of the main rivers and urban centres are also illustrated (coordinates from1949 New Zealand map grid). Cross section line A-A' is presented in Figure 1.5.

1.4.2 RIVER SYSTEMS IN THE AREA

The study area is located between two main catchments, the Waimakariri and Ashley River catchments. A brief description of the main rivers composing these catchments is given as follows.

1.4.2.1 Waimakariri River

The Waimakariri River flows at the south of the study area (Figure 1.4). It is characterised by a wide braided channel into which other rivers such as the Eyre and the Cust drain.

The source of the Waimakariri River is situated east of the main divide of the Southern Alps. At the study area, the river is braided and flows west to east across the Canterbury Plains.

1.4.2.2 Eyre River

The Eyre River is an intermittently flowing river situated to the north of the Waimakariri River. It extends from the eastern foothills of the Southern Alps to the west of Oxford, in an easterly direction into the Canterbury Plains. In the past, the river flowed into the Kaiapoi River, with its mouth where the Kaiapoi township is located, but in 1928 the river was diverted into the Waimakariri River (Earl, 1997).

1.4.2.3 Cust River

The Cust River is a tributary of the Waimakariri River (Figure 1.4) and it flows north of the Eyre River. The river drains from the foothills of the Southern Alps (north of the Oxford township) into the Canterbury Plains, with a southeasterly direction. Northeast of Kaiapoi, in 1869, the Cust River was accidentally captured during the enlargement of a drain constructed to drain the Rangiora Swamp, stretching from Rangiora to the Waimakariri River. Today, this drain constitutes the present river channel of the Cust River (Waimakariri Irrigation Ltd, 2000).

Within the study area, the river undergoes changes in both direction and river channel pattern. According to Cowan (1992) the actual Cust River valley corresponds to an ancestral channel of the Ashley River which was active ~20,000 years ago during the late glaciation.

1.4.2.4 Ashley River

The Ashley River is the second major river in the area, and is located at the north end of the study area, with several major tributaries such as the Okuku and Makerikeri Rivers (Figure 1.4). Within the study area, the river is diverted by anticline growth (Cust Anticline) which caused a change in flow direction from southeast to west-east direction after crossing the anticline, until it reaches the sea (Sisson et al., 2001).

1.5 TOPOGRAPHY AND GEOLOGY

Topographically, the study area is characterised by a very low relief, consisting of extensive plains, and in the northern part, to minor degree, of low hill-slope topography. The relief is directly related to the geology, with a composite landscape created by the multiple fluvial aggradation and degradation surfaces that constitute the Canterbury Plains.

1.5.1 OUTLINE OF THE GEOLOGY OF THE STUDY AREA

The geology described here is mainly based on the stratigraphic nomenclature of Browne and Field (1985), Browne et al. (1988), Wilson (1989) and Field et al. (1989). Only the geology relevant for this study is explained.

The study area is underlain by a basement of Mesozoic indurated sandstone and argillite (Torlesse Supergroup) and a Cretaceous-Tertiary cover sedimentary sequence of about 750-2000m thickness. This Mesozoic and Cenozoic bedrock is in turn overlain by a Quaternary succession of unconsolidated deposits dominated by sandy gravels, forming the ~7500 km^2 Canterbury Plains.

The Canterbury Plains are comprised of a series of coalescing alluvial fans formed by different rivers that emerge from the Southern Alps and foothills (e.g. the Waimakariri River).

1.5.1.1 Basement

The basement rocks in the Canterbury region correspond mainly to the Torlesse Supergroup, alternating indurated sandstones and argillite (informally referred to as greywacke) deposited in a variety of environments, with ages ranging between Permian to early Cretaceous (Bradshaw,

1989). The Torlesse Supergroup in Canterbury consists of two terranes: the Rakaia (Triassic-Jurassic) and Pahau (early Cretaceous). These terrenes are separated by the Esk Head Melange (Silberling et al., 1988) an 8-10 km wide formation formed of pillow lavas, limestone, and chert in a matrix of sandstone and mudstone.

1.5.1.2 Cover Sequence

Overlying the Torlesse Supergroup, there are a series of sedimentary formations deposited during marine transgressions and regressions, with ages ranging from late Cretaceous to early Quaternary.

Late Cretaceous to Cenozoic Cover Sequence

Eyre Group

The Eyre Group represents the base of the Cretaceous-Cenozoic sequence in north Canterbury. This group was deposited during a marine transgression in the late Cretaceous to mid Oligocene and unconformably overlies the Torlesse Supergroup basement. The Eyre Group mainly comprises marine sedimentary units such as quartz-rich sandstone, glauconite sandstone and mudstone, and locally submarine igneous rocks such as pillowed, tholeitic and alkaline basalts. It is conformably overlain by Oligocene limestones (Amuri Limestone) or unconformably by the Motunau group (see below).

Amuri Limestone

In north Canterbury, the Mid Oligocene Amuri limestone conformably overlies the Eyre Group and is the most widespread formation in Canterbury. It comprises a centimetre to a decimetre bedded, light cream to green-grey, indurated, bioturbated fine grained limestone.

Motunau Group

The Motunau Group is located in eastern north Canterbury and unconformably overlies the Amuri Limestone. This group was formed during a marine regression which took place between the mid Oligocene to the early Quaternary, and is represented by limestones, greensands, siltstones, and conglomerates.

Several formations are included in the Motunau Group (principally the Omihi, Mt Brown, Greta and the Kowai Formation). In the study area the Motunau Group is mainly represented by the Kowai Formation which comprises c.75-100m of basal shallow marine sediments (i.e siltstone, fine sandstone and round pebble conglomerate) overlain by more than 500 m of conglomerate.

The sequence is poorly dated, but according to Field and Browne (1985), it is Nukumaruan (c.1.5-2 ma) near the top. Cowan (1992), concludes that the Kowai Formation should extend into the Pleistocene because it underlies a Holocene erosion surface and it is unconformably overlain by dissected fans of coarse locally derived late Pleistocene conglomerate capped by loess.

1.5.1.3 Late Quaternary Deposits

Late Quaternary sediments related to glacial and interglacial periods overlie the sequence described above. Climatic changes have resulted in coastal transgression and regression over the study area causing an accumulation of swamp, estuary, lagoon and beach deposits over the alluvial fans.

According to Wilson (1989), large volumes of sediment were carried by the rivers during glacial periods, whilst interglacial periods resulted in rivers with less load, that downcut into earlier outwash aggradation surfaces. During subsequent cycles, glacial outwash infilled these entrenched interglacial valleys and covered fan deposits from the previous glaciations. This pattern of aggradation-degradation cycles was repeated creating a complicated succession of very similar deposits.

Five different glaciations have been recorded in the Waimakariri Catchment (Table 1.2), and morainal features have been correlated to outwash deposit on the plains. The local Quaternary stratigraphic units are strictly formational units consisting of a body of sediments assigned to a specific glacial cycle. There has been a loose usage of the same terms to apply to the surfaces, particularly to the aggradation surfaces underlain by these bodies of sediments. Nevertheless, tectonic uplifting may produce "surfaces" underlain by gravels of disparate ages. Therefore, a more rigorous separation of formational units from geomorphic surfaces is necessary, but this is beyond the scope of this study.

The Quaternary sedimentary cover consists of a sequence of gravel, sand, and silt, interbedded with silt, clay, and shell, often with peat. The main characteristics of the surficial formation in the study area are compiled in Table 1.3, and a diagrammatic geological cross-section is presented in Figure 1.5 (see Figure 1.4 for location of this profile).

Table 1.2: Chronology and terminology for glacial events in the Waimakariri River (data from Gage, 1958, Browne et al. (1985) and Suggate (1990)).

WAIMAKARIRI RIVER GLACIAL ADVANCE NAME	APPROX. AGE OF MAXIMUM ICE ADVANCE (IN YEARS B.P)	STRATIGRAPHIC FORMATION NAME	NEW ZEALAND CORRELATION NAME
Poulter 2 advance	14,000 (13,750±)		Otira Glaciation
Poulter 1 advance	17,000		
Blackwater 3 adv.	<19,000	Burnham Formation	
Blackwater 2 adv.	22,200		
Blackwater 1 adv.			
Otarama advance	56,000-70,000	Windwhistle Formation	Waimea Glaciation
Woodstock advance	150,000	Woodlands Formation	
Avoca		Hororata Formation	Waimaungan Glaciation

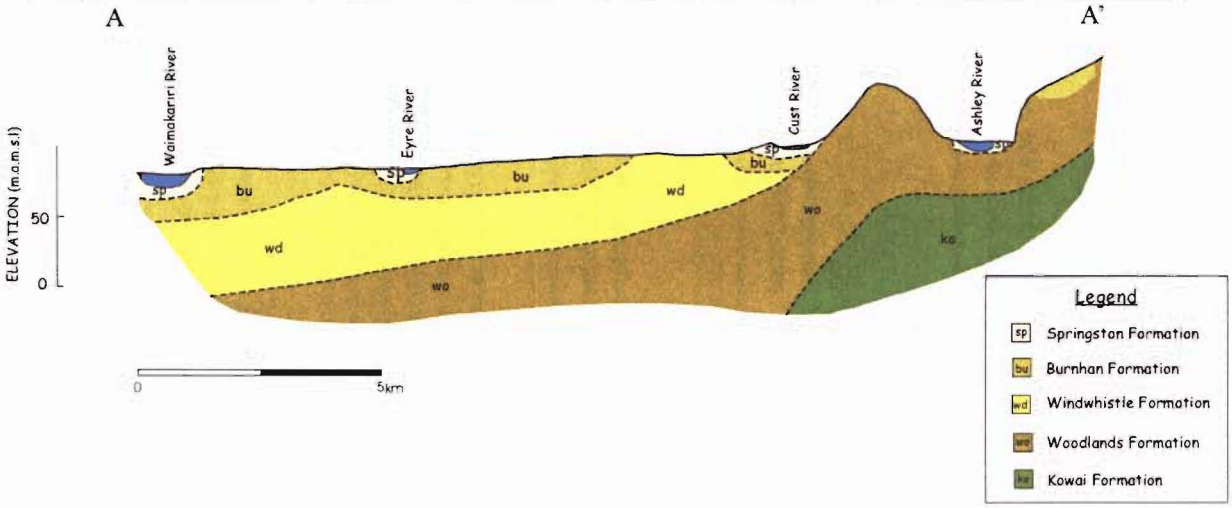

Figure 1.5: Diagrammatic geological cross section of the study area (see Figure 1.4 for location of the section line; modified from Bowden, 1982).

Table 1.3: Quaternary Formations of the study area.

FORMATION	LITOHOLGIC CONTENT	DEPOSITIONAL ENVIRONMENT AND AGE	GEOGRAPHIC DISTRIBUTION	STRATIGRAPHIC RELATIONSHIPS
Hororata Formation	Unstratified rounded and weathered medium gravel with a few boulders, overlain by a thick loess layer	Glacial outwash derived river deposit possibly from Wimaunga and Nemona Glaciations (Suggate, 1965 in Browne et al., 1988), but its age is uncertain	Inland Canterbury Plains	
Woodlands Formation	This Formation consists of moraine and outwash deposits of moderately-weathered gravel and poorly sorted ice-contact material that are moderately dissected and locally loess covered (Gregg, 1964)	This Formation is the result of the Woodstock glacial advance in the Waimakariri Valley. Glacial outwash derived river deposits during the Waimea Glaciation (Suggate, 1965 in Browne et al., 1988). 150,000 years ago	Inland Canterbury Plains	
Windwhistle Formation	Moderately sorted and rounded gravel in a weathered sand and silt matrix	Glacial outwash derived river deposits during an early Otiran ice advance about 70,000-40,000 years ago (Suggate (1965 in Browne, et al., 1988)	Inland Canterbury Plains	Underlies Springston Formation. Unconformable overlies the Woodlands Fm.
Burnham Formation	Moderately sorted, slightly-weathered, rounded outwash gravel in a sand matrix	Outwash streams during the Blackwater 1 and 2 glacial advances in the late Otiran Glaciation, about 25,000-18,000 years ago. It constitutes the major fans of the Canterbury Plains	Canterbury Plains	Usually unconformably overlain by the Springston Formation
Springston Formation	Well sorted rounded gravel with dominantly sand matrix and lenses of silt and clay	Lag and fan deposits of river gravel and overbank silt and coastal flood channels that followed glacial retreat at the end of the Otira Glaciation. This formation includes all postglacial deposits, excluding those of present-day river channel and flood plains. 0-14,000 years	Canterbury plains-floodplains immediately adjacent to rivers on inland plains but fanning out towards coast	Overlies Burnham Formation and is interbedded with the contemporaneous Christchurch Formation

1.6 GEOLOGICAL STRUCTURES IN THE AREA

Apart from the Springbank Fault, other structures have been recognized in the study area prior to this study. These structures include folds and faults such as the Cust Anticline, the Ashley and Loburn Faults, and backthrust structures off the Springbank Fault. They confirm the active tectonic setting in the area and provide evidence of complex structural interactions.

Cust Anticline

The Cust Anticline is part of a fold belt that extends to the northeast (Cowan, 1992). The anticline is a fault-propagated fold that has been associated with a backthrust off the Springbank Fault (Jongens et. al. 1999) and is also closely associated with a restraining step-over in the Ashley Fault (see below; Campbell et al., 2000).

The Anticline changes its trend from almost north-south to west-east (Figure 1.6). This swing in strike orientation is interpreted as having been caused by interaction between reactivated east-west Cretaceous basement faults and the principal horizontal compression, orientated northwest/southeast (Jongens et al., 1999).

The west limb of the Cust Anticline is limited by a 1.5 km long fault trace, the Cust Fault, which has uplifted the western limb, causing important changes in the drainage pattern in the field area (Cowan, 1992). According to Cowan (1992), an ancestral Ashley River, which today runs along the northern flank of the Cust Anticline, flowed along the valley now occupied by the Cust River (southern flank of the Anticline). The ancestral Ashley River was deflected to its actual position by uplifting on the Cust Anticline.

The fault bordering the northern limb of the anticline has been correlated by to the projection to the Ashley Fault (see below).

Ashley and Loburn Faults

The Ashley Fault and its splay the Loburn Fault, are parallel structures with a west-east strike, located north of the Ashley River (approximately 5 km northwest of Rangiora). The structures are reverse-slip with a dextral oblique-slip component. The traces appear to converge to the west, close to the Ashley River (Figure 1.6; Sissons et al., 2001).

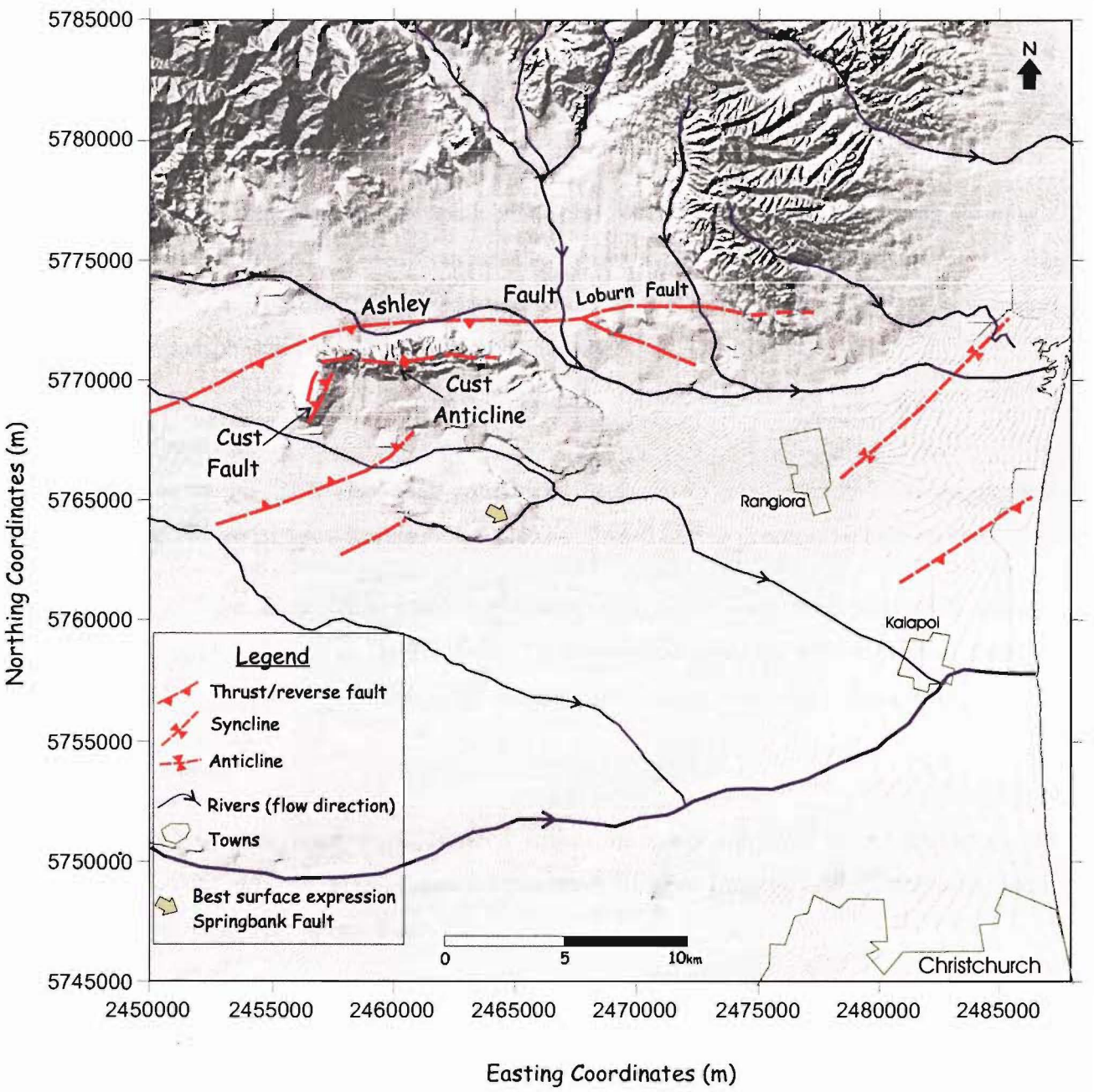

Figure 1.6: Other structures in the study area. This figure illustrates the location and extent of structures recognized prior to this study. The structures are compiled from different studies that include geological and geophysical investigations.

The Loburn Fault was recently discovered (Sissons, 1999) and is inferred to be the older of the two structures, with its activity transferred to the Ashley Fault, and the latter having been more active since about 10,000 years ago (post deposition of the Burnham Formation). The Ashley Fault is projected westward, and is inferred to continue as the structure bordering the northern limb of the Cust Anticline.

The Loburn Fault dips towards the south while the Ashley Fault dips to the north forming a wedge of elevated ground uplifted between the two as a result of late Quaternary reverse-slip activity on both faults. Some indirect geomorphic evidence also indicates a component of dextral oblique-slip transpression on these faults (Sissons, 1999).

Backthrust structures

Backthrust structures have also been recognized in the field area, mainly from geophysical investigations. Some of these features have been confirmed during geomorphologic surveys.

Backthrusts off the Springbank Fault are mainly recognized from the Indo-Pacific seismic reflection lines (Jongens et al., 1999). Some backthrusts intercept the western end of the Cust Anticline and suggest that the Anticline is fundamentally related to the Springbank Fault.

Hororata Fault

Although the Hororata Fault is not located within the study area, but to the southwest, the description of this structure is important for this study because Jongens et al. (1999) infer that it may be linked to the Springbank Fault.

The Hororata Fault is a thrust structure that uplifts late Cretaceous-Tertiary rocks to the surface. Correlation with nearby geology (Kowai gravels) indicates that the fault has a vertical throw of ~800M (Jongens et al., 1999). These authors also suggest that the Hororata Fault is a major basin boundary fault that commenced in the early-mid Pleistocene, according to onlaps of the Quaternary gravels.

Stratigraphic correlations in the Malvern Hill indicate that the hanging wall, west of the emergent Hororata Fault, is folded and broken by a series of both east and west facing thrust, presumably

breaking up from a basal decollement. These are thought to be analogous to the less well exposed structures associated with the Springbank Fault.

The Hororata Fault, together with the Springbank Fault have been correlated with a major northeast-southwest trending step occurring in the basement between Rangiora and Ashburton. This step is indicated by both geology and gravity data. The analysis suggests that the Hororata Fault is a master fault in a series of backthrusts, which together represents a tectonic wedge (Jongens et al., 1999).

1.7 METHODS AND TECHNIQUES

The initial step in fault characterisation, and assessment of its associated seismic hazard, is the determination of the basic characteristics of the fault such as location, extent and slip direction. This is achieved using conventional geomorphic and geologic mapping on the superficial expression of the structure.

The initial mapping performed in the study area indicated that, apart from the surface expression of the fold observed near to the Springbank Settlement, the Springbank Fault does not have any other evident geomorphic expression. The fault does not rupture the surface, and its associated fold is not even observable along the total projected fault extension. Consequently, conventional geological and geomorphological mapping is not enough to establish the basic characteristics of the fault.

Early in the project it became clear that many of the conventional techniques used in seismic hazard studies would not be applicable due to the blind nature of the Springbank Fault.

Seismic hazard studies are usually based on geological fault characteristics that can be observed in the field. In the case of blind faults such as the Springbank Fault, other conventional methods, including trenching interpretation, fault scarp morphology analyses, and dating of material displaced by the fault, do not lead to the recognition and characterization of their potential seismic hazard (Bullard and Lettis, 1993).

When there is no instrumental or historical record of ruptures along a fault, trenching across the structure is commonly used to establish the timing and character of past ruptures, which constitute important input information in seismic hazard assessment.

Due to the limitations of trenching, typically a narrow excavation of 2-4 m of depth across a recently active, well constrained fault scarp, this technique is not applicable to the Springbank Fault because the fault rupture does not reach the surface.

Fault scarp morphology analysis is another technique that utilizes the characteristics of the fault scarp on the surface to establish the character of the fault and the timing of paleoearthquakes. This technique cannot be used either because the Springbank Fault does not have a scarp, but does have a related fold.

Because there is no direct access to the material that has been displaced by the fault, conventional dating techniques (i.e. radiocarbon dating) to establish timing of paleoearthquakes and subsequently the rate of activity of the fault are also not directly applicable.

The dating problem in the study area is more complicated. The geological character of the study area, extensive alluvial plains formed during glacial and interglacial periods, has a lack of datable material directly related to the age of these surfaces.

The recognition that the various conventional techniques used in analysis of seismic hazard associated with geological faults are not applicable in this study, led to the search and application of other methods. Since the commencement of this investigation, it was always clear that the project would involve limitations restricting the achievement of the proposed objectives.

In this study various alternative methods and techniques have been adopted in order to analyse the surficial and shallow subsurface (<500 m) expression of the Springbank Fault. The key objectives are the determination of the location and extent of the fault, as well as its geometric/structural characteristics, even where there is no evident topographic expression available. This information will be used in turn to infer the potential seismic hazard associated with the Springbank Fault.

The methods used here include:

1. Conventional geomorphological mapping and Global Positioning System (GPS) topographic surveys
2. Morphometric analysis along rivers and subtle topographic features
3. Geophysical (seismic reflection) investigations
4. Seismological studies
5. Computer fold modelling and
6. Use of empirical equations for seismic hazard assessment.

1.7.1 BASE INFORMATION

As with any research project, at the commencement all the information from previous studies relating to geological, geomorphological, and topographical data of the study area were compiled. This information is summarised on a map which in turn constitutes a base map onto which new information is added progressively.

Conveniently for this study, the information related to previous studies carried out in the study area had been already compiled on a database. The database is contained in the Geographic Information System (GIS) of the Department of Geological Sciences at the University of Canterbury. The information on this GIS has been collected from both published and unpublished reports of the north Canterbury region, including geological and geophysical investigations from previous postgraduate research projects. This database was progressively complemented with information collected from the field investigations carried out for this study.

1.7.2 FIELD INVESTIGATIONS

The field investigations consisted of geomorphological mapping, morphometric analyses and geophysical (seismic reflection) surveys.

1.7.2.1 Geomorphological mapping

Detailed mapping (scale 1:10,000) was carried out in the area surrounding the Springbank Fault. The aim was to establish the surface characteristics, associated wider zone of deformation and fault-related micro-topographic features of the Springbank structure.

Mapping was based on interpretation of aerial photographs (scale ~1:15,000 and enhanced air photos in scale ~1:7,500), and several visits to the field. Global Positioning System (GPS) surveys were also undertaken along both the main geomorphological features and the subtle topography associated with the fault.

1.7.2.2 Global Positioning System (GPS) surveys

GPS technology was used to survey features related to the Springbank Fault. Both main landforms and subtle topographic features related to the fault were surveyed using mainly carrier-phase, and in some cases code-phase, in differential GPS technique (see Appendix 1 for an introduction to GPS technology).

Carrier-phase surveys involve vertical errors less than 0.1m, which allow very accurate measurements. These surveys were conducted on foot, taking a measurement every second, which corresponds to taking one measurement approximately every metre.

Some of the surveys consisted of profiles along the topography in order to outline changes in slope (convex topography) that could be associated with the Springbank Fault-related fold. In others, the topographic feature was surveyed completely and then modelled with computer assistance, in order to determine, on the basis of its characteristics, if the feature is or is not fault-related.

Code-phase differential GPS was mainly used along roads with approximately perpendicular direction to the fault trend, in order to determine local convex topography that could document folding caused by an underlying structure. Due to uncertainties related to the location of the fault (because of its lack of topographic expression) and considering that thrust faults may consist of different segments with changing strike, these surveys were carried out for multiple kilometres along each road.

Consequently, the surveys along roads were undertaken in a car, making the measurement every second, which at approximately 10km/h constitutes a measurement every ~3m. This, together with the characteristics of the code-phase surveys (see Appendix 1), resulted in less accurate measurements than those undertaken with carrier-phase. Errors in the vertical may reach ~1m or more in some cases.

1.7.3 MORPHOMETRIC ANALYSES

Morphometric analyses are quantitative and qualitative examinations of different topographic features to establish if they are affected by tectonic deformation. In this study, the morphometric analyses are mainly focused on the river systems.

The analyses include longitudinal stream profile, stream gradient index and river sinuosity analysis. A detailed explanation of the morphometric analysis performed on the drainage within the study area will be given in the next chapter.

1.7.4 GEOPHYSICAL (SEISMIC REFLECTION) INVESTIGATIONS

In order to establish the near-surface characteristics of the Springbank Fault, two shallow (<600 m) seismic reflection surveys were carried out at different locations in the study area. These surveys were analysed together with the seismic line previously undertaken by Indo-Pacific in 1998, which provides deeper penetration but lacks near surface information.

The basis of the shallow seismic reflection technique is to measure the time taken for a seismic wave to travel from a source, go down into the ground, where it is reflected (by layers of different characteristics known as a reflectors) and come back to the surface again. This time is known as the two-way travel time (TWTT; Reynolds, 1997).

The location of the source and the receivers on the surface used to measure the TWTT is known. Then, the problem is to convert the two-way travel time into depths of the different reflectors, which is directly related to the seismic velocity of the media.

This conversion involves complex computer processing of the seismic data. The theoretical and technical aspects of this processing are not explained here, only the aspects directly related to the

acquisition and processing of the seismic data for the two seismic lines undertaken as part of this project (Appendix 2).

1.7.5 EARTHQUAKE DATA ANALYSIS

One of the initial objectives of the study was to install a wide-band seismic network surrounding the field area, in order to establish microearthquake activity and focal mechanisms related to the Springbank Fault. This was not possible due to the unavailability of the required seismic equipment.

It was then decided to analyse the available seismic information of the area. Two earthquake catalogues were examined and compared. One corresponds to the earthquake information compiled by the Institute of Geological and Nuclear Sciences (GNS), and the other to the earthquakes registered as part of a temporary microearthquake network installed for a period of almost three months in 1990 (Cowan, 1992).

The information from both catalogues is processed from the point of view of earthquake location and distribution, and the results are compared considering the quality of data and the station distribution of each network with respect to the study area.

The focal mechanisms (fault plane solutions) determined by Cowan (1992) are also analysed to establish the kinematic character of the faults within the field area. This analysis is presented in Chapter 3.

1.7.6 COMPUTER FOLD MODELLING

Because the Springbank Fault is a blind structure expressed topographically as a fold developed at the fault tip, computer modelling was used to reproduce the characteristics of such a fold and simulate the most probable character of the underlying structure.

The computer software developed by Allmendinger (1998, 2003) is used to determine Springbank Fault parameters such as the fault slip, tip propagation, and fault geometry by using inverse modelling of the geometry of its associated fold. These parameters are constrained by the near-surface characteristics determined from the geophysical surveys.

1.7.7 EMPIRICAL EQUATIONS

Due to the blind nature of the Springbank Fault and to the lack of historical and instrumental information related to large earthquakes produced by the fault, the estimation of the earthquake magnitude that the structure is capable of producing cannot be directly determined. The estimation of earthquake magnitudes is a parameter necessary in seismic hazard analysis; consequently, empirical equations relating fault parameters such as subsurface rupture length or rupture area with earthquake magnitudes are used in this study.

Additionally, recent updated empirical attenuation relationships are used to estimate ground motion distribution in different urban centres in the near-fault zone of the Springbank Fault in the case of an earthquake produced by the structure.

Chapter 2
GEOMORPHOLOGIC EXPRESSION OF THE SPRINGBANK FAULT

2.1 INTRODUCTION

The Springbank Fault is a blind structure whose best surface expression is a fold developed at the fault tip close to the surface. The fault does not rupture the surface and its associated fold is not topographically observable along the whole length of the structure. Consequently, the total extent of the fault is not evident from its geomorphologic expression.

In order to determine the location and extent of the Springbank Fault, a combination of conventional geomorphologic mapping with other techniques that include GPS surveys, and morphometric analyses along rivers was necessary.

This chapter describes the location and further extension of the Springbank Fault based on the evident and subtle geomorphological expression of the structure determined from conventional mapping, GPS surveys and drainage morphometric examinations.

The chapter includes:

- The combined results of the geomorphologic mapping and GPS surveys (see Figure 2.1 for GPS survey locations) along the topographical expression of the Springbank Fault
- The results of the morphometric analyses over the main river systems in the area, including, river longitudinal profiles, gradient index and sinuosity analyses, and
- The proposed location and extension of the Springbank Fault and other structures based on those analyses.

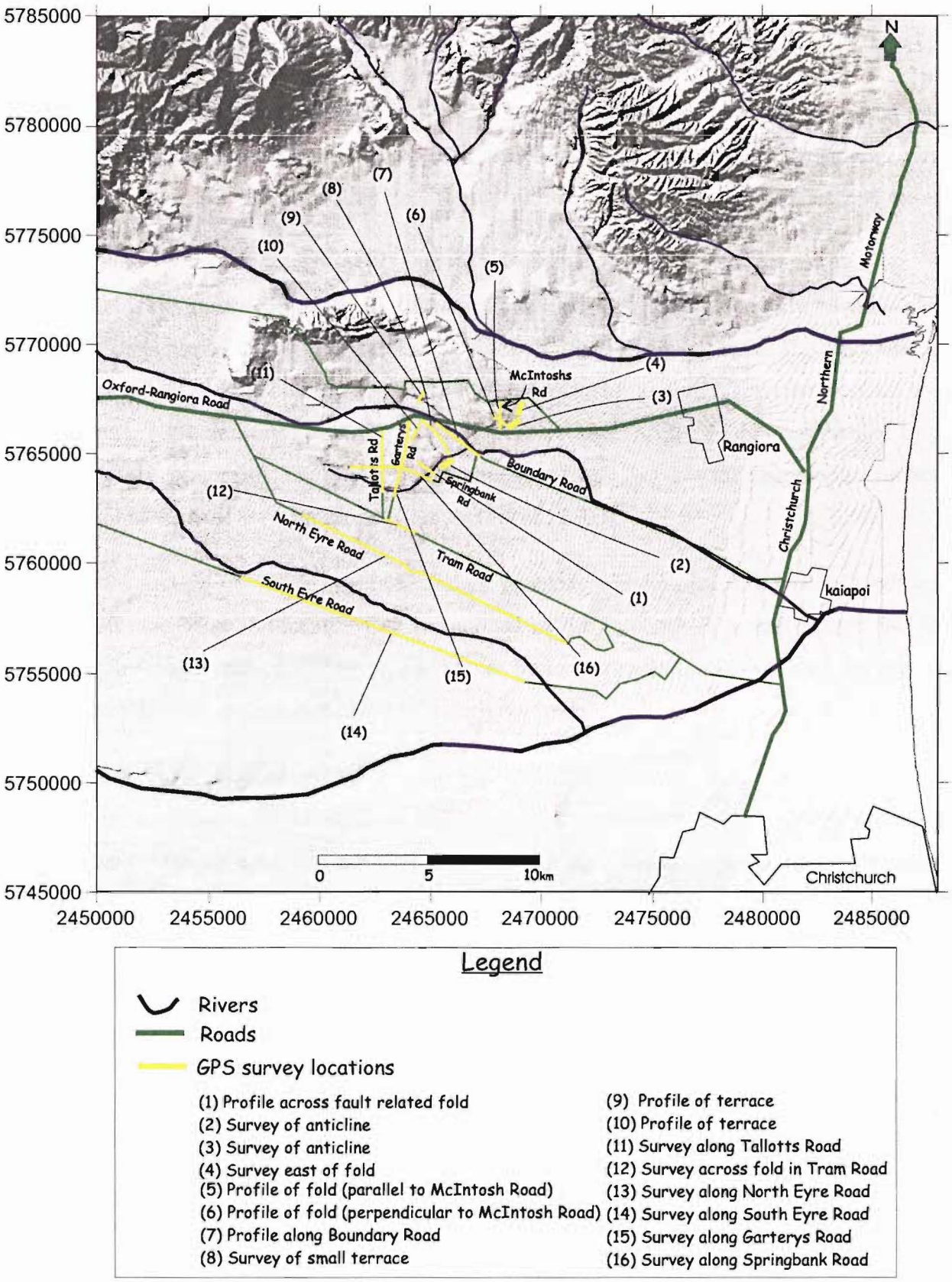

Figure 2.1: GPS survey locations within the study area.

2.2 TOPOGRAPHIC EXPRESSION OF THE SPRINGBANK FAULT

The tectonic deformation accommodated by the Springbank Fault includes an associated fold topographically expressed as: (i) an uplifted anticlinal; (ii) changes in river patterns; (iii) lineaments, and (iv) minor related landforms and deformation along terraces and other geomorphic surfaces.

The strata overlying the tip of the Springbank Fault closest to the surface have been broadly folded in response to the reverse movement along the fault plane at depth. The fault fails to reach the surface and the best expression of its fault-related fold occurs between the Cust and Eyre Rivers, close to Springbank (Figure 1.4). At this location, the fold is represented by a higher surface previously interpreted as a remnant of a higher glacial aggradation surface preserved between the river channels (Campbell et al., 2000).

The eastern margin of the surface is a straight northeast-trending broadly convex landform (Figure 2.2 and Map 1) that was first recognized as the forelimb of a fault-related fold in 1998, when seismic reflection surveys undertaken by Indo-Pacific Ltd showed that this curved surface was directly related to the folded underlying strata.

The differences in morphology between the eastern margin of the surface, where the forelimb of the fold is located, and the northern and southern margins, where degradational terracing truncate this elevated area, had not been recognized before the Indo-pacific seismic surveys (Campbell et al., 2000). The eastern margin corresponds to a broad flexure representing the fault-related fold deforming the broad fluvial surfaces. In contrast, the northern and southern margins comprise the typical, steep geomorphology of degradational terraces cutting into these relict uplifted surfaces (Figure 2.3).

Within this elevated area corresponding to the Springbank Fault-related fold, two different geomorphic units, the Cust and Springbank Units (Figure 2.4; Map 1) were recognized during this study. The separation between units was based on lithological and geomorphologic differences related to elevation, degree of incision, drainage features and loess cover.

The Cust Unit is a moderately to highly dissected surface attaining the maximum elevations. The Springbank Unit corresponds to a much less dissected unit with lower elevations. Both surfaces exhibit linear ridges trending approximately N45°W, but they are more evident in the Cust Unit (Figure 2.4; Map 1).

Figure 2.2: Broad convex landform located at the eastern margin of the elevated area. The landform is the topographical expression of the Springbank Fault-related fold forelimb. Yellow arrows illustrate the top of the fold and white arrows the curvature. (Photograph location grid reference NZMS 260 M35 652 641).

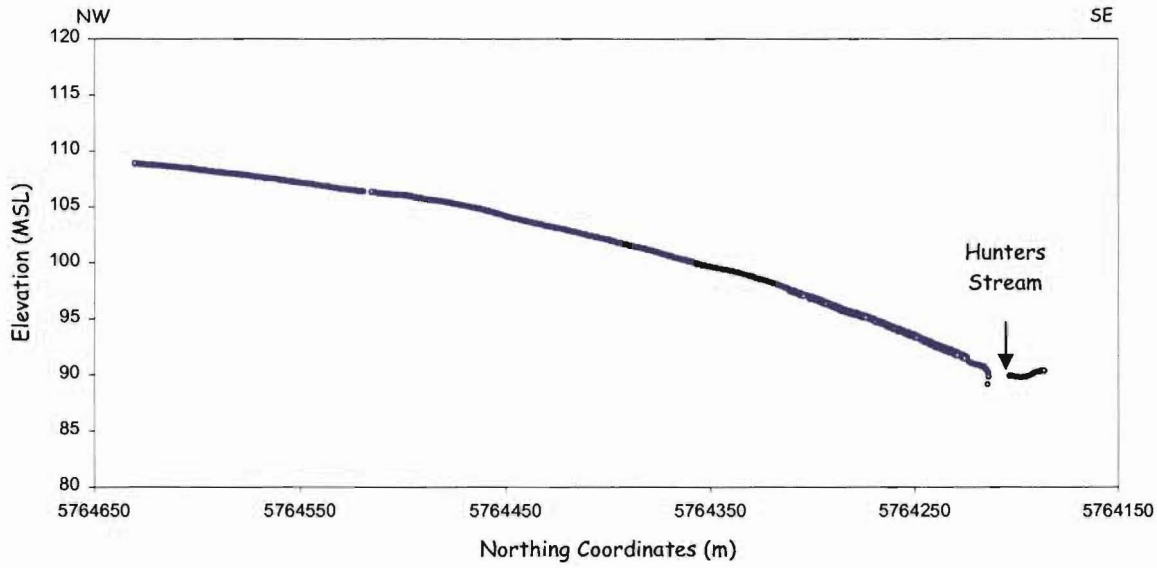

(A)

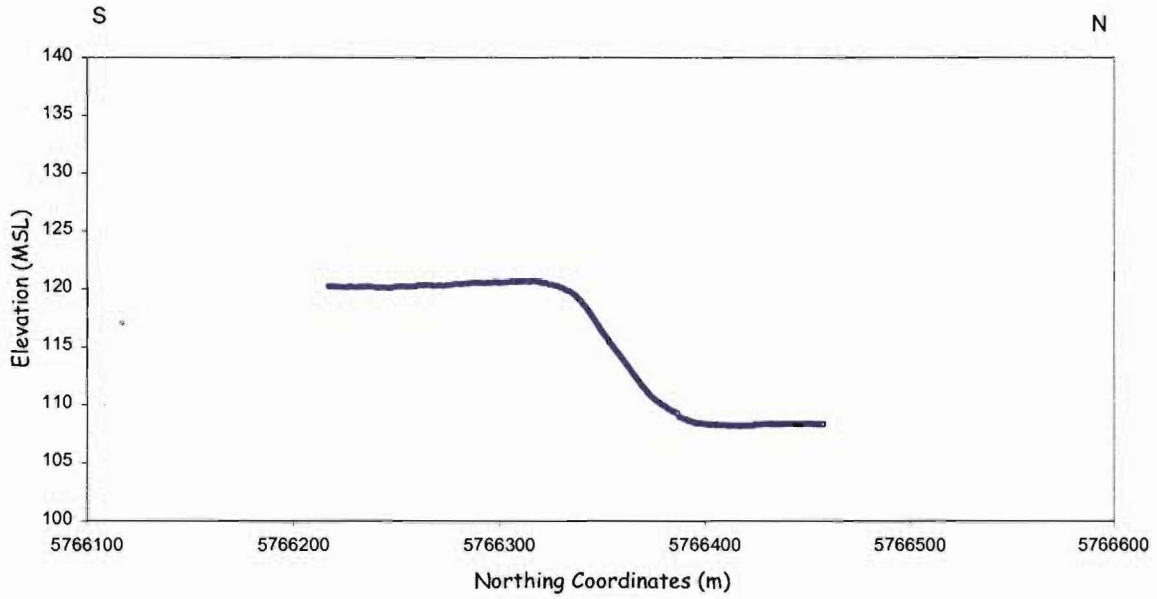

(B)

Figure 2.3: Topographic profiles (surveyed using carrier-phase in differential GPS) across the eastern and northern margins of the Springbank Fault-related fold (GPS surveys (1) and (10) in Figure 2.1). Both profiles are illustrated in the same scale (vertical exaggeration x 6). Profile (A) corresponds to the eastern margin and shows a broad flexure representing the forelimb of the fold. Profile (B) was carried out in the northern margin and comprises the typical geomorphology of a degradational terrace.

The Cust Unit also presents a distinctive "dune topography" that is not observable in the Springbank Unit (Figure 2.4). Within this dune topography, former river channels that have been affected by the fold evolution are expressed as semi-parallel linear ridges. These ridges are not substantial in the Springbank Unit. In contrast, this unit is less dissected and presents significant incision only in the terrace located along the northern margin of the elevated area. The southern terrace, within the Cust Unit, does not present significant incision (Figure 2.4; Map 1)

There are also lithological differences within the gravel deposits comprising each unit. The gravels comprising the Cust Unit are more weathered than those in the Springbank Unit. Unfortunately, these units have not been directly dated and there is not unanimity about their age. Gregg (1964) classified the gravels at Cust as Woodland Formation (150,000 years) and those in Springbank as Burnham Formation (25,000-18,000 years). Wilson (1989) has considered the gravels in the Cust Unit to be Woodland Formation but those in the Springbank Unit to be Windwhistle Formation (70,000-56,000 years). Moreover, Tonkin (*Personal communication*, 2003) considers the gravels of the Springbank Unit to be older than the Burnham Formation. It was not possible to establish the age of the gravels during this study. An attempt to assign them ages is based on the age of the loess cover overlying the Springbank Fault-related fold.

Berger et al. (2001) used luminescence chronology in a 6 m thick sequence of loess-paleosol cover over the Cust unit (Map 1). They dated three samples at this location: the base of a loess-paleosol unit (L3) at the bottom of the sequence, the base of a loess paleosol unit (L2) in the middle, and the base of a loess paleosol unit (L1) at the top of the sequence. The resulting ages were 73±13 ka, 41±5 ka and 27±3 ka, respectively.

Tonkin (*Personal communication*, 2003), in a preliminary interpretation of the stratigraphy of the loess cover across the Cust and Springbank units (along Chapmans-Boundary-Garterys Road; Figure 2.5 and Map 1), indicated that the top of the gravels is at about the same level, and that the difference in geomorphological characteristics between units is directly related to the loess cover.

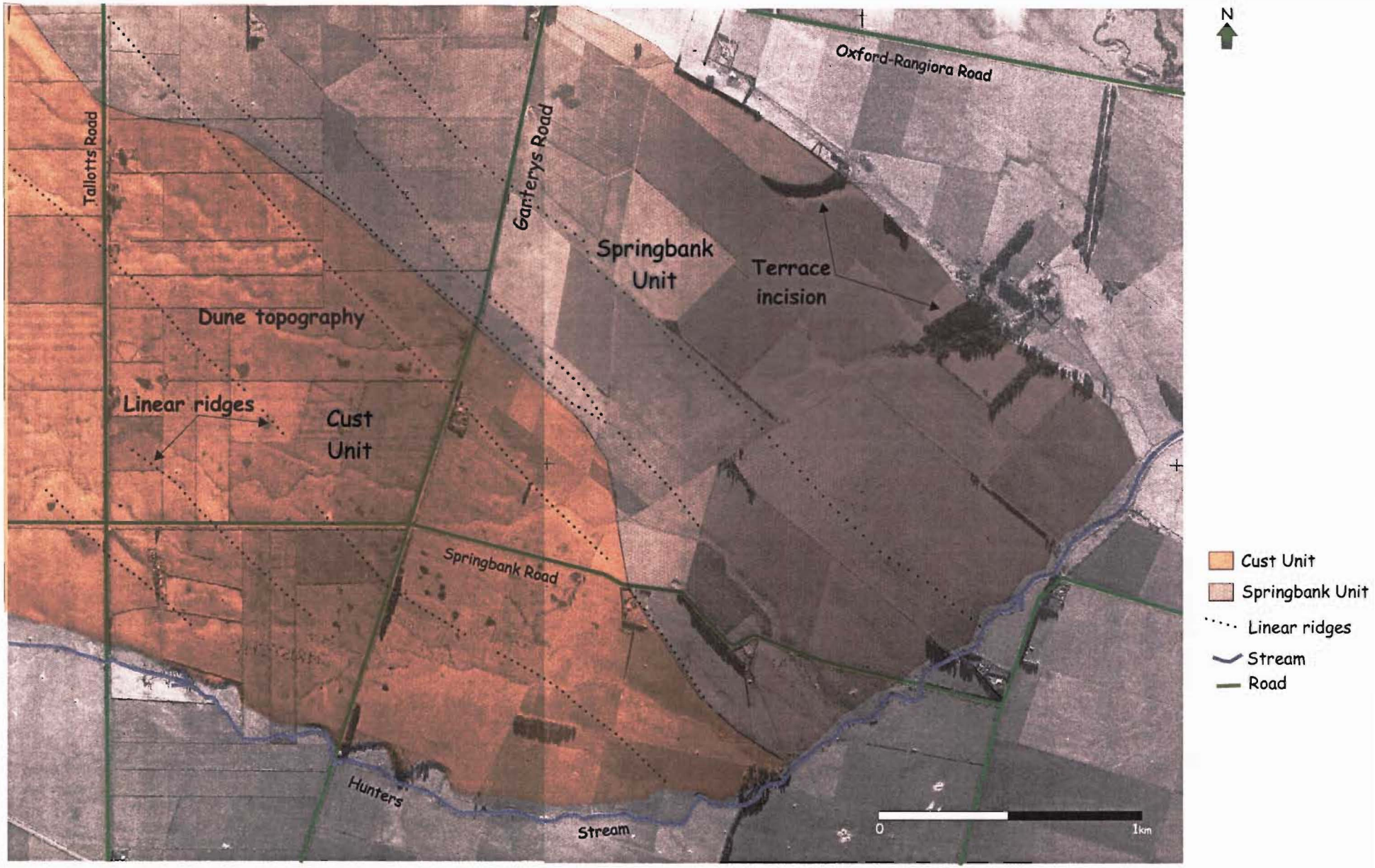

Figure 2.4: Air photograph of the elevated area associated with the Springbank Fault-related fold. Lithological and geomorpological differences within the area allowed its subdivision into two geomorphological units: the Cust and Springbank Units. The Cust Unit presents a highly dissected "dune topography". The Springbank Unit corresponds to a much less dissected unit with lower elevations. See text for discussion.

According to this preliminary interpretation, the Cust Unit is covered by the loess units L1, L2 and L3, and the Springbank Unit is covered by the loess units L2 and L3 (Figure 2.5). Therefore, the gravels underlying the Cust Unit must be older than 73,000 years, and the gravels under the Springbank Unit must be older than at least 41,000 years.

A possible geomorphological evolution of the area that represents the best expression of the Springbank Fault is provided in the following section. The evolution is based on the present-day drainage distribution, the geomorphic characteristics of the elevated area, and the ages of the loess cover.

2.2.1 EVOLUTION INTERPRETATION

Currently, the Cust River is flowing with a south-easterly direction between the elevated area constituted by the Cust and Springbank Units, and another elevated aggradation surface immediately to the north (Mairaki Unit in Map 1). At the northern margin of the Mairaki Unit, the Ashley River is flowing with east-southeast direction (Figure 2.6).

The Hunters stream is draining toward the southeast, in the southern margin of the Cust Unit (Map 1) but changes its direction to northeast to continue flowing in front of the elevated surface that represents the maximum expression of the Springbank Fault (Figure 2.6 and Map 1). Finally, the Eyre River is flowing toward the souteast, at the south of the area (Figure 2.6)

2.2.1.1 Possible Geomorphic Evolution

1. It is likely that before the deformation caused by the Springbank Fault, gravels older than 73 ka would have been part of a broad, braided outwash plain across which channels migrated (stage 1 in Figure 2.7). As uplift of this surface commenced the channels migrated to the north and south with respect to the axis of the uplifted zone. The channels that migrated to the north allowed the deposition of L3 (the loess paleosol unit dated 73±13 ka). The progressive river migration to the north incised and abandoned several channels represented today by the linear ridges mainly observed in the Cust Unit. Uplift and channel migration caused incision (trenching) along the northern margin of the elevated surface (new aggradation material would fill these trenches).

At this point, the Cust Anticline was in the first stages of development.

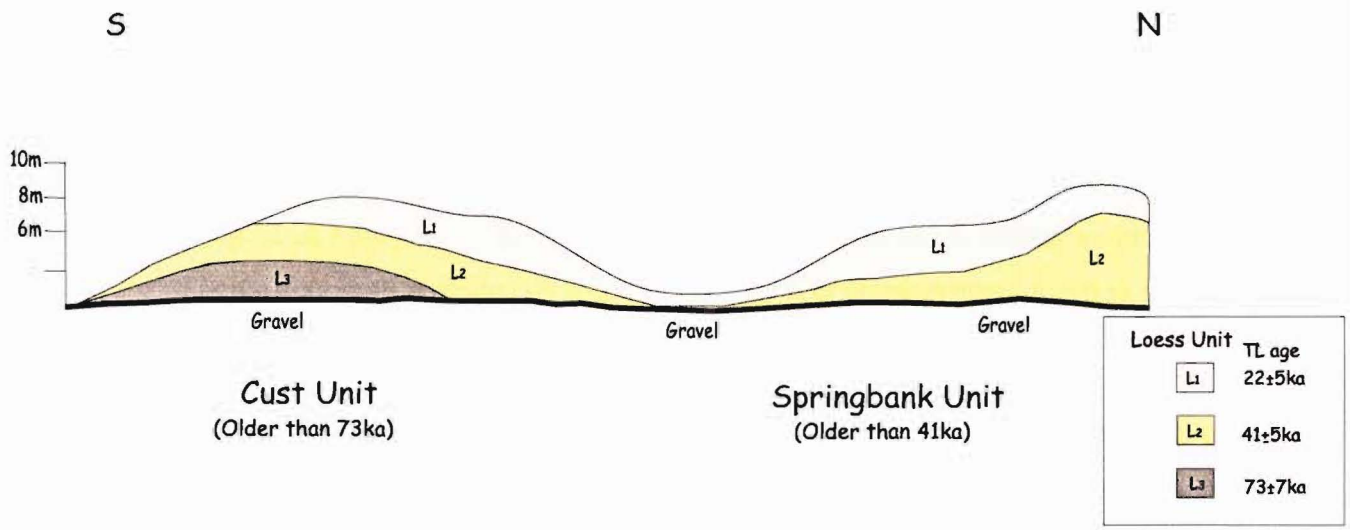

Figure 2.5: Preliminary stratigraphic interpretation of loess cover along Chapman-Boundary-Garterys Road (Tonkin, *personal communication*, 2003). Gravels assigned to the Cust Unit are covered by loess paleosol units L1, L2 and L3. Gravel constituting the Springbank Unit are covered by loess paleosol units L1 and L2.

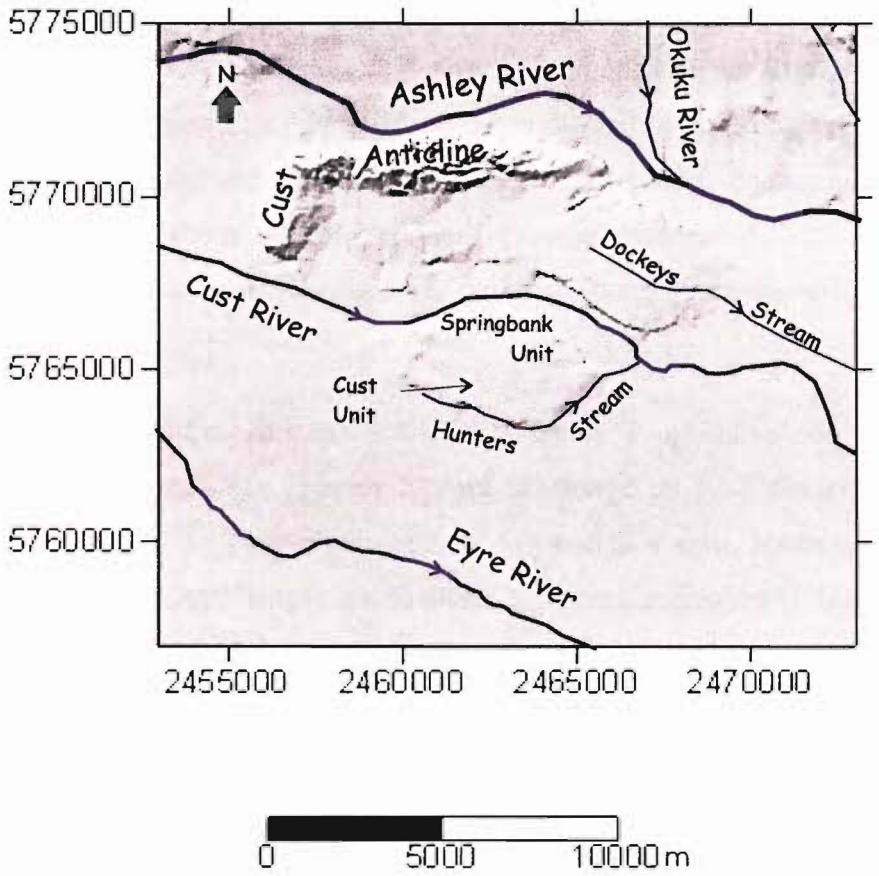

Figure 2.6: Current drainage distribution surrounding the elevated area formed by the Cust and Springbank Units.

2. A new aggradation cycle takes place and gravels older than 41 ka (the Springbank Unit) are deposited on areas not uplifted and in the trenches caused by river incision (stage 2 in Figure 2.7). River incision and progressive uplift related to the Springbank Fault affect both surfaces. A former Ashley River channel starts incision into the new aggadation surface (Figure 2.7)

3. L2 (the loess paleosol unit dated 41±5 ka) was probably deposited as a channel became confined within the crest of the fold and the new aggradation surface (stage 3 in Figure 2.7). The content of L2 is distinctive and thought to be locally derived from an adjacent river bed (Tonkin, *Personal communication*, 2003).

4. The Cust Anticline growth diverts the Ashley River toward its northern flank (Cowan, 1992) which corresponds to its present-day location. Progressive uplift associated with the Springbank Fault causes the confined river to abandon its channel and shift into the valley previously occupied by the ancestral Ashley River, immediately to the north (Cowan, 1992). Currently, this river corresponds to the Cust River. The Cust River migration related to this uplift is also indicated by swampy areas (Stage 4 in Figure 2.7). The progressive uplift also causes continuous river migration to the south. The widespread cover of L3 (the loess paleosol unit dated 27±3 ka) post-dates active antecedent channels, leaving only the minor consequent drainage now incised into the elevated surfaces.

5. Younger fluvial deposits cover the plains. Progressive fold growth toward the northeast forces the Hunters Stream to change its flow direction from southeast to northeast at the southern margin of the elevated area, south to the Cust Unit. The Hunters Stream changes its direction to continue flowing in front of the Springbank Fault-related fold forelimb. Progressive fold growth toward the northeast causes incision of the Dockeys Stream, in the Mairaki Unit. Progressive fold growth toward the southwest deflects the Eyre River (stage 5 in Figure 2.7).

Therefore, for practical purposes, the gravels comprising the Cust and Springbank Units are assigned ages of 75,000 and 45,000 years, respectively.

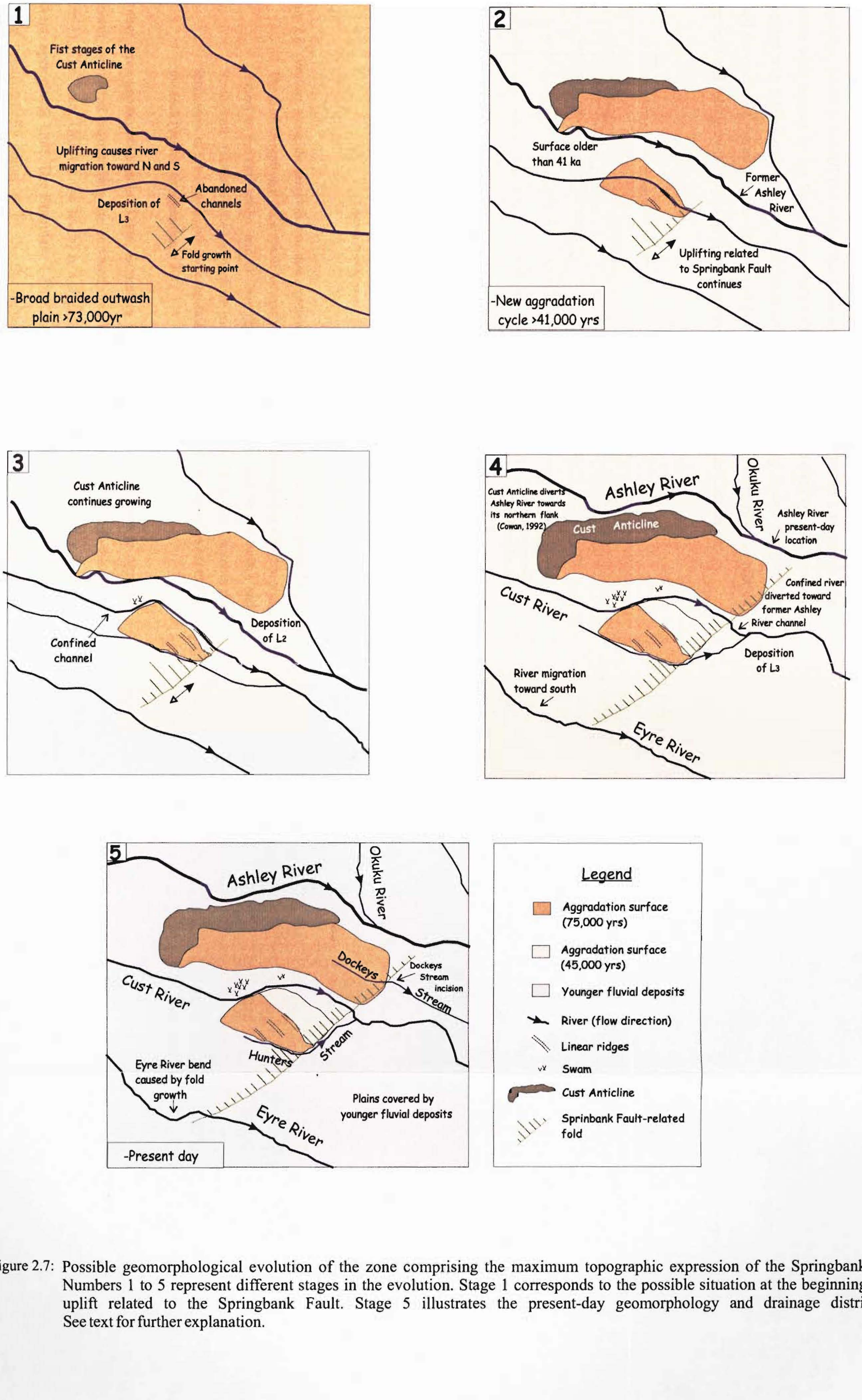

Figure 2.7: Possible geomorphological evolution of the zone comprising the maximum topographic expression of the Springbank Fault. Numbers 1 to 5 represent different stages in the evolution. Stage 1 corresponds to the possible situation at the beginning of the uplift related to the Springbank Fault. Stage 5 illustrates the present-day geomorphology and drainage distribution. See text for further explanation.

The topographic gradient of the elevated surface formed by the Cust and Springbank Units presents an inclination toward both the southeast and northeast. Figure 2.8 illustrates GPS topographic profiles carried out along the Cust and Springbank Units, in a perpendicular direction with respect to the Springbank Fault strike. The gradient toward the southeast is associated with folding and with the natural inclination of the Canterbury Plains. The gradient toward the northeast, parallel to the direction of the Springbank Fault, is interpreted as related to the fault and fold growth toward the northeast (this will be discussed in Chapter 4).

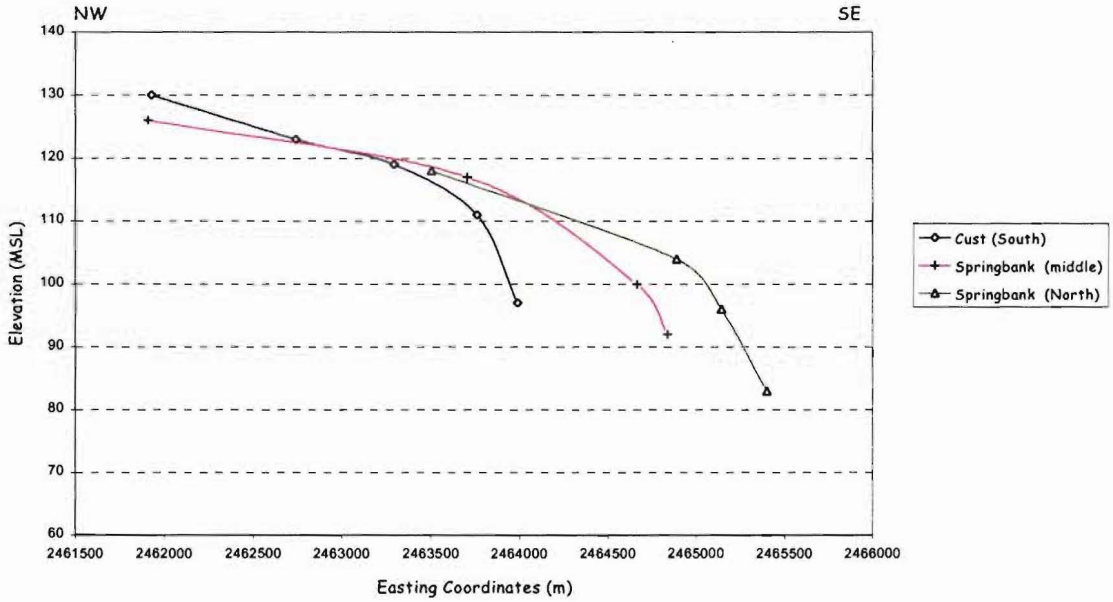

Figure 2.8: Profiles along the elevated area that represents the best expression of the Springbank Fault. The profiles represent the slope of the area in the approximately perpendicular direction with respect to the fault strike, and in three different localities: Cust unit (to the south), and Springbank (at the middle and northern part of the surface). The figure also illustrates the inclination of the fold to both the southeast and to the northeast in the direction parallel to the fault (vertical exaggeration x 37).

Another three geomorphic units (Tram, Boundary 1, and Boundary 2 Units) were recognized at lower elevations surrounding the elevated area formed by the Cust and Springbank Units (Map 1). The Tram Unit (to the south) is a slightly dissected aggradational surface younger than the Springbank Unit. The Boundary 1 Unit corresponds to a small terrace (to the north) that has been partially deformed by the Springbank Fault, and the Boundary 2 Unit is the youngest surface related to recent fluvial processes (Map 1). This surface is considered by Tonkin (*Personal communication*, 2003) to be of Holocene age.

GPS surveys along the Boundary 1 and 2 Units indicate that they are affected by deformation associated with the Springbank Fault. Figure 2.9 illustrates a digital elevation model of the terrace comprising the Boundary 1 Unit. The terrace is orientated approximately perpendicular to the fault direction and is warped, indicating tectonic deformation. Figure 2.10 shows the GPS topographic profile for the Boundary 2 Unit. The profile shows an inclination to the southeast that is stronger than the natural inclination of the Canterbury Plains, which suggests that it is also related to tectonic deformation associated with the Springbank Fault. The profile also presents a slight convexity possibly associated with folding.

The topographic fold expression progressively disappears to the north and south (Map 1). North of the Cust River, the fold is also expressed in another higher surface of aggradation (Mairaki Unit), but its manifestation is not as remarkable as it is immediately to the south (Figure 2.11). There is no topographic expression further to the north, at the Ashley River.

To the south of Springbank, the last clear superficial evidence of the Springbank Fault-related fold occurs at the Tram Road (Figure 2.12). At this road, the fold, however subtle, can still be observed (Figure 2.12).

South of the Tram Road, a very slight flexure is observed along the North Eyre Road (Figure 2.1). Code-phase GPS surveys were undertaken along the road but they did not confirm the flexure. This, however, could be related to the lower accuracy of the code-phase surveys.

If this flexure is an expression of the Springbank Fault south of the Tram Road, it would reflect its southern-most expression, and it would indicate a change in fault strike direction as well. This flexure is situated to the west of the expected southern projection of strike of the fault before this study (according to the GIS database of the Department of Geological Sciences, University of Canterbury).

In addition to the major Springbank Fault-related anticline, there are other minor topographic features that include minor anticlines and lineations. Two minor anticlines were surveyed east of the main fold (Figures 2.13 and 2.14, and Map 1), one south of the Cust River, and another on its north flank. The anticlines are small and have slightly different orientations. These minor anticlines seem to be directly associated with the folding process because their orientation is very similar to the projected orientation of the Springbank Fault to the surface.

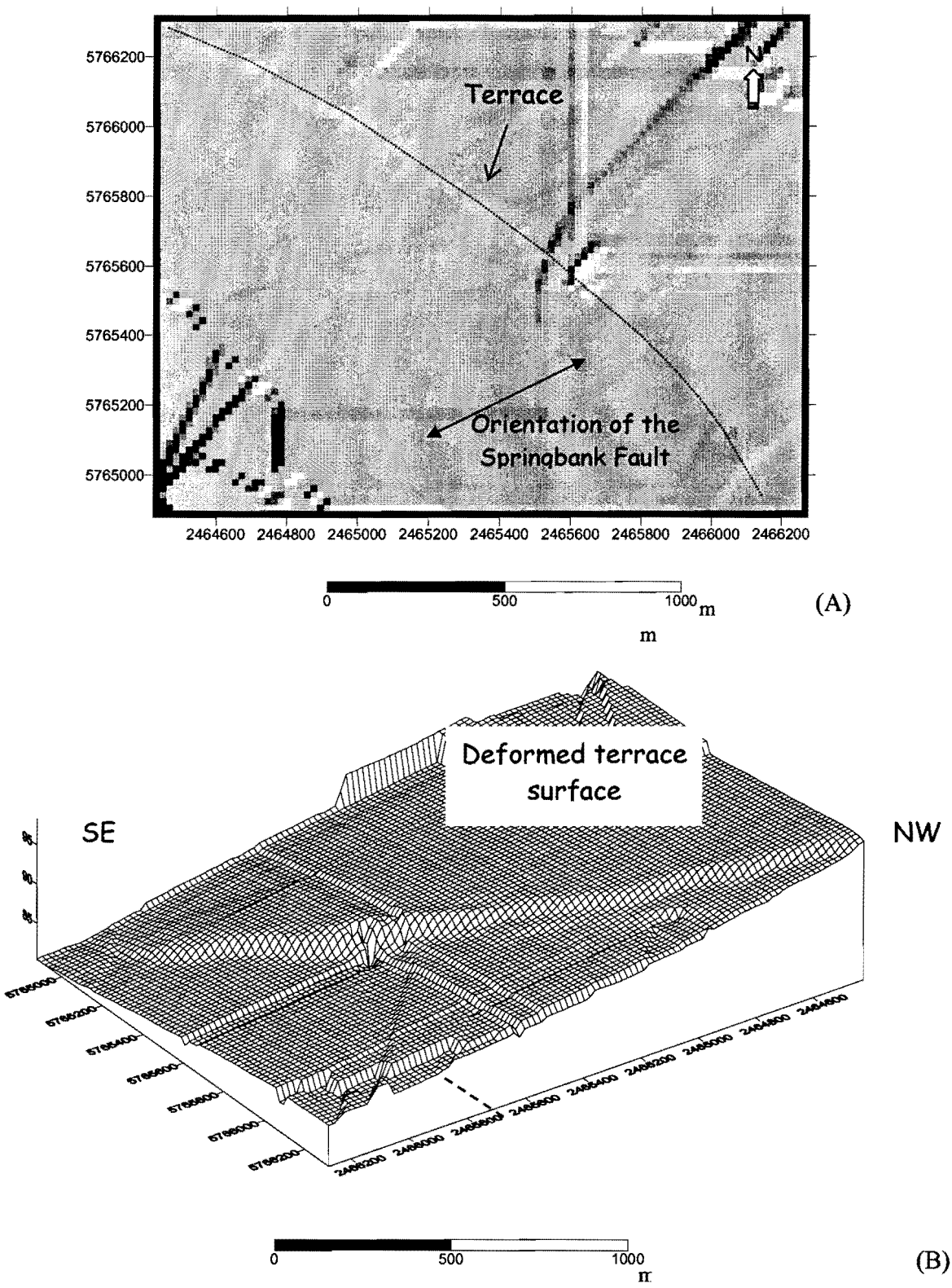

Figure 2.9: (A) Digital elevation model of GPS survey data showing the orientation of the terrace (Boundary 1 Unit) with respect to the schematic trend of the Springbank Fault (GPS survey (8) in Figure 2.1). (B) 3D model of schematic location of the Springbank Fault (dashed line) with respect to the terrace. The terrace surface is deformed by the fault.

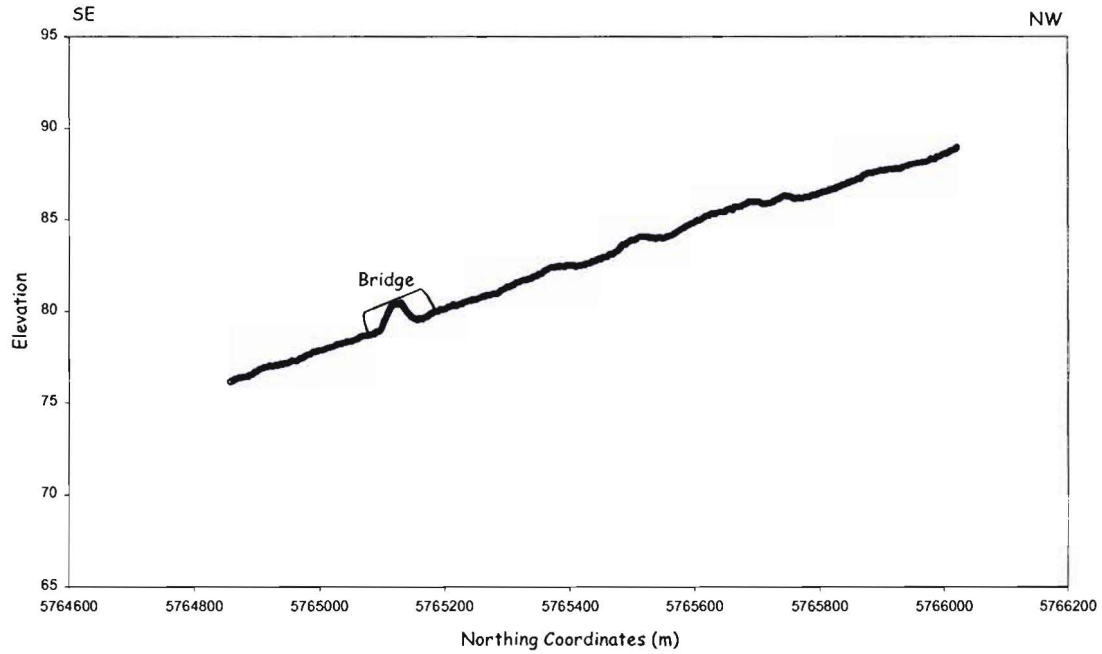

Figure 2.10: GPS survey along the Boundary 2 Unit (GPS survey (7) in Figure 2.1) showing the inclination, presumably affected by deformation produced by the Springbank Fault (vertical exaggeration x 30).

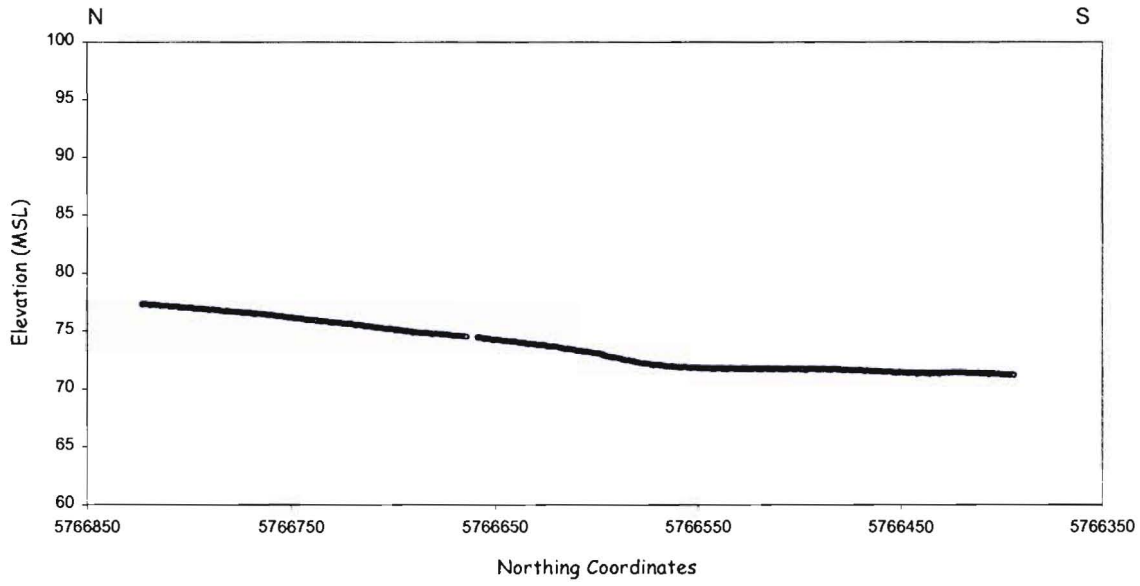

Figure 2.11: GPS profile across the fold expression between the Cust and Ashley Rivers in the Mairaki Unit (GPS survey (5) in Figure 2.1).

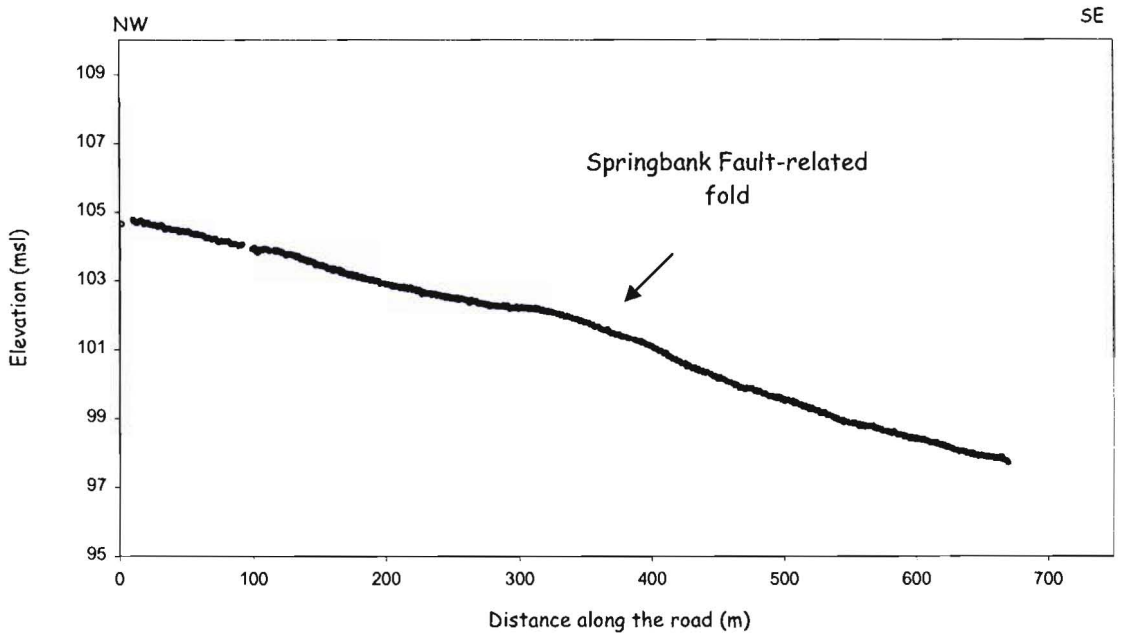

Figure 2.12: Differential GPS profile along the Tram Road (GPS survey (12) in Figure 2.1) showing a broad flexure related to the Springbank Fault-related fold. This corresponds to the southern-most clear surface expression of the fault (vertical exaggeration x 30).

The continuation of the Springbank Fault, north of the Ashley River and south of the Tram Road, is uncertain, at least from its topographic expression. The trend of the fault suggests that it may cross the Ashley River and then join to the Ashley Fault, on the northern flank of the river (Figure 1.6), but there is no superficial expression related to this interaction.

There are some photogeological lineaments to the northeast of the Ashley Fault, which have a similar trend to the Springbank Fault and suggest that they could be the expression of the fault to the northeast. There are several possibilities related to the continuation of the Springbank Fault to the north of the Ashley River, including:

(1) The Springbank Fault may cross the Ashley River and join the Ashley Fault in a complex interaction, to continue to the northeast with a slight change in direction. The expression of this could be represented by the photogeological lineaments observed to the northeast of the study area.

(2) The Springbank Fault may die out at, or before the junction with the Ashley Fault. This is suggested by the progressive decrease in the associated fold expression towards the Ashley River, and the lack of expression of the Springbank Fault close to the Ashley Fault.

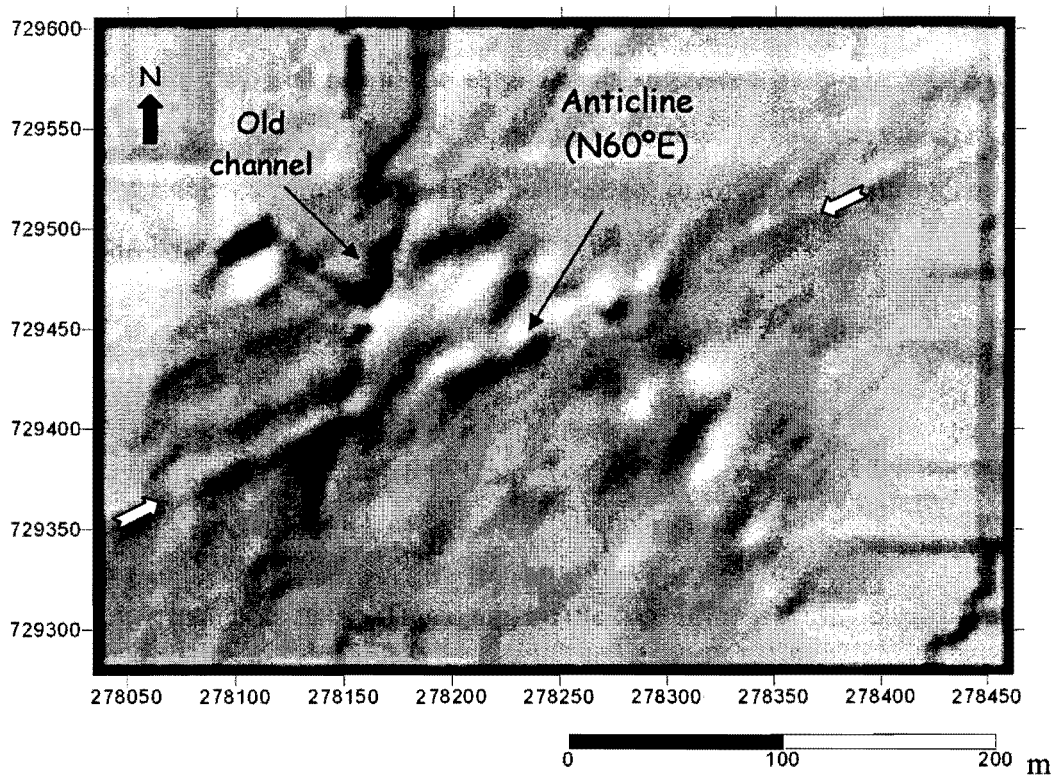

Figure 2.13: Digital elevation model of GPS data (GPS survey (2) in Figure 2.1) of a small anticline located to the east of the Springbank Fault-related fold. White arrows indicate anticline orientation.

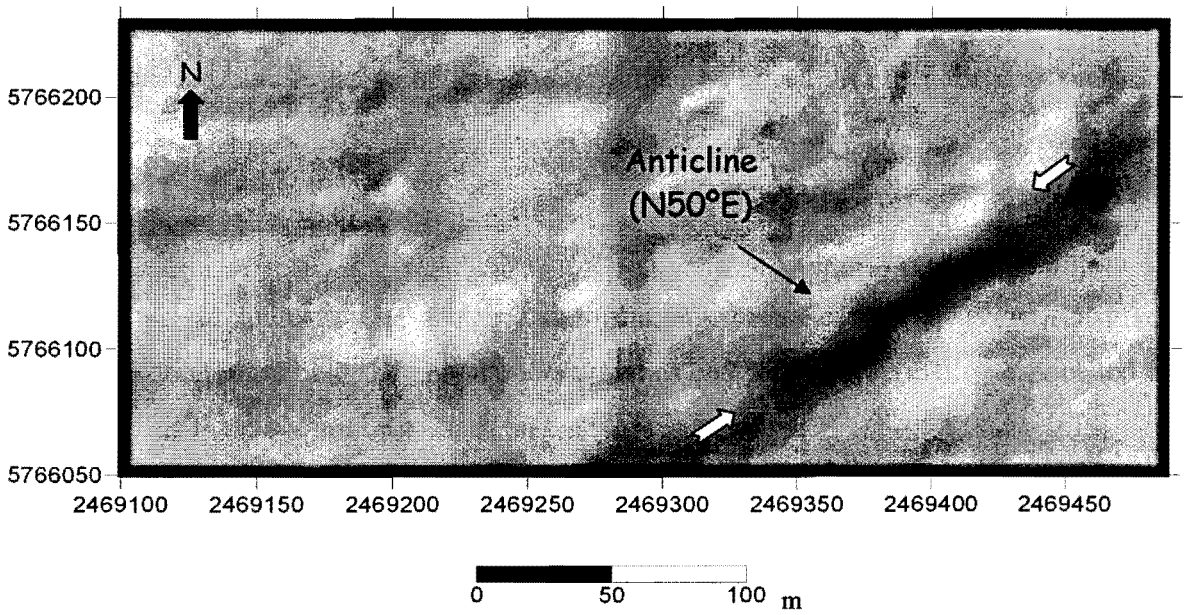

Figure 2.14: Digital elevation model of GPS data (GPS survey (3) in Figure 2.1) of a small anticline located to the east of the Springbank Fault-related fold and to the northeast of the anticline in the previous figure. White arrows indicate anticline orientation.

(3) The Springbank Fault may die out at or before joining with the Ashley Fault, and another segment of the fault may step out to the east. This is suggested by the lack of expression of the fault towards the Ashley Fault, by the topographic features (small anticlines) located to the east of the fault associated fold, and also by the presence of another structure identified on the basis of the morphometric analysis along the rivers (see below).

There are also several possibilities related to the continuation of the Springbank Fault to the south:

(1) The fault may die out south of the Tram Road. This is suggested by the lack of clear topographic expression south of the road.

(2) The fault may change its strike. This could be the case if the flexure observed on the North Eyre Road is directly related to the Springbank Fault.

(3) The Springbank Fault may correspond to a fault zone consisting of several segments with slightly different orientations. Consequently, expressions of fault strands may occur to the west or to the east from the projected location of the Springbank Fault.

The analysis of the topographic expression alone is not enough to conclude which one of the above possibilities is correct. To determine the further location and extent of the Springbank Fault, the surface manifestation of the structure must be based on other features such as the river system.

2.3 DRAINAGE ANALYSIS

Rivers are useful indicators of tectonic deformations because they are very sensitive to changes in channel gradient. Drainage characteristics can reflect deformation associated with faults and folds that may not be evident on the surface.

River channel characteristics may depend on many factors, including: (1) lithological characteristics of the river bed, (2) sediment load, (3) climate, (4) entrance of tributaries, (6) stream power, (7) regional slope, (5) local topography and (6) human activity, among others.

When anomalous changes in the drainage characteristics cannot be explained from changes in the above factors, the river may show evidence of ongoing tectonism (Jackson et al., 1996; Burbank and Anderson, 2001; Schumm, 1986; Schumm et al., 2000; Guccione et al., 2002).

The type of response to tectonic deformation will depend on the type of river and on the characteristics of the tectonic movement (Ouchi, 1985; Schumm, 1986; Schumm et al., 2000). It is not possible to predict consistently the pattern and the channel changes because different types of rivers will respond differently (Schumm, 1986)

Alluvial rivers, those that flow through sediments that have been eroded and deposited by the river (Schumm et al., 2000), have been classified into different channel patterns, including: (i) straight, (ii) sinuous, (iii) braided, and (iv) combinations of these (Schumm, 1986; Figure 2.15). There are also other patterns composed by multiple channels, that are termed anastomosing, anostomosed, or anabranch channels (Schumm, 1986).

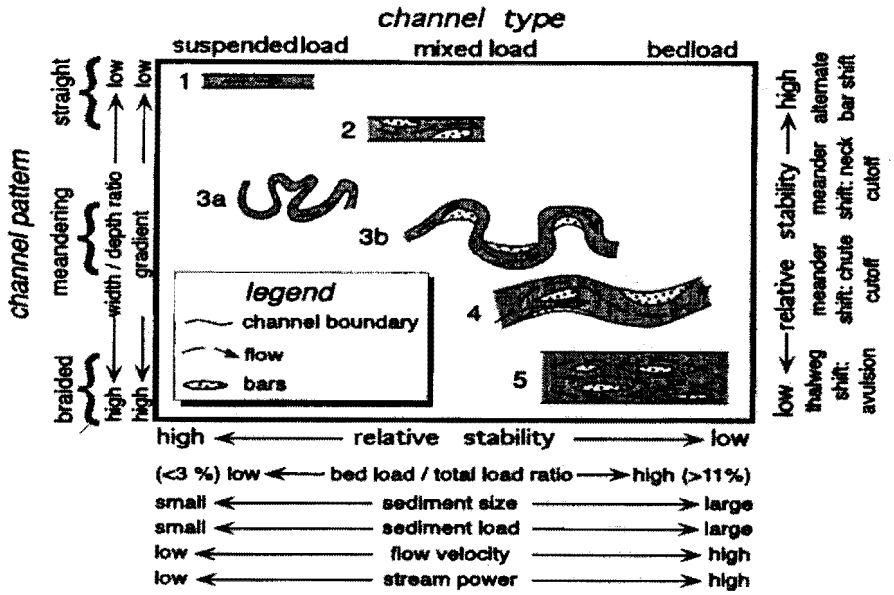

Figure 2.15: Classification of alluvial rivers. The different channel patterns (straight, braided and meandering) are the result of different factors such as nature of sediment load, velocity, stream power and slope gradient (after Schumm, 1996).

Studies have shown that a change of valley-floor slope may cause changes in channel pattern (Schumm, 1986). In the case of changes of the valley-floor slope caused by tectonism, the response along the river will depend on the type of channel and on the characteristics of the movement (Ouchi, 1985; Schumm, 1986; Schumm et al., 2000).

If a river is crossing a vertical uplift caused by faulting or folding, the valley-floor slope will change before and after the uplifted zone. Before the axis of the uplift, the river bed slope will be reduced, and after the axis, the slope will be increased. These changes will disrupt the

normal equilibrium and will induce different responses by the river. The first response will be deformation in the river longitudinal profile along the uplifted zone. Knickpoints, convexities or concavities will develop (Schumm, 1986). Then, the river could be forced to change its characteristics. If the river does not have enough stream power to overpass the uplift it will change its direction. Alternatively, if the river has enough stream power, it will adjust to the slope changes (Schumm et al., 2001).

At the axis of the uplift, rivers will start incision in order to maintain a constant gradient. With incision (degradation), the sediment load increases, and this together with the change of slope may cause changes in the river pattern (Keller and Pinter, 1996). Therefore, changes in sinuosity on both the upstream and downstream side of the uplift axis or local narrowing or widening along the river channel can be used to infer adjustments of bedform to tectonic disturbances of the stream bed (Ouchi, 1985; Schumn, 1986; Campbell and Yousif, 1985; Litchfield, 1995; Schumm et al., 2000).

Ouchi (1985) showed that the main observable effects of superficial uplift across rivers are changes in their channel patterns, and induction of aggadation and degradation processes. According to his experiments, braided and sinuous channels have different behaviour (Table 2.1). Braided channels are unable to change their pattern as a result of uplifting. They respond with degradation and terrace formation in the central part of the uplift (Figure 2.16). The sediment produced by the incision will cause aggradation after the uplifted zone. Ouchi (1985) showed that the braiding tendency in the reach upstream from the uplift might be less than in the downstream reach. If the tilting is significant the channel may incise meanders on the upstream side. Multiple thalweg channels with submerged bars may form before the uplifted zone and a strongly braided stream may develop after the uplift.

Alternatively, Ouchi (1985) indicated that meandering channels respond with an increase in sinuosity on reaches with steepened slopes (downstream of the uplift axis). This may be accompanied by bank erosion and point-bar growth. On the upstream side of the uplift, a damming processe occurs, accompanied with deposition, and a tendency to establish multiple stable channels (anastomosing pattern). As a result, a swampy condition with deposition of fine material is expected (Figure 2.16). Adjustment of the meandering channel results in increased overbank flooding upstream of the anticline uplift and in an increase in sinuosity dowmstream (Jin, 1984 in Schumm, 1986).

Table 2.1: Response of experimental channels to uplift. Braided and meandering river behaviour before, at the centre and after uplifting (modified after Ouchi, 1985).

	Axis of Uplift		
Braided channel	Aggradation Frequent thalweg shift; submerged bars	Degradation Terraces	Aggradation Strongly braided; central bars
Meandering channel	"Flooded" Indistinct thalweg; multiple channels (Anastomosing pattern)		Sinuosity increase Bank erosion; point-bar growth

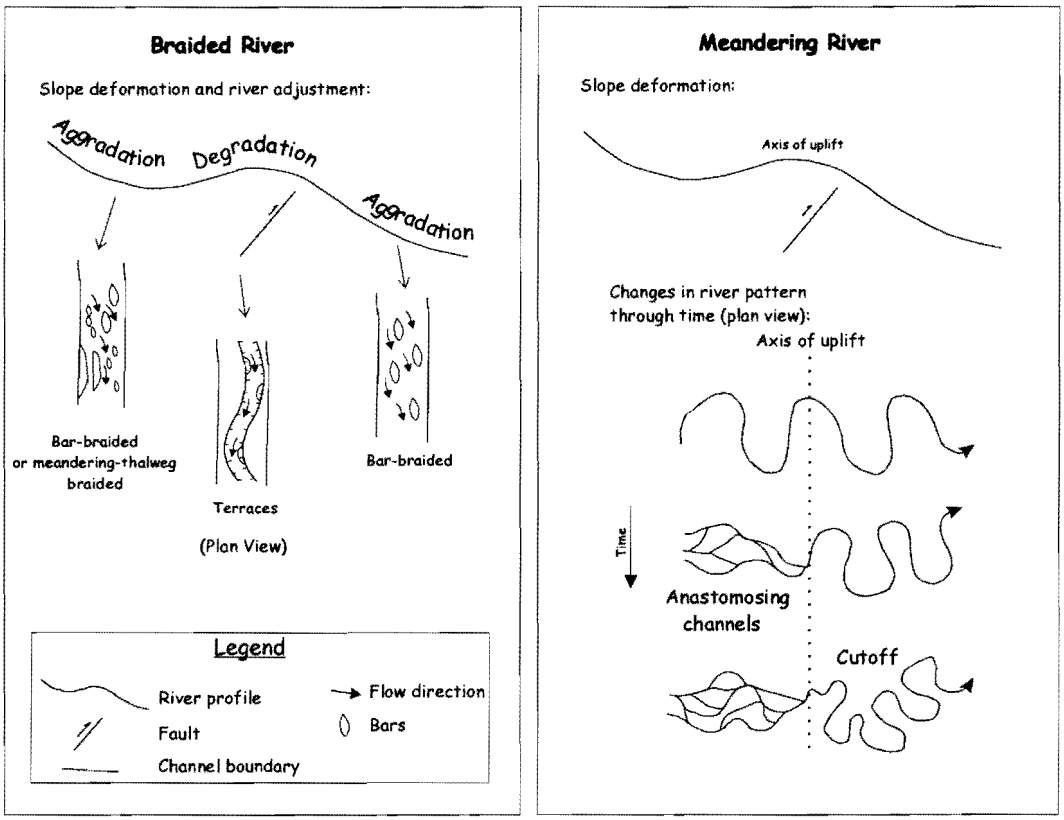

Figure 2.16: Schematic response of braided and meandering rivers to the growth of an anticline caused by inverse faulting. Left panel shows the deformation along the river profile and a plan view of a braided river response before, in the central part, and after the uplift. Right panel shows deformation along the river profile and a plan view of the response and evolution of a meandering river over time (modified after Ouchi, 1985).

In summary, river systems can indicate the presence of tectonic deformation across their channels. "Anomalies" on the river longitudinal profile, changes in channel direction, changes in sinuosity or channel bedform, and aggradation or degradation processes, suggest the presence of underlying structures that may not be obvious on the surface. Therefore, the river systems in the study area constitute a very useful tool to identify ongoing tectonism and they can be analyzed to reveal the location of the Springbank Fault across their channels.

In order to determine the location of the Springbank Fault where there is no evident topographic expression, different morphometric analyses along the rivers were undertaken. These analyses include river longitudinal profile analysis, and calculation of stream gradient index, and sinuosity index. The description of each analysis is given in the following section, together with the methodology followed for their measurement.

2.3.1 RIVER LONGITUDINAL PROFILES ANALYSIS AND STREAM-GRADIENT INDEX

Alluvial rivers develop a smoothly changing, concave longitudinal profile that is assumed to approximate a single exponential curve. Changes in this ideal smooth shape may reflect variations in the lithology of the river bed, or tectonic perturbations (Keller and Pinter, 1999; Schumm et al., 2000; Burbank and Anderson, 2001). Consequently, perturbations in river profile that are not related to lithologic contrast may be interpreted as responses to ongoing tectonism (Burbank and Anderson, 2001).

The river longitudinal profile can be directly plotted from topographic maps. The accumulated distance, from the source of the river, of straight lines between points at which the river crosses consecutive contours, is plotted against the contour elevations (Figure 2.17).

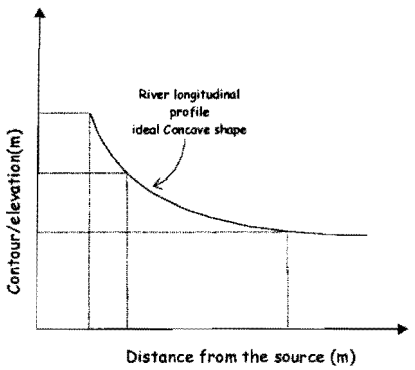

Figure 2.17: Schematic plot of a river longitudinal profile.

Perturbations along the river longitudinal profile can be observed directly from the plot as reaches with anomalous slopes that differ from the expected concave shape. Although these may be observed in the profile, a practical method for measuring and highlighting such perturbations is the stream-gradient index (Hack, 1973). The stream-gradient index (GI) is the product of the slope of a specific reach times the distance from the source of the river. In a homogeneous zone, the stream-gradient index will

remain approximately constant along the river length. Variations of the stream-gradient index reflect changes related to lithology, tectonism or other disturbances.

2.3.1.1 Calculation of Stream-Gradient index

Because the profile of a river is assumed to follow a characteristic exponential form, a mathematical relationship can be used to determine the "ideal" gradient for any reach of the river. This calculated value can be compared to the actual reach gradient in order to determine anomalous reaches. Figure 2.18 shows the parameters used to calculate the stream gradient index (GI).

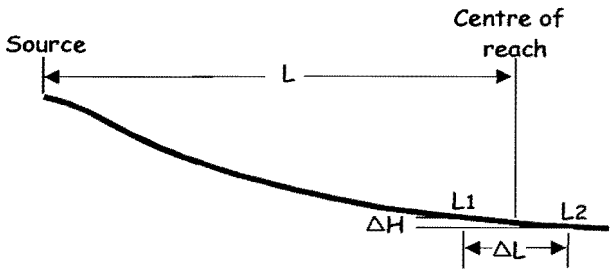

$$GI = \frac{\Delta H}{\Delta L} \times L \quad \text{or} \quad = \frac{\Delta H}{Ln(L_2) - Ln(L_1)}$$

Figure 2.18: Parameters used in calculation of gradient index. The parameters are explained in the text (re-drawn from Hack, 1973). ΔH is the difference in elevation between the ends of a reach, ΔL is the length of the reach, and L is the length measured from the source of the river to the middle of the reach.

For this study, the stream-gradient index is calculated following the methodology applied by Yousif (1987). GI is calculated for each reach between the points at which the stream crosses consecutive contours. This is made by direct measuring of the river length between contours (every 20m or 10m) using digitized maps in Autocad Map® and topographic maps.

GI of each reach is then compared to the gradient index (K) of the entire profile, defined by:

$$K = \frac{Hi - Hj}{Ln(Lj) - Ln(Li)}$$

Where Hi is the highest topographic contour crossed by the river and Hj is the elevation at the downstream limit of the river (the mouth, or if a tributary, at its junction with the next lowest stream). Lj and Li are the distances from the source of the river to its downstream limit and the highest topographic contour crossed by it, respectively.

Values in the ratio GI/K close to 1 indicate a profile close to the ideal shape. Very low (i.e GI/K<0.3) or high values (i.e GI/K>2) indicate reaches with gradients significantly different to those expected in the ideal profile. These reaches indicate perturbations that could be related to tectonism if other causes are eliminated.

2.3.2 SINUOSITY INDEX ANALYSIS

Sinuosity is the ratio between river length and thalweg length. In order to be consistent with the previously described analyses (river longitudinal profile and the stream gradient index), that are based on the reaches of the river between consecutive contours, the sinuosity index (SI) here is calculated as:

$$\mathbf{SI} = \frac{\text{The length of the river between consecutive contours (RL)}}{\text{The straight line distance between those consecutive contours (SL)}}$$

The length of the river between contours is measured on air photographs. The location at which the river crosses different contours is extracted from topographic maps and marked on the photographs, defining different reaches. The river at each reach is divided into straight line segments that approximately represent the river sinuosity.

Subsequently, the lengths of the straight segments that define each reach are added together. This corresponds to RL. Then, the distance of a straight line between the points at which the river crosses the consecutive contours is measured, and it constitutes SL. The sinuosity index (SI), the ratio between RL and SL, is then calculated for each reach.

The sinuosity analysis is represented as a two coordinate plot in which the SI values calculated for each reach are plotted on one axis, against the point at the mean distance between the contours in the other axis.

This process was carried out manually and several uncertainties were observed. There is an intrinsic error in measuring the sinuosity that depends of the scale used. The larger the scale and the track of the channel used to measured the sinuosity, the larger the length of the river at each reach. This results in different sinuosity values for the same river.

In practice, there are other difficulties measuring the sinuosity. For example if the river divides into different channels, the sinuosity of these channels within the same reach may be

different, and consequently the sinuosity index may vary depending on the channel used for its calculation. Consequently, braided or anastomosing rivers are excluded from the analyses.

Another uncertainty related to the application of the sinuosity concept is related to the dynamic nature of the rivers. The river sinuosity index measured on photographs taken in different years may show different values. Changes in sinuosity can be seen on photographs taken a few years apart. These changes do not represent tectonic adjustment but "instantaneous" changes related to other factors (i.e changes induced by flooding events). Therefore, the sinuosity values should be compared accross photographs of different periods to establish whether they are truly representative of the river characteristics.

Alternatively, the direct measurement of the channel width at different points along the river may resolve some of the above difficulties. Differences in channel width may be good indicators of changes in river sinuosity through time. The channel width at different places along the river is a straight line, whose length is not depending on the scale. The line is unique to each point along the river, therefore there is no uncertainty involved in choosing which line to measure. Finally, changes in channel width through time can be seen in air photographs and places where the channel is narrowing or widening can be detected and considered to be part of the analysis. These types of changes are important because they represent significant changes in sinuosity over time and may be evidence of ongoing tectonism. Consequently, river channel width examination at places where the river crosses different contours is included within the analysis of river sinuosity.

2.4 APPLICATION OF DRAINAGE MORPHOMETRIC ANALYSES

River longitudinal profile analysis, gradient index and sinuosity measurements were undertaken on the Cust, Eyre, Waimakariri, Ashley, Makekeri Rivers and Stony Creek (Figure 1.4). The analyses showed a direct relationship between the presence of different structures, including the Springbank Fault, and the examined river characteristics.

The locations along the channel where the river showed changes in its characteristics (i.e deformation along its longitudinal profile, changes in sinuosity or channel width, etc) were compared with geological maps and the information contained in the GIS database, to establish if geological structures or lithological changes had been previously determined at that particular location.

In most of the analyses there is a direct relationship between the river characteristics and the presence of a fault or fold. Variations in river characteristics related to lithological changes are not significant because, with some exceptions, most of the sections of the river relevant to this study flow over thick gravels of similar nature.

At most of the places where the river showed changes in the parameters analysed, a fault or fold has been previously mapped or inferred. In the other cases, no structures have been directly mapped at that location, but a prolongation of nearby mapped structures could explain the river characteristics at that point.

This confirmed the utility and validity of drainage analysis to detect underlying structures in the study area. The river characteristics can be used to establish the location of structures, such as the Springbank Fault that have not been mapped and are represented by only a very subtle surface expression.

The first river to be discussed is the Cust River because the location of the Springbank Fault, and its related fold, with respect to the river, is known from geomorphological mapping and especially from geophysical studies (next chapter). Therefore, the river behaviour at the place where it is flowing across the fold can be directly examined and the results can be extended to the other rivers in the study area to establish the direct effect of the Springbank Fault along their channels.

2.4.1 CUST RIVER ANALYSIS

Figure 2.19 contains the Cust River longitudinal profile together with the values of the ratio between the gradient index at each reach (GI) and the gradient index of the entire river (K). The high contrasting values in the GI/K ratio, measured for the different reaches along the river, closely correlates with mapped structures and previously recognized subsurface structures.

The known occurrence of the Springbank Fault and its propagation fold is manifested in the profile around the reach located between the 80m and the 70m contours (elevation), at ~26,000m from the source (Figure 2.19). At this point, the GI/K value changes from 2.9 to 4.2 reflecting the steep gradient developed by the river after crossing the fold on the hanging wall of the Springbank Fault.

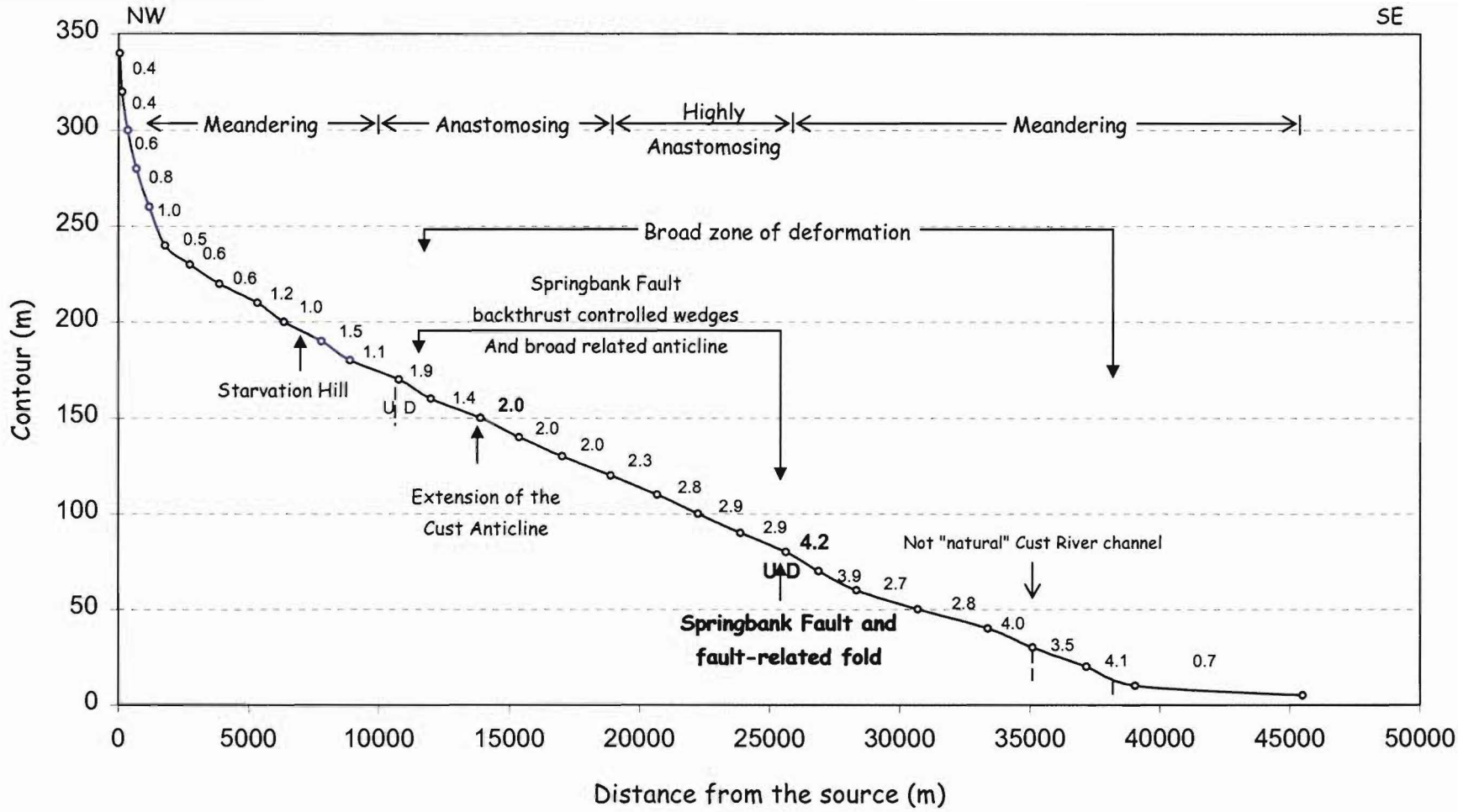

Figure 2.19: River longitudinal profile and values of the GI/K ratio for the different Cust River reaches. The location on the Springbank Fault-related fold with respect to the river is illustrated together with the location of other structures along the profile. Solid arrows represent previously mapped structures, dashed lines represent possible structures underlying the river. Changes along the Cust River channel pattern are illustrated at the top of the figure.

High GI/K values are also measured on reaches of the river located between the 170m and the 10m contours suggesting a broad zone of deformation. Within this zone, between the 170 and 80 m contours the river reflects tectonic perturbations that are directly related to Springbank Fault backthrust structures and the broad anticline related to the fault (the location of these structures is confirmed by previous geophysical investigations).

Anomalous high values are also observed at the reaches of the river between the 40m and the 10m contours. These values occur within the zone where the Cust River was accidentally trapped for the swan drain built in 1868 (see Section 1.4.2.2), and may not correspond to natural values; however they may reflect tectonic structures as well (the structures are outlined with dashed lines in Figure 2.19).

The presence of an extension of the Cust Anticline is indicated from the high value (2.0) in the GI/K ratio at the intersection between the Cust River and the 150m contour.

The Cust River response to the uplift produced by the Springbank Fault is also indicated by changes in the characteristics of the river channel. The river undergoes significant changes, from a meandering pattern, close to the source, to progressive development of multiple channels (anastomosing pattern) before the fold location, and finally, an increase in sinuosity, accompanied by incision, after the fold (Figures 2.19 and 2.20).

This behaviour reflects the channel pattern changes obtained by Ouchi (1985) on experimental meandering rivers crossing tectonic uplift. With uplift, damming effects may create an anastomosing channel pattern in the upstream side of the anticline, while on the down-stream side of the uplift the river increases its sinuosity and bank erosion as the valley floor is steepened.

The evident response of the Cust River to the occurrence of the Springbank Fault, manifested mainly by steeper river reaches and changes in channel pattern, and the certainty of the location of the subsurface fault with respect to the river, leads to the extrapolation of this analysis to the other rivers in the study area in order to establish the location of the Springbank Fault underneath their channels.

The same analysis is then undertaken for the Eyre and Waimakariri Rivers (south of the Cust River) and for the Ashley River, Makerikeri River, and Stony Creek (north of Cust River).

(A)

(B)

Figure 2.20: Cust River. (A) one of the multiple channels forming the anastomosing river pattern before crossing the Springbank Fault-related fold (photograph location grid reference NZMS 260 M35 644 672). (B) Terrace caused by incision of the single Cust River channel after crossing the fold (photograph location grid reference NZMS 260 M35 675 650).

2.4.2 EYRE RIVER ANALYSIS

The Eyre River is located ~8km south of the Cust River, within a zone where the Springbank Fault does not have any evident surface expression. To establish the presence of the Springbank Fault across the Eyre River, analysis of its longitudinal profile and changes in channel pattern were undertaken. Figure 2.21 illustrates the Eyre River longitudinal profile and the GI/K values for the different reaches between contours. A direct correlation between changes in river profile and structural features is also evident along this river. Contrasting GI/K values are present across important known fault zones such as the Townshend, Cooper Creek and Kowai Fault zones.

These faults are manifested as steeper river reaches located between the 640m and the 620m, the 480m and the 460 m, and the 330 and the 300m contours (elevations) respectively (Figure 2.21). Other structures along the Eyre River channel are also confirmed by the highly contrasting values in the G/K ratio. As indicated in the Cust River longitudinal profile, a broad zone of deformation is inferred for the high values (>>2) of the GI/K ratio underneath the lower reaches of the Eyre River, between its intersection with the 210m and 20m contours.

Within this zone, an especially high value (4.2) is observed between the intersection of the Eyre River with the 90m and 80m contour. This reach is comparatively steeper, and by analogy with the Cust River profile analysis, in which the most dramatic change (also 4.2) was directly related to the Springbank Fault-related fold, it indicates that a structure with similar characteristics to the Springbank Fault is located around the 90m contour in the Eyre River.

Nevertheless, this structure is not the direct strike continuation of the Springbank Fault to the south of the Tram Road (where it was first discovered) because its location is several kilometres displaced to the east relative to the expected location of the fault (according to the trend of the Springbank Fault observed to the north). This structure has not been mapped before.

High contrast in GI/K values also suggests minor structures within the zone of deformation. For example, high contrasts are calculated around the 180m contour, where there is a change in GI/K values form 2.7 to 1.6 (Figure 2.21); at the 160m contour (change in GI/K values from 2.7 to 1.6) or at the 130m contour (from 2.8 to 2). At these places minor structures are inferred.

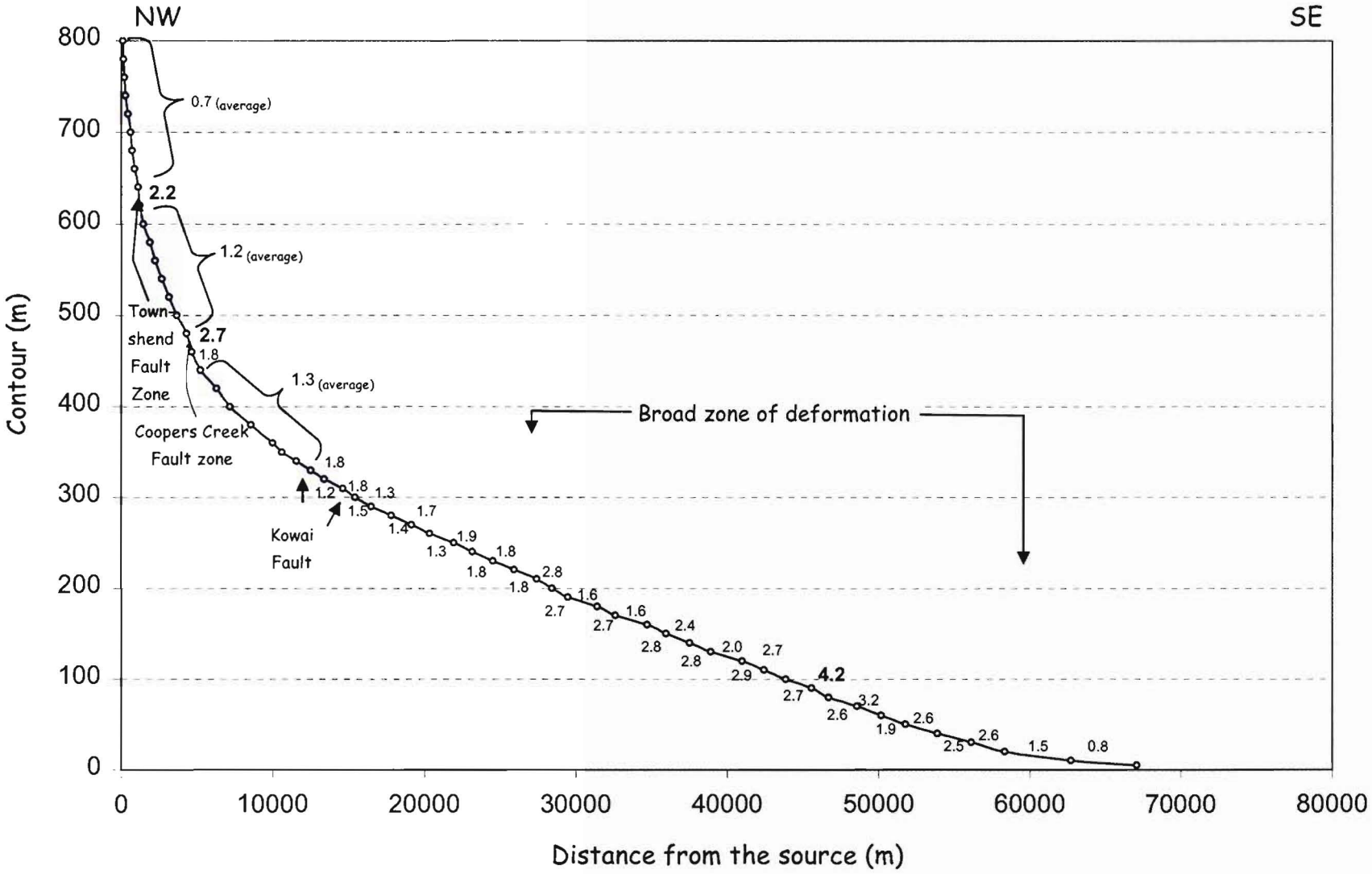

Figure 2.21: Eyre River longitudinal Profile. Values of GI/K ratio are measured for each reach. The location of previously mapped fault zones is showed with solid arrows, together with the GI/K values at those locations.

The broad zone of deformation and the possible occurrence of structures within it are also suggested by other morphometric analyses along the Eyre River. These analyses include topographic surveys contained in the database of the Environment Canterbury (formerly the Canterbury Regional Council), and sinuosity and width channel analyses carried out for this study (Figure 2.22).

An uplifted zone between the 80m contour and the 160m contours is indicated by two topographic surveys undertaken in the years 1924 and 1958 (Figure 2.22A). These surveys measured the mean bed level of the Eyre River at numerous places across the channel starting downstream from its diversion to the Waimakariri River. This uplifted zone may represent deformation possibly associated with folding related to the new inferred structure with similar characteristics to the Springbank Fault.

Figure 2.22B shows the sinuosity index and the width channel at different reaches of the Eyre River (the y-axis represents both the sinuosity index value and the channel width in kilometres). The sinuosity analysis indicates a major change in sinuosity after the river intersection with the 250m contour, and less significant changes at the reach located between the 170m and 160m contours, and at the reach located between the 90m and 80m contours. The major change is probably the result of the junction between the Eyre River and its tributary, the Coopers Creek, which takes place a few metres upstream. The change in sinuosity around the 160m contour and 80m contour seems to confirm the deformation related to folding associated with the new structure.

Minor changes in sinuosity were measured as well at reaches located between the 230-220m, 200-190m, 140-130m and 110-100m contours. Changes in the river longitudinal profile were are also present at the 200-190m, 140-130m and 110-100m contours indicating minor structures at those places.

In addition, significant changes in river width were noted around the intersection of the river with the 180m and with the 110m contour (Figure 2.22B). The Eyre River channel is progressively increasing its width after the 250m contour. This is probably related to the joining with the Coopers Creek, just a few metres upstream. There is a decrease of the channel width at around the 200m contour to gradually increase towards the 180m contour, where the channel reaches its maximum width, and then decrease again until the 160m contour. This shows a river adjustment that is probably related to uplift associated with the new inferred fault.

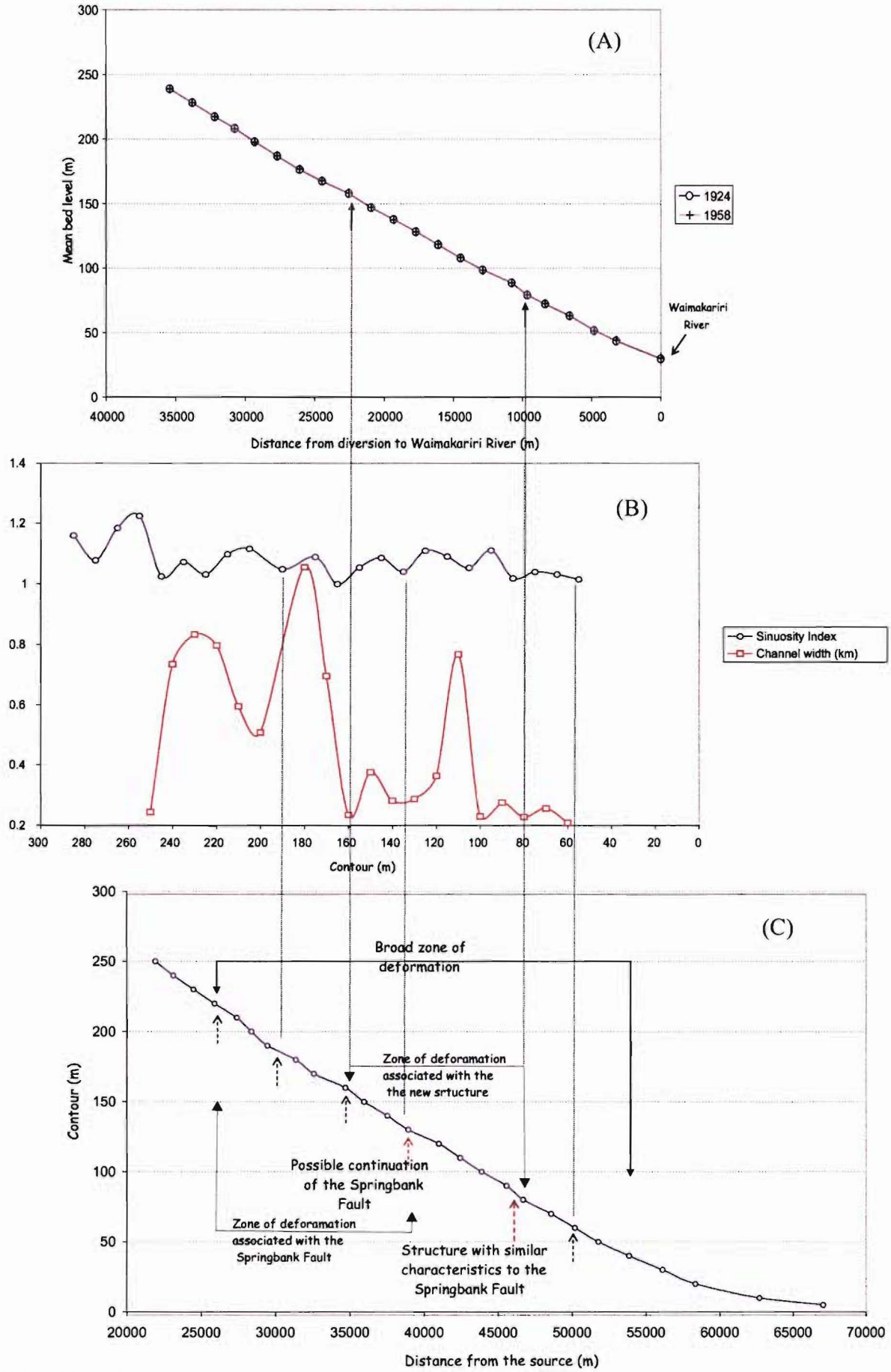

Figure 2.22: Correlation between different morphometric analyses along the Eyre River. (A) Longitudinal profile from topographic data collected in 1924 and 1958 (data courtesy of Environment Canterbury). (B) Sinuosity index (blue line) and channel width (red line). X-axis represents the intersection of the Eyre River with a contour, and y-axis represents both the sinuosity index value and the channel width in kilometres. (C) Plot of the longitudinal profile of the lower reaches of the Eyre River illustrating the structures proposed (dashed arrows) based on the morphometric analyses.

At around the 110m contour there is a major change in the river width indicating a significant change in river sinuosity. At this location there is a minor proposed structure, but this change may be related to the tectonic deformation associated with the inferred structure around the 130m contour.

Figure 2.22C compiles the structures proposed on the basis of the different morphometric analyses along the Eyre River. The structures include both previously mapped faults and unknown (inferred) structures underlying the river. A broad zone of deformation is inferred at the lower reaches of the river (Figure 2.22C). Within this zone, a fault with similar characteristics to the Springbank Fault, a related fold, and other minor structures are proposed.

It is possible that one of the structures proposed within the broad zone of deformation (the structure located around the 130m contour) corresponds to the continuation of the Springbank Fault to the south. At this point, the Eyre River has a significant change in direction possibly related to fault and fold propagation toward the southeast (Figure 2.7 and Map 2). This structure is situated close to the place at which the Springbank Fault should continue under the Eyre River, if the flexure observed at the North Eyre Road (see section 2.2) does corresponds to a topographical expression of the fault. This suggests a change in fault strike direction to the south.

The deformation measured between the 210m and the 130m contours (where the continuation of the Springbank Fault is inferred) is interpreted here as the manifestation of a broad anticline associated with the Springbank structure.

2.4.3 WAIMAKARIRI RIVER ANALYSIS

The Waimakariri River is a braided river situated to the south of the Eyre, and is the major river in the study area. The morphometric investigations on the Waimakariri River allowed the extrapolation to the south of some of the structures inferred from the analysis of the Eyre River.

The morphometric investigations conducted on the Waimakariri River include analysis of its longitudinal profile and gradient index determination for the different reaches between consecutive contours. This was supplemented with examination of aggradation and degradation processes along the river to corroborate its response to the different inferred

structures. The location of reaches where there is aggradation or degradation is based on periodic topographic surveys undertaken by Enviromment Canterbury. The analysis of sinuosity changes is not possible due to the braided nature of the Waimakariri River.

The Waimakariri River longitudinal profile is illustrated in Figure 2.23. Due to the long length of the river, and in order to present all the data in the same figure, it was necessary to average the GI/K values among some reaches. Only reaches with similar GI/K values are averaged together.

As is the case for the Cust and the Eyre Rivers, the Waimakariri River longitudinal profile and the GI/K values calculated for the different reaches, indicate the presence of underlying structures (Figure 2.23). The existence of previously mapped fault zones, including Harper, Porters Pass, Kowai and Hororata Faults are manifested by deformation along the profile and for high contrasting values in the GI/K ratio.

As observed on the Eyre and Cust Rivers, a wide zone of deformation is present in the lower reaches of the Waimakariri River. Within this zone, the river changes from southeast to easterly direction, suggesting structural control.

Two high values in the GI/K ratio (4.3 and 4.7) are determine for reaches located between the 90m and 80m contours and the 60m and 50m contours respectively, suggesting the presence of two structures. The location of the structure around the 80m contour is probably the continuation to the south of the structure with similar characteristics to the Springbank Fault inferred on the Eyre River. High GI/K values are also measured upstream of the above structures, suggesting a zone of deformation related to folding associated with this structure.

Changes in gravel volume on the Waimakarirri River bed, from the gorge to the river mouth, have been measured over the years by river monitoring programs, and are compiled on a database maintained in Environment Canterbury. These changes in volume are based on the measurements of the river bed levels during different periods. In brief, the river bed levels are surveyed by using a Total Station, EDM and Theodolite set up on concrete benchmarks on the stopbank system of the river. The exact locations and heights (above MSL) of these benchmarks have been coordinated recently by real-time GPS. The survey data are then analysed with computer assistance (TrimMap and Cross-Set software packages) to determine the mean bed level and gravel volumes at each survey cross-section (Youngs, *personal communication*, 2003).

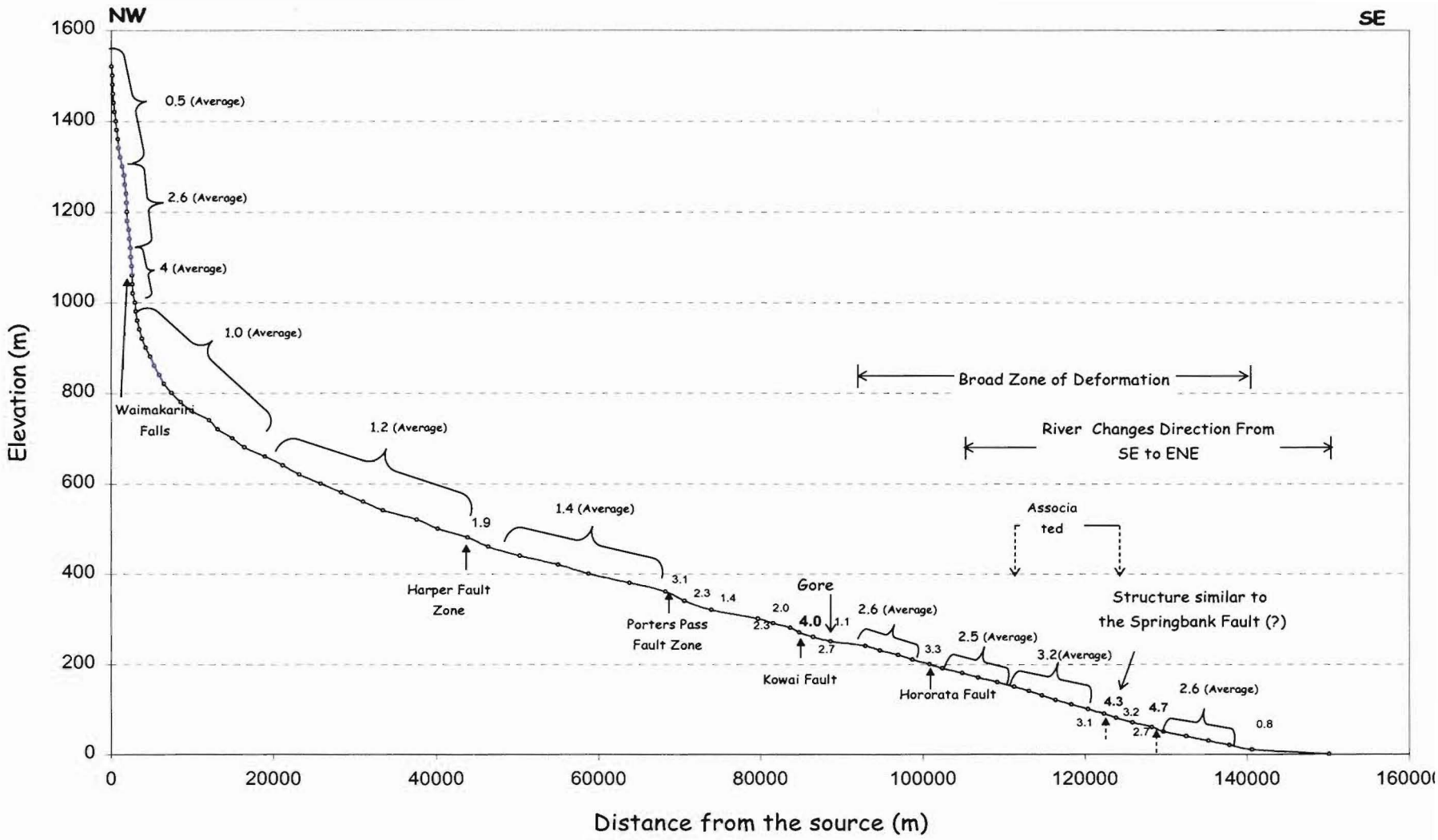

Figure 2.23: Waimakariri River longitudinal profile. Values of GI/K are measured for each reach. The location of previously mapped fault zones and other inferred structures are illustrated (solid and dashed arrows, respectively).

The gravel volume changes through time allow the determination of places where persistent agradation or degradation processes are taking place. Figure 2.24 includes the data from the topographical surveys carried out from 1967 until 1997. In this figure, the volume changes along the river bed are compared with the river bed level measured between 1960 and 1964.

Places of aggradation or degradation along the lower reaches of the Waimakariri River are illustrated in Figure 2.25 together with the inferred structures from the longitudinal profile analysis. The proposed structures, located around the 80m contour, and around the 160m contour (Figure 2.25), are interpreted as a structure with similar characteristics to the Springbank Fault and as a backthrust or backlimb, respectively. Both structures form an uplifted zone that affects the Waiamakariri River and induces degradation, as illustrated in Figure 2.25.

The incision produced by the river as a response to the uplifted zone is also evident in the river terraces. The Waimakariri River terraces developed at this location are comparatively higher than the terraces observed downstream, where aggradation processes are taking place (Figure 2.26).

The structure proposed around the 190m contour is also related to a change in river behaviour. At this location the river changes from degradation to aggradation, suggesting the presence of a structure with different characteristics from those inferred dowmstream. There is not an evident change in river behaviour related to the structure proposed around the 60m contour.

The analyses carried out in the Waimakariri River do not show any evidence of the continuation of the Springbank Fault from its possible location underneath the Eyre River, which suggests that the fault may die out south of to the Eyre River.

2.4.4 ASHLEY RIVER ANALYSIS

In order to identify the Springbank Fault to the north of the Cust River and determine its relation to other structures such as the Ashley Fault, similar morphometric analyses were conducted on the Ashley River and some of its tributaries.

The Ashley River is affected by active tectonism related to different structures such as the Ashley Fault and the Cust Anticline. The Ashley River longitudinal profile is presented in Figure 2.27.

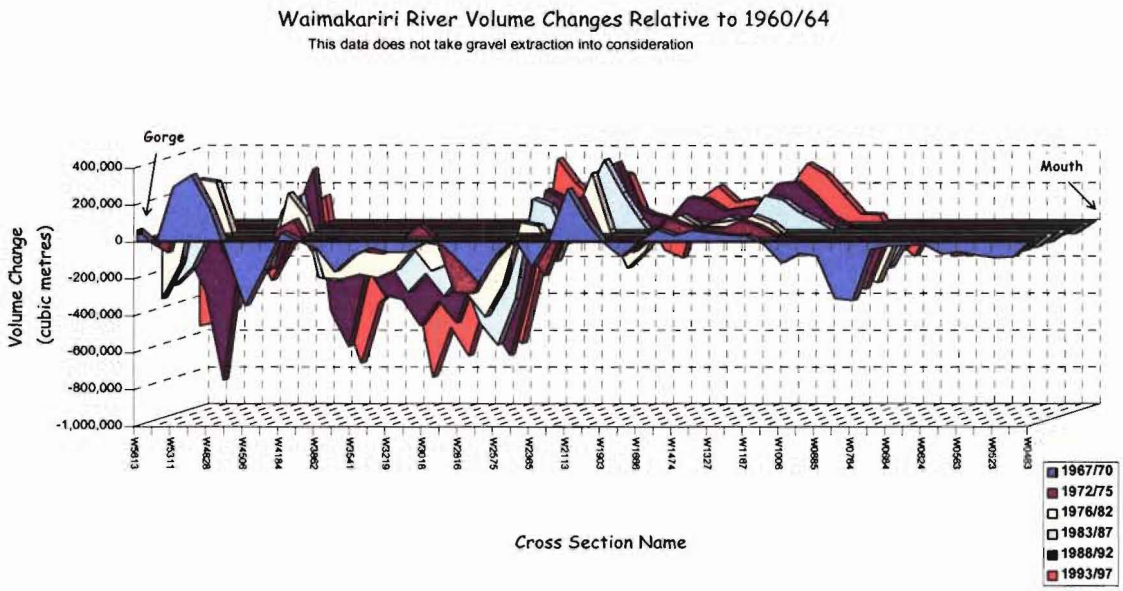

Figure 2.24. Waimakariri River volume changes. Comparison between river gravel volumes measured at different cross sections along the river (from the Gorge to the mouth) during different years. The x-axis comprises the name of the section where the measurements were taken, and the y-axis the volume change relative to the 1960 to 1964 period. Volume changes values above zero indicate aggradation processes and below zero indicate degradation (modified from Environment Canterbury).

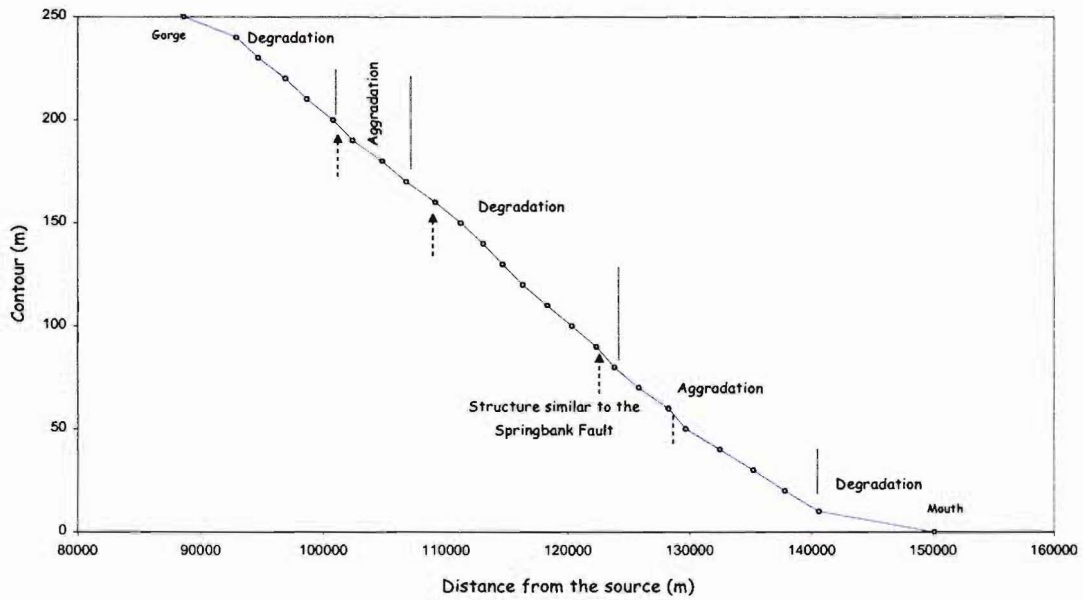

Figure 2.25. Correlation between the proposed structures (dashed arrows) and aggradation/degradation processes along the Waimakariri River.

(A)

(B)

Figure 2.26: Waimakariri River terraces formed across (A) and after (B) the proposed uplifted zone located between the newly identified structure and its backlimb. The higher terrace in (A) implies river incision maybe in response of folding. ((A) location grid reference NZMS 260 M35 595 506; (B) location grid reference NZMS 260 M35 712 526).

The values of the GI/K ratio are illustrated as well, together with the location of previously mapped structures. As in the preceding analyses, highly contrasting GI/K values are observed at reaches that are affected by faults, and minor changes are measured at places where the river flows through different sedimentary formations. Highly contrasting GI/K values are calculated around the Glentui Fault Zone, Cust Anticline, and the prolongation of the Ashley Fault along the river (Figure 2.27).

If the Springbank Fault continues from its expression between the Tram Road and the Cust River, across the Ashley River without any major change in strike, it should be manifested on the river longitudinal profile at around the 60m contour. It would be expected to show strongly contrasting GI/K values at this area, not only because of the presence of the Springbank Fault, but also because of the closeness of the Ashley Fault (immediately to the north), implying complex tectonic interactions.

At this point, the GI/K values, although exceeding 2, are not as strongly contrasting as expected. It is not possible to establish without further information (i.e geophysical studies) if this value correspond either to the extension to the north of the Springbank Fault, or the prolongation to the east of the Ashley Fault, but it is unlikely that these values reflect a strong uplift interaction between both structures.

High contrasting GI/K values are observed downstream, around the 30m contour, suggesting the presence of another structure with similar characteristics to the Springbank Fault at this point.

Information related to aggradation/degradation processes along the river was used to examine its response to the inferred structures. As for the Waimakariri River, these data were extracted from the river monitoring program executed by Environment Canterbury. Changes in gravel volumes in the Ashley River are illustrated in Figure 2.28. This information corresponds to surveys undertaken along the river from one kilometre downstream of the intersection with the Okuku River, to the river mouth, during 1976, 1986 to 1988 and 1997. Figure 2.28 compiles the changes in gravel volumes at different locations along the river, by comparing the river bed levels with those measured during 1960-1962. Increase or decrease in gravel volume indicates aggradation or degradation, respectively. The zones of aggradation or degradation along the longitudinal profile of the lower reaches of the Ashley River (between the intersection with the Okuku River and the mouth) are illustrated in Figure 2.29.

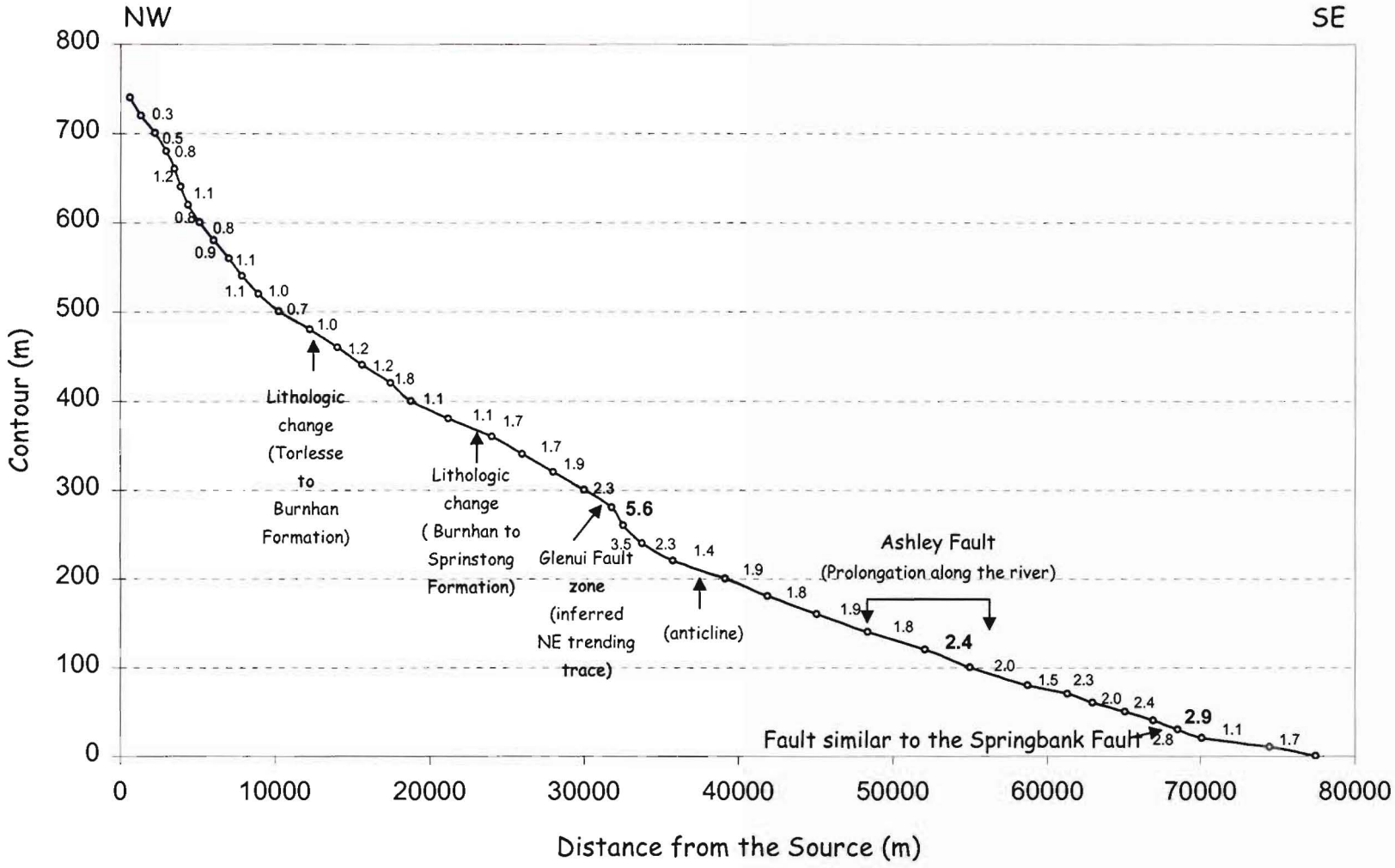

Figure 2.27: Ashley River longitudinal profile and values of GI/K ratio. The location of mapped fault zones and lithological changes are illustrated with solid arrows. Note that, as for the previously analysed rivers, there is not a significant change in the river profile and GI/K values with lithological changes.

Small zones of aggradation take place between the Ashey River intersection with the 100m and the 10m contours. The river at this section could be interpreted as experiencing mainly degradational processes as a result of a broad uplifted zone. This zone may correspond to the deformation associated with the inferred new structure, located at around the 30m contour and its backthrust or backlimb, located around the 60m contour.

The Makerikeri River, a tributary of the Ashley River, flows across the location at which the Ashley and the Springbank Faults should interact, if this is the case. Consequently, the Makerikeri longitudinal profile should be strongly deformed as a result of this complex interaction. The profile is presented in Figure 2.30. The river does not show strong deformation or highly contrast GI/K values. In contrast, the profile follows a nice concave shape, that ideally would be expected for alluvial rivers. The highest GI/K value (2) could be directly related to the prolongation of the Loburn Fault to the east, suggesting that there is a continuation of this structure towar the Makerikeri River.

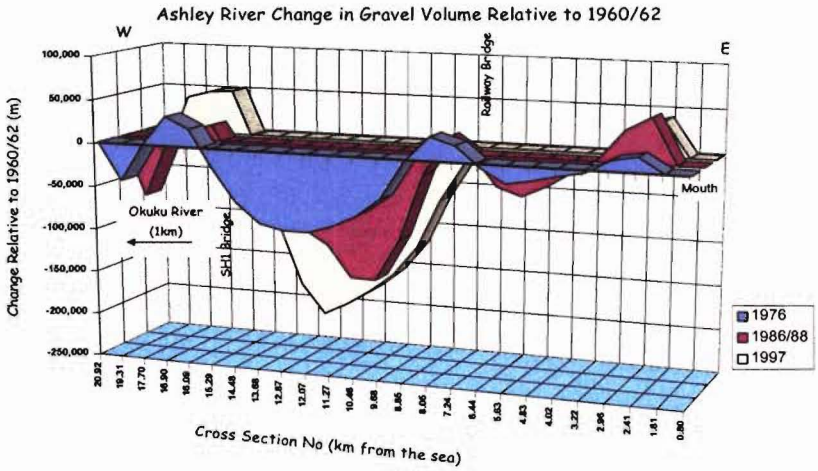

Figure 2.28: Ashley River volume changes. Comparison between river gravel volumes measured at different cross sections along the river (from one km downstream of intersection with Okuku River to the mouth) during different years. The x-axis comprises the distance of each cross section from the mouth, and the y-axis the volume change relative to the period 1960 to 1962. Volume change values above and below zero indicate aggradation and degradation respectively (modified from Environment Canterbury).

The morphometric analysis conducted on the Ashley and Makerikeri Rivers suggests that the Springbank Fault dies out towards the Ashley Fault. There is no superficial evidence, either topographical or related to changes in the rivers characteristics, for extending the Springbank Fault beyond the Ashley Fault.

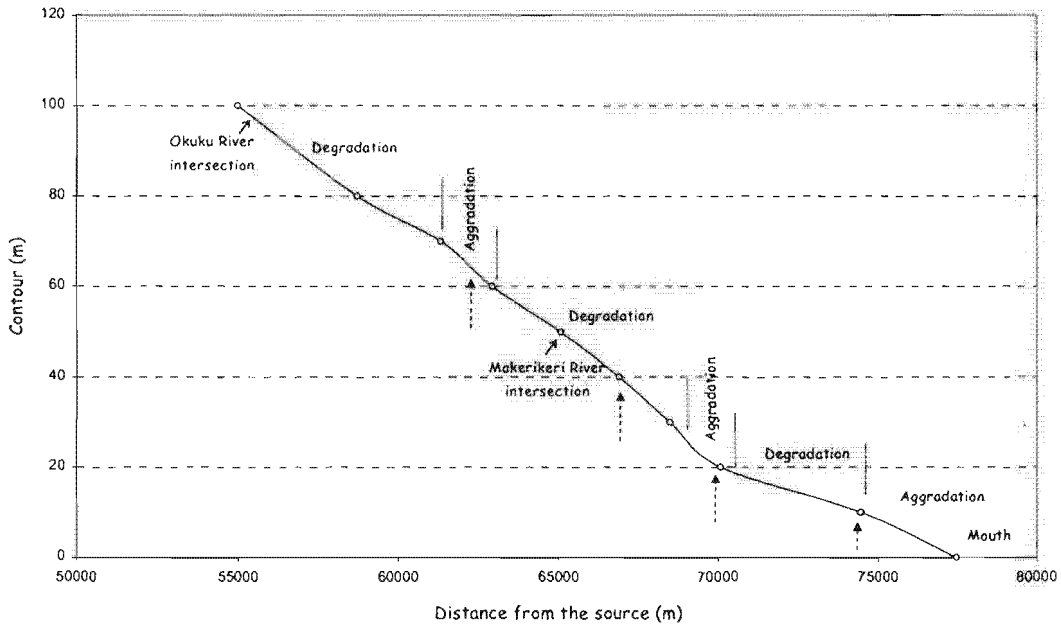

Figure 2.29: Longitudinal profile of the lower reaches of the Ashley River. The location of inferred structures (dashed arrows) is illustrated together with the location of aggradation or degradation processes along the river. The river intersection with its tributaries, the Okuku and the Makerikeri Rivers are also presented.

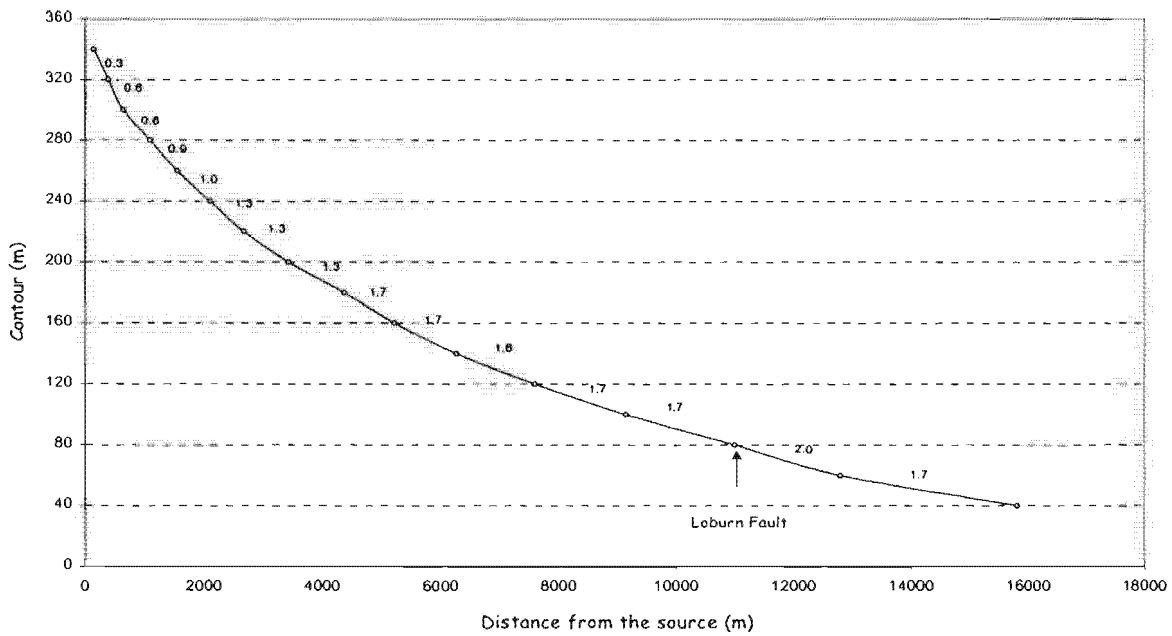

Figure 2.30: Makerikeri River longitudinal profile. The arrow shows the possible continuation of the Loburn Fault across the river. There is no evidence of the Springbank Fault.

It is probable that the structure inferred to the east, at around the Ashley River intersection with the 30m contour, may correspond to a splay of the Springbank Fault that steps out to the east or to a structure with similar characteristics. The longitudinal profile of Stony Creek, a small river situated to the northeast of the proposed structure around the intersection between the Ashley River and the 30m contour, indicates the presence of a structure close to the creek intersection with the 40m contour (Figure 2.31). If this structure is related to the proposed one in the Ashley River near the 30m contour, then the structure is trending to the northeast with a similar strike to the Springbank Fault.

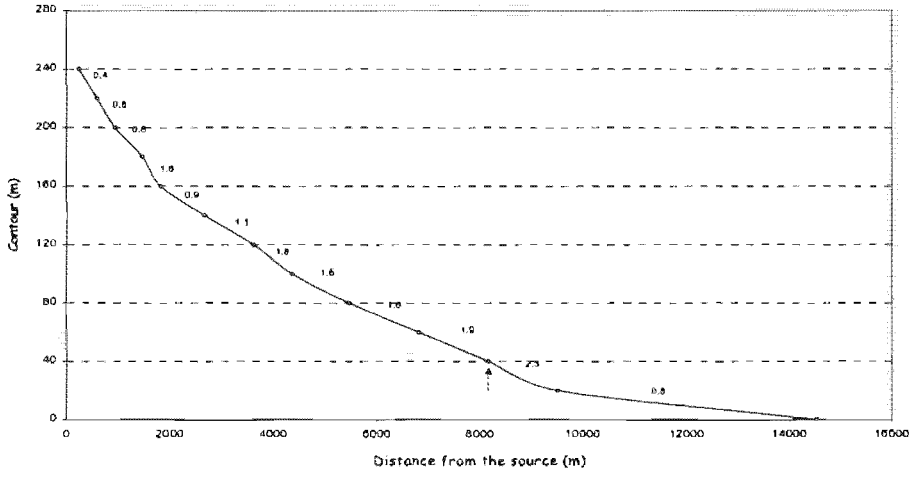

Figure 2.31: Longitudinal profile of Stony Creek. The profile indicates a structure around its intersection with the 40m contour which may correspond to the continuation of the proposed structure at the Ashley River around its intersection with the 30m contour.

2.5 SUMMARY AND CONCLUSIONS

The Springbank Fault is a blind structure located at depth beneath the north Canterbury Plains, to the northwest of Christchurch. The best topographic expression of the fault corresponds to an associated fold developed at the fault tip close to the surface. The fold is a doubly plunging structure that progressively dies out toward both the northeast and southwest and has its maximum amplitude between the Tram Road and the Cust River.

The surface that represents the maximum topographical expression of the fold is defined by two differentiated geomorphic units: the Cust and Springbank Units. The ages of the units, 75,000 and 45,000 yearrs, are not well constrained and are assigned based on published luminescence dating from an overlying loess cover (Berger et al., 2001).

Other minor geomorphological features such as deformed terraces, small microtopographic anticlines, and inclined surfaces are also circumstantially related to the Springbank Fault. Nevertheless, their analysis is not enough to establish the total extension of the fault. Alternatively, the rivers in the study area present a significant response to the deformation induced by the Springbank Fault and other structures. From morphometric analyses along the Cust, Eyre, Waimakariri, Ashley, Makerikeri Rivers as well as the Stony Creek, it is possible to determine the probable location and extension of the Springbank Fault and other structures where no obvious topographical expression is available. Figure 2.32 and Map 2 compile the location and extension of the structures based on the geomorphologic and the morphometric analyses. These analyses allowed the confirmation and extent of several structures identified prior to this study. Some of the structures that are recognized along the rivers can be directly related to previously mapped structures or their projection (Figure 36).

From the geomorphic and morphometric analyses, it is possible to establish that the Springbank Fault is a reverse/thrust structure extending for ~16 km between the Ashley River, to the north, and the Eyre River to the south. The structure is associated with a broad anticline whose forelimb has a clear topographical expression close to Springbank (Map 1); its backlimb occurs several kilometres (~14km) to the west, and is probably associated with backthrust systems. The Springbank Fault experiences a change of strike from N45°E in the north, to N75°E in the south.

Two new structures with similar characteristics to the Springbank Fault are inferred from the morphometric analyses, one located to the southeast of the Springbank Fault and another one to the northeast. Both structures appear to be associated with broad anticlines with similar dimensions to the anticline associated with the Springbank Fault. The structure located to the southeast of the Springbank Fault, identified here as Eyrewell Fault, is a reverse/thrust fault trending N20°E. This structure is located to the west, very close to Christchurch, and this may represent a significant seismic hazard. The northern end of the Eyrewell Fault occurs close to the North Eyre Road, but the southern end is not defined by this study. The structure situated to the notheast of the Springbank Fault, named here the Sefton Fault, is a reverse/thrust fault trending N50°E. This structure presents similar characteristics to the Springbank Fault, suggesting that it could correspond to a segment of the same fault system that stepped out to the east. The presence of these structures must be confirmed with other studies (i.e. seismic reflection investigations).

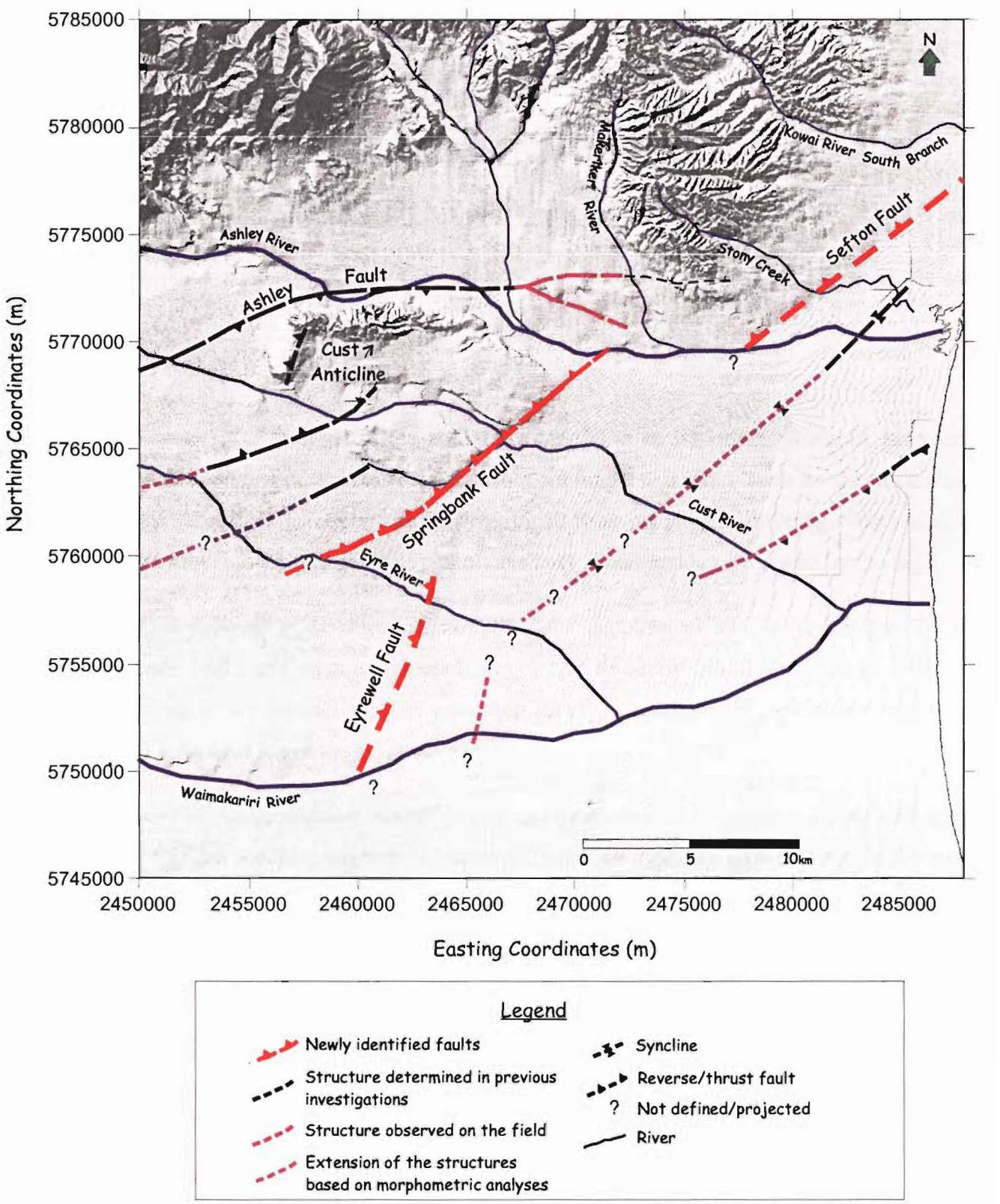

Figure 2.32: DEM of the study area showing the compilation of the structures identified from morphometric analyses along the rivers. The location and extent of the Springbank Fault and the two newly identified faults, the Eyrewell and Sefton Faults are illustrated in red. (See also Map 2).

Chapter 3
SUBSURFACE CHARACTERISATION OF THE SPRINGBANK FAULT

3.1 INTRODUCTION

The geometry of a fault (fault dip and strike length) is an important parameter in seismic hazard assessment. For structures that do not rupture the surface, such as the Springbank Fault, the subsurface geometry can be determined from geophysical investigations and from analysis of focal mechanisms (fault plane solutions) of earthquakes generated by the fault.

This chapter presents the interpretation of three geophysical studies undertaken on the Springbank Fault: one seismic reflection survey carried out by Indo-Pacific Ltd in 1998, and two separate multi-channel shallow reflection surveys undertaken as part of this study (see Figure 3.1 for location of the seismic lines).

The results of the geophysical investigations are supplemented by analyses of the earthquake activity and the focal mechanism solutions of small earthquakes recorded within the study area. Two different earthquake databases are analyzed and compared: the earthquakes compiled for the Institute of Geological and Nuclear Sciences (GNS), and the earthquakes registered by a microearthquake network installed in 1990 and monitored for a period of 2.5 months (Cowan, 1992).

In the last part of the chapter, eleven focal mechanisms obtained by Cowan (1992) within the study area are discussed.

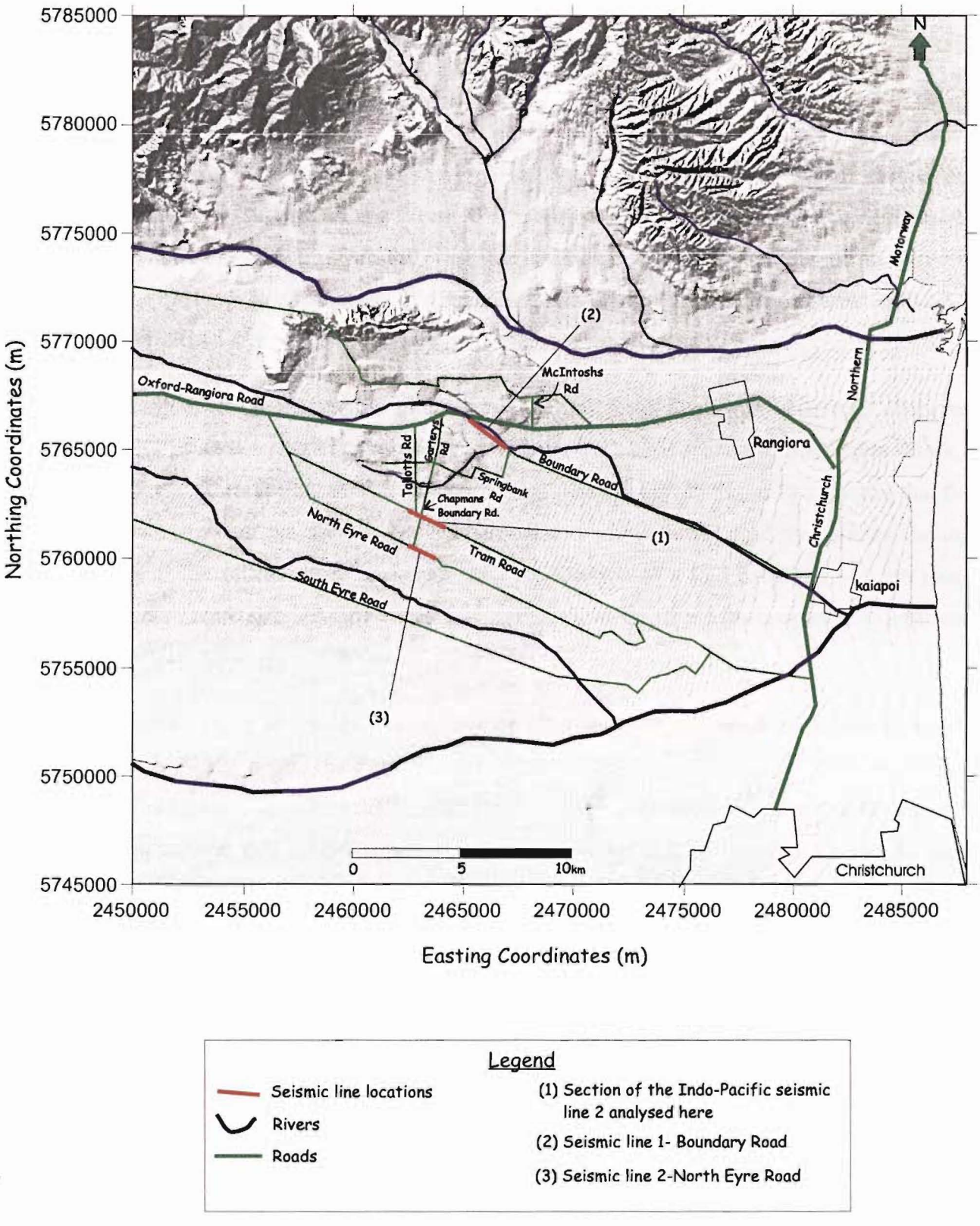

Figure 3.1: Locations of seismic lines analysed in this study.

3.2 GEOPHYSICAL INVESTIGATIONS

3.2.1 INDO-PACIFIC SEISMIC LINE (TRAM ROAD)

The Springbank Fault was first discovered in 1998, when Indo-Pacific (Ltd) carried out seismic reflection surveys in the North Canterbury Plains. The surveys were designed to penetrate several kilometres into the crust, for hydrocarbon exploration. One of the surveys, conducted on Tram Road (Indo-Pacific seismic survey 2), revealed the Springbank Fault close to the Tram Road-Chapmans Boundary Road intersection (Figure 3.1).

Only the top of that profile, in the zone where the Springbank Fault was discovered, (between shot points 1600 and 1900) is analysed here (Figure 3.2). This section of the profile shows a major reverse fault dipping ~60° to the northwest. The seismic stratigraphy indicates that the fault does not reach the surface but it is associated with a broad fold that affects the top reflectors of the seismic line. Backthrust and the location of a fold backlimb ~14 km away from the fault were also identified occurring to the northwest (these features are not illustrated in Figure 3.2).

Jongens et al. (1999) concluded that even though the Springbank Fault does not break the late Quaternary gravels above the Pliocene-early Pleistocene Kowai Formation, they are folded, and that the strong onlapping relationships between the late Quaternary gravels and the Kowai Formation suggest that the deformation commenced in the early or mid-Pleistocene. Jongens et al. (1999) identified a vertical throw across the fault of about 250-300m. They also suggest that the broadly anticline related to the fault is associated, but not directly connected with, the Cust Anticline, located immediately to the east-northeast (Map 2).

A compilation of the geometric characteristics of the Springbank Fault and is associated fold, observed in the section of the Indo-Pacific seismic line analysed here (between shot points 1600 and 1900), is presented in Table 3.1. Different characteristics (Figure 3.3) such as fault dip (θ), vertical throw (Z), length (L) and dip of the fold limb (δ) above the Springbank Fault, and angle between the fold limb and the not-deformed reflectors (γ, γ^*) are measured within reflectors of the Kowai Formation.

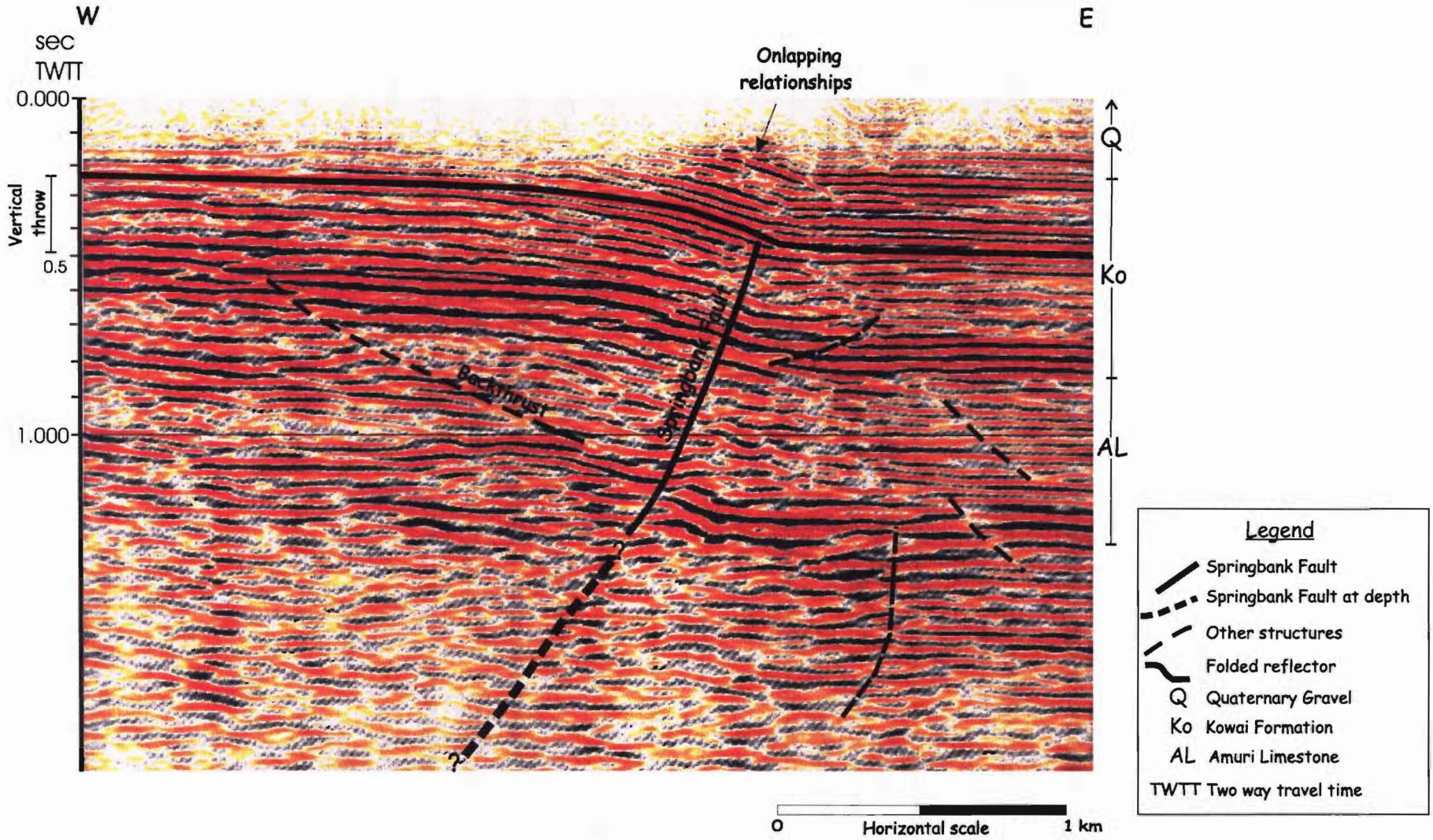

Figure 3.2: Expression of the Springbank Fault in the Indo-Pacific seismic line (seismic survey 2) where was initially discovered. The seismic profiling evidenced a reverse structure dipping 60° to the NW, without reaching the surface but folding the top reflectors. Other structures such as backthrust and minor faults are also illustrated. The continuation of the fault at depth is not clear but is assumed to be listric, progressively flatten out with depth. Stratigraphic units correlated to the profile are illustrated on right side.

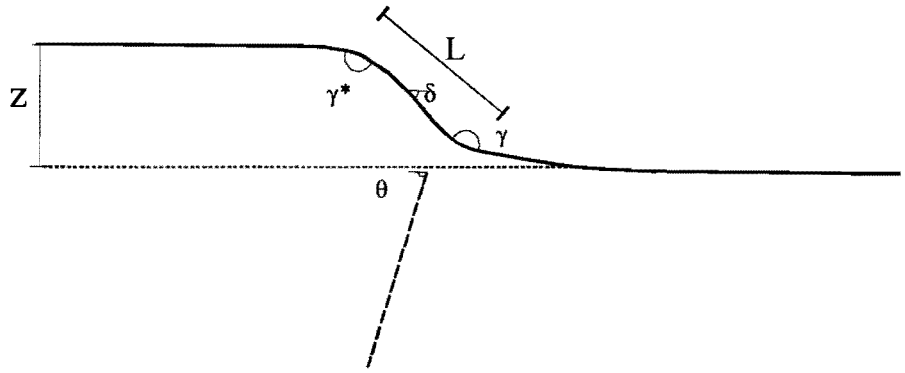

Figure 3.3: Schematic fold showing geometric relationships.

Table 3.1: Geometric characteristics of the Springbank Fault and associated fold measured in the Indo-Pacific seismic line.

Fault Dip Close to Surface(θ)	Vertical Throw (Z)	Fold Limb Length (L)	Fold Limb Dip (δ)	Fold Concave Angle (γ)	Fold Convex Angle (γ*)
60°	300m	910m	16°	85°	86°

The Indo-Pacific seismic line was designed to penetrate several kilometres into the crust, consequently its near surface resolution is poor. In order to supplement the information provided for the Indo-Pacific seismic line, and to determine the near surface characteristics of the Springbank Fault, two separate multi-channel shallow reflection surveys were undertaken as part of this study (see Appendix 2 for seismic surveys data acquisition and processing). The new seismic lines were located both to the north and south of the Indo-Pacific profile location (Tram Road), along Boundary Road and North Eyre Road, respectively (Figure 3.1). The location of these seismic lines was based on the inferred continuation (before this study) of the Springbank Fault towards the north and south, with respect to its location at the Tram Road.

3.2.2 SEISMIC LINE 1: BOUNDARY ROAD

Seismic line 1 was conducted along 1930m on Boundary Road, between Kennedys Road-Boundary Road intersection and Oxford to Rangiora Road-Boundary Road intersection (Figure 3.1).

The topography along Boundary Road is very subtle and the seismic line was assumed to be flat. No changes in elevation between geophones were incorporated in the calculations. Nevertheless, a GPS survey carried out at this location (Figure 2.10) showed a change in elevation of up to 10m along the profile. This change is linear along the length of the seismic line, and therefore does not affect the calculations.

Figure 3.4 shows the profile obtained for seismic line 1. The top ~500m are presented. The data displays strong reflectors, delineating a broad fold structure. On the west side of the profile, the reflectors are approximately parallel to the ground surface. In the central part of the profile, between shot points (sp) 200 and 600, a roll-over structure develops into an east facing monocline that corresponds to the Springbank Fault-related fold.

Comparisons with the previous geophysical study by Indo-Pacific, as well as outcrop ties, confirm that the reflector located at ~0.25s (TWTT-two way travel time), on the east side of the profile, represents the top of the Kowai Formation. As explained before (see section 1.5.1.2), the age of the Kowai Formation has not been well constrained but is generally accepted as Pliocene to lower Pleistocene in age. Consequently, the material above this reflector corresponds to sediments primarily of late Pleistocene and Holocene age.

The Springbank Fault is not clearly defined in this seismic profile and it is not possible to unequivocally determine its geometry. Nevertheless, it seems to be located below the shot point 500 (Figure 3.4) suggesting a high angle reverse fault, dipping to the north-west.

There is no evidence of large fault displacement in the profile, but from the characteristics of the associated fold, a vertical throw of approximately 200m is identified at this location.

Minor synthetic and antithetic faults are also observed (Figure 3.4). These structures are inferred to be related to the movement along the Springbank Fault. The pattern of observed thrust/reverse minor synthetic, antithetic and major backthrust faults is similar to some theoretical and physical models predicting secondary fault patterns in thrust fault zones (i.e. Rogers and Rizer, 1981). As predicted by the physical models, the seismic line 1-Boundary Road illustrates backthrusts formed in the hanging wall of the Springbank Fault together with a pattern of synthetic and antithetic minor faults. Similarly, synthetic reverse splay faults have developed in the footwall of the Springbank Fault (Figure 3.4).

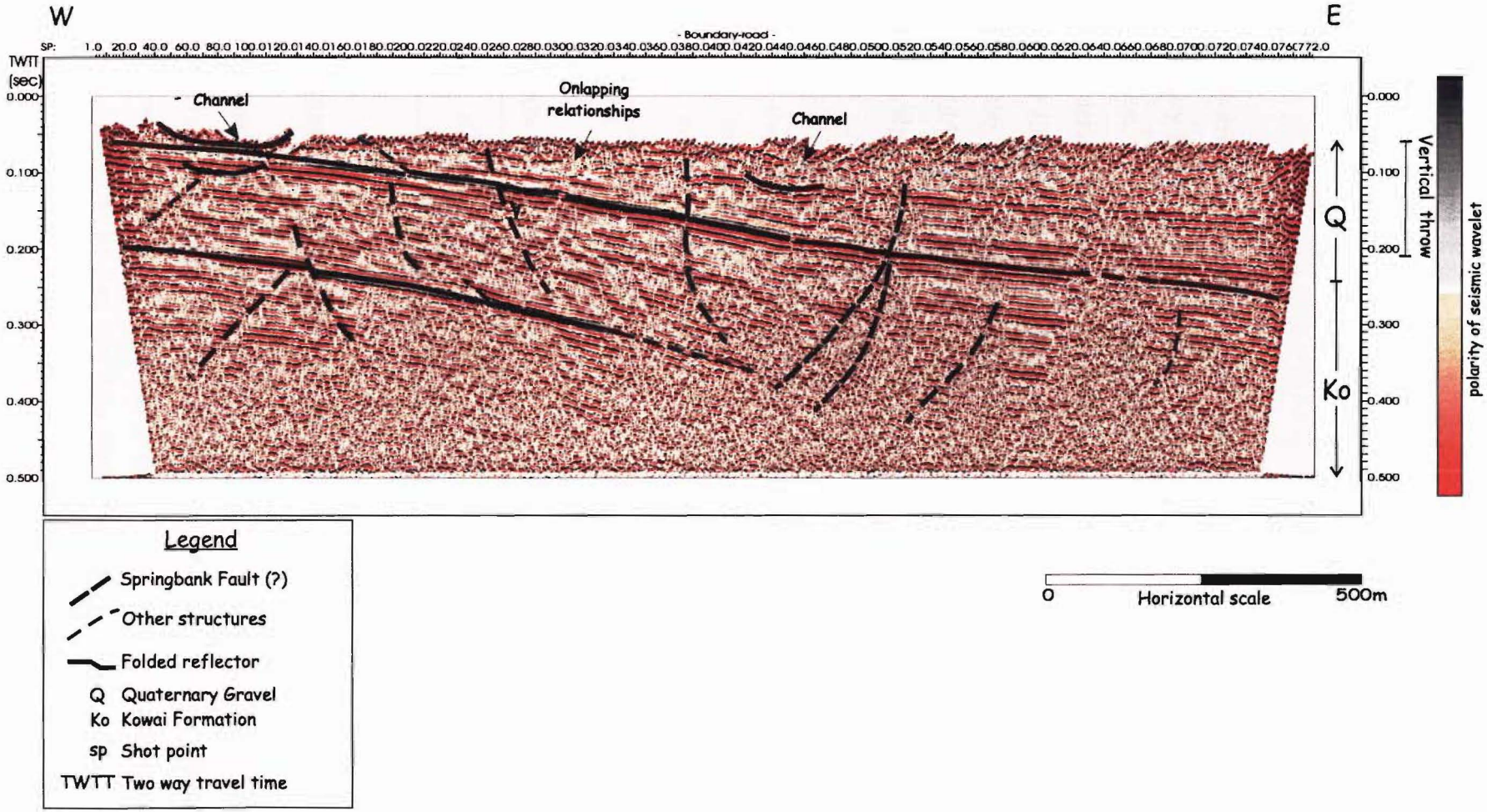

Figure 3.4: Boundary Road seismic line. The seismic profile indicates the broad fold associated with the Springbank Fault. The fault is not well imaged. Other features such as backthrusts, minor faults and channels are illustrated. The vertical throw of the fold observed in this profile is lower that the one in the Indo-Pacific seismic line. Stratigraphic units correlated to the profile are illustrated on the right side.

Other features in the profile include old channels and stratigraphic unconformities. Strong onlapping relationships are mainly exemplified within the Quaternary sediments, above ~0.25s on the east side of the seismic line indicating that the deformation is of Quaternary age.

The geometric characteristics of the Springbank Fault and associated fold on the seismic line 1-Boundary Road are summarized in Table 3.2. These characteristics, as for the Indo-Pacific seismic line, were measured within reflectors of the Kowai Formation. The fold identified in the Boundary Road seismic line has lower vertical throw, fold limb length and fold limb dip that those in the Indo-Pacific seismic line, indicating lower development of the structure at this location. This suggests that the displacement associated with the fault is maximum close to its middle point (which corresponds to its maximum topographic expression) and progressively decrease toward the fault ends.

Table 3.2: Geometric characteristics of the Springbank fault and associated fold measured in seismic line 1: Boundary Road. The values in brackets correspond to the same parametres measured in the Indo-Pacific seismic line and presented in Table 3.1.

Fault Dip Close to Surface(θ)	**Vertical Throw (Z)**	**Fold Limb Length (L)**	**Fold Limb Dip (δ)**	**Fold Concave Angle (γ)**	**Fold Convex Angle (γ^*)**
60° (60°)	200 m (300m)	860m (910m)	10° (16°)	87.5° (85°)	85° (86°)

3.2.3 SEISMIC LINE 2: NORTH EYRE ROAD

Seismic line 2 was conducted along 1200m on the North Eyre Road, south of Tram Road (Figure 3.1), at the location where the fault was predicted to extent before this study. As for seismic line 1-Boundary Road, the topography of the North Eyre seismic line 2 is very subtle and was assumed to be flat. The data acquisition and processing for this seismic line 2 is presented in Appendix 2. Figure 3.5 shows the profile obtained for seismic line 2-North Eyre Road. The top ~600m are presented. In contrast to the observed in seismic line 1-Boundary Road, the reflectors obtained in this profile show do not image the Springbank Fault or its associated fold.

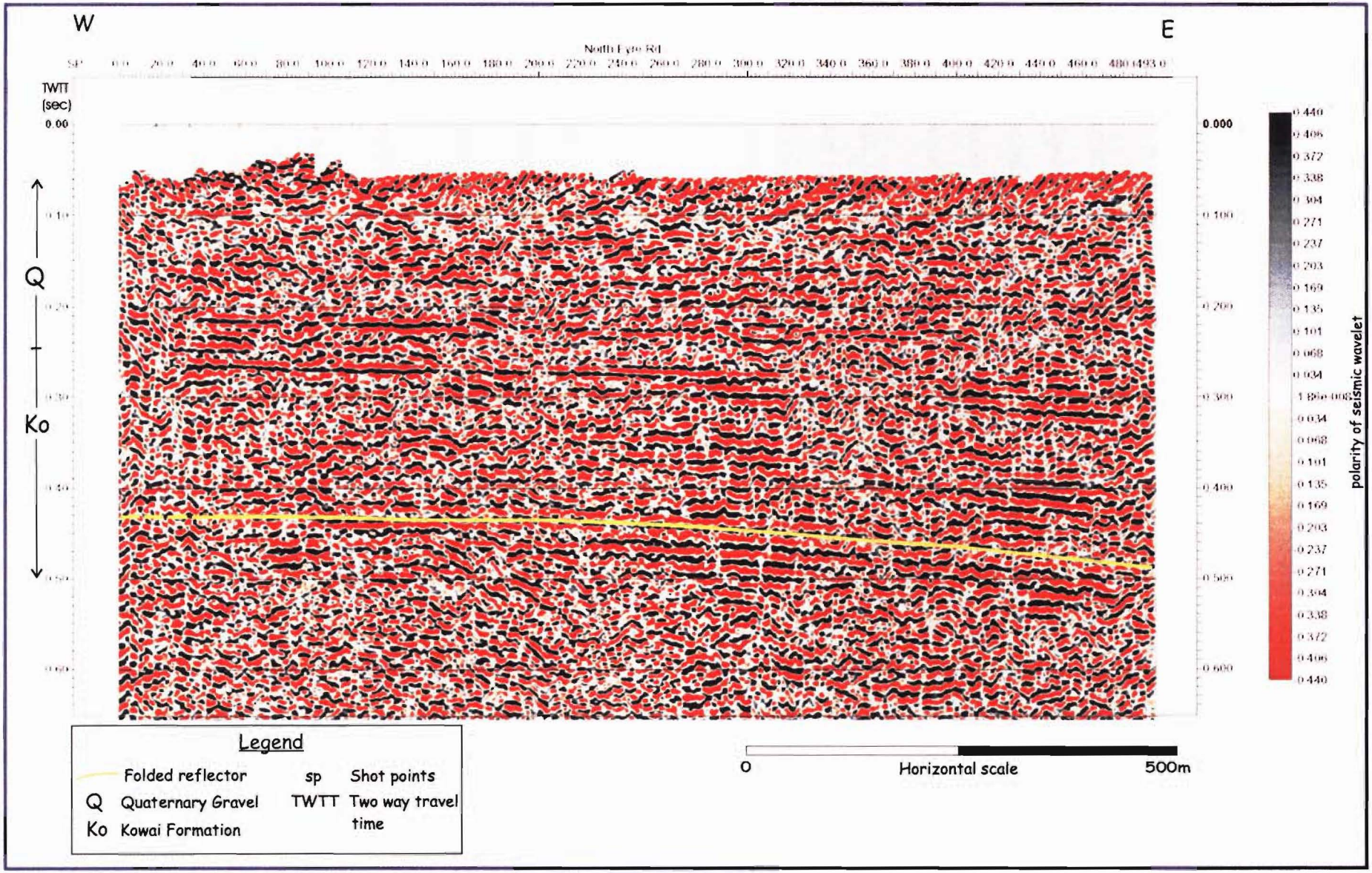

Figure 3.5: North Eyre Road seismic line. The profile does not show any evidence of the Springbank Fault. The reflectors are deformed into a broad flexure toward the right side of the seismic line suggesting another reverse fault to the east.

Seismic line 2 was undertaken before the morphometric analyses along the rivers and its location was chosen with the expectation of intercepting the predicted continuation, inferred before this study, of the Springbank Fault south of Tram Road. This profile indicates that the Springbank Fault or its associated fold are not present at this location but, the reflectors show evidence of a incipient monocline towards the eastern end of the profile (Figure 3.5) indicating the presence of a structure to the east of the Springbank Fault.

The characteristics of this structure are very similar to those related to the hanging wall side of the Springbank Fault. The folded reflectors suggest that a fault dipping to the west would underlie this structure at depth. This seismic line confirms both a change in the strike of the Springbank Fault from that at Tram Road to the north, and the new structure, the Eyrewell Fault, identified on the basis on the drainage analysis already discussed in Chapter 2.

Although, the profile obtained along North Eyre Road does not show the Sprinbank Fault and its related fold, this seismic line was essential for this study. The profile demonstrates that the Springbank Fault is not located where it was inferred prior to this investigation, and confirmed both the change in strike of the Springbank Fault to the south, and supports the presence of the Eyrewell Fault to the southeast.

3.3 EARTHQUAKE ACTIVITY ANALYSIS

The earthquake activity in the study area will be analyzed next in order to determine a possible relationship between the earthquakes and the proposed structures.

There are no reports of large historical or instrumental earthquakes related to the Springbank Fault or the nearby structures within the study area, even though moderate to large earthquakes have occurred beneath the north Canterbury region.

According to two separate earthquake databases analysed here, the seismicity in the study area is shallow (<30 km depth) and of small magnitude (M_L <4). The first database corresponds to the earthquakes compiled by the Institute of Geological and Nuclear Sciences (GNS), and the second is based on earthquakes registered by a microearthquake network installed by Cowan et al.(1990).

The earthquakes from both catalogues have different characteristics regarding hypocentral locations. This is related to the types of instrument used, the data processing, and especially, to the instrument distribution with respect to the study area.

3.3.1 COMPARISON BETWEEN THE GNS AND 1990 MICROEARTHQUAKE NETWORK CATALOGUES

3.3.1.1 GNS Earthquake Catalogue

The GNS earthquake catalogue, analysed for this study, comprises information from 1949 to September 2002. The quality of the catalogue has improved over the years. Better locations have been achieved with the progressive increase in the number of recording stations, better network arrays, and finally implementation of new technology. In 1987, the national seismic network was changed from analogue to digital seismographs, improving significantly the quality of the data. Before this, many events in the catalogue have restricted depths, events with depth of 5, 12 or 33 km assigned for the purpose of hypocentre determination (McGinty, 2001).

The study area is not closely surrounded by the stations of the GNS network (Figure 3.6), consequently, the earthquake locations are not optimum. The GNS station array (large spacing between stations) and the characteristics of the earthquakes in the zone (shallow, and of small magnitudes), has resulted in uncertainties related to hypocentral locations, especially with respect to depth control.

Until September 2002, the GNS network had registered 109 earthquakes within the field area (Figure 3.7). Of these earthquakes, 59% (64 earthquakes) have restricted depths. The rest, 41% (45 earthquakes) have hypocentral locations of less than 32 km. Of that 41%, two have depths of less than 12 km, four are located between 12 and 18 km and, 39 have depths between 18 and 32 km (Figure 3.7).

There is not an obvious relationship between the GNS earthquake locations and the active geological structures in the study area. Although some earthquakes appear to be related to some structures, for example to the Springbank Fault and specially near the Eyrewell Fault (Figure 3.7), the location uncertainties mentioned above make it difficult to establish an unequivocal relationship between earthquake and causative fault.

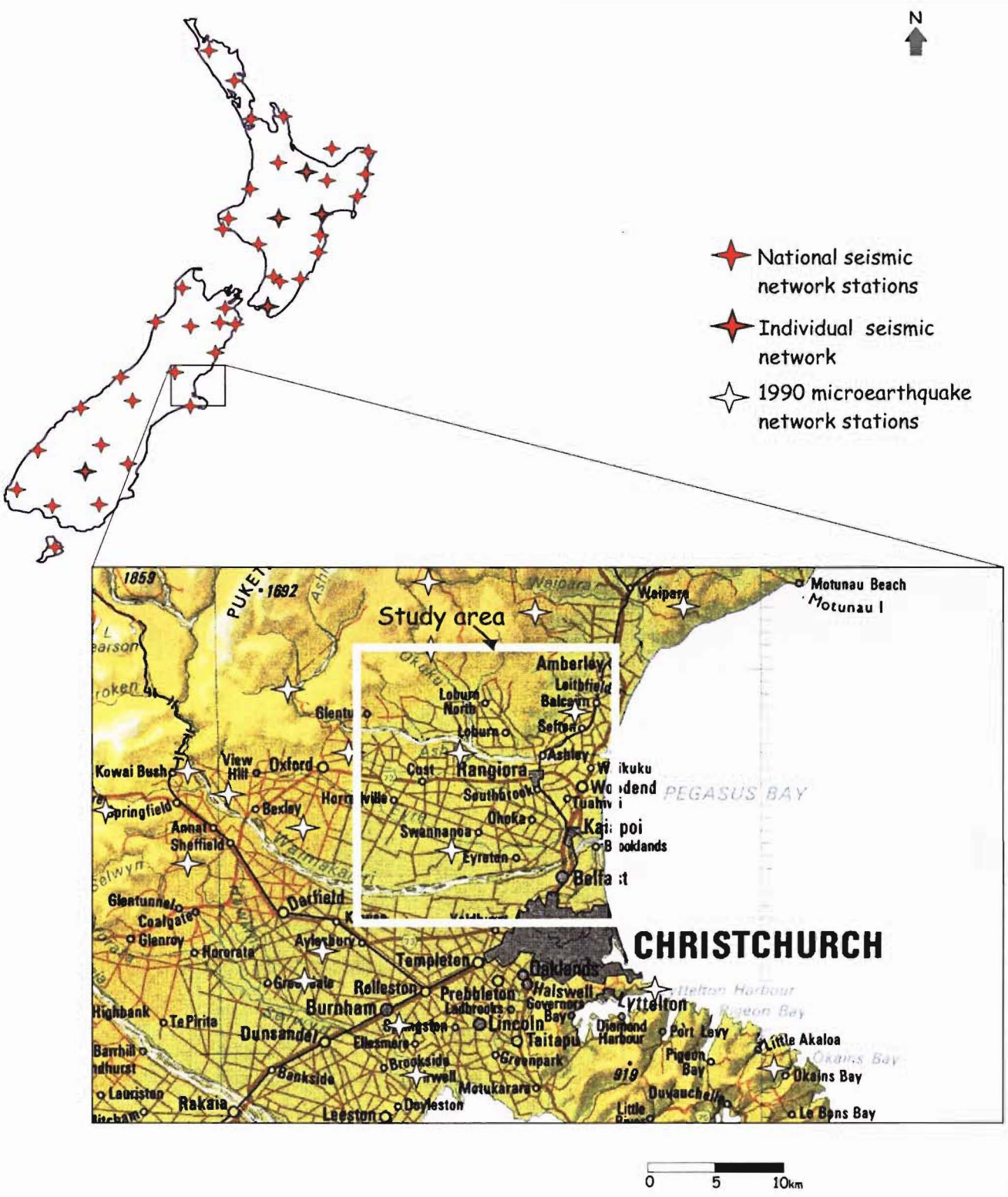

Figure 3.6: Location of the GNS network (red stars) and the 1990 microeartharquake network (white stars) with respect to the study area (white square). The location of the GNS network was obtained from Anderson and Webb (1994), and the location of the 1990 microearthquake network was extracted from Cowan (1992).

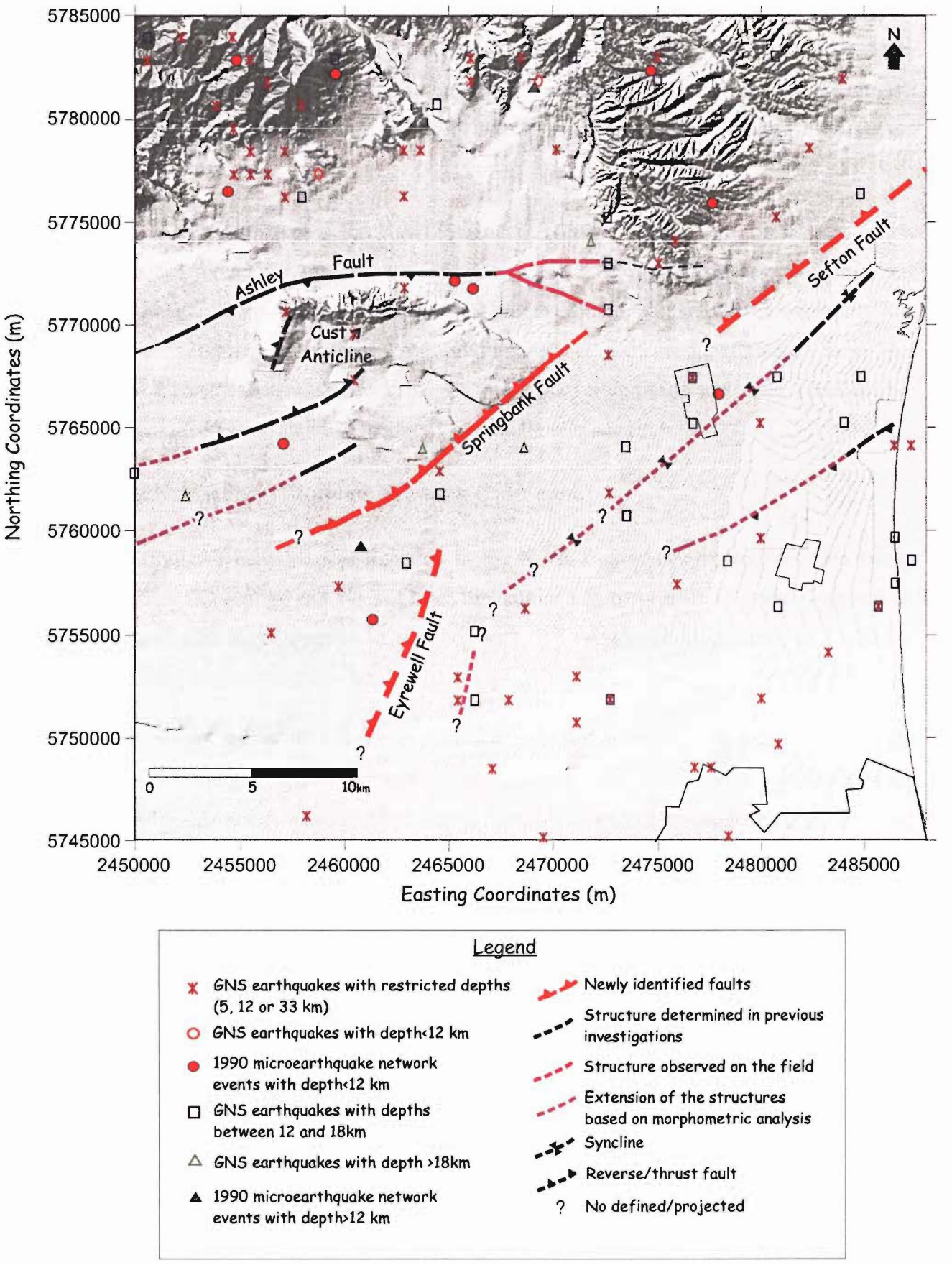

Figure 3.7: Earthquakes in the study area registered by GNS and the 1990 microearthquake network, and location of geological structures including the Springbank, the Eyrewell and the Sefton Faults.

There is another problem related to the events with restricted depths mentioned above. More than half of the registered events within the area have assigned depths of 5, 12 or 33 km, but these depths do not correspond to their actual depths, and any attempt of relating this event to the structures is useless.

McGinty (2001) reconstructed the New Zealand earthquake catalogue to be used in a new seismic hazard model for the country. McGinty developed a methodology to assign new depths to those events with restricted depths. The new methodology split the seismicity into overlying and subducting plate zones, but it did not relocate the events within each zone. This is adequate for use in seismic hazard analysis, but it is of little use in assigning a relationship between earthquakes and faults (McGinty, *personal communication*, 2002)

3.3.1.2 1990 Microearthquake Network Catalogue

A microearthquake network was installed in the North Canterbury region (between Banks Peninsula, Lake Coleridge and Waiau) from September 1 to November 15, 1990 (Figure 3.6). 24 portable digital seismographs were used, with an average station spacing of 15-20 km (Cowan, 1992; Reyners and Cowan, 1993;).

The study area for this project was completely surrounded by this microearthquake network. The station distribution with respect to the study area, together with the short spacing between stations, allowed good quality hypocentral locations and the determination of focal mechanisms for many earthquakes.

The microearthquake network registered 12 events within the study area (Figure 3.7). More than 80% (10 earthquakes) have hypocentral depths of less than 12 km. The rest, less than 20% (two earthquakes) have hyopocentral locations deeper than 18 km (Figure 3.7). An aseismic zone between 12 and 17 km was detected under most of the north Canterbury region and has been related to a mid-crustal decollement (Cowan, 1992; Reyners and Cowan, 1993).

The earthquake hypocentres determined from the microearthquake network significantly differ from those determined from the GNS database. Figure 3.8 shows a comparison between the hypocentral distribution on both catalogues. According to the data registered in the microearthquake network, most of the earthquakes within the study area can be related to structures in the upper crust. In contrast, the data in the GNS database, suggests that the earthquakes in the study area are related to structural process in the lower crust.

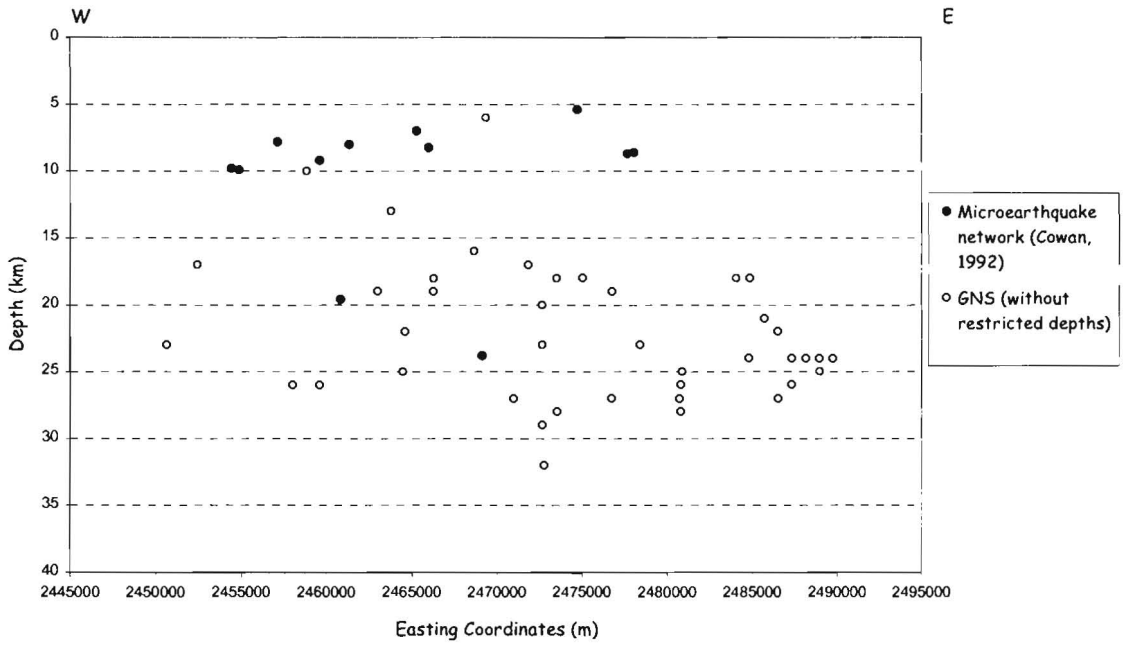

(A)

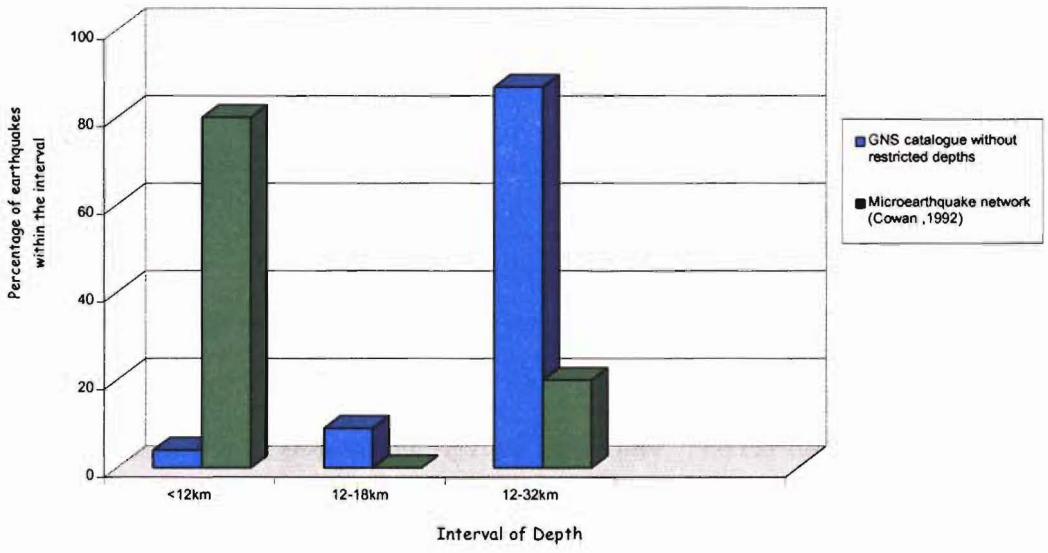

(B)

Figure 3.8. (A). Cross-section of the study area showing the distribution at depth of the earthquakes registered by GNS (empty circles) without restricted depths, and by the 1990 microearthquake network (solid circles). The total earthquake activity is projected on the cross-section. (B) Histogram showing a comparison between the hypocentral distributions of the earthquake activity registered by GNS (blue) and by the 1990 microearthquake network (green).

3.3.2 ANALYSIS OF FOCAL MECHANISMS

Eleven focal mechanisms solutions out of the twelve events recorded by the 1990 microearthquake network within the study area were determined by Cowan (1992). The fault plane solutions were derived from the P-wave first motion polarities recorded at different stations (Appendix 3). The solutions were assigned to different categories of confidence based on how tightly the nodal planes are constrained by the recorded motion (Cowan, 1992).

Focal mechanism denoted in Figure 3.9 as 7, 10 and 11 correspond to the highest quality. The other solutions are not very well constrained (Cowan, 1992). A summary of the type of faulting indicated by each focal mechanism is presented in Table 3.3.

Table 3.3: Description of the type of faulting indicated by the eleven focal mechanisms obtained by Cowan (1992) in the study area.

	FOCAL MECHANISM	COMMENTS
STRIKE SLIP	1,7,9,10, and 11	If the fault generating the earthquakes is assumed to have ENE strike, then these focal mechanisms indicate a right lateral displacement.
REVERSE SLIP	8	Focal mechanism 8 appears to be directly related to the Ashley Fault.
OBLIQUE SLIP	2, 3, 4, 5 and 6	Events 2, 4 and 6 correspond to strike slip displacement with a significant normal component. Events 3 and 5 indicate strike slip displacement with a significant reverse component.

The focal mechanism 3 is of special interest for this study. The earthquake location seems to be directly related to the newly identified structure at the southeast of the Springbank Fault, the Eyrewell Fault. The earthquake was generated at a depth of 8 km and about 2000 m west of the projection of this fault at the surface, which indicates that with a fault plane dipping 70° to 80° to the west, the Eyrewell fault could be the causative structure of this event. The focal mechanism of this microearthquake corresponds to strike slip displacement with a significant reverse movement component. One of the nodal planes corresponds to plane trending N22°E which strongly coincides with the strike of the newly identified structure. Consequently, if this nodal plane is related to the fault plane, the focal mechanism indicates a reverse fault with a strong left-lateral displacement.

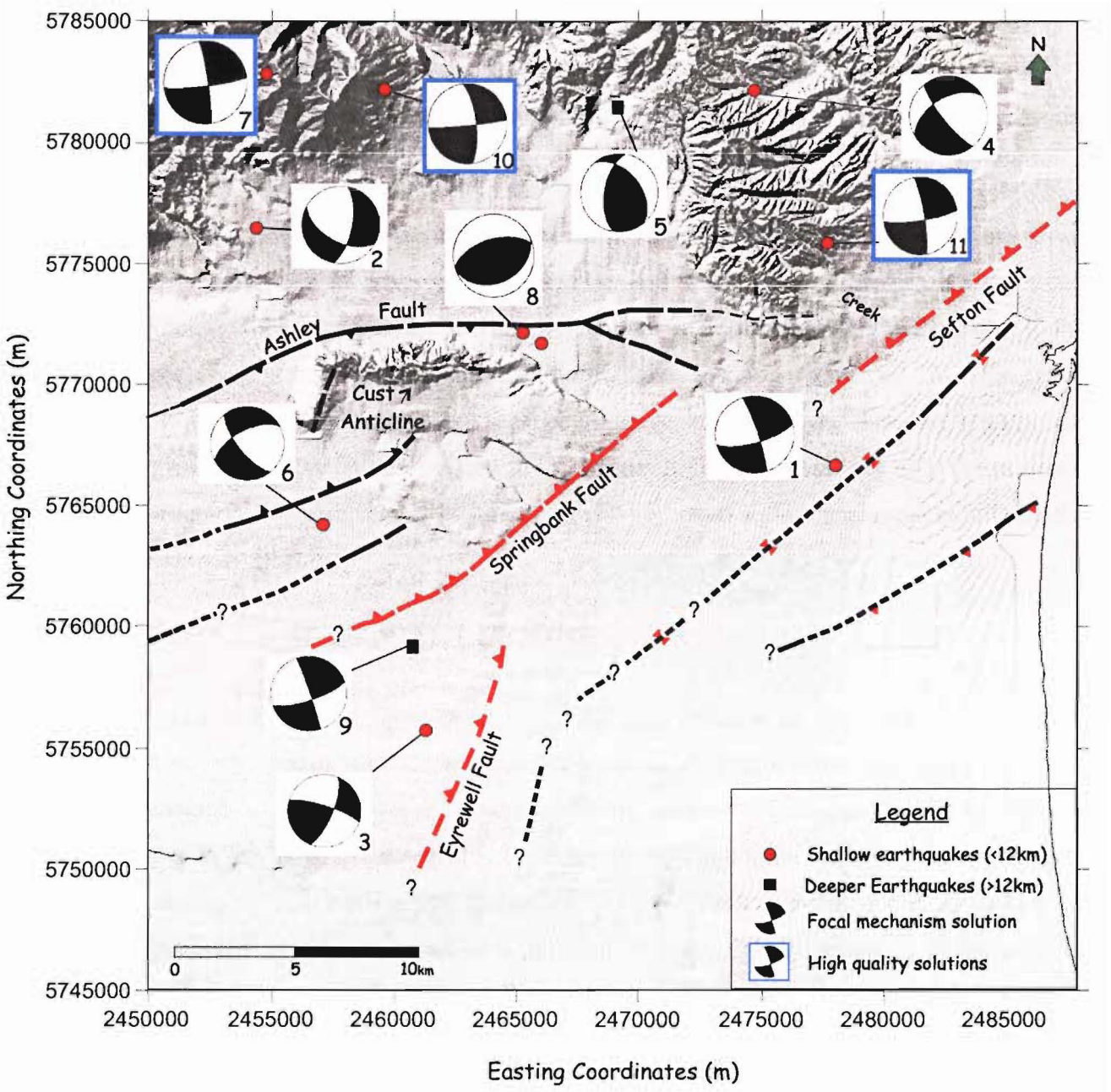

Figure 3.9: Focal mechanism obtained by Cowan (1992) in the study area, and location of geological structures. Focal mechanism framed in blue correspond to high quality solutions.

Nevertheless, the fault plane determined from the focal mechanism solution 3, obtained by Cowan (1992), is dipping 71° to the southeast, rather the actual fault plane that must dip to the northwest according to the seismic interpretation of the North Eyre Road seismic line 2. This discrepancy may be related to the quality of the solution. A nodal plane (fault plane) dipping to the northwest can also fit the data related to the P-wave first arrivals, or alternatively, this mechanism could be related to a backthrust off the Eyrewell Fault.

The seismicity registered by both networks confirms the presence of active tectonic structures within the area. For the purposes of correlation between earthquakes and causative structures, the 1990 microearthquake network is more reliable due to its configuration with respect to the study area. The good quality of the earthquake locations obtained in this 1990 microearthquake survey confirms the presence of active structures very close to Christchurch. The microearthquake tentatively related to the Eyrewell Fault suggests not only the presence of this structure, but also that it is active which may have significant implications for the seismic hazard of the city.

3.4 SUMMARY AND CONCLUSIONS

The Springbank Fault was discovered in 1998 when Indo-Pacific Ltd carried out seismic reflection surveys across the North Canterbury Plains. A seismic line undertaken on Tram Road indicated a major reverse structure dipping ~60° to the northwest. The seismic stratigraphy in this profile showed that the Springbank Fault does not reach the surface but that it is associated with a broad fold that affects the top reflectors of the profile. Jongens et al. (1999) concluded that the deformation associated with this fold commenced in the early to mid-Pleistocene.

Backthrust structures and the location of a fold backlimb 14 km away from the fault were also identified occurring to the northwest of the Springbank Fault.

Two new seismic profiles were undertaken as part of this study in order to supplement the information extracted from the Indo-Pacific seismic line. Two shallow reflection surveys (<600 m depth) were carried out along Boundary Road, north to the Indo-Pacific seismic line, and along North Eyre Road, to the south.

The seismic profile obtained in Boundary Road clearly illustrates the Springbank Fault-related fold, but the fault itself is not well imaged. The characteristics of the fault-related fold

observed in this profile differ from those observed in the Indo-Pacific seismic line. The fold at Boundary Road appears to be less developed than at Tram Road (Indo-Pacific seismic line). The Springbank Fault-related fold development appears to be a maximum close to the middle point of the fault where is topographical expression is also maximum.

The seismic line obtained along North Eyre Road, to the south of Tram Road, does not show either the Springbank Fault, or its related fold, but circumstantial evidence clearly indicates the presence of a reverse structure to the east. This profile confirms the results obtained from the morphometric analysis along the rivers presented in Chapter 2. The Springbank Fault changes in strike from its northeast orientation at the Tram Road to an east-northeast orientation toward the south, and supports the newly proposed structure (the Eyrewell Fault), identified to the southeast of the Springbank Fault.

The two earthquake databases analysed here, the earthquake database compiled for the Institute of Geological and Nuclear Sciences (GNS), and the database recorded by a microearthquake network installed by Cowan et al. (1990) present different characteristics with respect to the study area. According to the data comprising in the GNS database, the earthquakes in the study area are related to processes in the lower crust. In contrast, the more accurately located earthquakes registered in the 1990 microearthquake network, suggests that most of the microseismic activity within the study area is related to structures in the upper crust.

Due to the better station coverage with respect to the study area, and the short spacing between stations, the earthquakes recordered by Cowan et al. (1990) have better hypocentral locations. This also allowed the determination of 11 focal mechanisms within the study area (Cowan, 1992).

The good quality of the earthquake locations obtained in the microearthquake survey confirms the presence of active upper crustal structures within the study area, including the Eyrewell Fault.

Chapter 4

SPRINGBANK FAULT EVOLUTION AND STRUCTURAL MODEL

4.1 INTRODUCTION

The general character of the Springbank Fault and the presence of two new structures, the Eyrewell Fault and the Sefton Fault, have been identified in the study area based on geomorphology, drainage analysis and geophysical investigations. These three structures correspond to reverse/thrust faults with slightly different geometric characteristics, each structure is probably associated with folding on their upthrown (hanging wall) side but they have different strike lengths and orientations.

The purpose of this chapter is to establish a geological/structural evolution model for the Springbank Fault and its associated fold, and its relation to the newly identified faults and the other structures in the study area.

The chapter includes:

1. An explanation of the development of the Springbank Fault and its associated fold based on fault growth theories
2. A classification of the Springbank Fault-related fold by comparing the fold geometry with different fold structural models
3. Computer fold modelling in order to establish the fault parameters that may produce a fold with the particular geometry observed in the Springbank Fault-related fold
4. Estimation of further fault characteristics based on the fault-related fold features
5. Relationship between the Springbank Fault and other structures in the area; and
6. A structural evolution model for the Springbank Fault.

4.2 FAULT GROWTH AND FOLDING

The information analysed in the previous chapters suggested that the Springbank Fault and its associated fold are dying out toward both the northeast and the southwest direction, and that the combined (fault and fold) related displacement is a maximum close to the midpoint of the structure, at their maximum topographic expression. This characteristic is consistent with different theories that propose that faults originate at a point and grow radially (Williams and Chapman, 1983) or laterally (Scholz, 1990) with accumulated slip.

Different studies indicate that faults increase their length through repeated earthquakes (Walsh and Watterson, 1988; Jackson et al.,1996; Burbank and Anderson, 2001). A bow-shaped displacement variation has been identified in theoretical prediction, laboratory experiments and other field studies (Burbank and Anderson, 2001). The bow-shaped model suggests that there is no displacement at the fault tips, but the displacement gradually increases until it reaches a maximum near the midpoint of the fault (Figure 4.1).

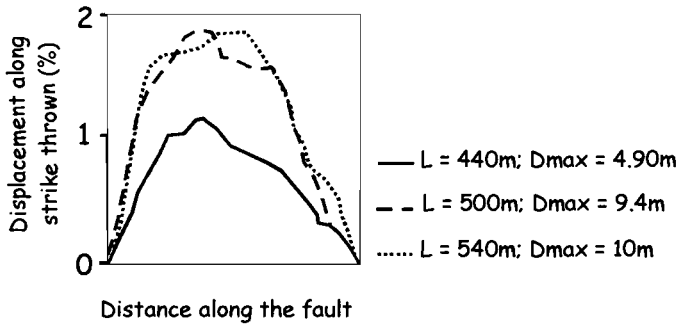

Figure 4.1: Schematic representation of displacement versus distance along fault traces on normal faults of different lengths (440, 500 and 540m) where the characteristic bow-shaped displacement variation is illustrated (modified form Burbank and Anderson, 2001).

Similarly, Elliot (1976) showed that in plan view, thrust faults increase in length as they increase in translation and that the maximum displacement generally occurs near the middle point of the fault (in Williams and Chapman, 1983), although the distribution of displacement over the fault plane can be variable and affected by factors such as interaction with adjacent faults.

The geometric characteristics of the Springbank Fault and its associated fold, indicate that the fault is growing in both the vertical and lateral direction and that the displacement is

maximum close to its middle point. This interpretation is based on the seismic profiles, on the preservation of elevated topography and on the diversion of drainage away from the central section of the fault. The analysis also suggests that the fold is asymmetric and has a substantial displacement toward the northeast.

4.3 FOLD CHARACTERISTICS

In the next section, the characteristics of the Springbank Fault associated fold will be explained and related to different fold models in order to classify the structure. The fold geometry will be used in turn to establish further features of the Springbank Fault at depth.

4.3.1 FAULT-RELATED FOLD MODELS

Different models have been proposed to explain the origin and shape of folds related to blind thrust/reverse structures such as the Springbank Fault. The main models include fault-bend folds (Suppe, 1983), fault-propagation folds (Suppe and Medwedeff, 1990), detachment folds (Jamison, 1987), and trishear folds (Erslev, 1991), (Table 4.1).

The importance of these models is that they relate fold shape (observable in the field or from geophysical studies) with the geometry of the blind fault (sometimes not even observable in geophysical investigations), which is an essential parameter in seismic hazard analysis.

Choosing the model that explains the fold and consequently the characteristics of the underlying fault is relevant because different models result in different fault geometry solutions, which has direct implications in seismic hazard assessment. In the same way, one model cannot explain every example of fold geometry (Thorbjornsen and Dunne, 1997).

In order to determine which fault-related fold model best explains the characteristics of the Springbank Fault-related fold, a brief description of the main models is presented in Table 4.1, together with a comparison between the fold model features and the observed features of the Springbank Fault-related fold.

The characteristics of the Springbank Fault-related fold are extracted from both the geomorphological mapping and mainly from the geophysical studies (i.e. Indo-Pacific seismic line and Boundary Road seismic line 1 of this study).

Table 4.1: Comparison between the main fault-related fold models and the Springbank Fault-related fold (all figures from Burbank and Anderson, 2001).

MODEL	BRIEF DESCRIPTION OF THE MODEL	SPRINGBANK FAULT-RELATED FOLD CHARACTERISTICS	
		For	Against model
Fault-bend fold (Suppe, 1983)	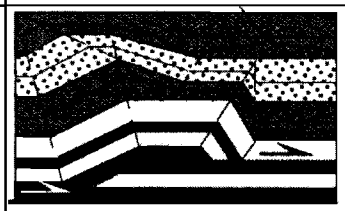 -Symetric folding caused by deformation over a ramp of a non-planar thrust fault, which consists of a flat-ramp-flat transition. -The resulting fold develops straight limbs and narrow axial zones known as kink-band geometry.	- N/A	-The Springbank Fault-related fold is asymmetric. - The Springbank Fault is not a flat-ramp-flat structure. - The fold does not present kink-band geometry.
Classical fault-propagation fold (Suppe and Medwedeff, 1990)	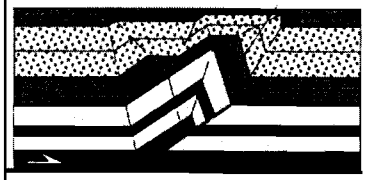 -Asymmetric folding caused by a blind fault with changing dip. -Displacement is not constant along the fault. -The forelimb dip does not vary during the process. -The up dip projection of the thrust terminates at the syncline. -An extensive backlimb is present and is the consequence of a change in fault dip from low to high angle. -Kink-band geometry.	- Springbank Fault associated fold is asymmetric. - The Springbank Fault changes dip. -No evident variation in forelimb dips.	-Not topographical evidence of backlimb, but seismic reflection surveys and morphometric analysis indicate its existence. -No kink-band geometry.

Model	Brief description of the model	Springbank Fault-related fold characteristics	
		For	Against model
Detachment fold (Jamison, 1987)	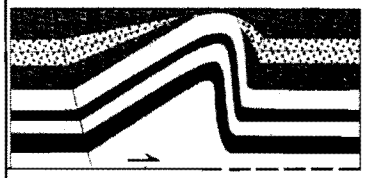 -Either symmetric or asymmetric folding produced above a fault that is parallel or subparallel to original layering. -Fold grows because displacement dies out toward a fault tip.	-N/A	- The Springbank Fault is, according to the seismic profiles, a high angle structure with a fold associated with the fault tip. Consequently, the fault associated with the Springbank Fault does not correspond to a detachment structure.
Break-thrust fold (in Woodward, 1997)	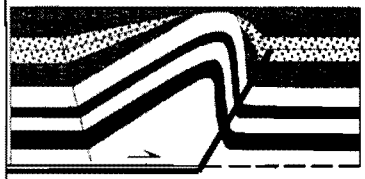 -Asymmetric folding that is cut by a fault propagation. - The fold may begin as a detachment fold and continues grow by folding ahead a propagation fault. -When the fold develops a close interlimb angle it locks, and is cut by a ramping thrust.	-N/A	-The fold is developing at the up dip propagating fault tip and is not entirely cut by the fault. - The fold interlimb angle is open.

Model	Brief description of the model	Springbank Fault-related fold characteristics	
		For	Against model
Trishear fold (Erslev, 1991)	Growth triangle trishear zone Velocity vectors 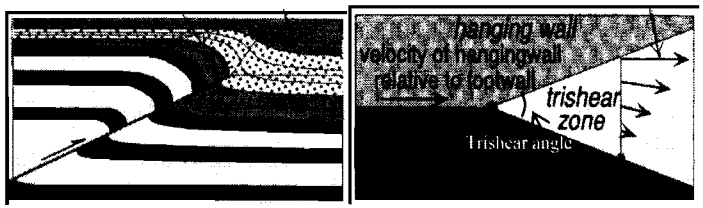 -Trishear folding develops when a triangular zone of distributed shear (trishear zone), which is symmetrical with respect to the dip of the fault, propagates ahead of the fault tip. -A differential slip (variations in both orientation and magnitude) occurs within the trishear zone (see figure above). At the top, slip vectors are equal to the master fault but they decrease progressively in magnitude until no-slip on the lower boundary of the trishear zone. -The relative rate of fault tip propagation (P) to fault displacement (s) causes both bed thickness and forelimb dips to change with fold growth. -This model does not require change in fault dip or the presence of any decollement, or regional back dips. -The up dip projection of the thrust terminates at the syncline.	-The monoclinal shape of trishear fold is very similar to the observed shape of the Springbank Fault associated fold forelimb.	- The Springbank Fault-related fold does not present significant variation in both bed thickness or forelimbs dips that are required for the model.

As illustrated in Table 4.1, none of the ideal geometries of the different models accurately describes the geometry of the Springbank Fault-related fold. The fold fits the general definition of a fault propagation fold given by Suppe (1985), in which a fault propagation fold is a deformation that takes place in front of the propagating fault plane, and in which the displacement on the fault is transferred to the fold with amplitude increase (Suppe, 1985; Couzens and Dunne, 1994). Of the models analysed, the classical fault propagation fold, defined by Suppe and Medwedeff (1990) and the trishear model defined by Erslev (1991), are fault propagation folds as defined by Suppe (1985).

A combination between the classical fault propagation fold and the trishear fold, satisfactorily explains the geometry observed in the Springbank Fault associated fold. The fold has the general shape of a trishear fold and some characteristics of the classical fault propagation fold model. The general geometry of the leading edge of the fold (forelimb), a broad flexure with open interlimb angles, strongly resembles a trishear fold, but the relatively straight limbs are associated with the classical fault propagation model.

An interdependency between the trishear model and the classical fault propagation model is possible as indicated by several studies (i.e Erslev and Mayborn, 1997; Allmendinger, 1998; Johnson and Johnson, 2002; Cardozo et al.,2003).

Allmendinger (1998) developed a computer program for trishear fold modelling based on initial parameters such as fault dip, fault tip location, fault slip, angle of trishear and tip propagation to slip ratio (P/S). He found that the shape of a fault propagation fold is directly related to the P/S ratio, which determines how rapidly the tip line propagates relative to the slip on the fault itself. Allmendinger's computer experiments showed that with some changes in the P/S ratio, trishear folds are completely compatible with the classical fault propagation model described by Suppe and Medwedeff (1990).

Changes from low P/S to high P/S, increase the propagation of the tip. Higher P/S ratios result in more open and gentle folds. Low P/S values produce fold geometry with relatively straight limbs and narrow rounded axial zone, which can be defined as the kink surface described by Suppe and Medwedeff (1990). Furthermore, when changes in the dip of the fault are introduced to the trishear fold computer model, the resulting fold is analogous to the fold geometry and kinematics described in the classical fault propagation model of Suppe and Medwedeff (1990).

Additionally, Johnson and Johnson (2002) demonstrated that trishear-like folds form in isotropic material and kink-like parallel folds in anisotropic viscous material. According to their study, anisotropy in the sedimentary cover has a significant influence on the fold geometry and can determine a trishear-like or a classical fault propagation-like geometry. The forelimb in isotropic cover increasingly thickens upward from the tip of the fault where the limbs are steeper, to the top surface where the limbs are shallower, producing a trishear geometry. In anisotropic cover, the forelimb is essentially of constant width and dip, resembling a kink fold with rounded hinges (Johnson and Johnson, 2002).

Cardozo et al. (2003) also indicated that different material characteristics (i.e. experimental incompressible material and compressible frictional materials) results in different fold styles. Trishear styles are produced with incompressible material, and compressible frictional materials produce a fold with similar characteristics to the classical fault propagation fold.

Consequently, a fold is the result of several parameters not only related to the characteristics of the underlying fault but also to the characteristics of the surrounding rocks. A specific combination of, or changes among different factors result in different fold shapes.

The theoretical fold models do not involve all of these parameters. The specific mixture of the Springbank Fault characteristics and the particular features of the sedimentary cover, within which the propagation fold develops, cannot be quantified and nor it is possible to incorporate them in any purely geometric model, and as a result, neither of them can accurately explain the geometry of the fold.

Nevertheless, the model that most closely explains the characteristics of the Springbank Fault propagation fold is the trishear fold. Therefore, the program developed by Allmendinger (1998, 2003), Trishear 4.5.4, was used to search for the combination of fault and trishear fold parameters that would produce a fold with similar characteristics to the Springbank Fault propagation fold.

4.3.2 FOLD MODELLING USING TRISHEAR 4.5.4 SOFTWARE

The program developed by Allmendinger (1998, 2003) for modelling trishear folds was used to estimate the parameters that may produce the Springbank Fault propagation fold. The geometry of the fold in the Indo-Pacific seismic line was used for this analysis.

There are five main parameters that define a trishear geometry: (1) trishear angle, (2) fault slip, (3) fault dip, (4) propagation to slip ratio, P/S, and (5) fault tip location. P/S and trishear angle are the parameters with more influence in fold shape, but of the two, P/S is more important (Allmendinger, 1998).

The Trishear program applies an inverse method to estimate the parameters that produce a particular fold geometry. The determination of all parameters can be made by a numerical grid search in which the computer finds the statistically best-fitting combination of parameters within predetermined grid values (Allmendinger and Shaw, 2000). The result is the best particular combination of values that returns the strata to an original linear orientation (Allmendinger, 1998, 2003). Then, a forward method should be applied to compare the match between the fold created with the modelled combination of values and the actual fold characteristics.

4.3.2.1 Springbank Trishear Fold Parameters

The seismic stratigraphy observed in the Indo-Pacific seismic line was used as an input for the Trishear program following the procedure explained in Allmendinger (1998). The grid search finds the best-fit for a single horizon trace that is the reflector determined with most confidence. In the Indo-Pacific seismic line, a reflector within the Kowai Formation was chosen as the best horizon for modelling the geometry of the Springbank Fault propagation fold. This reflector corresponds to reflector 2 in Figure 4.2.

The Trishear program was run several times testing each time about 8,000 combinations of fault dip (between 50° and 70°), tip line position, slip (0 and 1000 m), trishear angle (between 20° and 120°) and P/S (1-10). Some of the best fitting models are presented in Figure 4.2.

It was decided that model 1 represents the best combination of parameters because it is the model that best matches the reflector 2 and because the modelled fault dip (60°) corresponds to the dip observed in the Indo-Pacific seismic line. The fault slip in this model is about 300m, the propagation distance of the tip line is 2,100 m, the P/S is 7 and the best fit trishear angle is 90°.

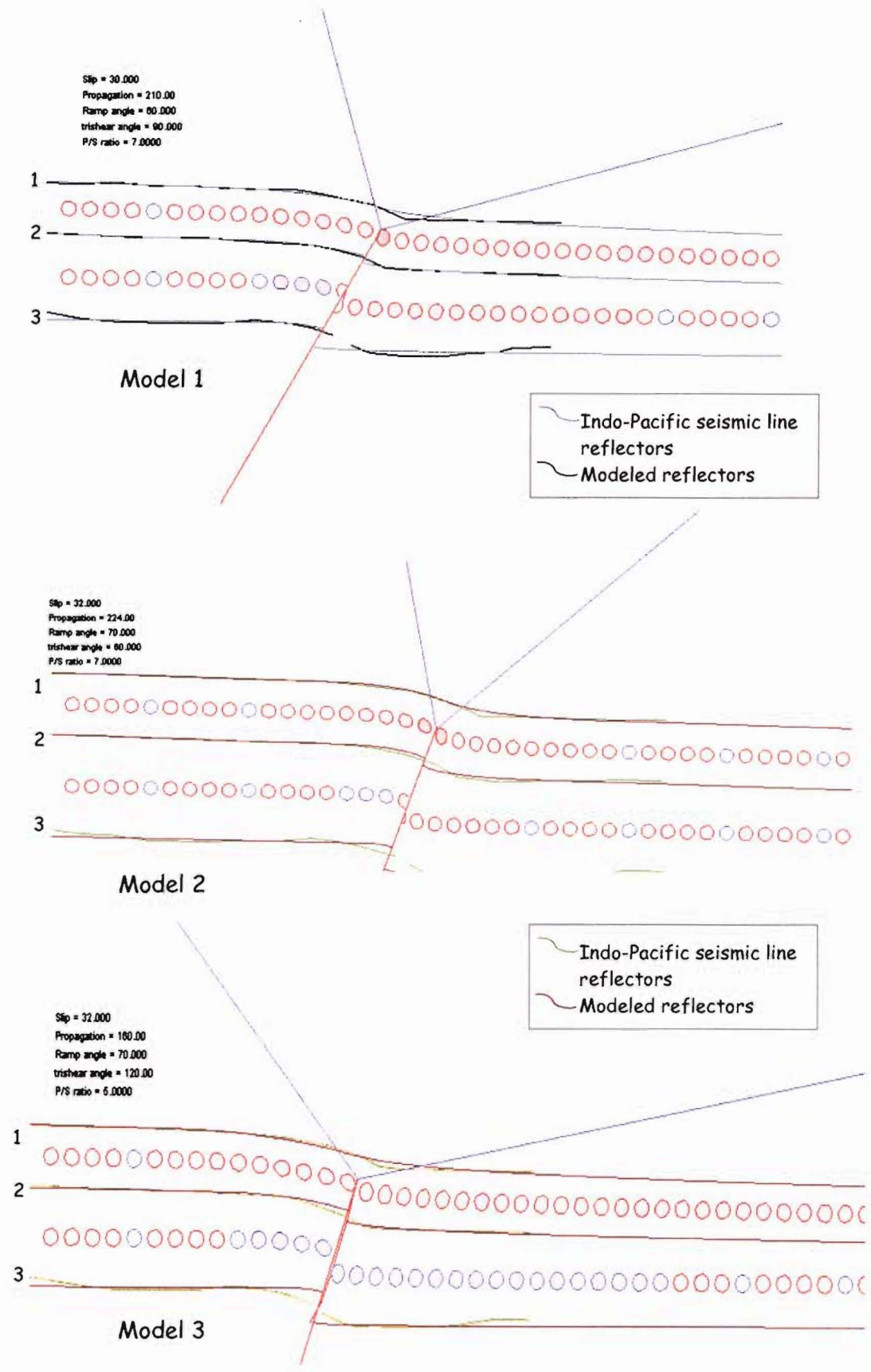

Figure 4.2: Different combination of values representing the best-fit of trishear parameters for modelling the Springbank Fault propagation Fold. Model 1 presents the best match for the reflector 2, used as a key horizon.

With the modelled parameters it is possible to reconstruct the position of the fault tip before the estimated slip was produced. According to the model, the tip of the Springbank Fault before it produced the estimated slip of 300m was located at an approximate depth of 2.2 km (based on the projected tip propagation along the fault plane (2,100m) and the present location of the fault tip, ~400 m).

Geometric relationships between the fault plane and the propagation fold dimensions can be used independently to estimate the fault slip, and confirm the slip calculated with the Trishear program. According to the fault propagation fold definition, a main feature of this type of folding is that folding and faulting occur synchronously. Before the emergence of the fault to the surface, the fault slip is completely accommodated by increase in fold amplitude without transfer of slip out of the fold (Couzens and Dunne, 1994). Consequently, there is a direct geometric relationship between the vertical throw of the fold (z) and the slip of the fault (s) (Figure 4.3).

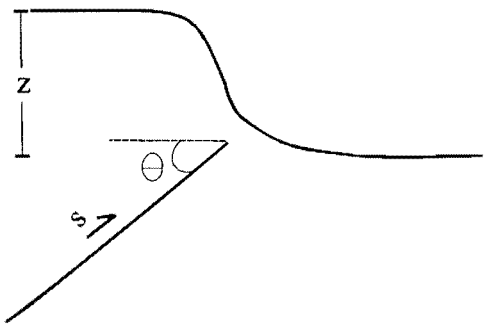

$$\sin\theta = \frac{z}{s}$$

$$\therefore s = \frac{z}{\sin\theta} \qquad (1)$$

Figure 4.3: Geometric relationship between fault and propagation fold parameters. Where θ is the fault dip, z is the vertical throw, and s is the fault slip.

From the Indo-Pacific seismic line, conducted at Tram Road, it is possible to determine a dip (θ) of 60°, and a vertical throw (z) between 250 and 300m in the top reflectors. The application of (1) in Figure 4.2, gives as a result a fault slip between 290 and 350m at this location, which is consistent with the 300m slip found with the Trishear program.

4.3.2.2 Springbank Fault Propagation Fold Backlimb

Backthrust structures and a fold backlimb associated with the Springbank Fault have also been recognized from the Indo-Pacific seismic line and from the morphometric analyses along rivers. The seismic stratigraphy indicated that the Springbank Fault propagation fold is a broad structure whose backlimb is located approximately 14 km away from the forelimb.

The development of a fold backlimb is associated with changes in fault dip. There is a direct correlation between the depth at which the change in dip occurs and the location of the backlimb. If the change in dip is shallow, the backlimb will develop close to the forelimb of the propagation fold. The deeper the change in dip, the farther away the location of the backlimb with respect to the forelimb.

Different fold models such as the fault bend fold and the classical fault propagation fold described by Suppe (1983) and Suppe et al. (1986), also show that the axial plane of the synform related to the fold backlimb projects to the change in slope on the fault plane. Trishear folds also present this characteristic with a fault dip change.

Therefore, the Trishear program (Allmendinger, 1998) was used to estimate the depth of the fault dip change along the Springbank Fault to develop a backlimb ~14 km away from the forelimb. The combination of parameters established from model 1 (section 4.3.2.1) was used as an input for the calculation (Figure 4.4).

According to the results (Figure 4.4), in order to develop a fold with the geometry observed in the Indo-Pacific seismic line, a fault (dipping 60, with a P/S of 7 and a trishear angle of 90°), would propagate from a pre-existing horizontal decollement located at a depth of ~14 km.

A subhorizontal decollement with similar characteristics has been inferred by several authors (Norris et al.,1990; Cowan, 1992; Nicol and Wise, 1994; Reyners and Cowan, 1993) under the Canterbury Plains. Furthermore, the microseismicity study carried out by Cowan (1992) indicated that the decollement is located within a ductile or aseismic zone situated between 12 and 17 km deep in the study area, which is consistent with the location of the decollement estimated with the Trishear program.

The morphometric analysis along the rivers in the study area (Chapter 2) also indicated a broad zone of deformation related to the Eyrewell and Sefton Faults. It was suggested then that this zone was the expression of backthrusts or fold backlimb associated with the faults.

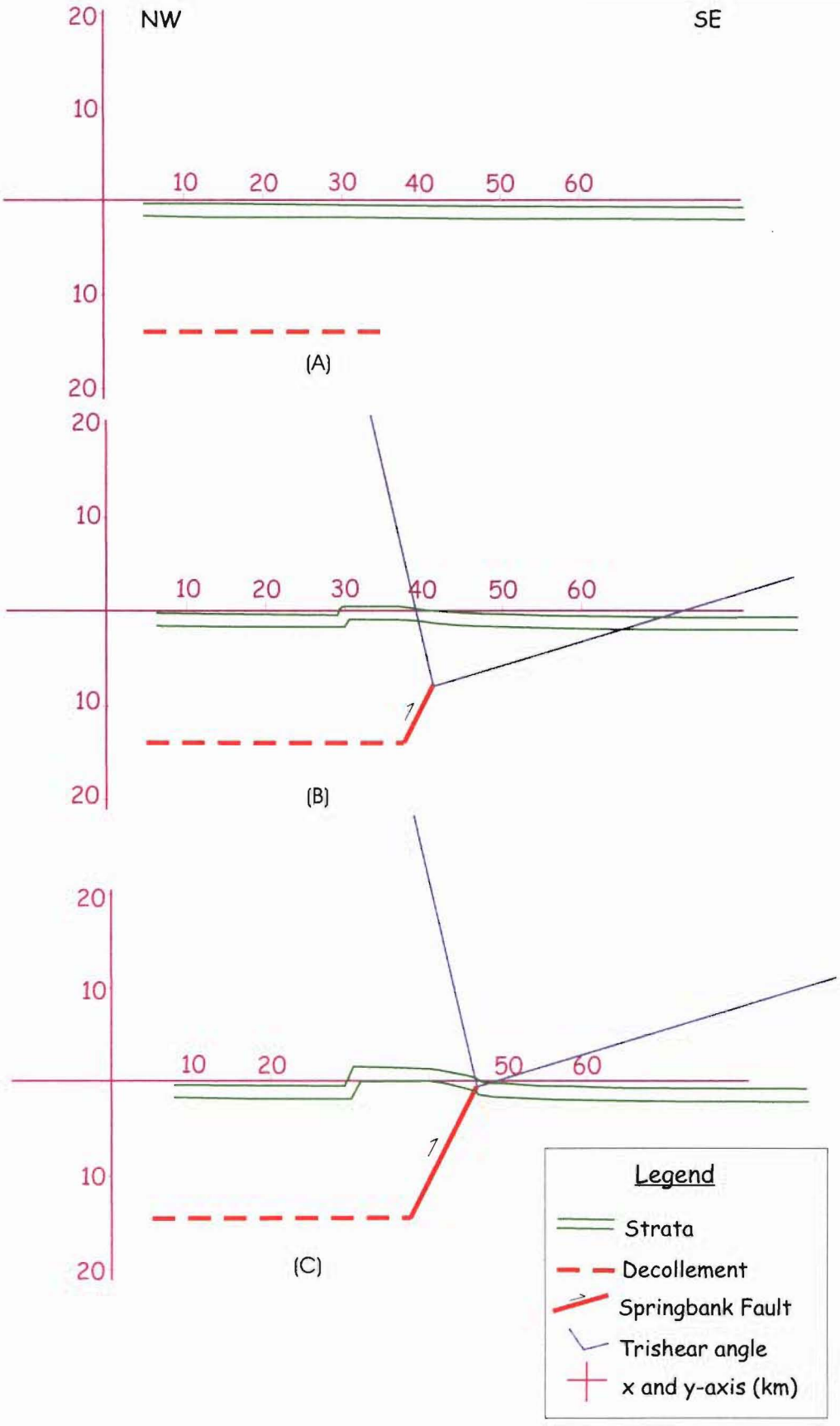

Figure 4.4: Illustration of different stages during the Springbank Fault propagation from a decollement located about 14 km deep (according to the Trishear program). (A) shows the original linear orientation of the layers without deformation. (B) shows an intermediate stage during the gradual deformation, and (C) illustrates the present situation in which the actual geometry of the Springbank Fault propagation fold is achieved.

The distance between the fault locations and the end of the deformation zone, is approximately 13, 12 and 12 km in the Cust, Eyre and Waimakariri Rivers, respectively. This suggests that, as for the Springbank Fault, the broad zone of deformation associated with the Eyrewell Fault, closer to Christchurch, may correspond to a broad fault propagation fold. Additionally, the dimensions of this fold are similar to those in the Springbank Fault, which suggests that the Eyrewell and Sefton structures are also propagating from the decollement zone located between 12 and 17 km.

4.3.3 GROWTH STRATA AND TIME OF DEFORMATION

The following analysis is based on the classical fault propagation fold characteristics apparently observed in the Springbank Fault propagation fold. According to Suppe et al. (1992), in a propagation fold, limbs increase in length as the fold grows, but if sedimentation takes place during the growth of the fold, the limb length will decrease upwards within the strata deposited during the deformation (growth strata). Fold geometry changes within the growth strata. Fold axial surfaces narrow from a constant width in the pre-growth strata (sediments deposited before deformation begins) to zero width at the current surface of sedimentation. The boundary between zones of constant width axial surfaces and zones of upwards progressively narrowing axial surfaces, represents the beginning of deformation (Suppe et al., 1992). At this point, the strata before deformation (pre-growth) and strata after deformation (growth) can be differentiated. Furthermore, the apex of the upward narrow axial surfaces, also called growth triangle (Figure 4.5), marks the end of deformation.

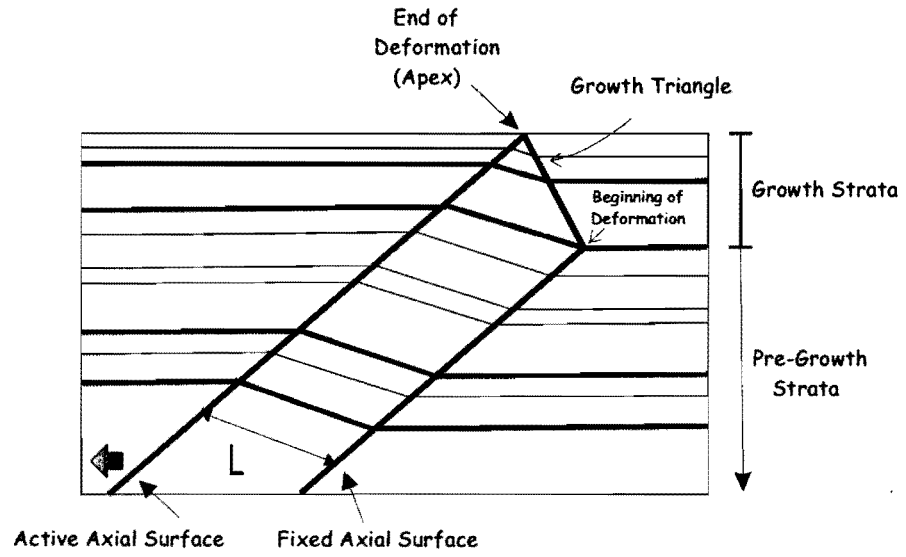

Figure 4.5: Schematic fold geometry related to growth strata (modified from Suppe et al., 1992)

Although the leading edge of the Springbank propagation fold rolls over a gently rounded monocline, as simulated by the trishear model, there are not significant changes in dip and bed thickness. This allows the determination of axial surfaces in the fold that corresponds to boundaries between regions of homogeneous dip.

Figure 4.6 illustrates the location of the axial surfaces in the profile obtained in the Boundary Road seismic line. This seismic line is used for this analysis because it is a shallow reflection survey with better resolution of the near-surface characteristics of the propagation fold than the Indo-Pacific seismic line.

The Boundary Road seismic line shows that the limb lengths represented by the reflectors below both the shot point 460 and the TWTT ~0.15s (below top of Kowai Formation) are longer than those above (Figure 4.6). At this point, the approximately constant-width axial surfaces start to decrease upwards, illustrating growth strata. This suggests that the deformation post-dates the deposition of the Kowai Formation (early Pleistocene; see section 1.5.1.2).

This is in accordance with other studies in North Canterbury (i.e. Cowan, 1992; Nicol et al., 1994). According to these authors, it is unlikely that measurable faulting and folding in the area began prior to the early Pleistocene, which represents the upper age limit of the Kowai Formation.

Unfortunately, it is not possible to establish without a doubt where the apex of the growth triangle is located because the top of the seismic profile was muted during processing (see Appendix 2). Nevertheless, the prolongation of the growth triangle lines shows that the apex may reach the surface (Figure 4.6), and, as the material at this surface is considered by Tonkin (*personal communication*, 2003) to be of Holocene age, this suggests that the Springbank Fault has been active in the last 10,000 years.

4.4 SPRINGBANK FAULT EVOLUTION AND ITS RELATIONSHIP TO OTHER STRUCTURES

The seismic profile interpretation and the morphometric analyses indicate that the geometry of the Springbank Fault close to the surface corresponds to a fault propagation fold. The data show that the Springbank Fault cuts through the sedimentary cover without reaching and rupturing the surface, and suggests that the fault flattens into a mid-crust decollement.

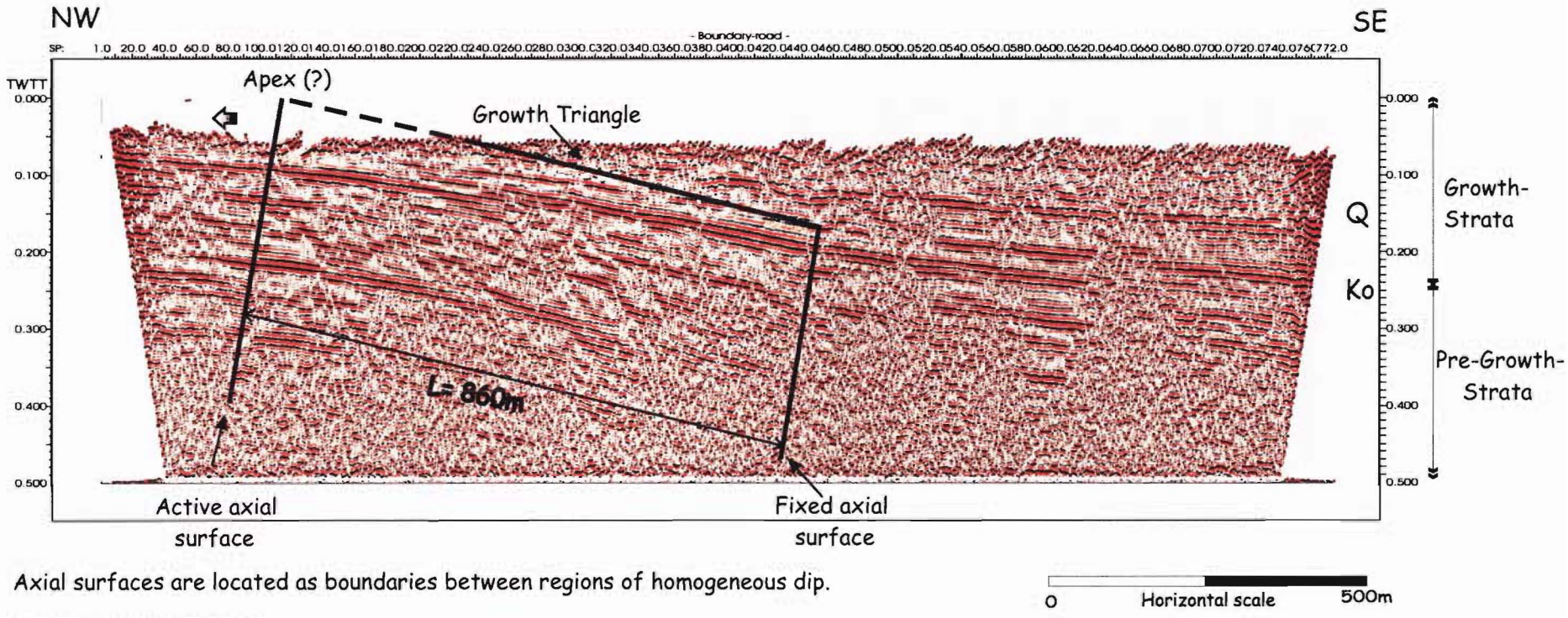

Figure 4.6: Parameters used to establish time of deformation within the Springbank Fault propagation fold. The boundary between pre-growth and growth strata illustrates the beginning of the deformation and, the apex of the growth triangle indicates the end of the deformation. See text for discussion.

The characteristics of the propagation fold suggest that the Springbank Fault is related to a decollement located at ~14 km beneath the Canterbury Plains. The propagation fold, a broad anticline whose backlimb is several kilometres away from the forelimb, was established from both the seismic profiling and the morphometric analysis along the rivers. A propagation fold with similar characteristics was also inferred from morphometric analysis for the two newly identified faults, the Eyrewell and Sefton Faults. This suggests that the three faults are related to the same basal decollement.

Consequently, the Springbank, the Eyrewell and Sefton Faults are interpreted as converging onto the subhorizontal mid-crust decollement that has previously been inferred under the Canterbury Plains by other authors (Norris et al.,1990; Cowan, 1992; Nicol and Wise, 1992).

The Springbank, the Eyrewell and Sefton Faults are directly related to the Hororata Fault, located bordering the southeast margin of the Malvern Hill, immediately to the southwest. The relationship between the Hororata Fault and the Springbank Fault has previously been proposed by Jongens et al. (1999), who suggested that these faults are correlated with a major northeast-southwest trending step in the basement at depth. The Hororata, Springbank, Eyrewell and Sefton Faults are considered to be part of the system of fold-thrust structures that are propagating eastward as backthrusts from the Alpine Fault (according to the model proposed by Norris et al., 1990).

4.4.1 SPRINGBANK FAULT EVOLUTION

According to the analysed data, it is likely that at the early stages, the Springbank Fault nucleated from the sub-horizontal decollement and gradually grew up dip and propagated bilaterally with consecutive earthquakes. Because the fault plane is dipping about 60° close to the surface, it is assumed, for modelling purposes, that the fault conserves this approximate inclination since its nucleation at the decollement.

The propagation from the decollement caused the development of the broad anticline whose backlimb may start to develop first, several kilometres away from the up dip propagating fault tip. The formation of the forelimb should have started at a later stage and is directly related to the fault tip propagation.

The deformation around the fault tip produced faulting of the prior Pleistocene materials (brittle deformation) and folding of Quaternary deposits (ductile deformation) close to the

surface. The measured deformation (~300m) associated with the propagation fold, observed in the seismic profiling and on the surface, started in the early Pleistocene (after the deposition of the Kowai Formation), as suggested by growth strata.

The Springbank Fault tip prior to this period of deformation would have been located at a depth of ~2.2 km. Later displacements in the fault, caused the propagation, accompanied by folding, of the fault tip until its actual position, at about 400m below the surface.

4.4.2 SPRINGBANK FAULT PROPAGATION FOLD EVOLUTION

The Springbank Fault propagation fold shape is controlled by the characteristics of the fault, the depth of the decollement and the characteristics of the sedimentary cover. The propagation of the fault from the decollement generated a broad propagation anticline in which the distance between the fore and backlimb is directly related to the depth of the decollement. The propagation anticline is assumed to reach its maximum amplitude close the middle point along the length of the fault, north of Tram Road.

The fold appears to experienced a progressive loss of amplitude toward the lateral tips of the fault (to the northeast and southwest), producing a double plunging anticline, as suggested by loss of surface expression, lower stream gradients and differences in fold amplitude in the seismic lines.

From its starting point at the decollement, the Springbank Fault has grown differentially, with more propagation toward the northeast than toward the southwest. This is indicated by the drainage evolution close to the maximum topographic fold expression, where the Cust River has slipped off to the north, and for an elongated topographical fold expression toward the northeast (Figure 4.7).

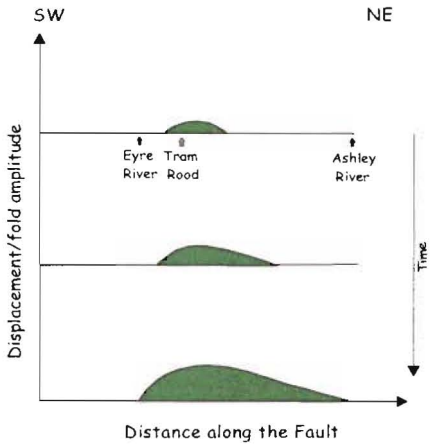

Figure 4.7: Schematic longitudinal-section of the Springbank Fault propagation fold forelimb showing differential growth toward the northeast

4.4.3 RELATIONSHIP BETWEEN THE SPRINGBANK FAULT AND OTHER STRUCTURES

The proximity of different structures such as the Springbank, Eyrewell, Sefton and Ashley Faults, the Cust Anticline, and other backthrust and minor structures, indicates complex tectonic interactions in the study area. This section contains a preliminary interpretation of these interactions.

The association of the Springbank, Eyrewell and Sefton Faults with the mid-crustal decollement located under the Canterbury Plains suggest that the three structures may have developed in a similar fashion. Unfortunately, the specific characteristics of the Eyrewell and Sefton Fault have not been established during this study. The strike of the Sefton Fault is very similar to the strike of the Springbank Fault, which suggest that these structures might be directly related.

4.4.3.1 Relationship between the Springbank, the Sefton and the Eyrewell Faults

The strong similarity between the Springbank and the Sefton Faults, regarding strike direction and topographic expression, suggests that the Sefton Fault may correspond to a part of the Springbank Fault that may have been displaced to the east by dextral strike-slip movement along the Ashley Fault (Map 2). Nevertheless, the morphometric analysis along the Ashley River did not show highly contrasting GI/K values where the interaction between the Ashley and the Springbank Fault was expected. This suggests that the Springbank Fault terminates before reaching the Ashley Fault without any direct interaction between them.

Furthermore, Holocene traces of the Ashley Fault indicate that it dies out to the east, approximately at the projected strike of the Springbank Fault. The Ashley Fault may function as a bounding transfer fault for the northern end of the upper plate of the Springbank structure (Sissons et al., 2001).

Moreover, the most recent movement on the Ashley Fault is mainly reverse instead of dextral, although Sissons et al. (2001) indicated that some indirect evidence suggest a long term dextral oblique-slip transpression across this structure.

Another alternative is that the Sefton Fault is simply another thrust/reverse structure belonging to the fault system in which the Springbank Fault is developing and that their similar orientations are the result of the tectonic regime of the area.

According to Nicol and Wise (1992), the orientation of the principal horizontal compressional stress in the North Canterbury Plains is northwest-southeast (~N50°W). These authors indicated that there has not been a significant change in this orientation since the late Pliocene-early Pleistocene (2-3ma).

An ideal model showing the orientation of different structures with respect to this direction of the principal horizontal compressional stress is illustrated in Figure 4.8. Reverse/thrust faults such as the Springbank, Sefton and Eyrewell Faults, and folds should form almost perpendicular to the stress orientation.

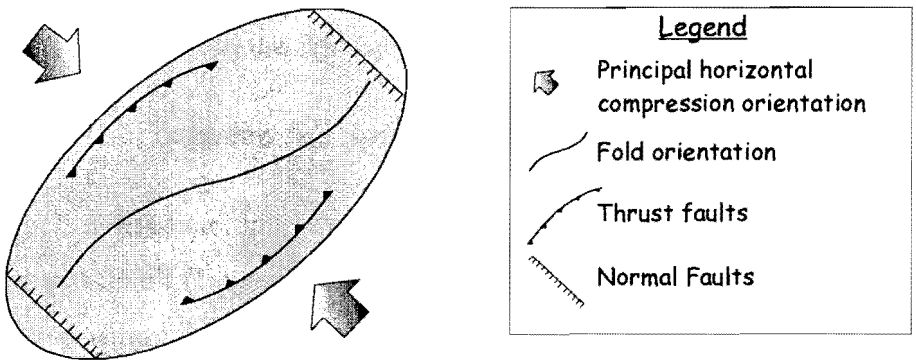

Figure 4.8: Ideal model illustrating the orientation of different structures with respect to the orientation of the principal horizontal stress (modified from Burbank and Anderson, 2001).

The Springbank (at least from north of its middle point) and the Sefton Faults are located almost perpendicular to the principal horizontal compressional stress orientation, but this is not the case for the Eyrewell Fault. The north-northeast orientation of the Eyrewell Fault could be the result of a local stress regime or the reactivation of a pre-existed structure.

However, if the structure is either formed during the current stress regime, or if it is a reactivated inherited fault, its actual sense of slip should respond to the current state of stresses. Consequently, the Springbank and the Sefton Fault should have an almost pure reverse slip, whereas the Eyrewell Faults should have an oblique displacement, with a strong left lateral component. The focal mechanism number 3 obtained by Cowan (1992) and

possibly correlated with the Eyrewell Fault (section 3.3.2) effectively corresponds to a left lateral slip.

The orientation of the Ashley Fault within the tectonic stress regime suggests that it may correspond to a reactivated structure. Field evidence indicates a reverse slip produced by the Ashley Fault, however, its orientation within the tectonic regime suggests a significant right lateral component of movement.

The geographic locations of the Springbank, Eyrewell, Sefton, and the Ashley Faults indicate that, although the faults are related, and in some cases present similar characteristics (particularly the Springbank and Sefton Faults), they can be considered as different and individual structures for purposes of seismic hazard analysis. Nevertheless, the Ashley Fault may form a northern bound to the Springbank Fault and may be synchronously reactivated.

4.4.3.2 Relationship between the Springbank Fault and the Cust Anticline

The Cust Anticline has been interpreted as a propagation fold associated with a backthrusts off the Springbank Fault (Jongens et al., 1999), and as a "pop-up" structure that has resulted from transpresion within a restraining bend along the Ashley Fault (Campbell et al., 2000).

The strong curved geometry of the Cust Anticline suggests that it is the result of complex tectonic interactions. The information analysed in this study suggests that the Cust Anticline, in addition to be associated with backthrust to the Springbank Fault and the Ashley Fault, may be also related to the backlimb of the Springbank Fault propagation fold.

The location of the Cust Anticline with respect the Springbank Fault and its propagation fold backlimb, strongly suggests a direct correlation between them. The Cust Anticline may be related to the backlimb of the Springbank Fault propagation fold associated with the maximum development to the fault, close to its middle point.

4.5 SUGGESTED STRUCTURAL MODEL

Figure 4.9 presents a schematic illustration of the model proposed for the Springbank Fault, and its relationship with other structures at different places along its strike. This figure illustrates the spatial variation of the Springbank Fault along three sections: at the Eyre River, close to the Springbank township (at its middle point), and at the Ashley River, together with their relation with the Eyrewell and the Sefton Faults and the Cust Anticline.

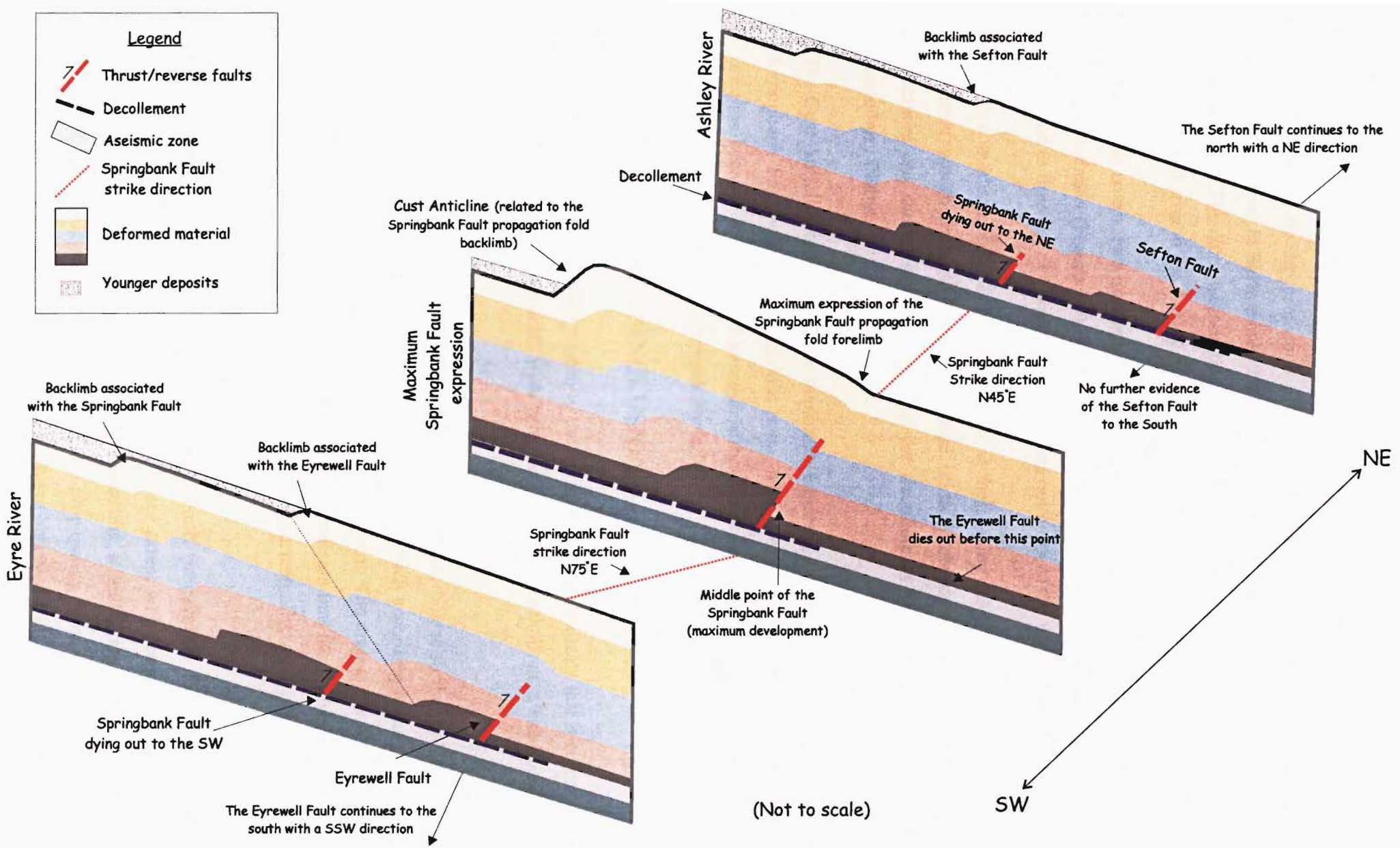

Figure 4.9: Schematic representation of the Springbank, Eyrewell and Sefton Faults at different locations across their strike: at the Eyre River, at the maximum expression of the Springbank Fault close to Springbank, and at the Ashley River (see text for explanation).

In summary, the up dip projection of the Springbank Fault is more significant close to its middle point, near to Springbank. The fault progressively dies out toward both the southwest and northeast. The data suggests that the Springbank Fault dies out south of the Eyre River in the south, and around the Ashley River in the north.

Along these rivers, two new structures are inferred to the east of the fault, the Eyrewell and the Sefton Faults (Figure 4.9). The Eyrewell Fault extents to the southeast of the Springbank Fault, and to the west of Christchurch, and dies out north of the Eyre River.

The first evidence of the Sefton Fault is at the Ashley River. The fault continues to the northeast but there is no further evidence of its presence south of the river. The three structures are shown propagating from the decollement located at ~14 km beneath the Canterbury Plains.

The Cust Anticline is related to the maximum expression of the backlimb associated with the Springbank Fault close to its middle point. The geomorphology of the Cust Anticline is complex because it is affected by other structures that may include the Ashley Fault and a major backthrust from the Springbank Fault.

4.6 SUMMARY AND CONCLUSIONS

The characteristics of the fold related to the Springbank Fault indicate that it corresponds to a propagation structure associated with progressive fault growth from a sub-horizontal mid-crustal decollement.

The maximum topographic expression of the fold is located close to the middle point of the longitudinal strike extension of the Springbank Fault, which according to the theories of fault growth is the location of the maximum fault displacement. The drainage evolution around the fold and the geophysical investigations undertaken indicate that the Springbank Fault and its propagation fold are growing both vertically and horizontally, especially in the northeast direction.

Fold modelling indicates that the Springbank Fault propagation fold is consistent with characteristics of a trishear structure and to a lesser extent with some features of the classic fault propagation fold. According to trishear modelling, a fault dipping 60°, with a slip of 300 m, P/S of 7, trishear angle of 90°, and initially propagating from a decollement located at a depth of ~14 km, may have produce a fold with the observed fault propagation fold attributes.

From this depth, the fault has broken up towards the surface creating a change in fault dip that is related to the development of the fold backlimb to the west.

The propagation fold has been formed during multiple episodes of movement along the Springbank Fault. The fold forelimb correspond to late stages of development. The seismic stratigraphy suggests that the deformation related to the forelimb started after the deposition of the Kowai Formation, and that the fault tip, before the leading edge deformation began, was located at ~2.2 km of depth.

Indirect evidence indicates that the Eyrewell and the Sefton Fault have propagation folds with similar characteristics to the Springbank Fault. This suggests that these structures are also associated with the same sub-horizontal decollement. This decollement has been previously recognized beneath the Canterbury region by several authors, and is considered to be part of a system of fold-thrust structures that are propagating eastward from the Alpine Fault, and in which the Hororata Fault is also taking part.

The location of these structures with respect to the northwest-southeast orientation of the principal horizontal compressional stress in the area indicate that the Springbank and Sefton Fault may have a mainly pure reverse slip, whereas the Eyrewell Fault may have a strong left lateral component.

Chapter 5
SEISMIC HAZARD ASSOCIATED WITH THE SPRINGBANK FAULT

5.1 INTRODUCTION

In general, seismic hazard is defined as the possibility of potentially destructive earthquake effects occurring at a particular location (Bommer, 2002). In other terms, seismic hazard refers to any phenomenon related to an earthquake that may produce adverse effects on human activities. This includes ground shaking, surface rupture, tectonic deformation, seismically induced landslides, tsunamis and liquefaction among others, and their effect on human infrastructure, land use and socioeconomic systems (Montana Bureau of Mines and Geology, 2003).

This chapter outlines the parameters considered in seismic hazard analysis and the assessment of the potential seismic hazard associated with the Springbank Fault. The chapter includes:

1. A brief description of the methodology used in seismic hazard assessment
2. The Springbank Fault characterisation and the explanation of the parameters taken into account for estimating the maximum earthquake that the fault is capable of producing
3. The methodology for estimating the maximum earthquake
4. A qualitative analysis of the factors that may affect ground motion distribution and their possible influence on different urban centres around the Springbank Fault
5. A quantitative estimation of ground motion distribution around the Springbank Fault using recently updated attenuation relationships.

5.2 SEISMIC HAZARD ASSESSMENT

Seismic hazard assessments can be performed both deterministically and probabilistically. The basis of deterministic seismic hazard (DSH) is to describe the earthquake scenario of a single event of known magnitude produced in a fault of known location. The essence of probabilistic seismic hazard (PSH) is to identify all possible earthquakes that could affect a site, including all possible combinations of magnitude and distance, and to characterise the frequency of occurrence of different earthquakes sizes. The two approaches require the determination of ground motion at specific places (Kramer, 1996; Abrahamson and Sheldock, 1997; Bommer, 2002).

In DSH, the hazard is defined as the ground motion at the site produced by a specific earthquake, whereas in PSH the hazard is defined as the mean rate of excedance of some chosen ground motion amplitude (Bommer, 2002).

In this study, the seismic hazard of the Springbank Fault will be estimated as the ground motion produced by a single structure at different places; therefore, the approach will be deterministic. The seismic source will be considered separately and the ground motion produced by a particular earthquake generated in the fault will be estimated at different sites.

In brief, a deterministic seismic hazard assessment involves:

1. Determining the location of the fault and its characteristics
2. Estimating the earthquake magnitude that the fault is capable of producing and the frequency of earthquakes at the seismic source
3. Estimating the ground motions and other earthquake-related phenomena that the seismic source will produce (Stirling et al., 2002b)

Each step of the process requires the estimation of different fault parameters. For the accomplishment of step (1), fault characterisation, it necessary to know the location, fault segmentation, fault geometry (i.e. fault dip and length), slip rate and the date of the most recent large earthquake.

The fault segmentation and the fault geometry define potential rupture lengths and are inputs to establish possible earthquake magnitudes. The slip rate and the date of the most recent large earthquake in the fault provide the basis for calculating earthquake recurrence intervals (Working group on California earthquake probabilities, 1999).

In order to estimate earthquake magnitudes (step 2), a combination of three factors is necessary (Stirling et al., 2002b): geological information (fault length, length of associated surface rupture, single event displacement); historical information (i.e records of large historical earthquakes produced by the fault); and paleoseismological information (date and magnitudes of past ruptures). When this information is not available, empirical equations relating fault characteristics, such as fault length or area of rupture, to earthquake magnitudes, can be used to establish expected earthquakes sizes.

Finally, the estimation of ground motion (step 3) can be achieved in different ways. These estimates are usually equations, called attenuation equations that express ground motion as a function of magnitude, distance and other parameters such as type of faulting (Abrahamson and Shedlock, 1997). Different factors affect ground motions and should be considered in seismic hazard analysis. These factors include type of rupture mechanism or type of faulting, site conditions and location with respect to the fault rupture.

5.3 ESTIMATION OF THE POTENTIAL SEISMIC HAZARD ASSOCIATED WITH THE SPRINGBANK FAULT

The characteristics of the Springbank Fault, the size of a maximum possible earthquake that the fault is capable of producing, and the expected ground motion at different sites are necessary to evaluate the seismic hazard.

In the next section, a compilation of the Springbank Fault characteristics is described and used as the basis for the calculation of the maximum earthquake that the structure is capable of producing.

The characteristics of the fault and the maximum earthquake will be used in turn to establish the ground motion at different sites. Initially, qualitative considerations regarding the factors that may affect ground motion and the role of thrust/reverse fault will be explained. Finally, a

quantitative estimation of ground motion at different sites around the fault will be established by using different attenuation relationships.

5.3.1 SPRINGBANK FAULT CHARACTERISATION

5.3.1.1 Springbank Fault Location

The combination between topographical fault expression, morphometric analysis along rivers and geophysical investigations allowed the determination of the probable location and extent of the Springbank Fault.

The fault is a northeast trending structure with a longitudinal extent of ~16 km, located approximately between the Eyre River (south end), and the Ashley River (north end).

Two other structures with similar characteristics to the Springbank Fault were also determined: the Eyrewell Fault, to the southeast of the Springbank Fault and the Sefton Fault towards the northeast.

The Eyrewell Fault is closer to Christchurch which may represent a serious seismic hazard for the City. This structure is trending north-northeast and is located from the North Eyre Road (north end), and extends towards the south, to the west of Christchurch. The limit of its southern end was not established by this study.

The Sefton Fault has a very similar trend and characteristics to the Springbank Fault. The first evidence of this fault occurs at the Ashley River, and from this location the fault trends to the northeast with similar strike to the Springbank Fault. The total length of this structure was not determined during this study.

5.3.1.2 Springbank Fault Segmentation

The Springbank, the Eyrewell and the Sefton Faults are considered as part of a fault zone propagating to the east, as explained in Chapter 4. This analysis assumes that each of these faults ruptures independently, without further segmentation.

5.3.1.3 Fault Geometry and Rupture Area

The Springbank Fault is a reverse/thrust fault with a length of ~16 km and dip of ~60° to the northwest. The fault propagates from a decollement zone located at a depth of approximately 14 km under the Canterbury Plains.

The decollement is located within an aseismic zone (according to Cowan, 1992), therefore, it is not considered as part of the seismogenic rupture area of the Springbank Fault.

The estimated length of the fault is assumed as the maximum length of the subsurface rupture plane, and the dip is assumed as approximately constant between the decollement junction and the fault tip closest to the surface. Therefore, the fault plane is modelled as a rectangular surface of 16 km x 16 km. Consequently, if the entire seismogenic part of the fault moves during an earthquake, the rupture area will be ~256 km^2.

5.3.1.4 Slip Rate

The slip rate of a fault is the rate of average displacement produced by the structure in a particular interval of time. To estimate the slip rate, it is necessary to know the displacement produced by the fault at features whose age can be determined.

In order to estimate the Springbank Fault slip rate, the tectonic displacement produced by the fault on different geomorphological units (Cust, Springbank and Boundary 2; in section 2.2) identified close to Springbank, was calculated and then divided into the assigned age of the unit.

The measurement of the Springbank Fault slip rate is approximate. The usual techniques of direct measurement of offset features across the fault plane are not applicable because of the blind character of the fault. Furthermore, the ages of the different units or sedimentary formations that the fault is deforming are not well constrained.

A slip rate of approximately 0.22mm/yr was estimated for the Springbank Fault following the methodology explained below. The vertical displacement caused by the fault was determined on its maximum expression: the maximum topographical expression of its propagation fold, between the Tram Road and the Cust River.

The vertical displacement is the difference in elevation between a point on the top of the fold, in the hanging wall, and a point in the footwall. The difference in elevation between points was calculated along different sections approximate perpendicular to the fault strike using surfaces of different age. The elevation of the different points in the field was measured using GPS carrier phase.

To calculate the Springbank Fault slip rate, several considerations were taken into account:

1. The slip of the Springbank Fault is completely accommodated by an increase in fold amplitude without transfer of slip out of the fold (according to the definition of propagation folds).
2. The displacement measured in the fold corresponds to vertical displacement. To estimate the fault slip it is necessary to project this vertical displacement on to the fault plane. This is achieved with the relation $s = z/\sin\theta$ (where s is the slip on the fault plane, z is the vertical displacement measured on the fold, and θ is the fault dip).
3. The loess cover of the different geomorphic units should be extracted from the analysis. 6 metres of loess cover are subtracted from the estimation of vertical displacement in the Cust Unit, and 4 metres of loess cover are subtracted from the analysis in the Springbank Unit.
4. The Canterbury Plains are not flat. There is a natural gradient (from the Southern Alps toward the ocean in the East Coast of the South Island) measured as averaging ~0.33° in the perpendicular direction to the Springbank Fault strike, at its central section. This gradient has been included in the calculation of the total vertical deformation caused by the fault.

Consequently, the difference in elevation between a point in the hanging wall and another in the footwall does not correspond to the net vertical displacement produced by the fault. The natural gradient of the North Canterbury Plains (0.33°) in the study area has to be included in the calculations together with the thickness of the loess cover. The gradient of the Plains may seem irrelevant, but over long distances, the difference in elevation between two points is highly significant.

In order to determine the tectonic vertical displacement, the point located on the hanging wall should be projected to an imaginary surface inclined 0.33° to the southeast, which would

correspond to the elevation of the point without tectonic deformation. The loess cover correction is made by subtracting its thickness from the difference in elevation between the point projected on the imaginary surface and the actual elevation of the point surveyed in the field, and this corresponds to the net tectonic displacement (Vt). Figure 5.1 illustrates the process.

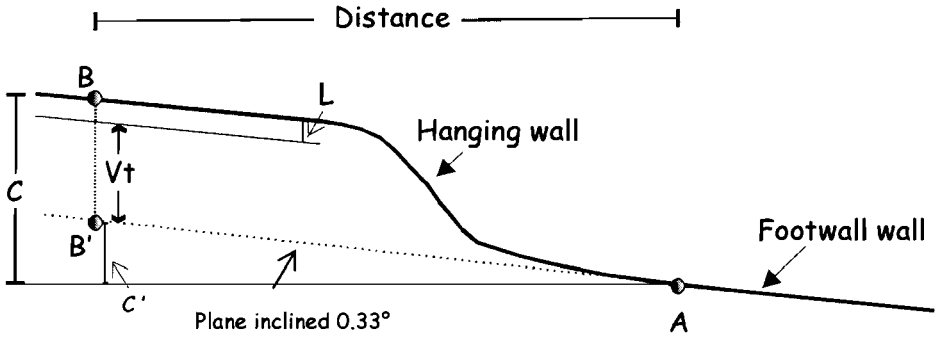

Figure 5.1: Diagrammatic representation of the calculation of the vertical tectonic deformation associated with the Springbank Fault. A and B are points surveyed in the field. Their difference in elevation is (C). The exact location of these points, including elevation (MSL), is known from GPS carrier phase surveys. B' is the projection of B on a surface inclined ~0.33°, that would correspond to the elevation of the point without tectonic deformation. The elevation of B' is calculated with respect to the distance between A and B, from which C' is determined. L is the thickness of the loess cover. The tectonic vertical deformation (Vt) is C-C'-L.

The net vertical displacement was calculated along different sections in the Cust, Springbank, and Boundary 2 Unit, and then converted to net slip on the fault plane. This slip was then divided into the assigned surface age to determine the Springbank Fault slip rate.

For example, in a profile located in the Cust Unit, at a perpendicular direction to the trend of the fault, the distance between a point in the footwall (A) and a point in the hanging wall (B) is 6,800m. The elevations for A and B in the field are 80 and 140m, respectively. Then, the difference in elevation between A and B is C=60m.

The projection of B along a line inclined 0.33° to the southeast (denoted as B') would have an elevation of C'= 39.17m with respect to A (where C' = 6,800 x tan 0.33). Then, the difference between C-C'-L, (L is the loess cover) is 14.8m (=60-39.17-6), which corresponds to the net vertical displacement (Vt).

Consequently, the slip (s) on the fault plane is 17.13m (s=14.8/sin 60°) and the slip rate is the division of the fault slip (17.13m) into the assigned age of the Cust unit (75,000 yrs) which corresponds to 0.23 mm/yr.

This process was repeated for several sections, and it was noticed that however, the distance between A and B was variable for each section, the estimated slip rate was very similar. It was found that the location of A and B does not have a significant influence in the slip rate estimation if the points are perpendicular to the fault strike, and point B is taken on the crest of the fold, beyond the forelimb. Table 5.1 summarises the input parameters and the results for three different sections in the Cust, Springbank and Boundary 2 Units.

Table 5.1: Input parameters for Springbank Fault slip rate estimation.

Geomorphic unit/ assigned age	**Distance between A and B (m)**	**Difference in elevation between A and B (C) (measured in the filed) (m)**	**Difference in elevation between A and B' (C') (m)**	**Vertical deformation (C-C'-L)** L=6m (Cust) L=4m (Springbank) L=0 (Boundary)	**Slip on the fault plane (m)**	**Slip rate (slip/age)**
Cust/75,000 yr	6,800	60	39.17	14.8	17.13	0.23 mm/yr
Springbank /45,000 yr	4,800	40	27.6	8.35	9.6	0.21 mm/yr
Boundary2/ 10,000 yr	1,930	13	11.12	1.88	2.18	0.22 mm/yr

All the estimated slip rates for the Springbank Fault are around 0.22 mm/yr. Nevertheless, this estimative correspond to an approximation because the ages of the units are reference ages,

they do not correspond to their exact (absolute) age, and because the footwall is covered by younger deposits that mask the actual vertical deformation. The thickness of this cover is unknown, and has been omitted from consideration here.

For example, for the Cust Unit, the age of 75,000 years was assigned based on the loess cover (section 2.2.1.1) and furthermore should be considered as the minimum age for this unit. It is not possible to quantify the error involve in the slip rate estimation because the ages of the units are not constrained and because the thickness of the younger sedimentary cover over the footwall is not established.

5.3.2 DETERMINATION OF MAXIMUM MAGNITUDE

Because of the blind nature of the Springbank Fault, the size or magnitude of earthquakes that the structure is capable of producing cannot be directly established by either geological or paleoseismological information. In addition, no historical records of large earthquakes produced by the fault exist.

The earthquake magnitude that a fault is capable of producing depends on its physical attributes. Fault parameters such as rupture length, rupture area, displacement per event, total fault length, rupture width and stress drop are directly related to the size of earthquakes.

Different authors (Bonilla et al., 1984; Shimazaki, 1986; Well and Coppersmith, 1994; Stirling et al., 2002a) have published empirical relationships relating magnitude to various fault parameters. These equations will be used here to estimate the maximum magnitude that the Springbank Fault is capable of producing. The empirical equations differ from one study to another. This is related to the earthquake database used, which in each case has been selected with different criteria.

5.3.2.1 Empirical Relationships Correlating Magnitude with Fault Parameters

The most widely used empirical relationships between magnitude and fault parameters are those established by Wells and Coppersmith (1994). They used a worldwide database of source parameters for 421 earthquakes with hypocentral depths less than 40 km and magnitudes greater than approximately 4.5.

The magnitudes established by the Wells and Coppersmith (1994) relationships are moment magnitudes (Mw or M). This magnitude has been preferred over surface wave magnitude, Ms, body wave magnitude, Mb, or Richter magnitude, ML, because these may become saturated and no-longer record large-scale faulting (Wells and Coppersmith, 1994).

M is directly related to seismic moment, Mo, of the earthquake by the relationship:

$$M = 2/3 \log Mo - 10.7 \text{ (with Mo in dyne-cm)} \quad [1]$$

The seismic moment, Mo, links earthquake size with fault rupture parameters by the relationship:

$$M = \mu DA \quad [2]$$

Where:

μ = Shear modulus (usually taken as $3x10^{11}$ dyne/cm^2)
D = Average displacement along the fault
A = Area of rupture.

Mo is considered a more accurate measure of the size of an earthquake because it is a direct measure of the amount of radiated energy, rather than a measure of the response of a seismograph to an earthquake (Wesnousky, 1986; Kramer, 1996; Wells and Coppersmith, 1994).

Analyses have indicated that the strongest correlations exist between magnitude (M) and surface rupture, subsurface length, rupture width and rupture area, and that the style of faulting is potentially significant for correlating earthquake magnitude and rupture parameters (Wells and Coppersmith, 1994).

Table 5.2 lists the empirical relationships established by Wells and Coppersmith (1994) between moment magnitude (M) and surface rupture length (SRL), subsurface rupture length (SSRL) and rupture area (RA), for thrust/reverse faults and all type of faults.

Table 5.2: Empirical relationships between magnitude and surface rupture length, subsurface rupture length, and rupture area, for thrust/reverse faults and all types of faults (from Wells and Coppersmith, 1994).

PARAMETERS	THRUST/REVERSE FAULT	ALL TYPES OF FAULTS
M estimated from surface rupture length (SRL)	M = 5.00+1.22 log (SRL)	M = 5.08+1.16 log (SRL)
M estimated from suburface rupture length (SSRL)	M = 4.49 + 1.49 log (SSLD)	M = 4.38 + 1.49 log (SSLD)
M estimated from rupture area (RA)	M = 4.33 + 0.9 log (RA)	M = 4.07 + 0.98 log (RA)

Other empirical relationships between earthquake magnitude and fault parameters are those established by Shimazaki (1986). From examinations of a set of well-determined source parameters of Japanese intraplate earthquakes, the author indicated that small earthquakes obey different scaling law from large earthquakes. For small events, the seismic moment (Mo) is related to the length of the fault (L) by the proportion $Mo \propto L^3$, whereas large earthquakes obey $Mo \propto L^2$.

Shimazaki (1986) divided that data set into small and large events at Mo = 7.5 x 10^{25} dyne/cm^2, and found the following linear regression equations for correlating fault length (L) to seismic moment (Mo):

$$\text{Log L} = 0.524 \log \text{Mo} - 12.44 \quad (\text{For Mo} \geq 7.5 \times 10^{25} \text{ dyne/cm})$$

And

$$\text{Log L} = 0.281 \log \text{Mo} - 5.98 \quad (\text{For Mo} < 7.5 \times 10^{25} \text{ dyne/cm})$$

Other authors such as Stirling et al. (2002a) proposed new relationships between surface rupture displacement and magnitude for crustal earthquakes. Their study used an expanded version of the earthquake database of Wells and Coppersmith (1994) supplemented by earthquakes from the pre-instrumental era (pre-1900) generated in New Zealand and other places such as California and Japan.

Stirling et al. (2002a) indicated that the empirical relations found by Wells and Coppersmith (1994) frequently produce smaller earthquake magnitudes than values derived from instrumental and paleosesimic data, and attributed this difference to the specific choice of data in the Wells and Coppersmith database. The authors established new relationships between moment magnitude (M) and surface rupture length (SRL) and rupture area (RA) with earthquakes from the instrumental and pre-instrumental era (Table 5.3).

The estimates of magnitude and surface displacement for earthquakes of the pre-instrumental era were based on felt intensities and field observations. Due to the uncertainties involved in this process, the equations extracted from pre-instrumental data are not going to be applied in this study.

Table 5.3: Empirical relationships between magnitude and surface rupture length, rupture area, from earthquakes from the instrumental and pre-instrumental era (from Stirling et al., 2002a).

PARAMETERS	INSTRUMENTAL	PRE-INSTRUMENTAL
M estimated from surface rupture length (SRL)	M = 5.45+0.95 log (SRL)	M = 5.89+0.79 log (SRL)
M estimated from rupture area (RA)	M = 4.54 + 0.89 log (RA)	M = 4.95+ 0.78 log (RA)

5.3.2.2 Earthquake Magnitude on the Springbank Fault using Empirical Equations

The empirical equations determined by Wells and Coppersmith (1994), Shimazaki (1986) and Stirling et al. (2002a) will be used to correlate earthquake magnitude with Springbank Fault parameters such as subsurface rupture length and fault rupture area.

To estimate earthquake moment magnitude, the following fault attributes will be used: a subsurface rupture length of 16 km (the total length established from the morphometric analysis), and a rupture area of 256 km^2 (determined from the subsurface rupture length, the depth to the decollement (14 km), and a fault dip of 60°). Table 5.4 compiles the results.

Table 5.4: Maximum earthquake moment magnitude that the Springbank Fault is capable of producing based on its physical attributes and different empirical equations

USED PARAMETER / EMPIRICAL EQUATIONS	SUBSURFACE LENGTH	RUPTURE AREA	LENGTH
Wells and Coppersmith (1994) (Thrust/reverse faults)	M=6.3	M=6.5	
Wells and Coppersmith (1994) (All type of faults)	M=6.2	M=6.4	
Shimazaki (1986) (Small events)			M=6.6
Shimazaki (1986) (Large events)			M=6.3
Stirling et al. (2002a) (Instrumental)		M=6.7	

The moment magnitudes estimated with the empirical equations range from 6.2 to 6.7, with an average magnitude of M=6.4. The difference is related to the different databases used to determine the empirical relationships.

A maximum magnitude of ~6.4 as the magnitude that the Springbank Fault is capable of producing, is consistent with the results of the study performed by Lettis et al. (1997). These authors compiled a worldwide database of 148 of thrust/reverse moderate to large magnitude earthquakes, and found that the occurrence of surface rupture is magnitude dependent. Lettis et al. (1997) established that the probability of co-seismic surface rupture increases from approximately 40% at Mw 5.0 to approximately 90% at Mw 7.2.

The data in the database showed that faults associated with folds and not with surface rupture, generate mainly magnitudes between Mw 6 and Mw 6.4. Lettis et al. (1997) concluded that because the probability of surface rupture is very high (>90%) for earthquakes greater than Mw 7.2, it appears that the presence of folds indicates that the maximum magnitude of potential earthquakes likely is limited to the range Mw 6.5 to 7.2.

Therefore, the determination of a moment magnitude equal to 6.4 as the magnitude that the Springbank Fault is capable of producing is reasonable.

5.3.2.3 Earthquake Recurrence

Usually, the fault slip rate and the date of the most recent large event produced by a fault provide the basis for calculating earthquake recurrence intervals where no other paleoseismic events are dated. The date of the most recent large earthquake is usually established from instrumental, historical or paleoseismological information. However, this information is not available for the Springbank Fault.

Alternatively, the maximum earthquake magnitude that the fault is capable of producing can be used to establish the earthquake recurrence, assuming that the fault characteristically ruptures at maximum displacement.

If the maximum magnitude that a fault is capable of producing is known, an estimation of the displacement per event can be calculated with the equations used to determine seismic moment (equations 1 and 2 in section 5.3.2.1). The displacement per event can be compared with the total displacement measured in the fault during a particular interval of time, in order to determine how many characteristics events have occurred in that particular period and, consequently the earthquake recurrence.

According to the equations (see below), an earthquake of moment magnitude of 6.4, the maximum that the Springbank Fault may generate, may produce a displacement per event of ~0.6m.

The comparison of this displacement with the ~2m of displacement measured in the Holocene Boundary 2 Unit, indicates that 3-4 events have been produced by the fault in 10,000 years. This suggests an earthquake recurrence of ~3,000 years.

$$\text{Log Mo} = 16.05 + 1.5\ \text{M (Mo in dyne-cm)}$$

$$\text{Mo} = 4.47 \times 10^{25}\ \text{dyne}$$

And,

$$D = \frac{Mo}{\mu A} = 58\ \text{cm}$$

Where :

$$\mu = 3 \times 10^{11}\ \text{dyne/cm}^2 \text{ and } A = 2.56 \times 10^{12}\ \text{cm}^2$$

Consequently, one event with average displacement (D) of 0.6m is produced each T = 3,000 yrs, which in turn leads to a slip rate (s=D/T) of 0.2mm/yr which is consistent with the slip rate of 0.22 mm/yr determined in section 5.3.4.

The same analysis on the Cust and the Springbank Units leads to the conclusion that approximately 28 events have occurred in 75,000 years and ~16 events in 45,000 years. This indicates earthquake recurrences of ~2,700 and 2,800 years, respectively.

5.3.3 GROUND MOTION

The final step in seismic hazard assessment, after establishing the fault characteristics and the maximum earthquake magnitude, is the estimation of ground motions that may be induced by an earthquake produced by the structure. The ground motion distribution depends on different factors such as earthquake magnitude, type of faulting, site location with respect to the fault, and site conditions.

Some of the factors that may have a direct influence on ground motion distribution, and their effect on selected urban centres close to the Springbank Fault are described below.

Different empirical attenuation relationships will also be used to estimate the values of peak ground acceleration (PGA) and the horizontal acceleration response spectra at the selected sites.

5.3.3.1 Qualitative Analysis of the Factors Affecting Ground Motion

Near-Fault Effects

The near-fault zone is the area within a distance of about 20-60 km from a fault (Stewart et al., 2001). The effects in the near-fault zone can be significantly different from those further away from the seismic source. Within this area, the rupture mechanism, the direction of rupture propagation, the site conditions and the tectonic deformation related to the surface rupture, strongly influence ground motion.

Several urban centres are located in the near-fault zone of the Springbank Fault (Figure 5.2). These include: Christchurch, Rangiora, Kaiapoi, Oxford, Cust, Amberley, Darfield, and

Rolleston, among others. The location of these towns with respect to the fault may result in serious effects during an earthquake produced by the structure.

Type of Rupture Mechanism

Information from different earthquakes indicates that dipping faults (thrust/reverse or normal faults) generate larger ground motions than vertical strike slip faults (Abrahamson and Shedlock, 1997; Oglesby et al., 1998, 2000a, 2000b, 2001).

Dipping fault earthquakes present larger ground motions in both the hanging wall and the footwall, but the effect is particularly pronounced on the hanging wall (Abrahamson and Somerville, 1996; Oglesby et al., 1998, 2000a, 2000b, 2001; Ouchi et al., 2001, Kelson et al., 2001). This effect is more significant in thrust/reverse than in normal faults. Motions from thrusts or reverse faults are larger than those from normal faults by a factor of two or more (Stein and King, 1984; Oglesby et al., 1998, 2000a).

Data from different reverse earthquakes (i.e San Fernando in 1971, Northridge in 1994 and Chi-Chi in 1999) presented a similar trend of an increase in ground motion on the hanging wall. This systematic difference is likely to be observed close to reverse faults in future reverse events (Abrahamson and Somerville, 1996; Somerville et al., 1996; Ouchi et al., 2001).

The difference in ground motion between the hanging and footwall seem to be distance-dependent. The hanging wall factor decreases with increasing magnitude and distance, so it is predominantly important in the near-fault field.

If the Springbank Fault produces a reverse slip earthquake, all the urban centres mentioned before (Christchurch, Rangiora, Kaiapoi, Oxford, Cust, Amberley, Darfield, and Rolleston) may be affected by the larger ground motions produced by this particular type of faulting. In addition, Oxford and Cust, both directly on the hanging wall of the fault, might experience stronger motion amplification due to the hanging wall effect.

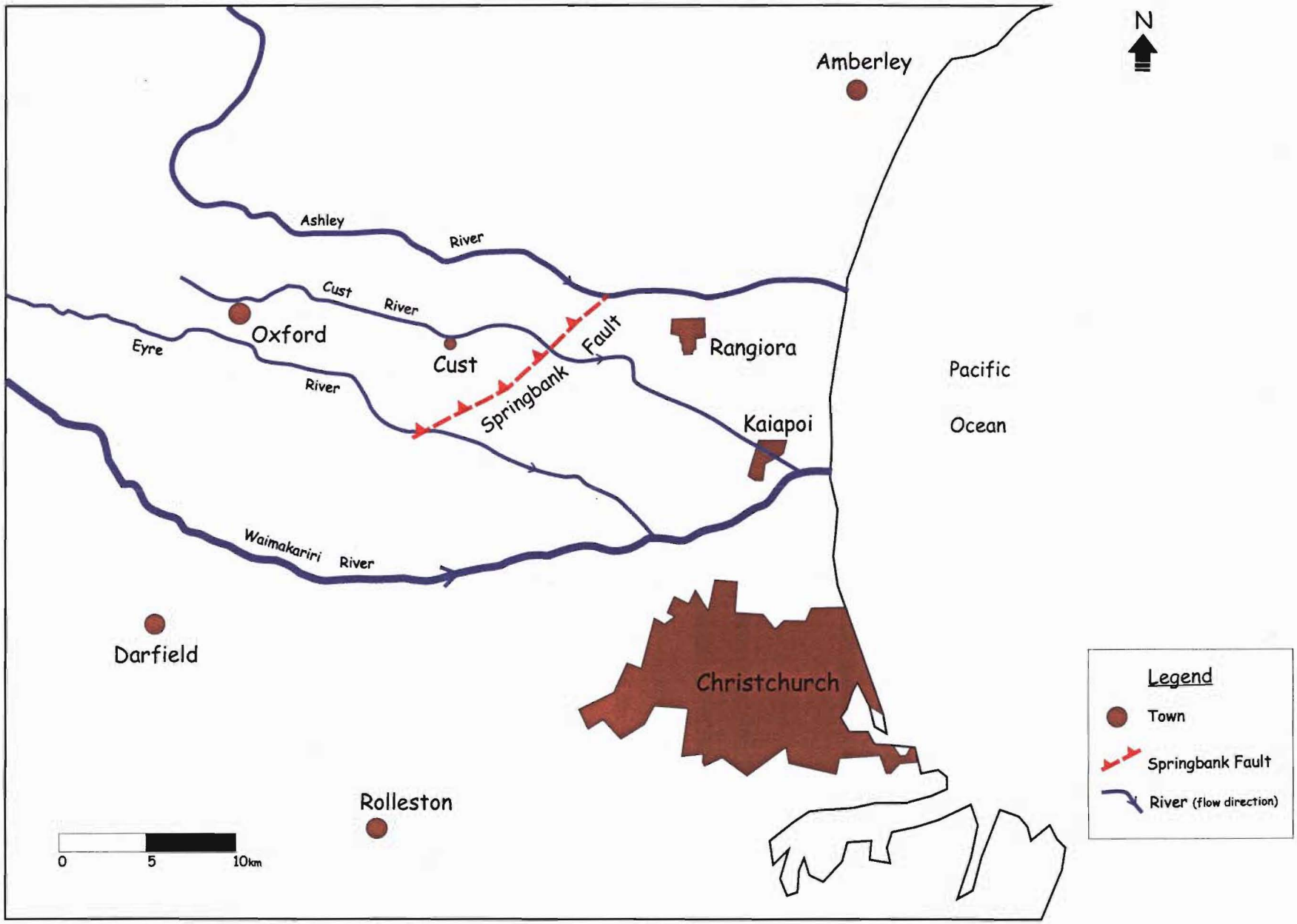

Figure 5.2: Location of urban centres within the near- fault zone of the Springbank Fault that were considered for the estimation of ground motion.

Directivity

When the direction of slip and the rupture on a fault propagate towards a specific site, a forward directivity effect occurs. As the rupture front propagates away from the hypocentre towards the site, energy is accumulated near the rupture front. The wave front arrives as a large pulse of motion (Gazetas et al., 1990; Somerville et al., 1997).

A constructive interference of S-waves radiating from successive positions of the rupture front takes place because the rupture propagates at a velocity only slightly less that the S-wave velocity. As a result, a large amplitude pulse is built at sites in the approximate direction of rupture propagation. These pulses contain much of the kinetic energy radiated from the fault (McVerry, 1997).

In dip-slip events or dipping faults, forward directivity occurs for sites located near the up dip projection of the fault plane. For thrust/reverse events, sites on both the hanging wall and the footwall close to the tip of the rupture will experience strong directivity effects that result in increased long-period motion on the component normal to the fault strike (Abrahamson and Somerville, 1996, Somerville et al., 1997). Dip-slip faulting produces directivity effects on the ground surface that are most concentrated up dip from the hypocentre.

More important forward directivity effects occur for smaller angles between the site and the fault strike and for larger sections of ruptured fault between the site and the hypocentre (Somerville et al., 1997). The parameters that influence the directivity effect in dip-slip faulting (Figure 5.3) are magnitude (M), rupture distance (r_{rup}), style of faulting, width ratio (fraction of fault dip that ruptures toward a site, Y), and angle between fault plane and ray path to site (θ). For dip-slip events, the angle θ and width ratio Y are measured from the hypocentre to the site in the vertical plane oriented normal to the fault.

Between the ends of a dip-slip fault, the variation of ground motion with θ depends of the rupture distance, r_{rup}. At the ends of a dip-slip fault, the directivity effects are not important because the effect operates in the up dip direction not along the strike as for strike slip faults. The region beyond the ends of the fault is not considered in the determination of directivity effects (Somerville et al., 1997), (Figure 5.3).

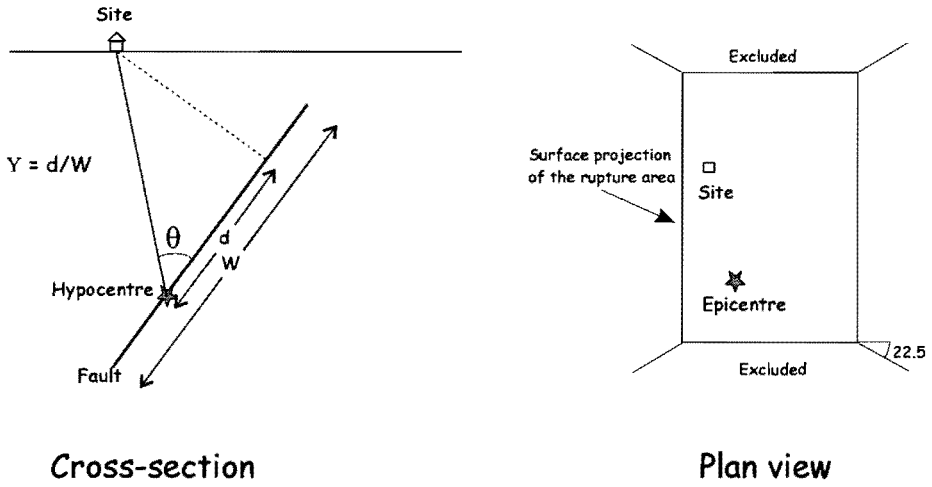

Figure 5.3: Definition of rupture directivity parameters θ and Y for dip-slip faults, and region off the end of dip-slip fault excluded from the model (after Somerville et al., 1997)

Urban centres such as Rangiora, Oxford, Kaiapoi, and Cust may experience important directivity effects due to their location close to the up dip direction of the Springbank Fault. Of these towns, Rangiora, on the footwall, and Cust, on the hanging wall may be the more affected because of the small angle between the fault plane and the path to their location.

Christchurch also may be affected by directivity from the Springbank Fault, but this effect will be less significant because the city is located at the southern end of the structure. In contrast, the location of Christchurch with respect to the inferred Eyrewell Fault, a few kilometres to the west of the city, indicates that in the case of an earthquake rupture produced on this fault, strong directivity effects may occur.

The location of Amberley, Darfield and Rolleston with respect to the Springbank Fault, indicates that they may not be affected by directivity. Amberley, situated away from the northern end, and Darfield and Rolleston both located away from southern end, are beyond the ends of the fault, where directivity effects are not considered significant.

Site Effects

The site conditions: sedimentary basins, local geological conditions, and topographic relief, may strongly influence shaking during an earthquake. Sedimentary deposit in basins, particularly deep basins, may produce significant amplification, or resonance, effects during an earthquake because the basin geometry may introduce complex effects within seismic waves.

The finite lateral extent of the basin allows the generation of surface waves at the edges and resonance in the lateral direction causing an increase in both the amplitude and duration of ground motion (Papageorgiou, 1998). The process can focus the waves from the bottom of the basin concentrating the intensity of strong shaking in small regions at the surface, while diminishing intensity at other sites.

Waves that become trapped in deep sedimentary basins can produce up to 50% stronger amplitudes at intermediate and low frequencies (f < ~1 Hz) than those recorded on comparable surface materials outside basins, and their durations can be twice as long (Graves et al., 1998 in Stewart et al., 2001).

Important amplification effects may be also related to superficial geological materials. Parameters such as type of geological material, average shear wave velocity in the upper 30m and geotechnical conditions have direct influence on ground motion.

Soft rocks (soft sediments) usually exhibit stronger shaking than hard rocks, causing larger amplification of seismic waves (USGS, 1996). In general, the less compact the rock the larger the ground shaking.

Seismic records have shown amplification levels on alluvial sediments of about two to five without a predominant period of amplification indicated by the spectra. Amplification spectra for sedimentary rock sites also lack a predominant period, and indicate amplification levels of about one to three. Quaternary deposits were found to be most critical at lower frequencies (Stewart et al., 2001).

The site response also depends on the match between the frequency content of the earthquake motions and the natural period(s) of the ground (Klohn-Crippen Consultants Ltd, 1994).

Another parameter that has been considered as affecting ground motion is the average shear wave velocity in the surficial materials. Wave propagation theory suggests that for a given earthquake, ground motion amplitude should depend on the density and shear wave velocity of near-surface media. Shear wave velocity has been used for representing site conditions due to density and has relatively little variation with depth (Bullen, 1965; Aki and Richards, 1980 in Stewart et al., 2001). Slower shear wave velocities imply softer ground and, therefore, larger site amplifications (USGS, 1996). Finn (1991) demonstrated that for many sites, surface motions are influenced primarily by the top 20m to 30m of soil (Klohn-Crippen Consultants Ltd, 1994). Table 5.5 presents a classification of the material based on shear wave velocity (Martin, 1994 in Stewart et al., 2001).

Table 5.5: Classification of the material based on mean shear wave velocity to 30m (modified from Martin, 1994 in Stewart et al., 2001).

DESCRIPTION	MEAN SHEAR WAVE VELOCITY TO 30m (m/s)
Hard rock	> 1500
Firm to hard rock	760-1500
Dense soil rock	360-760
Still soil	180-360
Soft clays	<180

Christchurch, Rangiora, Kaiapoi, Oxford, Cust, Amberley, Darfield, and Rolleston are all located on the Canterbury Plains, a sedimentary basin composed of a sequence of conglomerates, sandstone, limestone and mudstones with less compacted largely gravel dominated material at the top of the sequence. This particular site condition may have a significant influence on ground motion. The soft rocks and sediments within the sedimentary basin might produce a significant amplification and resonance effect.

The topographical effect is not significant in ground motion because the study area comprises a very subtle relief without major contrasts in topography.

Tectonic Deformation

Bonilla (1982) defined tectonic deformation as the permanent deformation of the ground caused by the sudden displacement of buried rock masses during an earthquake. This deformation includes both faulting that ruptures the surface and permanent distributed deformation around the earthquake-generating fault. Such definition includes, as a tectonic deformation, the permanent deformation associated with fault propagation folds.

Bonilla (1982) considered tectonic deformation to be a very significant hazard for most constructions. Some effects of tectonic deformation include; (1) propagation of the shear rupture plane to the ground surface, (2) differential settlement, (3) compressive or tensile horizontal strains at the surface, and (4) development of surficial tension cracks (Bray, 2001) These effects can disrupt buried pipelines and tunnels, and tilting of structures may also occur. Local deformation may directly affect houses, roads, railways, tunnels, bridges, embankment dams, and water wells, for example. The effects on structures depend on the type of structure, on the type, amount, and distribution of the tectonic deformation and its angle of intersection with the structure, and on the nature of the overlying earth materials (Bonilla, 1982; Bray, 2001).

The effect of tectonic deformation in seismic hazard was confirmed during the 1999 Chi-Chi earthquake. Large damage in the Chi-Chi earthquake was associated with the surface rupture zone. Most of the infrastructure on the rupture zone was destroyed regardless of type and quality of construction. The damage was concentrated in a 5-50m zone along the surface rupture and was caused by fault displacements. Some structures were tilted but not destroyed (Ouchi, et al., 2001).

Observations of the Chi-Chi earthquake also showed that the damage associated with the tectonic deformation, in this case with the direct effect of the fault rupture at the surface, was larger on the hanging wall than on the footwall (Ouchi, et al., 2001). This supports the large effect of the hanging wall on ground motion distributions observed in other studies.

Although in the field area there are no towns directly located on the area of deformation of the Springbank Fault, several farms are located on the fault propagation fold. These places may be directly affected by tectonic deformation if an earthquake in the fault takes place.

5.3.3.2 Quantitative Analysis of Ground Motion

Attenuation relationships have been commonly used in order to provide quantitative estimations of ground motion related to a particular earthquake. Recent modifications of attenuation equations attempt to include some of the parameters that have a direct influence on ground motion distribution. However, not all the parameters are included in all the relationships, and still some assumptions have to be involved in the analysis.

The purpose of this section is to estimate the ground motion (horizontal peak ground accelerations and horizontal acceleration response spectra) at the selected sites around the Springbank Fault, assuming that an earthquake of moment magnitude 6.4 is produced by the fault during a reverse slip event.

Attenuation Relationships

The attenuation relationships used here are mainly based on shallow earthquakes produced in active tectonic regions. Recent attenuation relationships include the effects of magnitude, distance, site conditions and rupture mechanism on ground motions.

The general form of the attenuation relationships is as follows (Stewart et al., 2001):

$$\ln IM = c_1 + c_2\, m + c_3\, m^{c4} + c_5 \ln r + f(F) + f(HW) + f(S)$$

Where *IM* is the parameter to be estimated (i.e. peak ground acceleration, peak ground velocity or spectral acceleration), c1 to c5 are constants established by the regression, F is the factor related to the fault rupture mechanism, HW is the hanging wall factor for dip-slip fault, and S is a site factor. m represents moment magnitude, r represents site-source distance measured differently by different investigations.

The different attenuation equations used in this study and the main parameters considered in each, are listed in Table 5.6.

Table 5.6: Summary of attenuations relationships for active tectonic areas used for this study.

MODEL	PERIOD RANGE	PARAMETER CALCULATED	SITE CONDITIONS	FACTORS CONSIDERED
Abrahamson and Silva (1997)	0.0-5.0.	PGA, PVA, Sah, Sav	Rock, deep soil	M, r_{rup}, F, HW
Boore, Joyner and Fumal (1997)	0.0-2.0	PGA, Sah	Vs in top 30m	M, r_{jb}, F
Campbell (1997)	0.0-4.0	PGA, PVA, PVH, PVV, Sah, Sav	Hard rock, soft rock, soil, D	M, Rseis, F
Sadigh et al., 1997	0.0-4.0	PHA, Sah	Rock, deep soil	M. Rrup, F

Where:

PGA = peak horizontal ground acceleration, PVA = peak vertical ground acceleration, PHV = peak horizontal ground velocity, PVV = peak vertical ground velocity, Sah = horizontal spectral acceleration, and Sav = vertical spectral acceleration.

Distance definitions: r_{rup} = closest distance to the rupture surface, r_{jb} = closest horizontal distance to the vertical projection of the rupture, r_{hypo} = hypocentral distance, r_{seis} = closest distance to the seismogenic rupture zone.

D = depth to basement rock.

Fault paramenters: M = moment magnitude, F = fault type (reverse, oblique, strike slip, normal), HW = hanging wall (different values for site on the hanging wall).

An attenuation equation developed from New Zealand earthquakes has also been used during this study. This relationship was developed by McVerry et al. (2000) as an attenuation relationship for 5% damped acceleration response spectra from a data set of New Zealand earthquake records, supplemented by data from overseas records.

This equation together with the attenuation relationships listed in Table 5.6 were used to estimate the horizontal peak ground acceleration (PGA) and the response spectra for the different selected sites in the near-fault zone the Springbank Fault. (A full description of the attenuation relationships in Table 5.6 may be found in the special issue of Seismological Research Letters, Vol 68, January/February, 1997).

The PGA values and the response spectra for different urban centres were calculated assuming an earthquake of moment magnitude 6.4 produced by the Springbank Fault during a reverse slip event. Table 5.7 shows the estimated PGA values for different sites in the near-fault zone. Appendix 4 contains the input parameters used in the different attenuation relationships and the response spectra for each site according to each relationship.

Table 5.7: Estimated values of PGA for Christchurch, Rangiora, Kaiapoi, Oxford, Cust, Amberley, Darfield, and Rolleston estimated as part of this study. The values are calculated using the attenuation relationships developed by Abrahamson and Silva (1997), Boore, Joyner and Fumal (1997), Campbell (1997), Sadigh et al. (1997) and McVerry et al. (2000), assuming an earthquake of moment magnitude 6.4 produced by the Springbank Fault during a reverse slip event.

Attenuation Relationship	**Christchurch PGA (g)**	**Rangiora PGA (g)**	**Kaiapoi PGA (g)**	**Oxford PGA (g)**	**Cust PGA (g)**	**Amberley and Darfield PGA (g)**	**Rolleston PGA (g)**
Abrahamson and Silva (1997) (soil)	0.14	0.4	0.21	0.35	0.51	0.16	0.15
Boore, Joyner and Fumal (1997)	0.12	0.31	0.16	0.29	0.42	0.13	0.12
Campbell (1997)	0.11	0.39	0.17	0.30	0.55	0.15	0.12
Sadigh et al. (1997) (soil)	0.14	0.43	0.21	0.27	0.46	0.16	0.15
McVerry et al. (2000)	0.15	0.40	0.21	0.37	0.47	0.17	0.16

The differences in PGA values and response spectra for each site (Appendix 4) are related to the intrinsic characteristics of each attenuation relationship and to the input parameters. The attenuation relationships used here are the most widely used for seismic hazard assessments

around the world, and is not the purpose of this study to determine which one is the best. The purpose of the study is to provide an estimate of ground motion distribution if the Springbank Fault generates an earthquake of the expected magnitude.

In order to provide an idea about the physical significance on the estimated peak ground acceleration values, a mathematical relationship obtained by Wald et al. (1999) between PGA and Modified Mercalli Intensities (Imm) is applied as follows. This relationship produces an approximate estimation of the possible effects and the way that a particular PGA might be felt.

The equation obtained for Wald et al. (1999) relates PGA to observed intensities (based on significant Californian earthquakes). The Imm is limited by the range V≤Imm≤VIII (see Appendix 5 for an abbreviated description of the Modified Mercalli scale). The equation relating PGA with Imm is:

$$Imm = 3.66 \log (PGA) - 1.66$$

The estimated PGA for the different sites (Table 5.7) ranges between ~0.1 g and ~0.5 g. Table 5.8 shows the estimated values of intensity on the Modified Mercalli scale for different PGA using the equation developed by Wald et al. (1999).

Table 5.8: Approximate Modified Mercalli intensity values for different PGA based on the relationship developed by Wald et al. (1999)

PGA [g]	MODIFIED MERCALLI SCALE INTENSITY
0.1	V-VI
0.2	VI-VII
0.3	VII-VIII
0.4	VII-VIII
0.5	VIII
0.6	VIII-IX

Summarizing, an earthquake of magnitude 6.4 generated by the Springbank Fault during a reverse slip may produce, in Christchurch, estimated values of PGA around 0.14g. This PGA may induce an intensity between V and VI, which means that everyone will feel the earthquake, windows and dishes will be broken, unstable objects overturned and some heavy furniture will be moved (see Appendix 5).

Alternatively, in Cust, for example, an earthquake with the same characteristics will produce PGA greater than 0.5g, which may result in Imm intensities about VIII, producing considerable damage in ordinary buildings, partial collapse, great damage in poorly or badly designed structures, and fall of chimney, columns, monument, walls, etc

5.4 SUMMARY AND CONCLUSIONS

The seismic hazard associated with the Springbank Fault has been estimated by a deterministic approach. A deterministic seismic hazard assessment requires the characterisation of the seismic source, the determination of the earthquake magnitude that the fault is capable of producing, and the estimation of ground motion distribution.

Due to the blind nature of the Springbank Fault, some of the parameters necessary to establish its potential seismic hazard cannot be directly evaluated. Nevertheless, a combination of field investigations, morphometric analyses, empirical equations and geometric relationships lead to the Springbank Fault characterisation.

In summary, the characteristics of the Springbank Fault include:

PARAMETER	VALUE
Strike	The Springbank Fault changes its strike from N75°E, at the south end, to N45°E.
Dip	60° to the northwest
Length	~16 km
Width	~16 km
Rupture area	~256 km^2
Slip rate	~0.22 mm/yr
Maximum magnitude	6.4 (moment magnitude)
Earthquake recurrence	~3,000 years

An earthquake of moment magnitude of 6.4 generated by the Springbank Fault during a reverse slip will produce significant ground motion in different urban centres including Christchurch, Rangiora, Kaiapoi, Oxford, Cust, Amberley, Darfield, and Rolleston. All these places will be directly influenced by their location in the near fault zone, and by their specific site conditions within a sedimentary basin. Additionally, towns such as Cust and Oxford may be significantly affected by the hanging wall effect, and Cust and Rangiora by directivity.

The values of PGA and acceleration response spectra estimated with different attenuation relationships present variations. The range of estimated values of PGA for the selected sites is:

URBAN CENTRE	ESTIMATED PGA
Christchurch	0.11<PGA<0.15
Rangiora	0.31<PGA<0.43
Kaiapoi	0.16<PGA<0.21
Oxford	0.27<PGA<0.37
Cust	0.42<PGA<0.51
Amberley	0.13<PGA<0.17
Darfield	0.13<PGA<0.17
Rolleston	0.12<PGA<0.16

These results indicate that the Springbank Fault represents a significant seismic hazard for several urban centres in mid-Canterbury but its degree of activity is low.

Chapter 6
DISCUSSION, CONCLUSIONS AND RECOMMENDATIONS

6.1 INTRODUCTION

The purpose of this chapter is to provide a discussion of the methodology used to evaluate the seismic hazard associated with the Springbank Fault, a compilation of the conclusions and their implications, and finally, to offer some recommendations for future studies.

The chapter is subdivided into the following:

- A discussion about the uncertainties related to the estimation of the seismic hazard associated with the Springbank Fault
- A compilation of the implications regarding the main results and conclusions; and
- Recommendations for future studies.

6.2 UNCERTAINTIES RELATED TO THE ESTIMATION OF THE SEISMIC HAZARD ASSOCIATED WITH THE SPRINGBANK FAULT

Seismic hazard assessments involve significant uncertainties related to the actual knowledge of the earthquake process and strong motions, and with the incomplete information related to fault parameters (Bommer, 2002). The degree of uncertainty increases for studies of seismic hazard related to blind structures, such as the Springbank Fault, because some fault parameters have to be inferred indirectly.

During this study, several assumptions were involved in order to provide an estimation of seismic hazard of a fault that may constitute a significant danger to many urban areas in Canterbury. Structures with similar characteristics have proven to be a significant hazard for

many places around the world. Some of these structures include the causative faults of important earthquakes such as El Asnam (Algeria, 1980), Coalinga (California, 1983), Northridge (California, 1994) and Tauramena (Colombia, 1995) (Philip and Meghraoui, 1983; Stein and King, 1984; Bullard and Lettis, 1993; Shaw and Shearer, 1999; Carena and Suppe, 2002)

The results of this study constitute a preliminary estimation of the potential seismic hazard associated with the Springbank Fault and they can be refined by further investigations and availability of new data.

Uncertainties related to the determination of the potential seismic hazard associated with the Springbank Fault will be described as follows in an attempt to recognize them and include them in the future analyses when new information becomes available. Sources of uncertainty include:

- Lack of dated material
- River knickpoint migration
- Errors related to seismic data acquisition and correlation
- Fold modelling errors with the Trishear program
- Possible variations in fault characteristics over time and space
- Errors related to slip rate calculation
- Uncertainties related to empirical equations

6.2.1 LACK OF DATED MATERIAL

The Quaternary stratigraphic units that have been defined in the study area are strictly formational units consisting of sediments assigned to a specific glacial cycle. The age of the formations is not well constrained and the nomenclature used for their classification is not rigorous.

The age of the geomorphologic units (Cust, Springbank and Boundary Units) defined during this study from geomorphologic and lithologic differences in the superficial sediments, and used to estimated the slip rate of the Springbank Fault, are based on indirect methods such as

loess cover, aggradation cycles, and river system evolution. These units are interpreted in the context of current literature on the late Quaternary history of Canterbury and the only direct dates from the area are from the loess sequence on the Cust Unit (Berger et al., 2001)

Direct methods of dating and a more accurate separation and classification of these units, are necessary in order to improve the estimations of total tectonic deformation produced by the Springbank Fault and its slip rate.

6.2.2 RIVER KNICKPOINT MIGRATION

The location of different structures such as the Eyrewell and the Sefton Faults is mainly based on morphometric analysis along the rivers in the study area. An important part of the analysis is related to the recognition of steepened river reaches (or knickpoints) associated with uplif.

At knickpoints, the river begins to adjust because the stream power increases across the steepened reach. This causes erosion and possibly knickpoint migration through time (Burbank and Anderson, 2001).

In some cases, steep inflections in channel profiles associated with structural controls or contrasting bed erodabilities remain stationary. In other cases, the knickpoint may diminish in a diffusive manner as slopes may decrease due to erosion upstream and deposition downstream; or the knickpoint may migrate upstream (Crosby, 2001).

The river analysis in the study area suggests that the knickpoint migration may not be significant because the location of fault zones and other structures identified before this study can be confirmed by the analysis of the river longitudinal profiles. Significant deformation in the profile is directly related to the location of the previously mapped structures. Furthermore, the direct correlation between the location of the Springbank Fault, established from geophysical investigations, and the location of the knickpoint related to the propagation fold forelimb at the Cust River, indicates either stationary knickpoints or comparatively recent deformation. Additionally, the topographic surveys along the Eyre River carried out in 1924 and 1958 show knickpoints at the same locations as the knickpoints obtained during this study, indicating no significant knickpoint migration.

It is possible that because of the characteristics of the Waimakariri and Ashley Rivers (larger rivers with more stream power), the conditions for knickpoint migration could be enhanced, but unfortunately if this is the case, the rates of migration are unknown.

As an example of an indication of the scale of error in locating the faults by this method, a knickpoint migration rate of 100mm/yr and an earthquake recurrence of 3000 years (as estimated for the Springbank Fault) are assumed. Under these conditions, the maximum upstream migration of the knickpoint would be in the order of 300m. Therefore, because the proposed location of the structures based on morphometric analysis along the rivers correspond only to their approximate projection on the surface, then a difference of 300m in their location is not considered to be significant in the context of this study.

6.2.3 ERRORS RELATED TO SEISMIC DATA ACQUISITION AND CORRELATION

There are intrinsic errors related to the acquisition, processing and depth conversion of seismic reflection data. These errors are related to the heterogeneous nature of the earth, subjective nature of the processing and different quality of the complementary information (i.e. well logs) used for depth conversion (Brooks et al., 2000).

During this study, the analysis and correlation of seismic lines lead to the estimation of a net slip for the Springbank Fault (from the seismic stratigraphic vertical throw) and some inferences related to the evolution of its propagation fold. Nevertheless, the errors related to seismic data acquisition and conversion of two way travel time (TWTT) to depth may induce uncertainties in the seismic stratigraphic interpretation and in the comparison between different seismic lines.

6.2.4 FOLD COMPUTER MODELLING ERRORS

The character of a propagation fold is directly related to the characteristics of the underlying fault and the geological and mechanical features of the sedimentary cover. Nevertheless, none of the kinematic/structural fold models involves the nature of the surrounding rocks or changes in fault characteristics over time and space.

Additionally, modelling of propagation folds with the Trishear program used for this study is limited by the assumption that the fault dip, tip propagation/slip ratio (P/S), trishear angle and depth to the decollement remain constant during the gradual fault/fold evolution; the physical validity of this assumption has not been demonstrated (Allmendinger and Shaw, 2000).

6.2.5 VARIATIONS IN FAULT CHARACTERISTICS

The characterisation of the Springbank Fault, including the determination of its geometry and rupture length, was based on the assumption that parameters such as fault dip and decollement depth remain constant over time and space. There is not enough information confirming that this is the case, and due to the heterogeneous nature of the crust, it is logical to think that these factors may vary. However, in the same way, there is no information indicating the amount and characteristics of this variation. Therefore, homogeneous parameters were used for simplicity in the calculations.

6.2.6 ERRORS RELATED TO SLIP RATE CALCULATION

The estimation of the tectonic deformation produced by the Springbank Fault was based on the difference in elevation between stratigraphically equivalent points, one in the hanging wall and another in the footwall of the fault, evaluated at the fault maximum topographic expression. This estimation of vertical deformation is only approximated and probably underestimated because younger deposits are covering the footwall and masking the actual vertical deformation. The tectonic deformation must be measured between points on synchronous surfaces and therefore, the thickness of the younger deposits must be included in the analysis. However, this thickness could not be estimated during this study because the top ~40 m of the surface cannot be imaged in the seismic lines as explained in Appendix 2.

6.2.7 USE OF EMPIRICAL RELATIONSHIPS

Several considerations have to be taken into account in order to apply the empirical relationships to estimate the maximum earthquake that the Springbank Fault is capable of producing and the ground motions around the fault. Some of these considerations are listed below:

- The magnitudes calculated by empirical relationships are approximate estimates and correspond to mean magnitude (Working group on California earthquake probabilities, 1999). The resulting estimates are expected values which could be exceeded 50% of the time (Bonilla et al., 1984; Wells and Coppersmith, 1994). However, if the input parameter, for example the rupture area, is considered the maximum value, then magnitude estimated using the empirical relations could be considered the maximum magnitude.

- In practice, different magnitudes could be related to the same values of fault parameters or vice versa. Such differences may be associated with a different shear modulus value (μ) on rock materials, that is a parameter directly related to seismic moment (Mo), which in turn is directly related to earthquake magnitude. Differences in shear modulus from place to place could explain observed variations in fault parameters associated with a given magnitude (Bonilla et al., 1984).

- Differences in magnitudes values between those predicted from the equations and the actual values could be associated with stress drop processes. Different studies have suggested that stress drop for medium magnitude events ($6 \leq M \leq 7$) may be less that those for large magnitude ($M \geq 7$) events. Consequently, stress drop for large magnitude events may significantly exceed the prediction of the regression equations (Wells and Coppersmith, 1994; Steward et al., 2001).

- The regression equations should not be extrapolated beyond the range of data sets used for the analyses (Bonilla et al., 1984; Wells and Coppersmith, 1994; Stirling et al., 2002). This also applies for the attenuation relationships.

- The attenuation relationships only provide an estimation of ground motions, and not everyone include all the parameters that may have a direct affect in ground motion distribution, such as specific site conditions, topographic effect and hanging wall effect.

- It is expected that the attenuation equations change when new digital seismic information from new earthquakes become available.

- Each region responds to its own attenuation laws and in order to provide a more accurate estimation of ground motions, a particular attenuation relationship should be developed from the specific site conditions of the region.

6.3 CONCLUSIONS

The main aim of this study was the characterisation of the Springbank Fault and the evaluation of its associated seismic hazard. To accomplish this, the project was divided into different objectives that, in summary, included: (i) detailed geomorphological mapping; (ii)

determination of subsurface fault geometry; (iii) estimation of fault slip rate; (iv) estimation of the approximate timing of the most recent earthquake ruptures; (v) analysis of microearthquake activity and focal mechanisms, and finally, (vi) estimation of ground motion and fault hazard assessment for an scenario earthquake.

Most of the objectives were achieved during the study, except the determination of the approximate timing of the most recent earthquake ruptures in the Springbank Fault. The following section provides the conclusions regarding each objective and their main implications.

In order to achieve the objectives, conventional techniques used in seismic hazard assessments of geological faults were supplemented with alternative and indirect methods, owing the blind character of the fault.

The blind nature of the Springbank fault made the determination of its location and total extent from conventional geomorphologic mapping, unviable. Additionally, the geomorphic expression of a blind structure significantly differs from the expression of faults that rupture to the surface. Trenching was not possible and consequently, data related to ages of displaced materials, and the date of the last earthquake produced by the structure were not available.

Therefore, conventional geomorphological mapping of landforms was accompanied by global positioning system (GPS) surveys, morphometric analyses along the rivers and seismic reflection surveys, in order to establish the location of the structure where its topographic expression is not evident.

The combination of these techniques were successful during this study. From the geomorphologic mapping and GPS surveys it was possible to establish the characteristics of the maximum fault expression, between Tram Road and the Cust River, and some attributes related to the Springbank Fault propagation fold, together with micro-topographic features associated with the deformation produced by the structure.

The morphometic analyses along the rivers proved to be an excellent tool in determining tectonic deformation. These analyses included river longitudinal profiles, determination of gradient index, analysis of sinuosity and channel changes, analysis of river channel width, topographical data along the riverbeds, and location of sites of persistent aggradation or

degradation. The combination of these analyses led to the determination of the tectonic deformation produced by both previously mapped structures and newly inferred faults.

The analyses indicate both that the Springbank Fault is not located where it was expected prior to this investigation, and the possible presence of two previously unrecognized faults, the Eyrewell and the Sefton Faults. The seismic reflection surveys further refined the location of the structures, mainly the Springbank and the Eyrewell Faults.

The basic fault characteristics necessary to establish the potential seismic hazard are estimated from these analyses: the Springbank Fault is a blind thrust/reverse structure located at less than 30 km from Christchurch, approximately between the Ashley and the Eyre Rivers, with an estimated strike extent of ~16 km and dip of ~60° to the northwest. The fault does not reach the surface but instead, produces a broad anticline that was classified as a propagation fold with the characteristics of both trishear and classical propagation fold, but mainly with the attributes of a trishear fold.

Further analysis of the Springbank Fault propagation fold suggests that its geometry is most closely modelled by a fault dipping 60°, with a tip propagation/slip ratio (P/S) of 7 and a trishear angle of 90°. In addition, the fault should propagate from a decollement located at a depth of ~14 km beneath the Canterbury Plains in order to produce a fold with the attributes of the Springbank Fault propagation fold.

The data also show that the two newly inferred structures, the Eyrewell and the Sefton Faults, appear to be related to propagation folds with similar characteristics to the fold related to the Springbank Fault, and consequently, they appear to be associated with the same decollement beneath the Canterbury Plains.

A decollement located in an aseismic detachment zone at the brittle-ductile transition has been suggested by several authors. Cowan (1992) suggested that the decollement is located between 12 and 17 km beneath the Canterbury Plains, which is consistent with the decollement at a depth of 14 km established during this study.

Therefore, the Springbank, the Eyrewell, the Sefton and also the Hororata Fault (a structure located to the southwest of the study area) are interpreted to be related to a fault system that is propagating toward the east, from a decollement associated with the development of a double side wedge geometry east of the Alpine Fault (Norris et al., 1990). Microearthquake activity

in the study area indicates seismicity associated with structures in the upper crust (Cowan, 1992), and probably related to this fault system.

Although the Springbank Fault belongs to this fault system, it is considered as a structure that behaves in a seismically independent way. The fault is assumed to move as a whole during and earthquake, without further segmentation, and with a rupture area of ~256 km^2.

In this analysis, the rupture area calculation is based on the estimates of subsurface length, dip and depth to the decollement, assuming that only the Springbank Fault ruptures. If the Eyrewell Fault and even the Sefton Fault branch from junctions linked above the basal decollement then it may be possible that a significantly larger area ruptures during a single rupture event, with a consequent increase in earthquake magnitude.

The Springbank Fault characteristics suggest Holocene activity and an earthquake of moment magnitude about 6.4 as the probable maximum magnitude earthquake for the fault, with a mean recurrence of approximately 3,000 years. There is no evidence of the date of the last earthquake produced by the Springbank Fault but the Holocene activity is indicated by deformation on surfaces of Holocene age. The magnitude of 6.4 is assumed as the maximum magnitude that the fault is capable of producing and implies the maximum stress drop in the fault. If this earthquake is assumed as a characteristic earthquake for the Springbank Fault, its recurrence, according to the amount of tectonic deformation on geomorphic units and their assigned age, may correspond to approximately 3,000 years. Nevertheless, it is expected that smaller and more frequent earthquakes may occur between the maximum events.

Further analyses, regarding the vertical displacement related to the fault at its maximum topographic expression, on the Cust, Springbank and the Boundary 2 Units, allow the estimation of a slip rate of ~0.22mm/yr. This indicates that, although the margin of error due to the unit age uncertainties is significant, the degree of activity of the Springbank Fault is low, and there is no indication of a change in slip rate through time.

If the Springbank Fault produces an earthquake of maximum magnitude 6.4 during a reverse slip event, urban centres such as Christchurch, Rangiora, Kaiapoi, Oxford, Cust, Amberley, Darfield, and Rolleston, among others, may be significantly affected. These towns are located in the near-fault zone, on the Canterbury Plains, which is underlain by a sedimentary basin containing a sequence of conglomerates, limestone, sandstone and mudstones with less compacted material at the top of the sequence. These conditions may strongly increase

earthquake shaking or modify the initial wave frequency and amplitude characteristics. Furthermore, urban centres such as Oxford and Cust may be significantly affected by the hanging wall effect, and Cust and Rangiora by directivity. Estimates of peak ground accelerations for these urban centres range between ~1.4g for Christchurch, to ~0.5g for Cust.

The results of this study suggest the presence of a previously unidentified fault system under the Canterbury Plains that may represent a significant and yet unstudied seismic hazard for many urban centres in Canterbury. This system is composed of thrust/reverse faults associated with propagation folds whose topographic expression may be considerably different from the topographical expression of faults that reach and rupture the surface.

The topographic expression of blind thrust/reverse faults may be very subtle, but it is possible to recognize them with detailed geomorphological mapping, supplemented with other techniques such as those used during this study, which include GPS surveys, morphometric analyses along the rivers and geophysical investigations.

This study showed that although the degree of activity of the Springbank Fault may be low, the close location of the structure with respect to many urban centres and its characteristics, make it a significant seismic hazard.

In the same way, the Eyrewell and Sefton Faults may also represent a significant seismic hazard for many urban centres. The hazard is related to the proximity and the location of the towns with respect to the inferred fault location, and with their site conditions.

The inferred Eyrewell Fault is especially important for Christchurch but neither this structure, the Sefton Fault, or the other possible structures beneath the study area have been subject to detailed analysis in assessment of seismic hazard or development of building codes.

6.4 RECOMMENDATIONS

Some recommendations considering both the uncertainties recognized during this study and its conclusions are presented below:

1. Use of alternative dating techniques such as optically stimulated luminescence (OSL), cosmogenic dating, and weather rind methods in order to provide a more accurate age of the gravels comprising the geomorphologic units identified in the study area. A better age

estimation of these units would provide in turn a better evaluation of both the Springbank Fault slip rate, and the geomorphologic fault and fold evolution.

2. Investigations regarding both river knickpoint migration or knickpoint behaviour in the study area, in order to improve the inferred location of the underlying structures.

3. Shallow seismic reflection surveys in order to confirm the location and extent of the Springbank Fault and its interaction with other structures such as the Ashley Fault and the Sefton Fault.

4. Detailed geomorphologic studies supplemented with other studies such as shallow seismic reflection surveys, GPS surveys and morphometric analyses in order to confirm the presence of the Eyrewell and Sefton Faults and their extent.

5. Deeper penetration seismic surveys to identify the projections and dip of faults into the basement, and the fault linkages.

6. Assessment of the potential seismic hazard associated with the Eyrewell, the Sefton and Hororata Faults. The location of these faults with respect to multiple urban centres in Canterbury, especially the location of the Eyrewell Fault with respect to Christchurch may result in a significant seismic hazard.

7. Further studies to identify other active structures beneath the Canterbury Plains in order to take them into account in seismic hazard analysis and building codes. This study showed that, however subtle, blind structures have geomorphic expressions that may lead to their recognition.

8. Detailed investigations regarding other earthquake related phenomena, such as landslide and liquefaction hazards, that may be induced by an earthquake generated by the Springbank Fault.

9. Application of the attenuation relationships currently developed for New Zealand by different researchers (i.e McVerry at GNS; and Stafford at the University of Canterbury) in future studies of the seismic hazard in different New Zealand regions.

REFERENCES

Abrahamson, N.A., and Somerville, P.G. (1996). Effects of the hanging wall and footwall on ground motions recorded during the Northridge Earthquake, *Bulletin of the Seismological Society of America* 87, 1B: S93-S99.

Abrahamson, N.A., and Shedlock, K. (1997). Overview (attenuation relationships), *Seismological Research Letters* 68, 1:9-23.

Abrahamson N. A., and Silva, W. J. (1997). Empirical response spectral attenuation relations for shallow crustal earthquakes, *Seismological Research Letters* 68, 1: 94- 127.

Allmendinger, R.W. (1998). Inverse and forward numerical modeling of Trishear fault-propagation folds, *Tectonics 17*, 4:640-656.

Allmendinger, R.W., and Shaw, J.H. (2000). Estimation of fault propagation distance from fold shape: implications for earthquake hazard assessment, *Geology* 28, 12:1099-1102.

Allmendinger, R.W. (1998, 2003). TRISHEAR 5.4.4 PROGRAM.

Anderson, H. and Webb, T. (1994). New Zealand seismic pattern revealed by the upgrated National Seismographs Network, *New Zealand Journal of Geology and Geophysics* 7, 4:477-493.

Atkins R. A., and Hicks S.R. (1979). Geophysical models along Ashburton River, Canterbury, New Zealand, *New Zealand Journal of geology and Geophysics* 22,6: 673-677.

Berger, G. W., Pillans, B. and Tonkin, P. (2001). Luminescence chronology of loess-paleosol sequences from Canterbury, South Island, New Zealand, *New Zealand Journal of Geology and Geophysics* 44: 501-516.

Berryman, K., and Beanland, S. (1991). Variation in fault behaviour in different tectonic provinces of New Zealand, *Journal of Structural Geology* 13, 2:177-189.

Bommer, J, J (2002). Deterministic vs probabilistic seismic hazard assessment: an exaggerated and obstructive dichotomy, *Journal of Earthquake Engineering*, Special Issue, 6: 43-73.

Bonilla, M. G. (1982). Evaluation of potential surface faulting and other tectonic deformation. USGS Open-File Report 82-732. [Online]. Available: http://geopubs.wr.usgs.gov/open-file/of82-732 [2002].

Bonilla, M. G. (1984). Statistical relations among earthquake magnitude, surface rupture length, and surface fault displacement. USGS Open-File Report 84-256. [Online]. Available: http://geopubs.wr.usgs.gov/open-file/of84-256 [2002].

Boore, D, M., Joyner, W.B., and Fumal T. E., (1997). Equations for estimating horizontal response spectra and peak acceleration from Western North American earthquakes: a summary of recent work. *Seismological Research Letter*s 68, 1: 128-153.

Bowden M.J., (1982). The water resources of the Ashley catchment: a report presented to the North Canterbury Catchment Board and Regional Water Board. 181p.

Bradshaw, J. D. (1989). Cretaceous geotectonic patterns in New Zealand region, *Tectonics* 8: 803-820.

Bray, J.D. (2001) Developing mitigation measures for the hazards associated with earthquake surface fault rupture. In Seismic Fault-Induced Failures Workshop, Japan Society for the promotion of Science, University of Tokyo, Japan, pp. 55-79.

Brooks, B.A., Sandvol, E., and Ross, A. (2000). Fold style inversion: Placing probabilistic constraints on the predicted shape of blind thrust faults, *Journal of Geophysical Research* 105, B6:13281-13301.

Browne, G. H. and Field, B. D. (1985). The lithostratigraphy of Late Cretaceous to Early Pleistocene rocks on Northern Canterbury, New Zealand, *New Zealand Geological Survey.* Record 6, 63 p.

Browne, L.J., Wilson, D. D., Moar, N. T., Mildenhall, D.C. (1988). Stratigraphy of the Late Quaternary deposits of the Northern Canterbury Plains, New Zealand, *New Zealand Journal of geology and Geophysics* 31: 305-335.

Bullard, T.F., and Lettis, W.R. (1993). Quaternary fold deformation associated with blind thrust faulting, Los Angeles Basin California, *Journal of Geophysical Research* 98, B5: 8348-8369.

Burbank, D. and Anderson R. (2001). Tectonic Geomorphology. Blackwell Science, 274p.

Campbell K, W. (1997). Empirical near-source attenuation relationships for horizontal and vertical components of peak ground acceleration, peak ground velocity, and pseudo-absolute acceleration response spectra, *Seismological Research Letters* 68, 1: 154-179.

Campbell, J.K and Yosif, H.S. (1985). Tectonic geomorphology of the Lower Waipara Gorge, North Canterbury, *Geological Society of New Zealand Miscellaneous Publication,* Report 32B, pp 53-69.

Campbell, J., Bennet, D. and Brand, R. (2000). Actively emergent, fault-related fold structures beneath the Canterbury Plains. 2000 New Zealand Petroleum Conference. Pre-Conference Field Trip Guide.

Canterbury Regional Council (1995). Ashley River floodplain management regional plan: Technical investigation. Report 95(6).

Cardozo, N., Bhalla, K., Zehnder, A., and Allmendinger R.W. (2003). Mechanical models of fault propagation folds and comparison to the trishear kinematic model, *Journal of Structural Geology* 25:1-18.

Carena, S. and Suppe, J. (2002) Three-dimensional imaging of active structures using earthquake aftershocks: The Northridge thrust, California, *Journal of Structural Geology* 24: 887-904.

Couzens, B., A. and Dunne, W.M. (1994) Displacement transfer at thrust terminations: the Saltville thrust and Sinking Creek anticline, Virginia, U.S.A., *Journal of Structural Geology* 16: 721-793.

Cowan, H. A., Reyners, M., and Taber, J. (1991). Present tectonics of the East Coast-Southern Alps plate boundary zone, North Canterbury, N.Z.: Inferences from seismicity, *Geological Society of New Zealand miscellaneous publication* 56: 11.

Cowan, H. A. (1992). Structure, seismicity and tectonics of the Porter's Pass-Amberley fault zone, North Canterbury, New Zealand. Christchurch, New Zealand, University of Canterbury, Thesis: PhD, 181p.

Cowan, H. A., Nicol, A., and Tonkin, P. (1996). A comparison of historical and paleoseismicity in a newly formed fault zone and a mature fault zone, North Canterbury, New Zealand, *Journal of Geophysical Research* 103, 3:6021-6036.

Crosby, B.T. (2001). Knickpoint migration in the Waipaoa River and its tributaries: and examination of the rate and form of transient migration in fluvial systems. [Online]. Available: http://darla.mit.edu/~montain [2003].

Earl, P.L (1997). The hydrogeology of the Eyre River aquifer and its influence on spring occurrence and distribution. Christchurch, New Zealand, University of Canterbury, Thesis: Bs Honours, 260p.

Elliot, D. (1976) The motion of thrust sheets, *Journal of Geophysical Research* 81, 5:949-963.

Erslev, E. A. (1991). Trishear fault-propagation folding, *Geology* 19: 617-620.

Erslev, E. A., and Mayborn, K. R. (1997). Multiple geometries and modes of fault-propagation folding in the Canadian thrust belt, *Journal of Structural Geology* 19, 3-4:443-461.

Field, B., D; Browne and others (1989). Cretaceous and Cenozoic sedimentary basins and geological evolution of the Canterbury Region, South Island, New Zealand. N.Z. Geological Survey Basin Studies 2.

Gage, M. (1958). Late Pleistocene glaciations of the Waimakariri Valley, Canterbury, New Zealand. *N.Z Journal of Geology and Geophysics* 1:123-155.

Gazetas, G. Dakoulas, P. and Papageorgiou, A. (1990). Local soil and source–mechanism effects in the 1986 Kalamata (Greece) earthquake, *Earthquake Engineering and Structural Dynamics* 19: 413-456.

Gregg, D. R (1964). Geological Map of New Zealand 1:250,000. Sheet 18, "Hurunui". N.Z. DSIR, Wellington.

Guccione, M.J., Mueller, K.J., Champion, J., Sheperd, S., Carlson, S.D., and Odhiambo, B. (2002). Stream response to repeated coseismic folding, Tiptonville Dome, Western Tennesse, *Geomorphology* 43: 313-349.

Hack, J.T. (1973). Stream-profile analysis and stream-gradient Index, *Jour. Research U.S Survey* 1, 4: 412-429.

Jackson, J., Norris, R., and Youngson, J. (1996). The structural evolution of active fault and fold systems in Central Otago, New Zealand: Evidence Revealed by Drainage Patterns, *Journal of Structural Geology* 18, 2/3: 217-234.

Jamison, W.R., (1987). Geometric analysis of fold development in overthrust terranes, *Journal of Structural Geology* 9: 207-219.

Jongens, R., Pettinga, J. R., and Campbell, J.K. (1999). Stratigraphic and structural overview of the onshore Canterbury Basin: North Canterbury to the Rangitata River. Unpublished Report for indo-Pacific Energy (NZ) Ltd. University of Canterbury. 31p.

Johnson K.M., and Johnson A. M. (2002). Mechanical models of trishear-like folds, *Journal of Structural Geology* 24:277-287.

Keller and Pinter, (1996). Active Tectonics: Earthquakes, Uplift and Landscape. 338 p.

Kelson, K., Kang, K.H., Page, W., Lee, C.T., and Cluff Ll. (2001). Representative styles of deformation along the Chelungpu Fault from the 1999 Chi-Chi (Taiwan) earthquake: Geomorphic characteristics and responses from man-made structures, *Geological Society of America Bulletin* 91, 5:930-952.

Knuepfer, P.L. (1992). Temporal variations in latest Quaternary Slip across the Australian-Pacific Plate boundary, northeast South Island, New Zealand, *Tectonics* 11, 3:449-464

King, G.C.P., and Vita-Finzi, C. (1981). Active folding in the Algerian earthquake of 10 October 1980, *Nature* 292: 22-26.

Klohn-Crippen Consultants Ltd. (1994). Amplification of ground motion. preliminary seismic microzonation assessment for British Columbia. [online]. Available: http://www.for.gov.bc.ca/RIC/Pubs/EarthSci/seismic/Seismicmicro-05.htm [2002].

Kramer, S.L. (1996). Geotechnical earthquake engineering. Prentice-Hall civil engineer and engineering mechanics series. 653p.

Lettis, W.R., Wells, D.L., and Baldwin J.N. (1997). Empirical observations regarding reverse earthquakes, blind thrust faults, and Quaternary deformations: Are blind thrust truly blind?, *Bulletin of the Seismological Society of America* 87, 5: 1171-1198.

Litchfield, N.J. (1995). Structure and tectonic geomorphology of the Lowry Peaks Range-Waikari Valley Distric, North Canterbury. Christchurch, New Zealand, University of Canterbury, Thesis: MSc, 260 p.

McClay, K. R., (Editor). (1992). Thrust Tectonics. Chapman & Hall. 447 p.

McGinty, P. (2001). Preparation of the New Zealand earthquake catalogue for a probabilistic seismic hazard analysis, *Bulletin of New Zealand Society for Earthquake Engineering* 34, 1:60-67.

McVerry G.H. (1997). Near-fault earthquake records and implications for design motions. New Zealand National Society for Earthquake Engineering. Pp 88-95.

McVerry, G, Zhao, J.X., Abrahamson, N.A, Somerville, P.G. (2000). Crustal and subduction zones attenuation relations for New Zealand earthquakes. Proceedings of the 12th World Conference of Earthquake Engineering 2000. Auckland, New Zealand.

Montana Bureau of Mines and Geology (2003). Earthquake studies: glossary of seismic terms [Online]. Available: http://mbmgquake.mtech.edu/seismic_glossary.html [2003].

Nicol, A., and Wise, D. (1992). Paleostress adjacent to the Alpine Fault of New Zealand: fault, vein, and styolite data from the Doctors Dome area, *Journal of Geophysical Research* 97, 12: 17,685-17,692.

Nicol, A., Alloway, B., Tonkin, P. (1994). Rates of deformation, uplift, and landscape development associated with active folding in the Waipara Area of North Canterbury, New Zealand, *Tectonics* 13, 6: 1327-1344.

Norris, R.J., Koons, P.O., and Cooper, A.F. (1990). The obliquely-convergent plate boundary in the South Island of New Zealand: Implications for ancient collision zones, *Journal of Structural Geology* 12, 5/6: 715-725.

Oglesby, D.D., Archuleta, R.J., and Nielsen, S.B. (1998). Earthquakes on dipping faults: the effects of broken symmetry, *Science* 280:1055-1059.

Oglesby, D.D., Archuleta, R.J. (2000a). Dynamics of dip-slip faulting: Explorations in two dimensions, *Journal of Geophysical Research* 105, B6: 13643-13653.

Oglesby, D.D., Archuleta, R.J., and Nielsen, S.B. (2000b). The three-dimensional dynamics of dipping faults, *Bulletin of the Seismological Society of America* 90, 3: 616-628.

Oglesby, D. D. and Day, S.M. (2001). Fault geometry and the dynamics of the 1999 Chi-Chi (Taiwan) earthquake, *Geological Society of America Bulletin* 91, 5:1099-1111.

Ouchi, S. (1985). Response of alluvial rivers to slow active tectonic movement, *Geological Society of America Bulletin* 96:504-515.

Ouchi, T., Lin, A., Chen, A., and Maruyama, T. (2001). the 1999 Chi-Chi earthquake: Earthquake fault and strong motions, *Geological Society of America Bulletin* 91, 5:966-976.

Papageorgiou. **A.** (1998). Long period ground motions and spatial variation review . [online]. Available: http://mceer.buffalo.edu/research/HighwayPrj [2001].

Patrick, M. (1999). An examination of stream profile data for characterizing active tectonics in Mendoza, Argentina. [Online]. Available: asuag.org/~mpatrick/cornell-thesis [2002].

Pettinga, J. R., Chamberlain, C.G., Yetton, M.D., Van Dissen, R.J., Downes, G. (1998). Earthquake source identification and characterization: Stage 1 (Part A) Earthquake hazard and risk assessment study. Canterbury Regional Council, publication No. U98/10. 121p.

Pettinga, J.R., Yetton, M.D., Van Dissen, R.J. and Downes, G. (2001). Earthquake source identification and characterization for the Canterbury region, South Island, New Zealand. *Bulletin of New Zealand Society for Earthquake Engineering* 34:282-317.

Philip, H., Meghraoui, M. (1983). Structural analysis and interpretation of the surface deformations of the El Asnam Earthquake of October 10, 1980, *Tectonics* 2, 1: 17-49.

Reyners, M., and Cowan, H. (1991). Crustal structure of the North Canterbury Region determined from earthquakes and explosions, *Geological Society of New Zealand miscellaneous publication* 56: 41.

Reyners, M and Cowan, H. (1993) The transition from subduction to continental collision: crustal structure in the North Canterbury region, New Zealand, *Geophys. J. Int* 115:1124-1136.

Reynolds, J. M. (1997). An introduction to applied and environmental geophysics. Wiley ed. 796p.

Rodger, D. A. and Rizer, W. D. (1981). Deformation and secondary faulting near the lending edge of a thrust fault. In: McClay, K. R and Price, N., J., (Editors). Thrust and Nappe Tectonics. Geological Society of London Special Publication No. 9. pp 65-77.

Sadigh, K., Chang, C. Y., Egan, J.A., Makdisi, F., and Young, R.R. (1997). Attenuation relationships for shallow crustal earthquakes based on California strong motion data, *Seismological Research Letters* 68, 1: 180-189.

Scholz, C. H. (1990). The mechanics of earthquakes and faulting. Cambrige University Press. 439p.

Schumm, S. (1986). Alluvial river response to active tectonics. In Active Tectonics. National Academic Press. Pp 80-94.

Schumm, S., Dummont, J., and Holbrook, J. (2000). Active tectonics and alluvial rivers. Cambridge University Press. 276 p.

Shaw, J. H., and Shearer, P. M. (1999). An elusive blind-thrust fault beneath metropolitan Los Angeles, *Science* 283:1516-1518.

Shimazaki, K. (1986). Small and large earthquakes: The effects of the thickness of seismogenic layer and the free surface, in Earthquake Source Mechanics. Das, S., Boatwrigth, J.,and Scholz, C. (editors). Geophysical Monograph 37. American Gephycial Union. Pp 209-216.

Sibson, R.H. (1989). Earthquake faulting as a structural process, *Journal of Structural Geology* 11, 1-2:1-14.

Silberling, N.J., Nichols, K.M., Brawshaw, J.D., Blome, C.D. (1988). Limestone and chert in tectonic blocks from the Esk Head Subterrane, South Island, New Zealand. *Geological Society of America Bulletin* 100:1213-1223.

Sissons, R. (1999). Paleoseismic investigation of the Ashley Fault, North Canterbury, New Zealand. Christchurch, New Zealand, University of Canterbury, Thesis: B.Sc Honours.

Sissons, R., Campbell, J., Pettinga, J., and Milner D. (2001). Paleoseismicity of the Ashley and Loburn Faults, North Canterbury, New Zealand. Report prepared for Earthquake Commissions Research Foundation. Project number 97/237.

Somerville, P., Saikia, C., Wald D., and Graves, R. (1996). Implications of the Northridge earthquake for strong ground motions from thrust Faults, *Bulletin of the Seismological Society of America* 87, 1B: S115-S125.

Somerville, P.G., Smith N.F., Graves, R. and Abrahamson, N.A. (1997). Modification of empirical strong ground attenuation relations to include the amplitude and duration effects of rupture directivity, *Seismological Research Letters* 68, 1: 199-222.

Stein, R.S., and King, G.C.P. (1984). Seismic potential revealed by surface folding: 1983 Coalinga, California, Earthquake, *Science* 224: 869-872.

Stewart., J., Chiou, S., and Bray, J., Graves, R.W., Somerville, P.G., and Abrahamson, N.A.,. (2001). Ground motion evaluation procedures for performance based design. Peer Report 2001/09. Pacific Earthquake Engineering Research Center. 229p.

Stirling, M., Rhoades, D., and Berryman, K. (2002a). Comparison of earthquake scaling relations derived from data of the instrumental and preinstrumental era, *Bulletin of the Seismological Society of America* 92, 2: 812-830.

Stirling, M.W., McVerry, G. H., and Berryman K. R. (2002b). A new seismic hazard model for New Zealand, *Bulletin of the Seismological Society of America* 92, 5: 1878-1903.

Suggate, R.P. (1990). Late Pliocene and Quaternary Glaciations of New Zealand, *Quaternary Sciences Reviews* 9, 2-3:175-197.

Suppe, J. (1983). Geometrics and kinematics of fault-bend folding, *American Journal of Science* 283, 7:684-721.

Suppe, J. (1985). Principles of Structural Geology. Prentice-Hall. 537 p.

Suppe, J., and Medwedeff, D. A. (1990). Geometry and Kinematics of fault-propagation folding, *Eclogae Geol. Helv.* 83, 3:409-454.

Suppe, J., Chou, G. T and Hook, S. P. (1992). Rates of folding and faulting determined from growth strata. In: McClay, K. R. (Editor). Thrust Tectonics. Chapman & Hall. pp105-132.

Thorbjornsen K.L and Dunne W. M. (1997). Origin of a thrust-related fold: geometric vs kinematic tests, *Journal of Structural Geology* 19, 3-4:443-461.

Trimble. The Global Positioning System (GPS) Tutorial. [Online]. Available: http://www.trimble.com/gps [2002].

USGS (1996). USGS Response to an Urban Earthquake -- Northridge '94. Open-File Report 96-263 *1996.*. [online]. Available: http://geohazards.cr.usgs.gov/northridge/localeff.htm [2002].

USGS (1998). Shallow earthquakes in active tectonic regions. [online]. Available: http://geohazards.cr.usgs.gov/engnseis/Eshmpage/shalactreg.htm [2003].

Waimakariri Irrigation Ltd (2000). The rivers of the Waimakariri plains. [online]. Available: www.wil.co.nz [2002].

Wald, D. J., Quitoriano, V., Heaton, T. and Kinamori, H. (1999). Relationships between Peak Ground Acceleration, Peak Ground Velocity and Modified Mercalli Intensity in California, *Earthquake Spectra*, 15,3: 557-564.

Walsh J.J., and Watterson J. (1988). Analysis of the relationship between the displacements and dimension of faults, *Journal of Structural Geology* 10:239-247.

Wells, D. L, and Coppersmith K. J. (1994). New empirical relationships among magnitude, rupture length, rupture width, rupture area, and surface displacement. *Bulletin of the Seismological Society of America* 84, 4:974-1002.

Wesnousky, S. (1986). Earthquakes, Quaternary faults and seismic hazard in California. *Journal of Geophysical Research* 91, B12:12587-12631.

Wilkerson, M.S., Apotria, T., Farid, T. (2002). Interpreting the geologic map expression of contractional fault-related fold terminations: lateral/oblique ramps versus displacements gradients, *Journal of Structural Geology* 24:593-607.

Williams, G., and Chapman, T. (1983). Strains developed in the hanging wall of thrust due to their slip/propagation rate: a dislocation model, *Journal of Structural Geology* 5, 6:563-571.

Wilson, D.D. (1989). Quaternary geology of Northwestern Canterbury Plains. Miscellaneous series map 14, 1:100.000, New Zealand Geological Survey, Department of Scientific and Industrial Research.

Woodward, N.B. (1997). Low-amplitude evolution of break-thrust folding, *Journal of Structural Geology* 19, 3-4:293-301.

Working Group on California Earthquake Probabilities (1999). Earthquake probabilities in the San Francisco Region: 2000-2030 – A summary of findings. USGS open file-report 99-517.

Yielding, G., Jackson, J.A., King, G.C.P., Sinvhal, H., Vita-Finzi, C., and Wood, R.M. (1981). Relations between surface deformation, fault geometry, seismicity, and rupture characteristics during the El Asnam (Algeria) Earthquake of 10 October 1980, *Earth and Planetary Science Letters* 56:287-304.

Yousif, H. S. (1987). The applications of remote sensing to geomorphological neotectonic mapping in North Canterbury, New Zealand. Christchurch, New Zealand, University of Canterbury, Thesis: PhD. 410p.

Appendix 1
GLOBAL POSITIONING SYSTEM (GPS)

This appendix presents an introduction and brief description of the GPS technology and surveying techniques. The information was mainly extracted from the online tutorial of Trimble®, the equipment used during this investigation. For additional reading, many references in the specialized literature and Internet exist.

A1. INTRODUCTION

The Global Positioning System (GPS) is a worldwide radio-navigation system formed by 24 NAVSTAR satellites and their ground stations.

The NAVSTAR satellites orbit the Earth every 12 hours and are used as reference points to calculate accurate positions on the Earth.

Ground Stations monitor both the performance and the exact position in space of the GPS satellites. These stations transmit corrections for the satellite's orbits (ephemeris) constants and clock offsets back to the satellites themselves. This information is incorporated and sent to GPS receivers on the Earth.

A.2 HOW GPS WORKS

Satellites in space are used as reference positions to locate points on the Earth. The exact orbit and position of each satellite is known, and is continually monitored by the ground stations.

In order to determine the exact location of a point of interest on the Earth, the distance between a satellite and the point is calculated using the travel time of a radio signal sent from the satellite to a receiver located at the point of interest. The radio signal is a very complicated digital code, named pseudo-random code, and is different for each satellite.

The receiver calculates the travel time of the signal by comparing its own pseudo-random code with an identical code in the signal sent from the satellite. The receiver's code is delayed with respect to the signal from the satellite, and it is "moved" until it matches perfectly. This amount of "movement" is equal to the travel time of the signal. Knowing the travel time and the velocity of the signal (i.e. speed of light), the distance between the receiver and the satellite can be calculated.

With the distances between three different satellites and the receiver located at a specific point, a "trilateration" process (a process similar to triangulation but without angles involved) is used to calculate the position of the point. A fourth satellite is employed to determine the exact position and to remove time errors.

A3. DIFFERENTIAL GPS TECHNIQUE

Different GPS techniques exist in order to achieve better accuracy in the measurements. During this study, the differential GPS technique was used to minimize positional errors.

Differential GPS involves two receivers working at the same time. One of them remains stationary while the other one is moving making positional measurements. The stationary receiver (base station) is located at a point of very well known position, usually a survey mark such as a trig station. This attaches the satellite measurements to a local reference and allows us to make position corrections if necessary.

The time signal that travels from the satellites to a receiver and that is used to calculate the position of a particular point, may contain errors related to technological or environmental factors. These errors may be caused by clock and/or satellite orbit inaccuracies, changes in signal travel path due to atmospheric layers, and environmental noises. The well known position of the base station permits us to determine and correct timing errors and provides the positional corrections to the moving receiver, improving the overall accuracy of the measurements.

Instead of using timing signals to calculate its position, the base station uses its known position to calculate timing. It compares the calculated travel time (what the travel time of the GPS signals

should be according to its position), with the actual measured travel time. The difference is an "error correction" factor that is used to correct the measurements of the moving receiver.

A.3.1 CODE PHASE AND CARRIER PHASE GPS

There are two different modes of determining positional locations in differential GPS technique: code and carrier phase. Both were used as part of this study. As explained above, the GPS receivers determine the signal travel time from the satellites by comparing pseudo-random codes. In code phase, pseudo-random codes that have a cycle width of almost a microsecond are compared. Due to the wide cycle of the signals, the compared pseudo-random codes can be out of phase and this will introduce an error in the location. This error may be of about 1 m or more.

Carrier-phase uses shorter wavelength signal which significantly reduces the positional errors. A carrier signal is a particular high frequency signal also transmitted by the satellites. The pulses of this signal are much closer together and consequently provide greater accuracy. The positional error in carrier-phase may be of around 10 cm.

Appendix 2

SHALLOW SEISMIC REFLECTION SURVEYS

Two shallow P-wave seismic reflection surveys were undertaken to define the near-surface geometry and fault characteristics of the Springbank Fault. Both surveys were carried out along gravel roads: Boundary Rd (seismic line 1) and North Eyre Rd (seismic line 2). This appendix explains the data acquisition and processing of both seismic lines.

An initial walkaway test was undertaken in the middle of the seismic line 1 (Boundary Road) in order to define the acquisition parameters and the optimum source for the reflection surveys. Conservative seismic acquisition parameters were chosen (Table A2.1) and several different sources were tried including Mini-SOSIE, 12 gauge pipe gun, and a hammer and plate.

The results from these tests indicated that the region of interest, the top 500 m of the sub-surface, would be imaged successfully by all three sources. It was therefore decided that the hammer and plate would be used, as it allows the most rapid field data acquisition, is very easy to use in the field, and involves minimal costs.

Using the information obtained from the walkaway test, the parameters present in Table A2.1 were chosen for both seismic lines.

Table A2.1: Seismic survey acquisition parameters.

Seismic Line	Survey Type	Seismic Line Length	Nearest Shot Receiver Offset	Furtherest Shot Receiver Offset	Shot Spacing	Geophone Group Spacing	No. Of Stacks
Boundary Road	Shots through north west end	1930m	25m	265m	10m	5m	6
North Eyre Road	Shots through west end	1200m	25m	265m	10m	5m	6

A2.1 DATA ACQUISITION

On both surveys the data was recorded by a Geometrics 48-channel Strata Visor® 24 bit seismograph. Groups of geophones, consisting of three 30Hz non-damped geophones, wired in series, were aligned parallel to the seismic line orientation (N55°W for seismic line 1 and N70°W for seismic line 2). Each geophone was spaced at ~1.66m, 1/3 of the group spacing apart.

Four, 24 takeout 6.6m spacing common mid point (CMP) cables were used for the connection of the geophones, and a 96 to 48 channel roll-along switch was used to select 48 continuous geophone groups out of the 96 available.

The seismic source shots were generated using a 10kg hammer and 15kg plate. Shot timing was determined electronically at the seismic source when the hammer hit the plate.

The raw field data was recorded without filters or other field processing functions so that all possible frequencies would be available. The Strata Visor® seismograph is equipped with a large amount of storage capacity reducing the need to select low sampling rates to reduce the data quantity (Geometrics, 1999). For the surveys a sampling rate of 0.25 ms was used and recording window of 2s. The sampling rate and window were reduced in later processing to speed computations.

A2.2 DATA PROCESSING

To obtain the maximum amount of information possible from the surveys careful processing of the raw data is necessary. All data processing was undertaken using the Visual Sunt® for PCs seismic processing software, running on an IBM Pentium PC.

The goal of the processing is to identify and enhance the reflection signals, eliminating as many non-reflection events as possible. This process is necessary for the accurate interpretation of the subsurface data.

Processing steps

Data processing involved the following steps for each seismic line:

Geometry Setting

The initial step in processing involves setting the geometry of the seismic line. Field notes were used to register the location of all seismic sources (shots) and receiver, and the general configuration of the line.

Data Conversion

The raw seismic data was converted from industry standard SEG-2 format to the propriety Visual Sunt format used by the processing software.

Trace Editing (Bad Trace Removal)

Independent trace editing or "killing" was used to remove unusually noisy traces or traces without any reflection signal. These traces are caused by several factors such as malfunctioning geophones, environmental noise or bad coupling between geophones and ground.

Bandpass Frequency Filtering

Some frequencies representing undesirable data such as airwaves, ground roll, environmental noise and refractions, among others, should be eliminated from the seismic record. To suppress as much "noise" energy as possible, a band pass frequency filtering process was applied.

To determine at which frequencies the reflected signals are enhanced compared to the coherent noise signal, a range of bandpass filters were evaluated and the optimum applied to all shot gathers in the line. Figure A2.1 in this Appendix shows the graphical record of the process for both seismic lines.

The analysis indicated that a band pass filter of (80Hz – 100Hz –180Hz – 240Hz) and (40Hz – 60Hz –120Hz – 160Hz) enhance the data of interest for seismic line one and two respectively. However, not all undesirable data is eliminated by this process, further techniques have to be used, as explained below.

Trace Scaling (Gain Correction)

To account for the decrease in amplitude of seismic waves caused by spherical divergence, attenuation and different geophone-source geometry, a gain correction was applied. This has the effect of normalizing the total energy within a user-defined window.

Different Automatic Gain Control (AGC) values of 10ms, 20ms, 50ms, 100ms, 150ms, 200ms, and 400ms, were analysed for each seismic line (Figure A2.2). The analysis showed that an AGC of 100ms gave the best results for both profiles.

First Arrival Muting

Undesirable signals representing direct waves and shallow refractions are the first ones to arrive and be recorded and they masked some of the reflections of interest.

Not all these signals can be removed by bandpass filtering, so further muting was manually carried out for the top of the profile.

Careful muting out of non-reflection data was done using a tapered mute. A disadvantage of the procedure is that approximately the first 50m in depth of the profile are also removed.

Surgical Muting of "Noise"

To increase the signal to noise ratio (S/N) of the reflection events, surgical muting is applied to the data to remove any airwave and ground roll data that has not been removed by bandpass filtering. At this stage, the non-reflection component of the profile should have been reduced to a minimum.

Common Mid Point (CMP) sorting

The traces were then Common Mid Point (CMP) sorted to produce CMP gathers. Each CMP gather represents the energy above a common mid point in the subsurface.

Velocity Analysis

A velocity analysis was done on the CMP sorted muted records. The aim of the analysis is to derive a detailed subsurface velocity model.

Velocities between 1600m/s and 3000m/s were evaluated, as shown in Figure A2.3. According to the analysis, a velocity of 2400m/s enhances the reflection signal.

Move Out Correction

Due to the seismic reflection energy having to travel longer to reach progressively farther away geophones, their travel times increase with distance. This causes a delay (move-out) for each seismic arrival on the seismic record. To correct this delay, a move-out correction was applied, using the velocities obtained from the previous step.

Stacking

In order to enhance the seismic signal at each CMP gatter, individual traces are summed together (stacking). This produces a two-way time (TWT) versus offset section display. Finally, the stacked section is scaled and gained applied to maximise the presentation of important features.

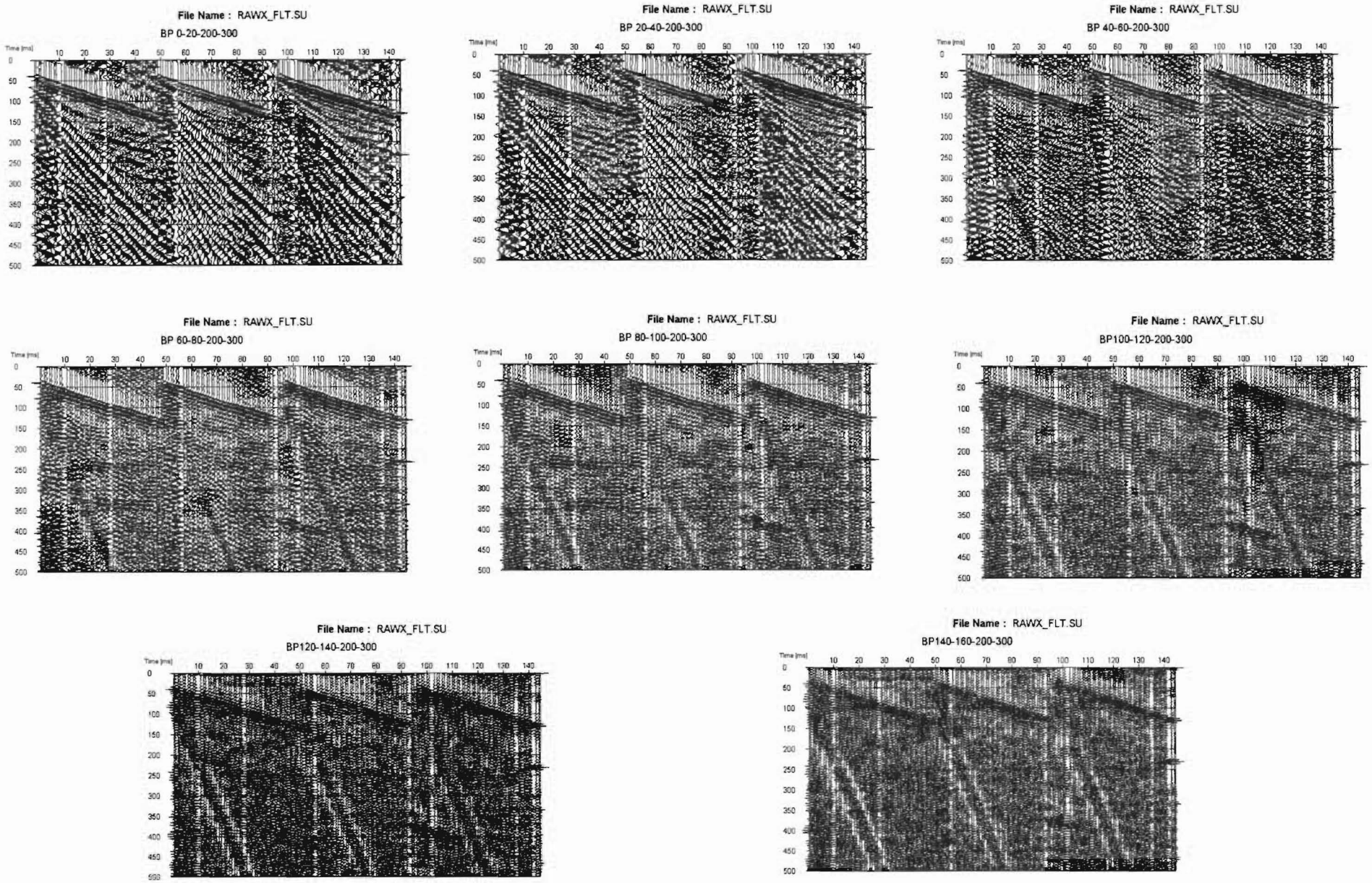

Figure A2.1: Band pass frequency filtering for seismic line 1-Boundary Road.

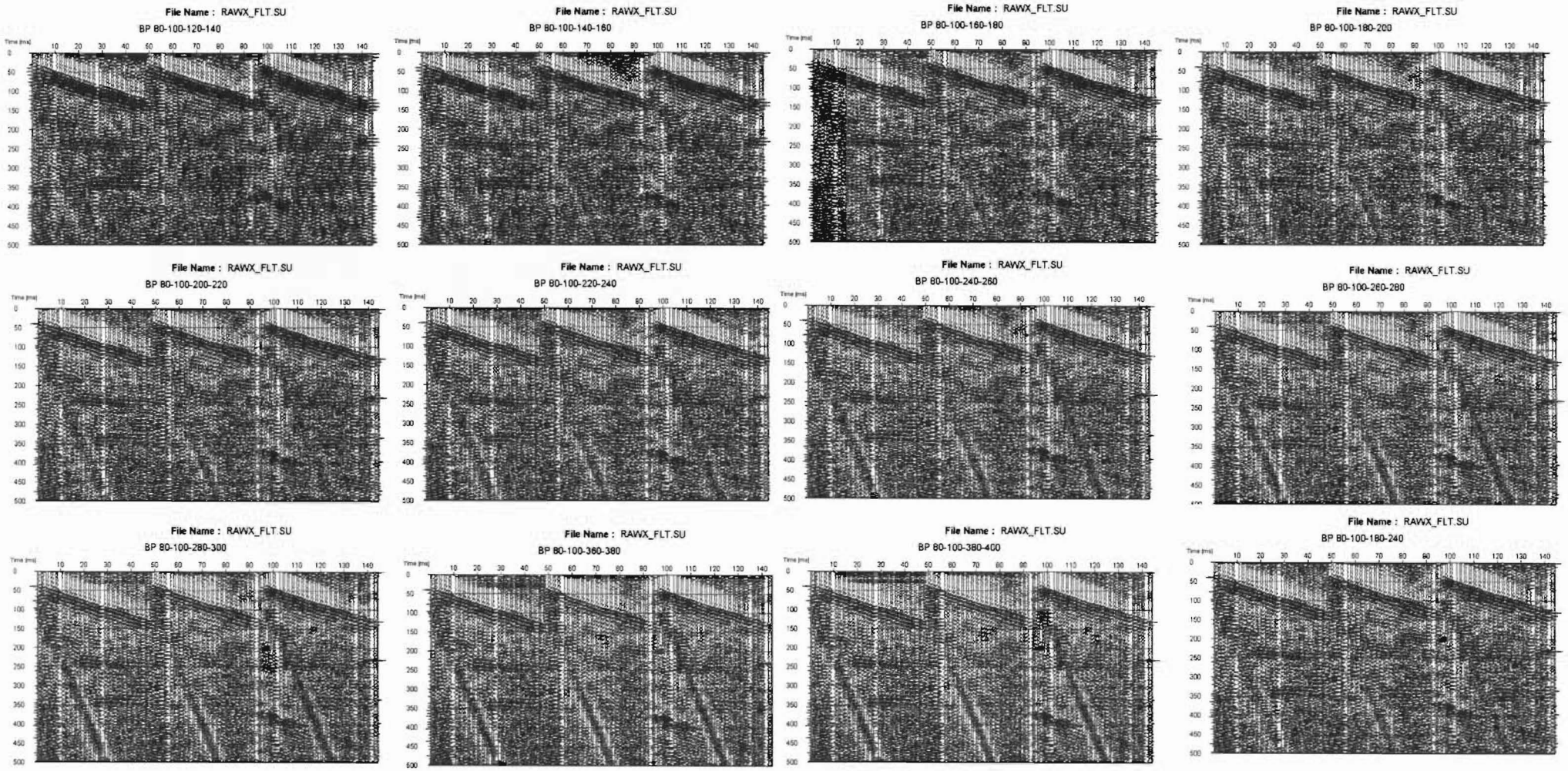

Figure A2.1 (continuation): Band pass frequency filtering for seismic line 1-Boundary Road.

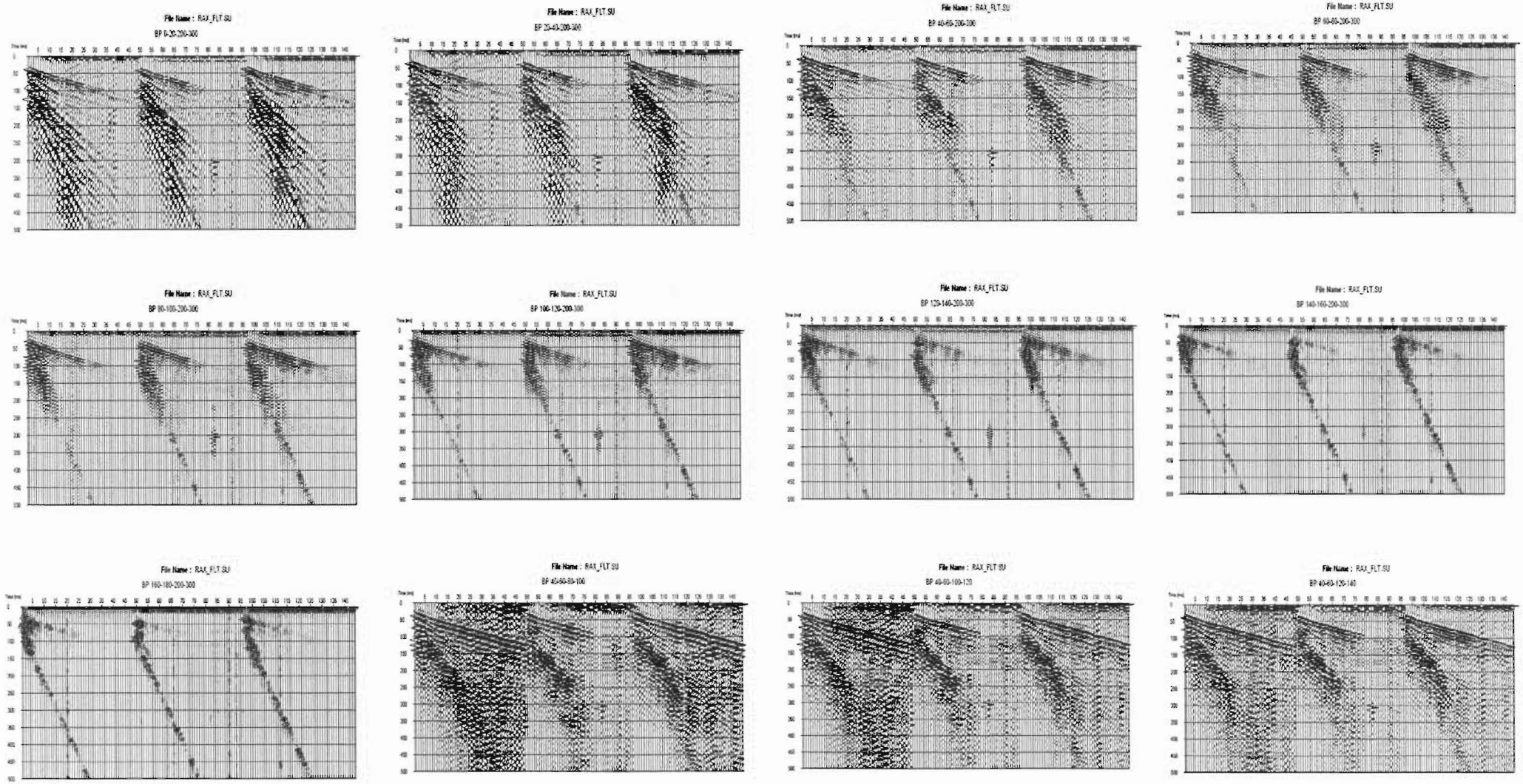

Figure A2.1 (continuation): Band pass frequency filtering for seismic line 2-North Eyre Road.

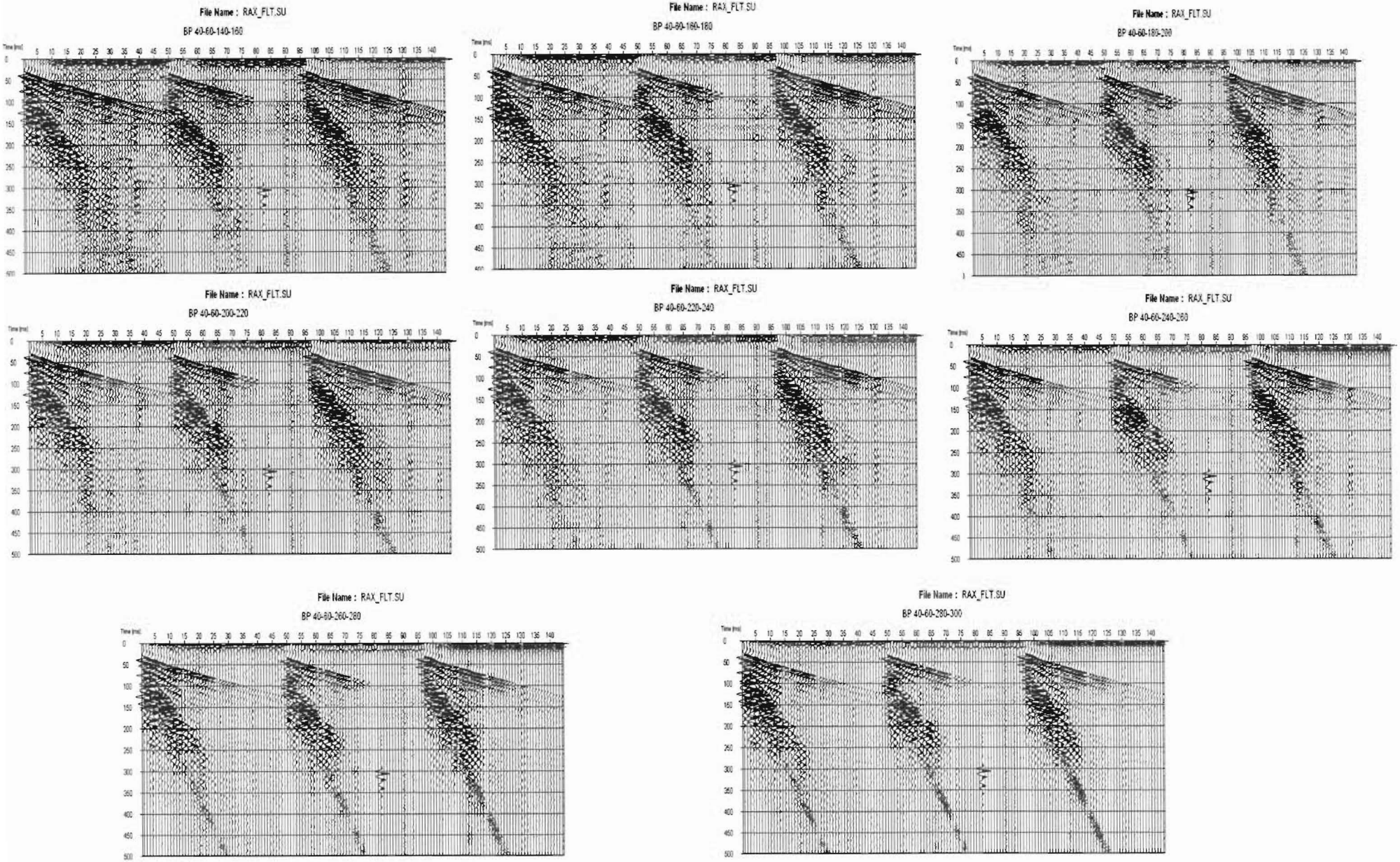

Figure A2.1 (continuation): Band pass frequency filtering for seismic line 2-North Eyre Road.

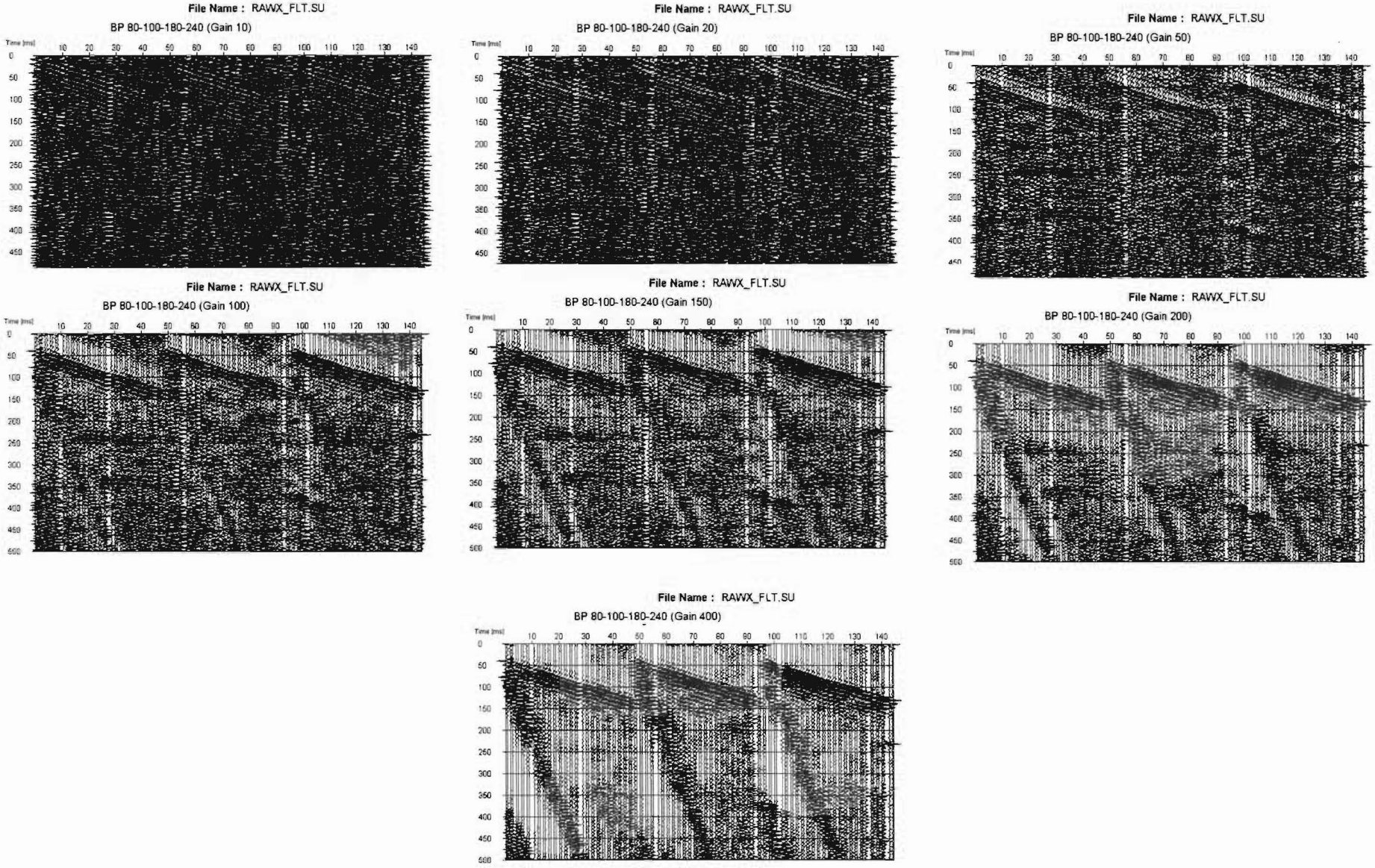

Figure A2.2: Trace scaling (gain correction) for seismic line 1-Boundary Road.

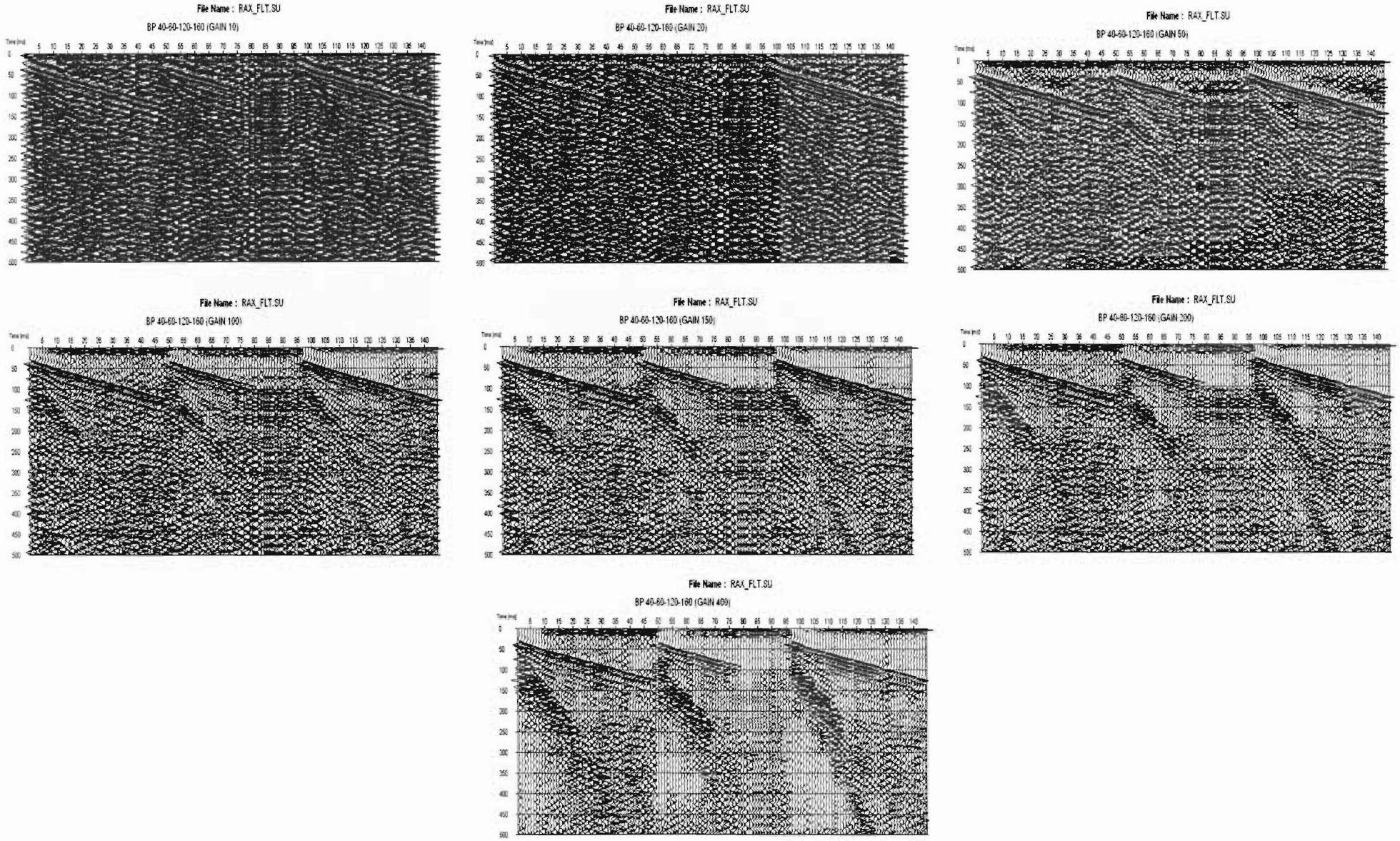

Figure A2.2 (continuation): Trace scaling (gain correction) for seismic line 2-North Eyre Road.

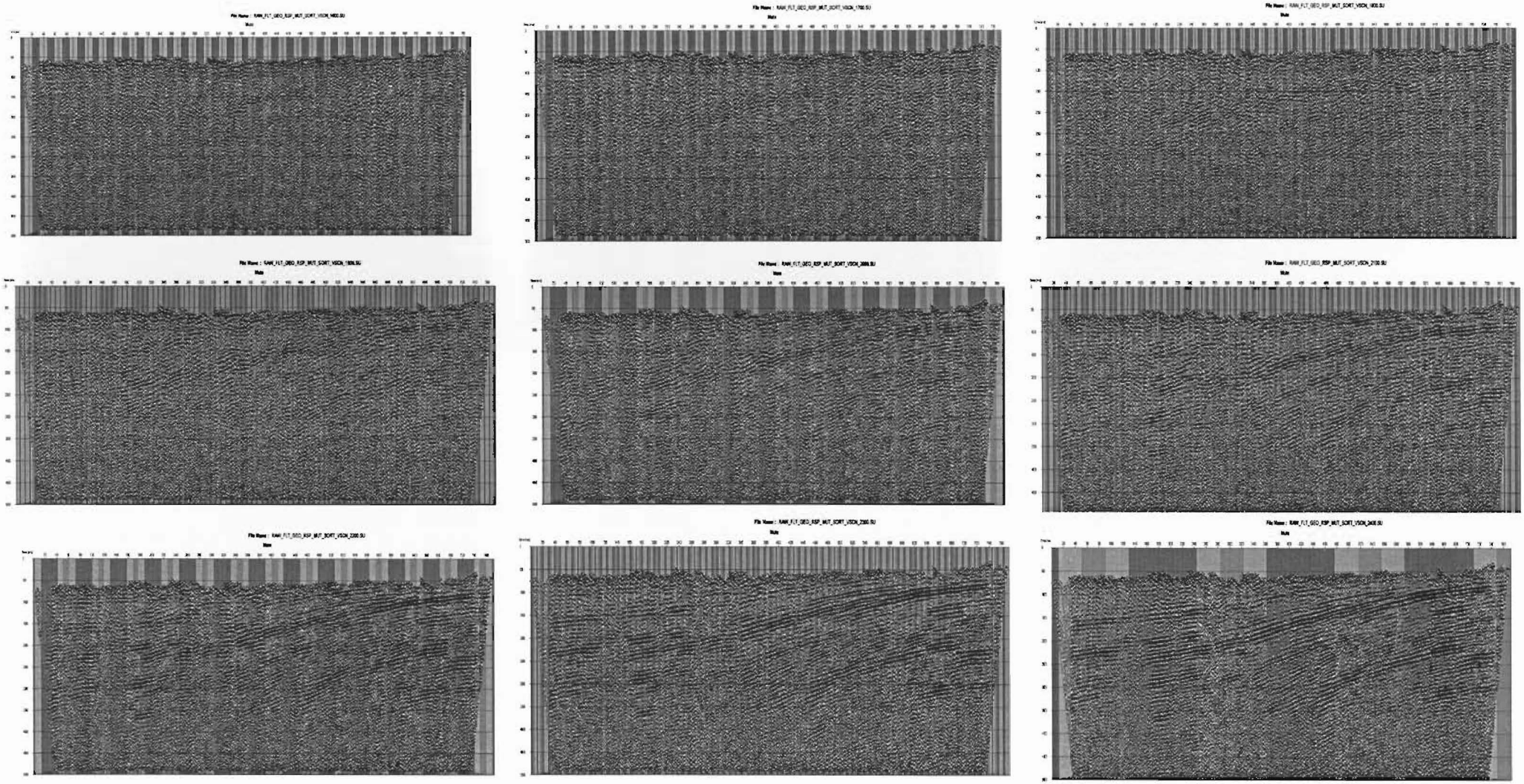

Figure A2.3: Velocity analysis

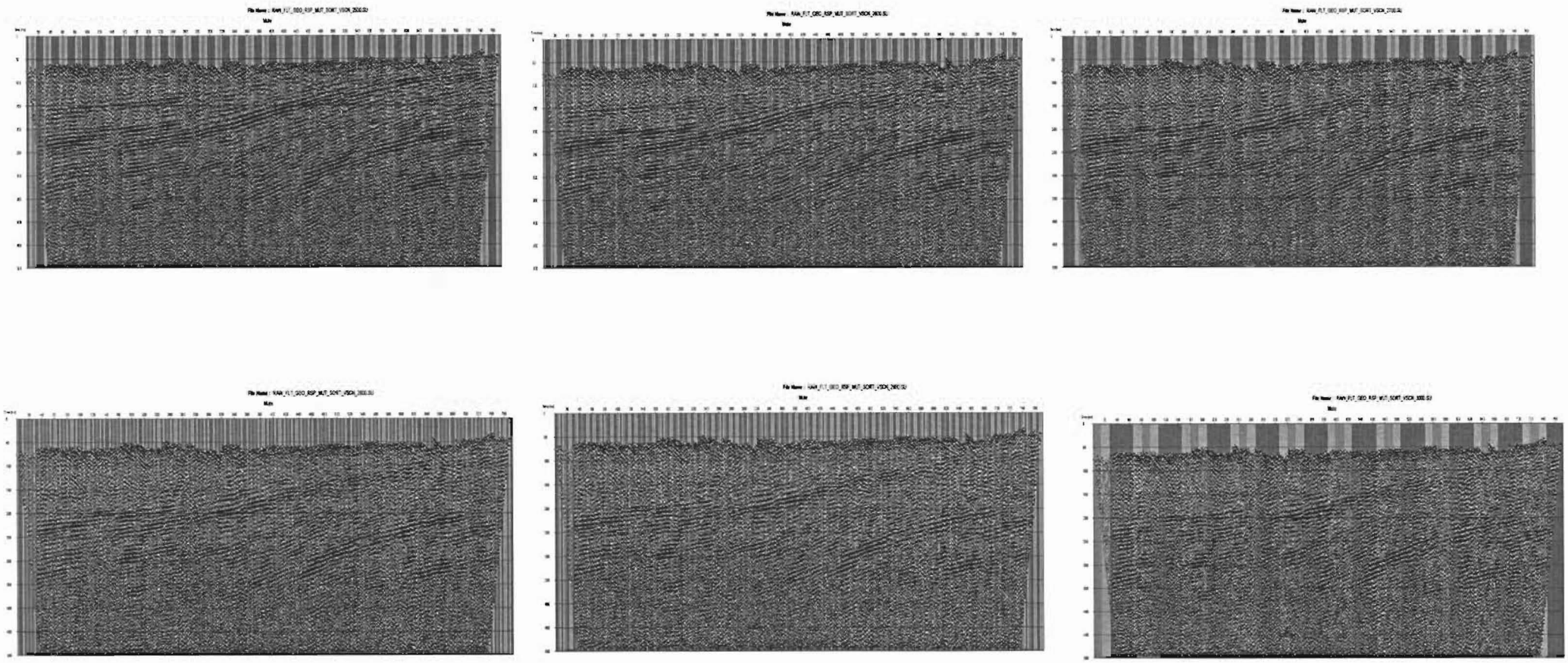

Figure A2.3 (continuation). Velocity analysis.

Appendix 3

FOCAL MECHANISMS

Eleven focal mechanisms were obtained by Cowan (1992) after 2.5 months of recording in a microearthquake network installed around the study area. Table A3.1 contains the hypocentral parameters used to establish these focal mechanisms. A description of each parameter is provided below:

YR	=	Year (1990)
EVT	=	Event number
DATE	=	Month and day
LAT	=	Latitude (°)
LONG	=	Longitude (°)
NORTHING	=	Northing coordinates in NZ map grid (1949)
EASTING	=	Easting coordinates in NZ map grid (1949)
MAG	=	Richter magnitude
SE	=	Standard error of residuals (sec)
NP	=	Number of phases used for location
NS	=	Number of station used for location
ERT	=	Standard error in origin time (sec)
ERY	=	Standard error in Latitude (°)
ERX	=	Standard error in Longitude (°)
ERZ	=	Standard error in depth (km). R is restricted depth

Table A3.2 contains the fault plane solutions obtained by Cowan (1992) for the events illustrated in Table A3.1.

Table A3.1: Hypocentral parameters recorded by the microearthquake network (Modified from Cowan, 1992).

EVT	YR	DATE	LAT	LONG	NORTHING	EASTING	DEPTH	MAG	SE	NP	NS	ERT	ERY	ERX	ERZ
1	90	Sep-05	43.307 S	172.606 E	5766638.19	2478045.64	8.6	1.6	0.08	17	11	0.03	0.002	0.003	0.4
2	90	Sep-20	43.217 S	172.316 E	5776484.12	2454436.21	9.8	1.6	0.09	13	8	0.03	0.002	0.003	0.3
3	90	Sep-25	43.405 S	172.399 E	5755650.83	2461330.17	8	1.7	0.11	18	12	0.04	0.002	0.004	0.4
4	90	Sep-25	43.167 S	172.566 E	5782174.91	2474719.21	5.4	2.2	0.13	20	16	0.04	0.002	0.005	1
5	90	Sep-26	43.173 S	172.497 E	5781476.76	2469112.5	23.8	1.7	0.07	17	10	0.03	0.002	0.003	0.4
6	90	Oct-01	43.328 S	172.348 E	5764173.95	2457132.49	7.8	2	0.08	22	12	0.02	0.001	0.002	0.3
7	90	Oct-04	43.16 S	172.322 E	5782820.07	2454872.19	9.9	2	0.07	26	16	0.02	0.001	0.002	0.2
8	90	Oct-10	43.257 S	172.449 E	5772120.51	2465271.52	7	2.1	0.05	10	6	0.03	0.002	0.002	0.3
9	90	Oct-13	43.373 S	172.393 E	5759202.3	2460818.35	19.6	1.9	0.1	21	12	0.03	0.002	0.004	0.3
10	90	Oct-18	43.166 S	172.38 E	5782190.26	2459593.87	9.2	1.9	0.07	32	19	0.02	0.001	0.001	0.2
11	90	Nov-12	43.224 S	172.602 E	5775857.37	2477676.95	8.7	1.7	0.12	22	12	0.05	0.002	0.004	0.4

Table A3.2: Fault plane solutions (From Cowan, 1992)

	Nodal plane 1			Nodal plane 2				
EVT	**STRIKE**	**DIP**	**SLIP VECTOR**	**STRIKE**	**DIP**	**SLIP VECTOR**	**P-AXIS**	**T-AXIS**
1	252	89N	252/07	342	83E	162/01	298/02	208-06
2	119	54S	293/08	23	82E	030/36	335/32	076/17
3	22	71E	193/23	283	67N	290/19	151/02	243/30
4	233	80n	051/12	141	78s	142/10	94/16	0/07
5	184	54W	230/46	320	44E	093/36	253/04	154/65
6	238	70N	052/20	141	70S	149/20	102/29	192/00
7	82	84S	263/06	352	84E	353/06	306/09	219/00
8	254	57N	338/56	68	34S	164/33	342/10	072/79
9	74	50S	251/03	341	87E	345/40	290/29	035/25
10	85	84s	264/18	353	72E	356/06	312/17	219/06
11	80	84S	261/09	350	81E	350/06	306/10	215/01

Appendix 4
ATTENUATION RELATIONSHIP PARAMETERS AND RESPONSE SPECTRA

This appendix contains both the compilation of the input parameters used in different attenuation relationships in order to estimate ground motions, and the horizontal acceleration response spectra of selected urban centres within the near-fault zone of the Springbank Fault.

The ground motion estimation was based on an earthquake of moment magnitude 6.4 produced by the Springbank Fault during a reverse slip event. The following recent updated attenuation relationships were used for the calculations: Abrahamson and Silva (1997), Boore et al. (1997), Campbell (1997), Sadigh et al. (1997) and McVerry et al. (2000). (A full description of these attenuation relationships, except McVerry et al. (2000), may be found in the special issue of Seismological Research Letters, Vol 68, January/February, 1997)

Table A4.1 contains the input parameters and Figures A4.1 to A4.7 illustrate the estimated horizontal acceleration response spectra for the different selected sites.

Parameters used in table A4.1:

Moment magnitude: M
Distance definitions: r_{rup} = closest distance to the rupture surface, r_{jb} = closest horizontal distance to the vertical projection of the rupture, r_{hypo} = hypocentral distance, r_{seis} = closest distance to the seismogenic rupture zone (as defined for each attenuation relationship).
Fault type: F, F_r, Cr (1 for reverse faults)
Hanging wall: HW (1 for sites over the hanging wall, 0 otherwise)
Site class: S, Ssr, Shr (S = 1 for deep soils; Ssr = Shr = 0 for firm and stiff Quaternary deposits with a depth grater than 10 m)

Table A4.1: Input parameters used in the different attenuation relationships

	Abrahamson and Silva (1997)	Boore et al. (1997)	Campbell (1997)	Sadigh et al. (1997)	McVerry et al. (2000)
Christchurch	M= 6.4 r_{rup}= 28 km F= 1 HW= 0 S= 1	M= 6.4 r_{jb}= 28 km F_{rs}= 1 Vs= 520 m/s	M= 6.4 r_{seis}= 31.3 km F= 1 Ssr= 0 Shr= 0	M= 6.4 r_{rup}= 28 km F= 1	M= 6.4 r= 28 km Cr= 1 HW= 0 Weak rock
Rangiora	M= 6.4 r_{rup}= 6 km F= 1 HW= 0 S= 1	M= 6.4 r_{jb}= 6 km F_{rs}= 1 Vs= 520 m/s	M= 6.4 r_{seis}= 10.2 km F= 1 Ssr= 0 Shr= 0	M= 6.4 r_{rup}= 6 km F= 1	M= 6.4 r= 6 km Cr= 1 HW= 0 Weak rock
Kaiapoi	M= 6.4 r_{rup}= 18 km F= 1 HW= 0 S= 1	M= 6.4 r_{jb}= 18 km F_{rs}= 1 Vs= 520 m/s	M= 6.4 r_{seis}= 21.5 km F= 1 Ssr= 0 Shr= 0	M= 6.4 r_{rup}= 18 km F= 1	M= 6.4 r= 18 km Cr= 1 HW= 0 Weak rock
Oxford	M= 6.4 r_{rup}= 13 km F= 1 HW= 1 S= 1	M= 6.4 r_{jb}= 6.9 km F_{rs}= 1 Vs= 520 m/s	M= 6.4 r_{seis}= 13.1 km F= 1 Ssr= 0 Shr= 0	M= 6.4 r_{rup}= 13 km F= 1	M= 6.4 r= 13 km Cr= 1 HW= 1 Weak rock
Cust	M= 6.4 r_{rup}= 5.2 km F= 1 HW= 1 S= 1	M= 6.4 r_{jb}= 0 km F_{rs}= 1 Vs= 520 m/s	M= 6.4 r_{seis}= 5.9 km F= 1 Ssr= 0 Shr= 0	M= 6.4 r_{rup}= 5.2 km F= 1	M= 6.4 r= 5.2 km Cr= 1 HW= 1 Weak rock
Amberley	M= 6.4 r_{rup}= 24 km F= 1 HW= 0 S= 1	M= 6.4 r_{jb}= 24 km F_{rs}= 1 Vs= 520 m/s	M= 6.4 r_{seis}= 24.5 km F= 1 Ssr= 0 Shr= 0	M= 6.4 r_{rup}= 24 km F= 1	M= 6.4 r= 24 km Cr= 1 HW= 0 Weak rock
Darfield	M= 6.4 r_{rup}= 24 km F= 1 HW= 0 S= 1	M= 6.4 r_{jb}= 24 km F_{rs}= 1 Vs= 520 m/s	M= 6.4 r_{seis}= 24.5 km F= 1 Ssr= 0 Shr= 0	M= 6.4 r_{rup}= 24 km F= 1	M= 6.4 r= 24 km Cr= 1 HW= 0 Weak rock
Rolleston	M= 6.4 r_{rup}= 26 km F= 1 HW= 0 S= 1	M= 6.4 r_{jb}= 26 km F_{rs}= 1 Vs= 520 m/s	M= 6.4 r_{seis}= 29.3 km F= 1 Ssr= 0 Shr= 0	M= 6.4 r_{rup}= 26 km F= 1	M= 6.4 r= 26 km Cr= 1 HW= 0 Weak rock

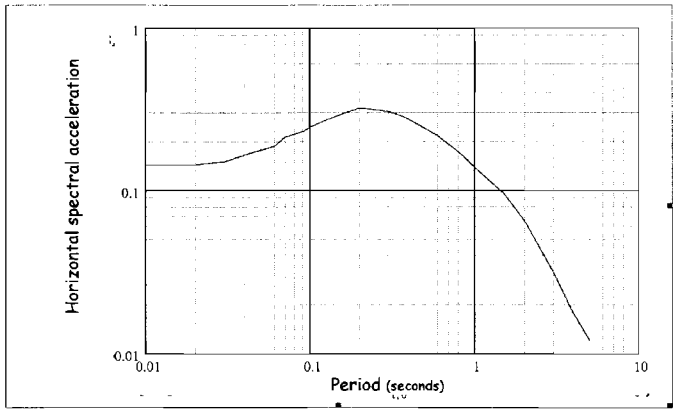

Abrahamson and Silva (1997)

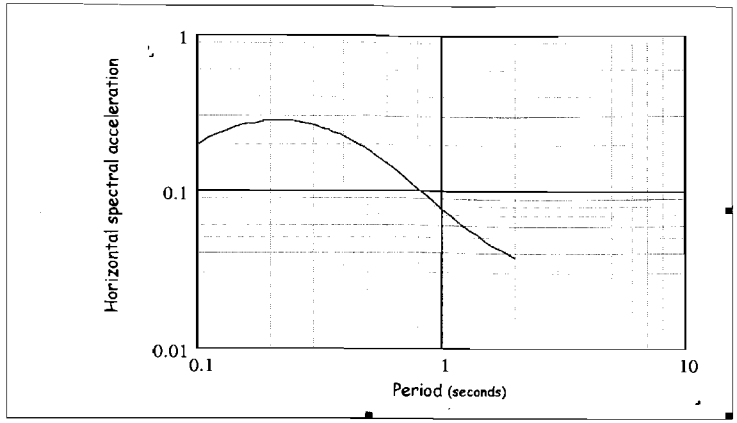

Boore et al (1997)

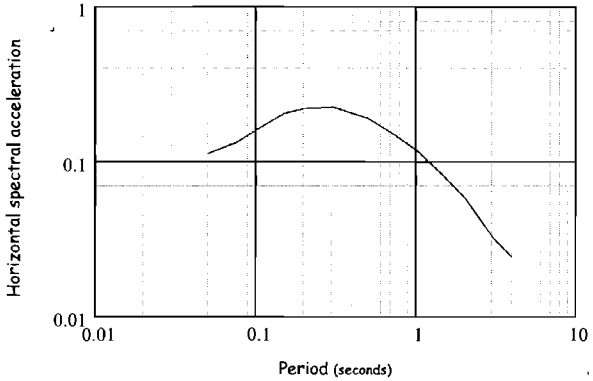

Campbell (1997)

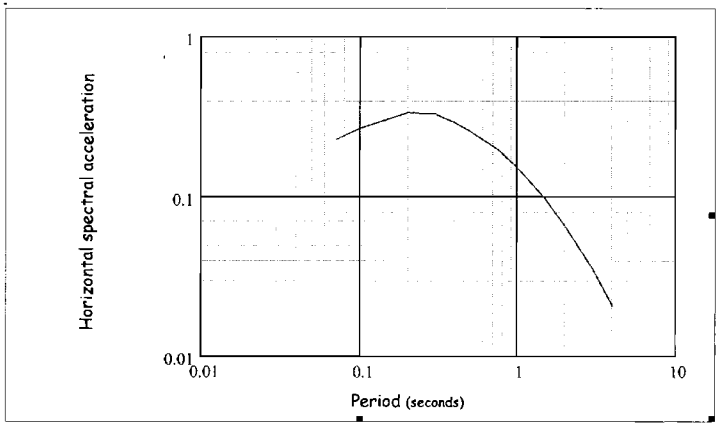

Sadigh et al (1997)

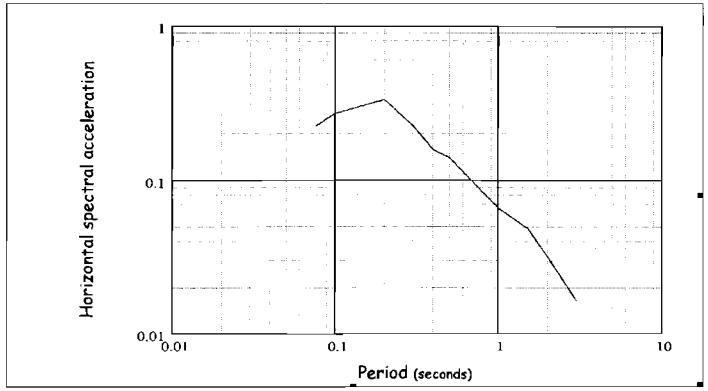

McVerry et al (2000)

Figure A41: Response spectra estimated for Christchurch according to the illustrated attenuation relationships

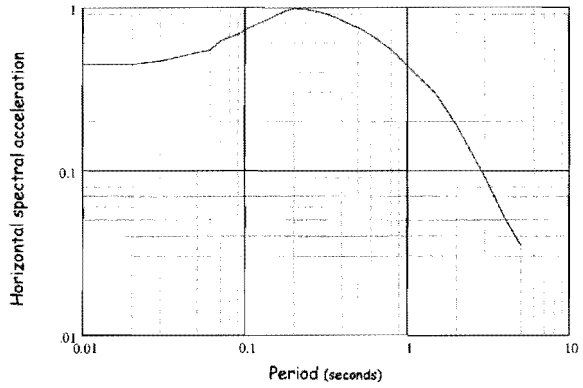

Abrahamson and Silva (1997)

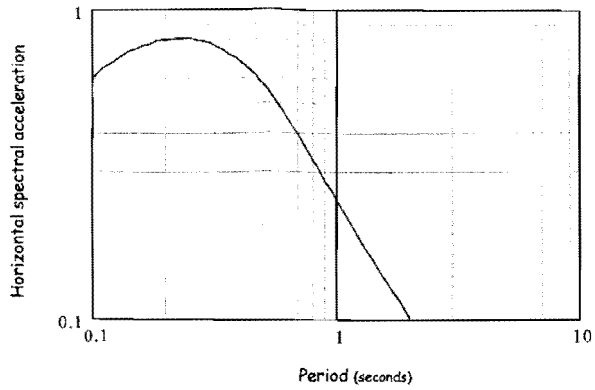

Boore et al. (1997)

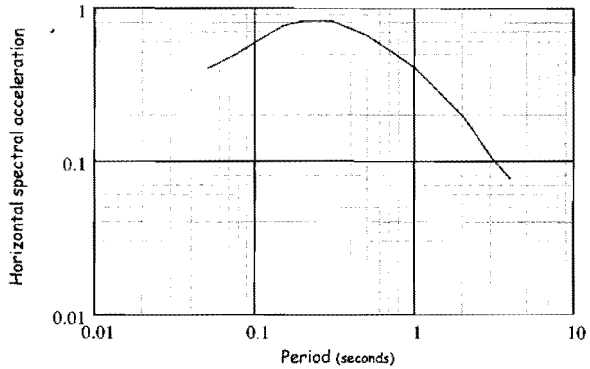

Campbell (1997)

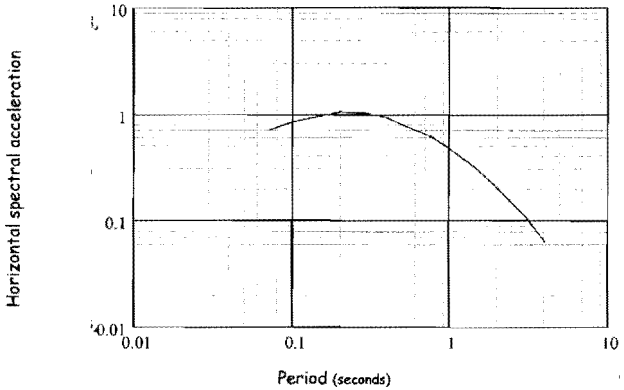

Sadigh et al. (1997)

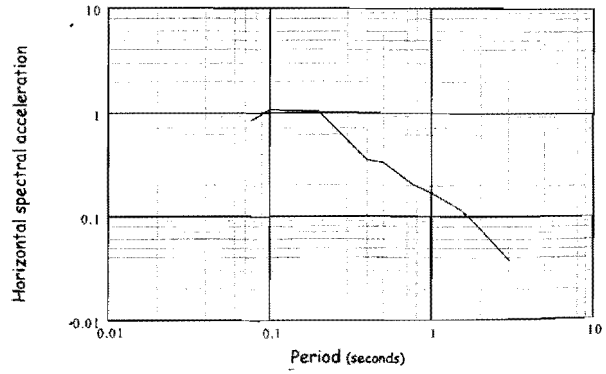

McVerry et al. (2000)

Figure A4.2: Response spectra estimated for Rangiora according to the illustrated attenuation relationships.

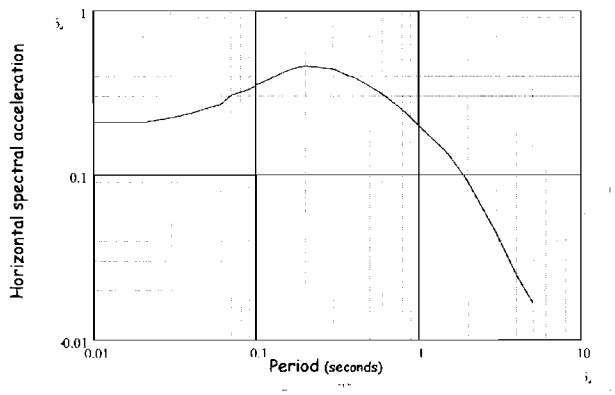

Abrahamson and Silva (1997)

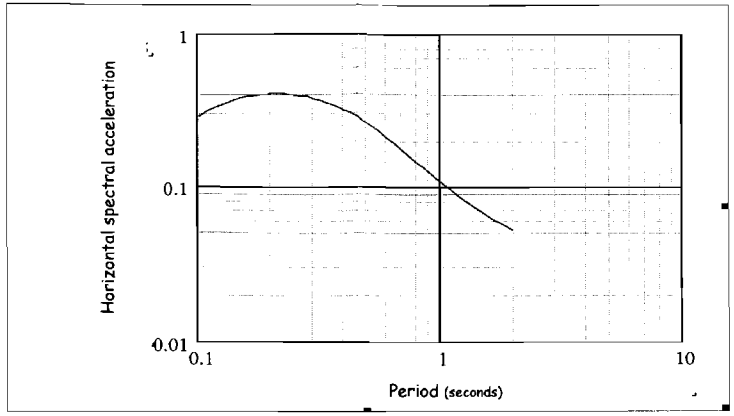

Boore et al. (1997)

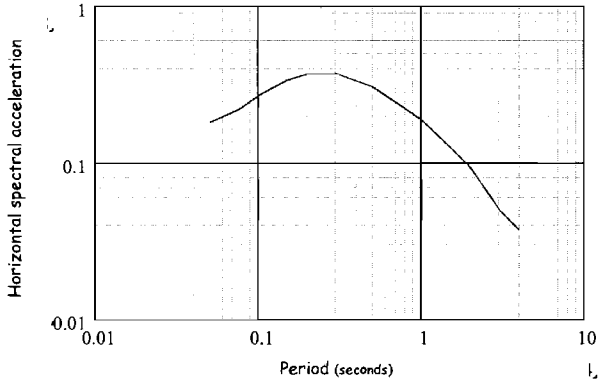

Campbell (1997)

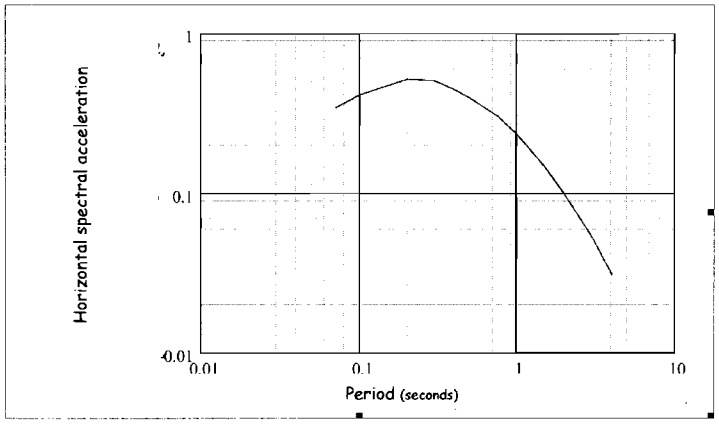

Sadigh et al. (1997)

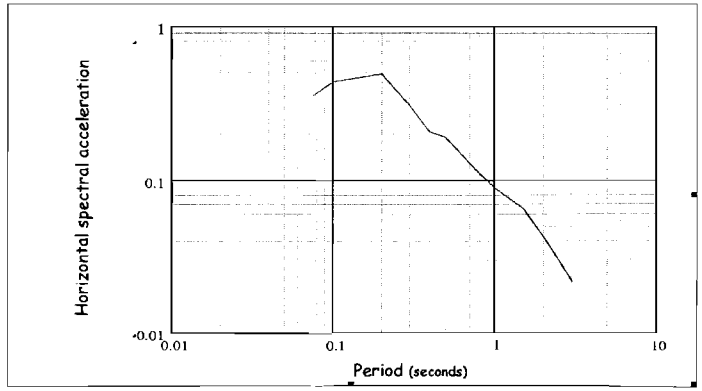

McVerry et al. (2000)

Figure A4.3: Response spectra estimated for Kaiapoi according to the illustrated attenuation relationships.

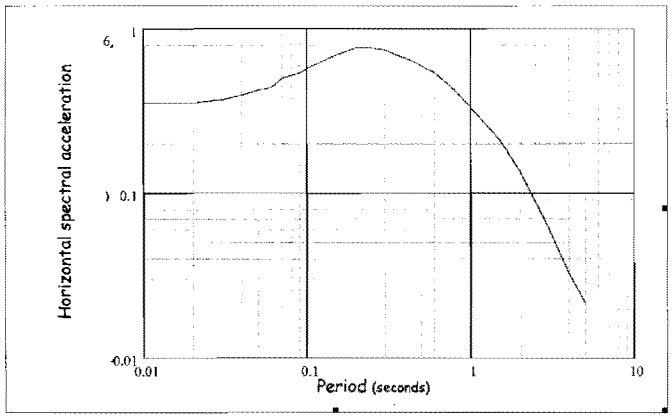

Abrahamson and Silva (1997)

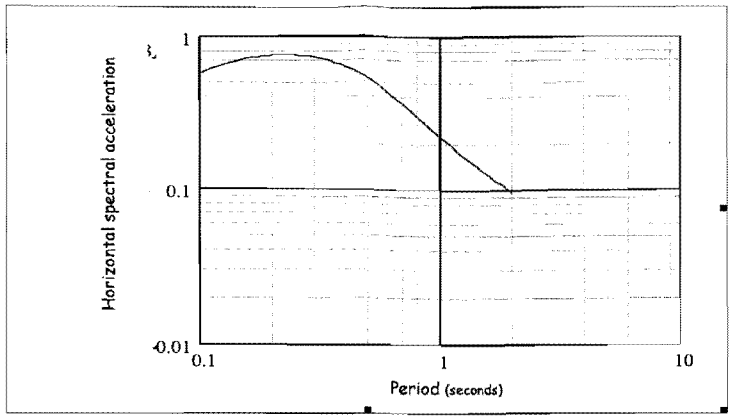

Boore et al. (1997)

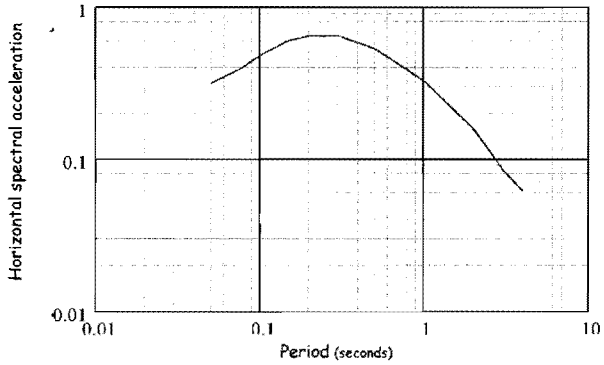

Campbell (1997)

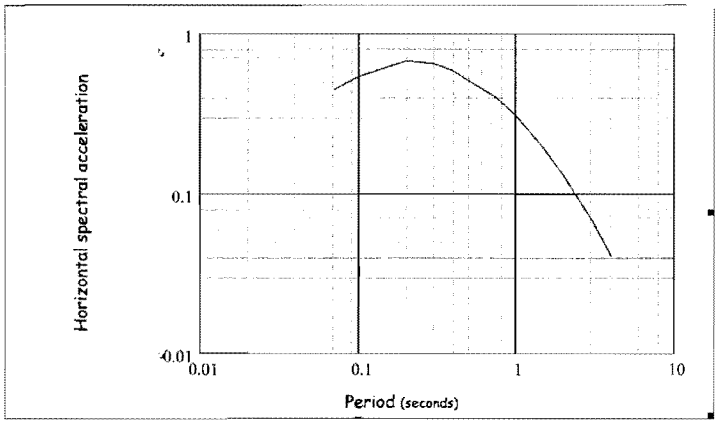

Sadigh et a.l (1997)

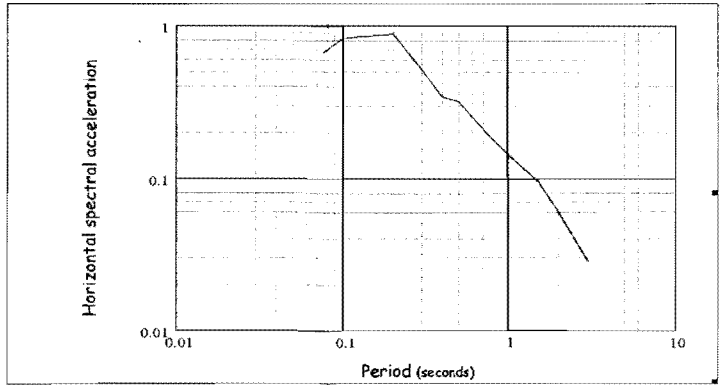

McVerry et al. (2000)

Figure A4.4: Response spectra estimated for Oxford according to the illustrated attenuation relationships.

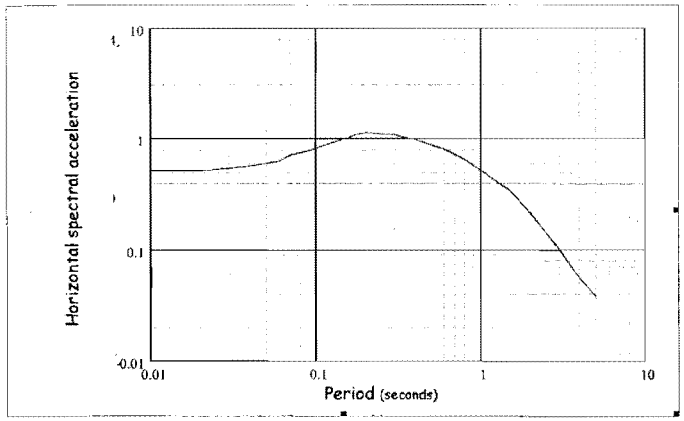

Abrahamson and Silva (1997)

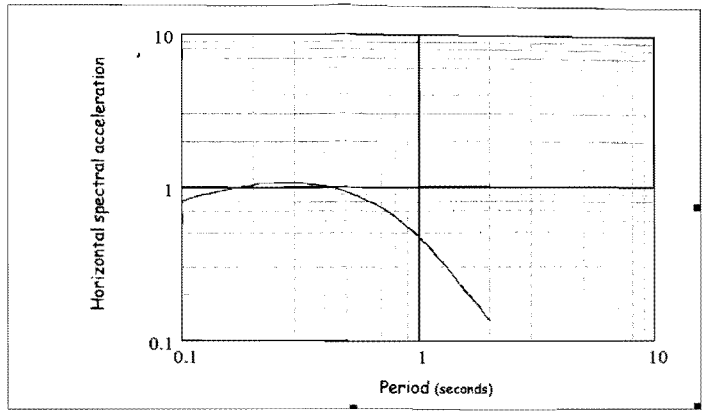

Boore et al. (1997)

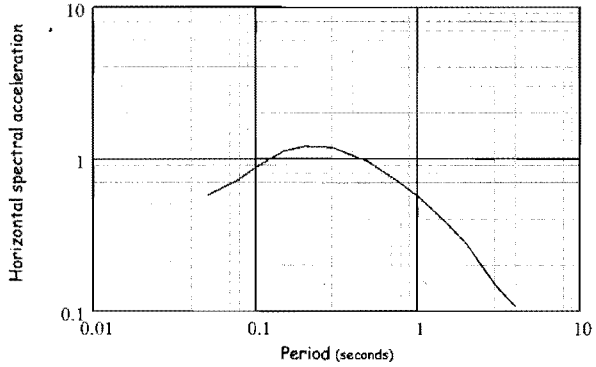

Campbell (1997)

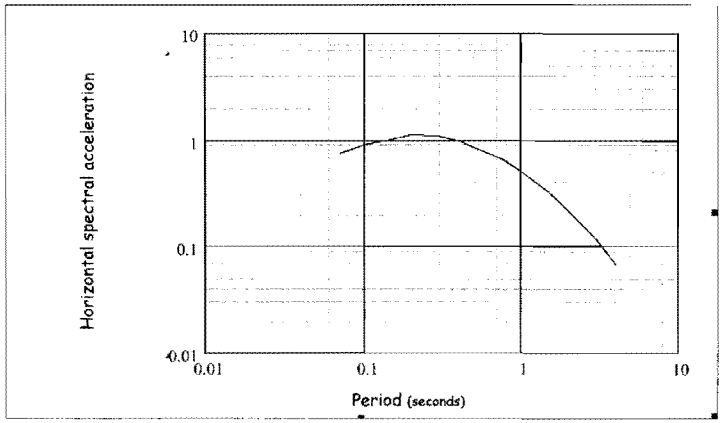

Sadigh et al. (1997)

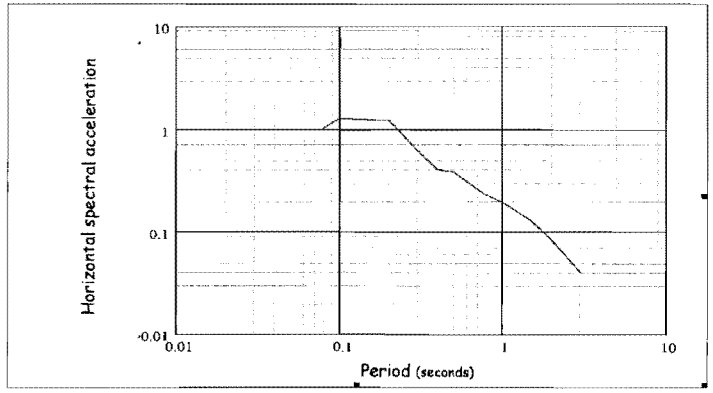

McVerry et al. (2000)

Figure A4.5: Response spectra estimated for Cust according to the illustrated attenuation relationships.

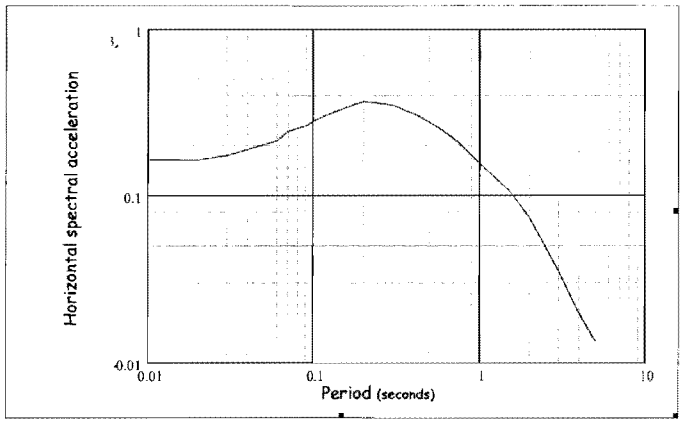

Abrahamson and Silva (1997)

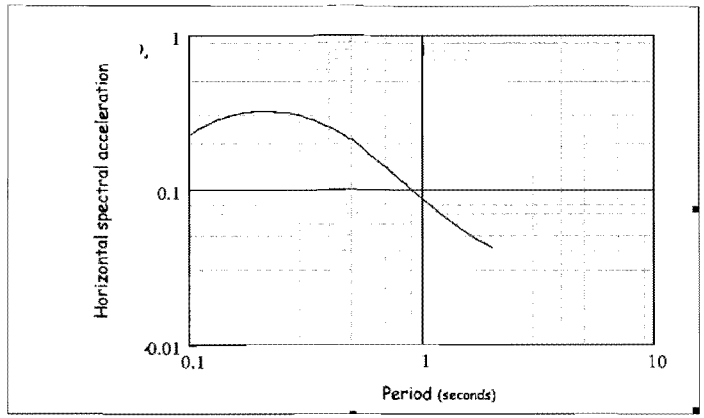

Boore et al. (1997)

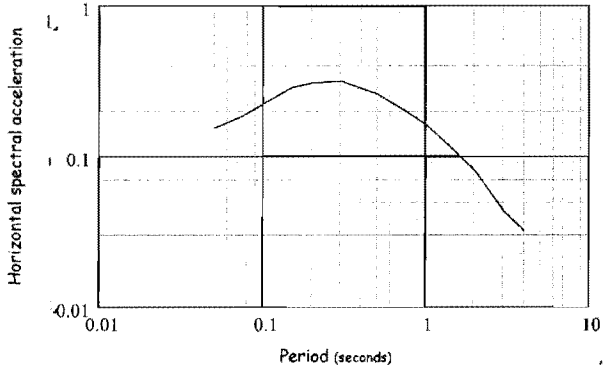

Campbell (1997)

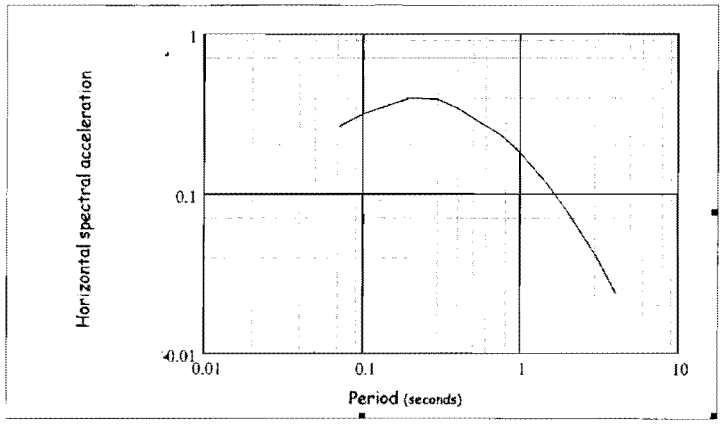

Sadigh et al. (1997)

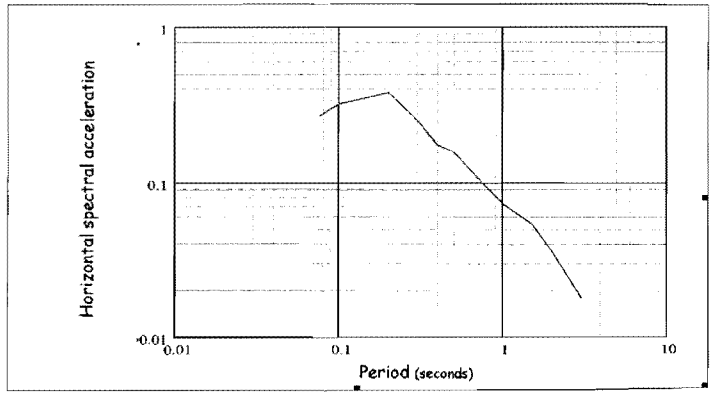

McVerry et al. (2000)

Figure A4.6: Response spectra estimated for Amberley and Darfield according to the illustrated attenuation relationships.

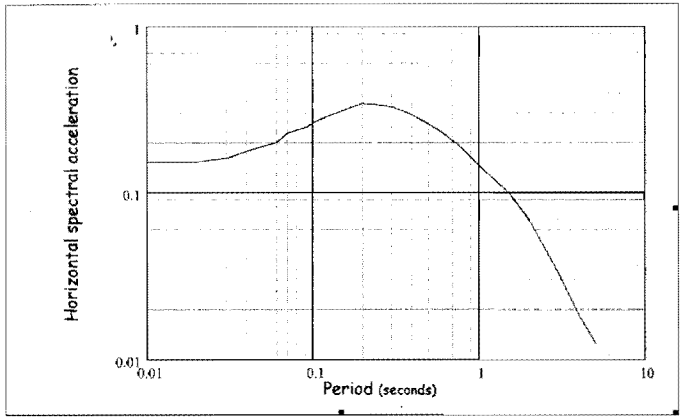

Abrahamson and Silva (1997)

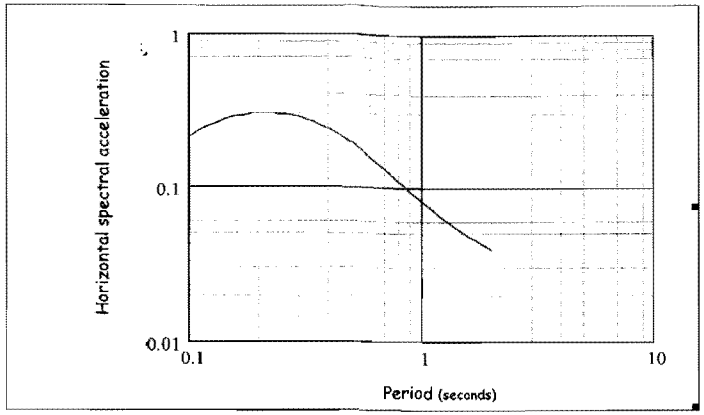

Boore et al. (1997)

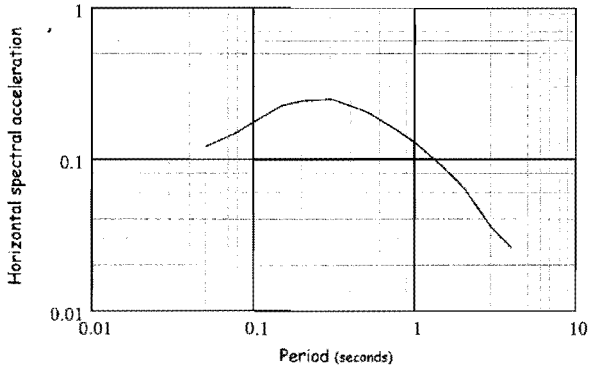

Campbell (1997)

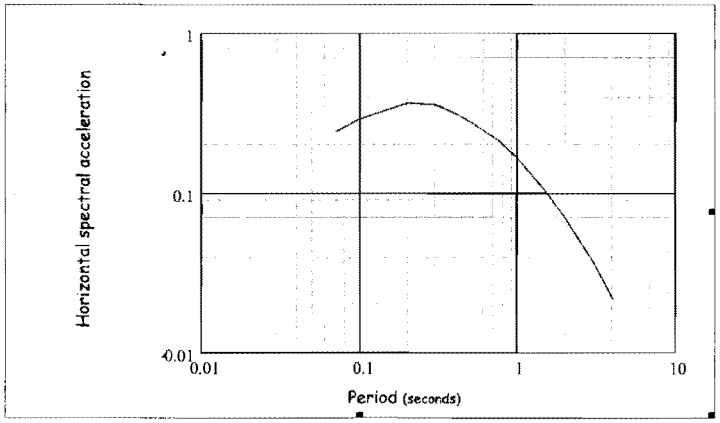

Sadigh et al. (1997)

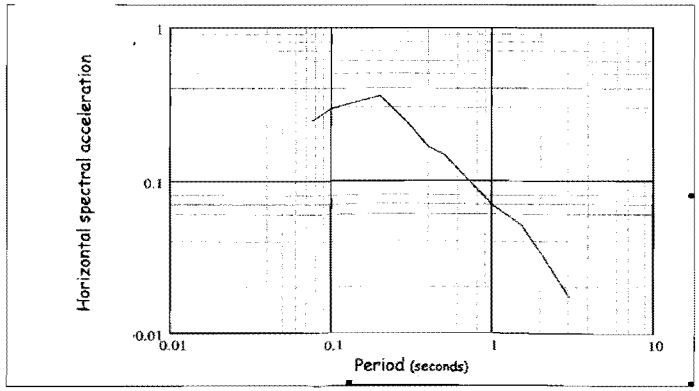

McVerry et al. (2000)

Figure A4.7: Response spectra estimated for Rolleston according to the illustrated attenuation relationships.

Appendix 5

MODIFIED MERCALLI SCALE

The following is an abbreviated description of the 12 levels of the Modified Mercalli Intensity scale (extracted from http://neic.usgs.gov/neis/general/mercalli.html).

I. Not felt except by a very few under especially favourable conditions.

II. Felt only by a few persons at rest, especially on upper floors of buildings.

III. Felt quite noticeably by persons indoors, especially on upper floors of buildings. Many people do not recognize it as an earthquake. Standing motor cars may rock slightly. Vibrations similar to the passing of a truck. Duration estimated.

IV. Felt indoors by many, outdoors by few during the day. At night, some awakened. Dishes, windows, doors disturbed; walls make cracking sound. Sensation like heavy truck striking building. Standing motor cars rocked noticeably.

V. Felt by nearly everyone; many awakened. Some dishes, windows broken. Unstable objects overturned. Pendulum clocks may stop.

VI. Felt by all, many frightened. Some heavy furniture moved; a few instances of fallen plaster. Damage slight.

VII. Damage negligible in buildings of good design and construction; slight to moderate in well-built ordinary structures; considerable damage in poorly built or badly designed structures; some chimneys broken.

VIII. Damage slight in specially designed structures; considerable damage in ordinary substantial buildings with partial collapse. Damage great in poorly built structures. Fall of chimneys, factory stacks, columns, monuments, walls. Heavy furniture overturned.

IX. Damage considerable in specially designed structures; well-designed frame structures thrown out of plumb. Damage great in substantial buildings, with partial collapse. Buildings shifted off foundations.

X. Some well-built wooden structures destroyed; most masonry and frame structures destroyed with foundations. Rails bent.

XI. Few, if any (masonry) structures remain standing. Bridges destroyed. Rails bent greatly.

XII. Damage total. Lines of sight and level are distorted. Objects thrown into the air.